Structural and Biophysical Analysis of Enzymes involved in the Amidation Process in the Cobalamin (Vitamin B_{12}) Pathway

A thesis submitted to the University of Kent for the Degree of PhD in the Faculty of Sciences

2019

Mary Durie Anderson

Declaration

Name: Mary D Anderson

Degree: PhD-Biochemistry

Title: Structural and Biophysical Analysis of Enzymes involved in the Amidation Process in the Cobalamin (Vitamin B_{12}) Pathway

No part of this thesis has been submitted in support of an application for any degree or other qualification of the University of Kent, or any other University or Institution of learning.

Abstract

Cobalamin, more commonly known as vitamin B_{12}, is a highly complex molecule whose biosynthesis in bacteria and archaea involves around 30 enzyme-mediated steps. The biosynthesis of vitamin B_{12} occurs by one of two distinct pathways, which are referred to as the aerobic and the anaerobic routes. The work described in this thesis relates to the aerobic pathway, and is mainly focussed on two enzymes responsible for the amidation of the corrin ring component of cobalamin, CobB which is the enzyme responsible for the amidation of HBA to its product HBAD and CobQ which amidates cobyrinic acid *a, c*-diamide to cobyrinic acid. These enzymes amidate the peripheral carboxylic acid sidechains of the corrin moiety, and produce hydrogenobyrinic acid (HBA) and adenosylcobyrinic acid *a, c*-diamide, respectively. CobB, amidates the *a* and *c* side chains attached to C2 and C7 of the corrin ring, of HBA. The product of this multi-functional enzyme is initially hydrogenobyrinic acid *c*-monoamide (HBAM) followed by hydrogenobyrinic acid *a, c*-diamide (HBAD).

The gene encoding CobB was cloned from *Brucella melitensis,* overexpressed and its encoded protein purified. After crystallisation of the *B. melitensis* CobB, the first X-ray crystal structure of this enzyme was solved using selenomethionine labelled protein to 1.6 Å resolution. Further high resolution structures were obtained containing substrate and co-factors.

To complement the structural information, kinetic data was acquired for the binding of CobB with its substrates, using stopped flow analysis. This kinetic approach helped identify a two-phase binding process, indicating that the initial HBA molecule binds quickly to the dimeric enzyme, whilst the second HBA molecule binds at a much slower rate. Collectively, the binding data suggest that CobB undergoes a conformational change upon binding the first HBA substrate that alters the binding affinity of the second HBA-binding site.

CobH, the enzyme prior to CobB in the cobalamin pathway, is known to bind its product (HBA) very tightly, which poses the question as to how CobB interacts with CobH in order to access its substrate. To investigate if CobB and CobH interact a model was constructed to determine if the two enzymes could form a complex that facilitates direct metabolite channelling. Evidence for direct metabolite transfer was obtained from fluorescence spectroscopy, where fluorescence emission was used to monitor changes associated with substrate transfer of HBA from CobH to CobB Co-crystallisation trials to obtain a complexed crystal structure of CobH/HBA/CobB was attempted, but this approach resulted only in the generation of CobH crystals.

CobQ, the second enzyme in the amidation process, was also produced recombinantly and purified. This enzyme amidates positions *b, d, e* and *f* on the corrin ring. Crystallisation trials were attempted, and a low resolution data set was collected (4.5 Å). However, the structure was not determined due to the poor quality of the data.

CobB and CobQ are key enzymes involved in the amidation process in the vitamin B_{12} pathway. To date there is no structural information in the literature as to how these enzymes function. Obtaining a crystal structure of either CobB or CobQ would enhance our knowledge on these multi-functional enzymes, enabling a clearer understanding on how they bind their substrates, and how these enzymes pass their product to the next enzyme in the vitamin B_{12} pathway.

Contents

Figures

Tables

Abbreviations

Å:	Angstroms
A_{280}:	Absorbance at 280 nm
ADP:	Adenosine diphosphate
ALA:	5-Aminolevulinic acid
ALAD:	5-aminoevulinic acid dehydratase
ALAS:	5-Aminolevulinic acid synthase
Amp:	Ampicillin
AMPPNP:	Adenylyl-imidophosphate
AS:	Ammonium sulphate
a.s.u:	Asymmetric unit
ATP:	Adenosine triphosphate
AU:	Absorbance units
B_{12}:	Vitamin $B_{12,}$ Cobalamin
Chl:	Chloramphenicol
Da:	Dalton
DEAE:	Diethylaminoethyl
DFDNB:	1, 5-difluoro-2, 4-dinitrobenzene
DLS:	DIAMOND Light Source
DMB:	5, 6-dimethylbenzimidazole
DMS:	Dimethyl sulphide

DMSP: Dimethyl sulfoniopropionate

DMSO: Dimethyl sulfoxide

DMP: Dimethyl pime limidate

DTT: Dithiothreitol

EDTA: Ethylenediaminetetraacetic acid

FPLC: Fast performance liquid chromatography

GATase: Glutamine amidotransferase

GluTR: Glutamyl tRNA (transfer ribonucleic acid)

Gln: Glutamine

Glu: Glutamate

GSA: Glutamate-1-semialdehyde

GTP: Guanosine-5'-triphosphate

HBA: Hyrogenobyrinic Acid

HBAM: Hydrogenobyrinic acid *c*-diamide

HBAD: Hydrogenobyrinic acid *a,c*-diamide

HCl: Hydrochloric acid

IPTG: Isopropyl-β-D-thiogalactopyronoside

kDa: Kilodaltons

LB: Luria-Bertani

MES: 2-(N-morpholino)ethanesulphonic acid

MOPS: 3-(N-morpholino)propanesulfonic acid

M-THF:	Methyl-tetrahydrofolate
MMA:	Methylmalonic acid
MPD:	2-Methyl-2,4-pentanediol
MST:	MicroScale Thermophoresis
MS:	Mass spectrometry
NADPH:	Nicotinamide adenine dinucleotide phosphate
nm:	Nanometres
NTY:	Na/Tryptone/Yeast broth
OD:	Optical density
PAGE:	Polyacrylamide gel electrophoresis
PBG:	Porphobilinogen
PBS:	Phosphate buffer saline
PEG:	Polyethylene glycol
PLP:	Pyridoxyl-5 phosphate
rpm:	Revolutions per minute
SAD:	Single wavelength anomalous dispersion
SAM:	S-Adenosyl-L-methionine
SDS:	Sodium dodecyl sulphate
SOC:	Super Optimal broth with Catabolite repression
SUMT:	S-adenosyl-L-methionine-dependent uroporphyrinogen III C methyltransferase

Tris:	2-amino-2-hydroxymethyl-propane-1,3-diol
2YTNN:	2 x Yeast/Tryptone Na/NH_5Cl
2YT:	2 x Tryptone/Yeast broth
Uro'gen III:	Uroporphyrinogen III
UV:	Ultra violet

Quotes

The most glorious moments in your life are not the so-called days of success, but rather those days when out of dejection and despair, you feel rise in you a challenge to life, and the promise of future accomplishments.

Gustave Flaubert

The adventure of life is to learn. The purpose of life is to grow. The nature of life is to change. The challenge of life is to overcome. The essence of life is to care. The opportunity of life is to serve. The secret of life is to dare. The spice of life is to befriend. The beauty of life is to give.

William Arthur Ward.

Acknowledgements

I would like to give a big thanks to Prof. Martin Warren for giving me the opportunity to be part of the Warren Lab, and for his help and support in the writing of this thesis.

Many thanks goes to the people in the Warren Lab. Especially Dr. Evelyne Deery who provided me with the many plasmids used, also Dr. Andrew Lawrence who helped me with mass spectrometry and last but not least Dr. Joe Baker for his contribution of the HBAM.

I would also like to thank Prof. Dave Brown for his invaluable help in solving the structures. Also Neil Paterson from Diamond Light Source, Oxfordshire, for his valuable help with the Se-Met data set.

Special thanks goes to Prof. Mike Geeves for the time he spent teaching me to use the stopped-flow and his patience in helping me in the interpretation of the data.

Thanks also goes to the Argenta team, Dr. Steve Irving, Colin Robinson and Richard Bazin, for their friendship and advice, also for allowing me to help myself to any materials that I required.

I would also like to thank my family and friends for their support. My daughter Georgette, my sister Margaret and my brother Billy, who despite going through their own trials have never faltered in their support for me. Lastly I want to thank my mother and father for their help and encouragement throughout my life. This thesis is dedicate to my father, William Reston who is no longer with us, but who I know would be extremely proud.

Chapter 1

Introduction

1.1 Macrocyclic tetrapyrroles - the pigments of life

Macrocyclic tetrapyrroles are a family of compounds that are essential for life. They are composed of four pyrrole rings that are arranged in a circular manner whereby the individual pyrrole rings are connected by methene bridges. Organisms synthesize these compounds either *de novo* or scavenge them from their environment.

The pyrrole rings of the tetrapyrrole framework are labelled A-D in a clockwise direction (Figure 1.1). Modified tetrapyrroles occur widely in nature and are involved in many critical biological processes such as electron and oxygen transport, photosynthesis, methanogenesis, sulphite and nitrite reduction and many enzymatic reactions. Naturally occurring tetrapyrroles include haem, sirohaem, haem d_1, chlorophyll, coenzyme F_{430} and cobalamin (vitamin B_{12}) (Figure 1.2) (Dailey 2013) (Banerjee and Ragsdale 2003a; Battersby 2000). Haem is responsible for the transport of oxygen (Hamza and Dailey 2012), while chlorophyll is pivotal for the transformation of light into chemical energy in plants during photosynthesis (Bollivar, 2006). In humans, cobalamin plays a key role in homeostatic functions and acts as cofactor and coenzyme for the enzymes methionine synthase and methylmalonyl-CoA, respectively. Methionine synthase is involved in the recycling of methionine whilst methylmalonyl CoA mutase is associated with the breakdown of certain amino acids and odd chain fatty acids (Banerjee and Ragsdale 2003b).

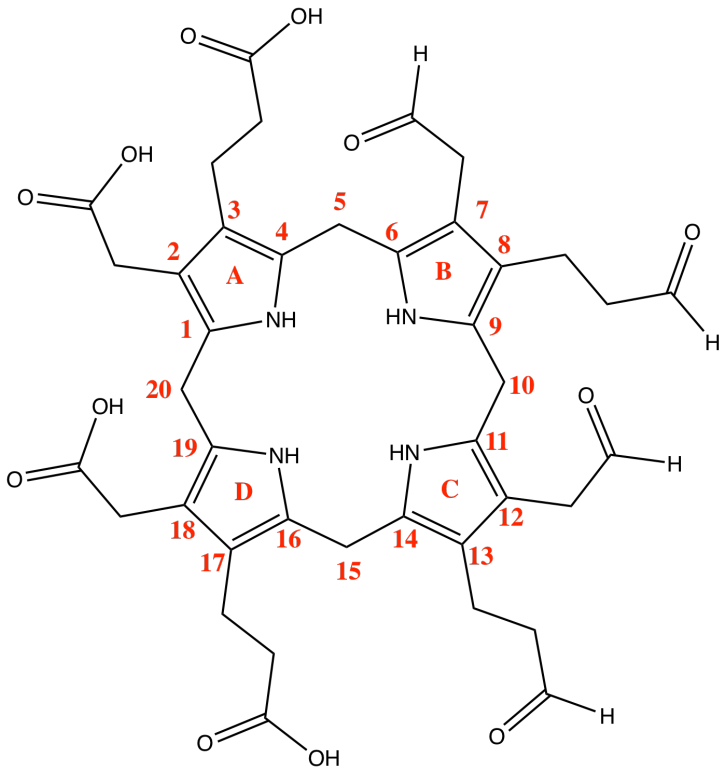

Figure 1.1: Structure of uroporphyrinogen III. Diagram shows the structure of the tetrapyrrole primogenitor uroporphyrinogen III and the numbering system for the mainframe carbons (red:1-20). The meso-bridge carbons are labelled 5, 10, 15 and 20, and the rings are labelled A-D in a clockwise direction.

Modified tetrapyrroles are found in all domains of life and are involved in many essential biological reactions. They are able to chelate metal ions in the ring system and these ions (Fe, Ni, Co and Mg) determine their function (Figure 1.2). It is this variation in the nature of the chelated metal ion and the oxidation state of the macrocycle that not only gives them their distinctive colour (Battersby 2000) but also determines their role within this family of molecules (Senge 2015) (Frankenberg, Moser and Jahn 2003).

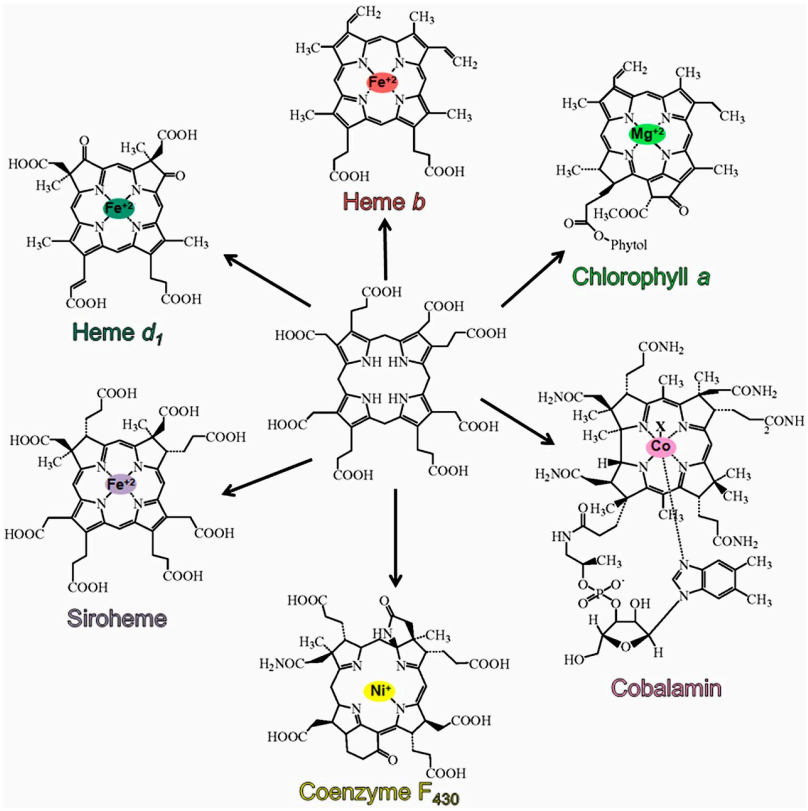

Figure 1.2: Cyclic tetrapyrroles derived from common precursor. Figure shows the main biological macrocyclic tetrapyrroles that originate from uroporphyrinogen III. The central metal ions are coloured to highlight the metallo tetrapyrrole. (Figure is taken from Dailey 2013).

Coenzyme F_{430} is a unique nickel containing tetrapyrrole involved in methyl - coenzyme M reductase activity. In the cobalamin pathway HBA is amidated at position C2 and C7, by CobB to form hydrogenobyrinic acid *a, c* – diamide. F_{430} Ni^{2+} - sirohydrochlorin is amidated also at positions C2 and C7 to form Ni - sirohydrochlorin *a, c* -diamide. Both of these pathways although completely different require Mg/ATP and Gln for enzyme activity. Although F_{430} is involved in methanogenesis and Cobalamin in cellular metabolism, two completely different processes, as with the other tetrapyrroles are all derived from a common precursor (uroporphyrinogen III) (Moore *et al.* 2017).

The aim of this thesis is to obtain structural and biophysical information on two enzymes involved in the aerobic biosynthesis pathway, leading to the production of vitamin B_{12}. The aerobic pathway has been studied extensively due to the relative stability of its pathway intermediates. However, even in this pathway there are still a number of enzymes which have been difficult to obtain structural information on. The two enzymes of specific interest to this research project are involved in amidation of the corrin ring. CobB, the first enzyme, amidates the corrin ring at position C2 (side chain *a*) and C7 (side chain *c*). The second enzyme CobQ is involved in the final stage of the aerobic branch of the pathway. This enzyme is involved in the amidation of the side chains (three propionic acids and one acetic acid) labelled *b, d, e* and *g* on the corrin ring.

1.2 Cobalamin

Cobalamin along with other corrinoids which contain cobalamin are unique due to the fact they do not have a methane bridge between rings A and D (Friedmann & Thauer, 1992). This molecule is the most complex of all the tetrapyrroles, and is the only tetrapyrroles to have an upper and lower ligand. The lower ligand is a nucleotide loop formed of dimethylbenzimidazole, and an upper axial ligand which can be aquacobalamin, methylcobalamin, adenosylcobalamin or cyanocobalamin. The two active forms of cobalamin are methyl and adenosyl-cobalamin. These two active forms use the properties of the cobalt carbon bond to promote a range of enzymatic properties such as rearrangement, methylation and reductive dehalogenation reactions (Banerjee and Ragsdale 2003a).

1.3 Haems

Heme is an iron containing porphyrin known as protoporphyrin IX. Haems are widely distributed and are found in eukaryotes, most bacteria and some archaea and has

been used as a cofactor for over 3,000 years. In the *Bacteria, de novo* biosynthesis of haem developed very early in the evolutionary path. However, there is an absence or incomplete pathway in some bacterial pathogens which may be due to secondary gene loss (Dailey *et al.* 2017) There are four types of haem *a*, *b*, *c* and *o*. The four types are all derived from haem *b* which is also referred to as protehaem (Kranz *et al.* 2009).

1.4 Chlorophylls

The most abundant of all tetrapyrroles in nature are the chlorophylls. Chlorophylls and bacteriochlorophylls are structurally related porphyrin compounds, and are indispensable components of the photosynthetic apparatus used by plants and bacteria to harvest energy and convert it to chemical energy (Reinbothe *et al.* 1996). Although the two are structurally related, in the later stage of the pathway the two porphyrin compounds use different enzymes to convert pro-tochlorophyllide to chlorin. It is therefore, suggested that bacteriochlorophyll is the bacterial equivalent of chlorophyll and may be representative of the evolutionary ancestor of chlorophyll (Reinbothe *et al.* 1996).

1.5 Sirohaem

Sirohaem is considered to be one of the most simplest tetrapyrroles, as after the synthesis of uro'gen III there are very few modifications. These modifications involve a two methylation step, oxidation and ferrochelation to form sirohaem. Sulphur and nitrogen are two elements that are essential for life, these compounds must be reduced to sulphate and ammonium. Sirohaem is an iron containing isobacteriochlorin and is a cofactor involved in the reduction of nitrite and sulphite (Dailey *et al.* 2017; Lobo *et al.* 2015; Tripathy, Sherameti and Oelmüller 2010).

1.6 Coenzyme F_{430} and haem d_1

Of all of the tetrapyrroles coenzyme F_{430} and d_1 are the most elusive as there is very little known about their synthesis. Coenzyme F_{430} is a nickel containing tetrapyrrole which is yellow in colour. This molecule is a cofactor of methyl-coenzyme M reductase and is involved in methanogenesis (Dailey *et al.* 2017; Moore *et al.* 2017; Thauer and Bonacker 2007).

Despite being named haem d_1 this molecule is not a member of the haem family and therefore is not a true porphyrin. It is in fact an iron containing isobacteriochlorin. Cytochrome cd_1 nitrate reductase is involved in the conversion of nitrite to nitric oxide in denitrifying bacteria, where haem d_1 is a cofactor for this reaction (Dailey *et al.* 2017; Moore *et al.* 2017; Thauer and Bonacker 2007).

The research described in this thesis deals with an important aspect of cobalamin biosynthesis and hence this chapter will focus largely on the corrin macrocycle. The biological forms of cobalamin are found with a range of different upper ligands. methylcobalamin (transfer of methyl groups between compounds), adenosylcobalamin and hydroxycobalamin (reductive dehalogenases) (Bridwell-Rabb, Grell and Drennan. 2018). Interestingly, cyanocobalamin, the commercial form of cobalamin, is a chemical artefact reflecting the purification of the nutrient from large scale bacterial cultures (Jahn. 2013; Martens *et al.* 2002) . Cobalamin is defined as a cobinamide which has 5, 6-dimethylbenzimidazole as a lower axial ligand.

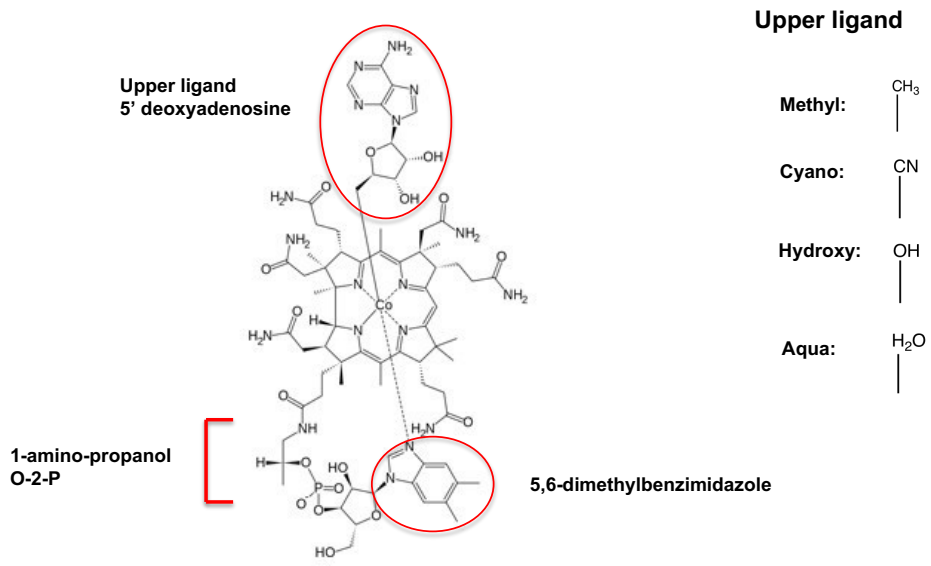

Figure 1.3: The structure of adenosylcobalamin. Structure shows the upper ligand (adenosyl) bound to cobalt, and the lower ligand 5, 6-dimethylbenzimidazole (DMB). Alternative upper ligands are shown on the right hand side.

1.7 History of Cobalamin (Vitamin B_{12})

It was in 1926 that two scientists (Minot and Murphy) discovered that by feeding patients with whole liver extracts they could control a condition known as pernicious anaemia (Minot and Murphy 1926). Another scientist, Whipple, also studied anaemia in dogs. His research involved bleeding dogs until they were anaemic, and then feeding them on special diets to note how quickly they recovered. Whipple found that dogs who ate large amounts of liver recovered quickly (Robscheit *et al.* 1920). In 1934 Minot, Murphy and Whipple were awarded the Nobel Prize for demonstrating that liver contained an anti-pernicious anaemia factor that was termed vitamin B_{12} (Moore *et al.* 2012). Researchers were therefore keen to isolate and characterise the anti-pernicious anaemia factor, with interest from Glaxo in the UK, led by a research team headed by Lester Smith (Smith L. 1948), and Merck in the USA, with a research team led by Karl Folkers (Rickes *et al.* 1948). This work was very difficult as the nutrient in liver was present in very small quantities (Battersby 2000).

In 1944 Mary Shorb, a microbiologist who worked on *Lactobacillus lactis* Dorner (LLD), similarly discovered that this bacterium would only grow in medium containing liver extract. Shorb suggested that *L. lactis* required the anti-pernicious anaemia factor too and that the bacterium could be used for its detection in various liver extracts. In 1947 she collaborated with Karl Folkers and his co-workers at Merck where her *L. lactis* assay was used to identify the presence of the anti-pernicious anaemia factor from liver fractions, which helped in the purification of vitamin B_{12}. For this discovery, Mary Shorb and Karl Folkers were co-recipients of the Mead Johnson Award from the American Society of Nutritional Sciences in 1949 (Shorb 1948).

Around the same time Lester Smith & Karl Folkers (Smith L. 1948) (Rickes *et al.* 1948), using chromatographic procedures, also isolated vitamin B_{12}, from which they were able to grow deep red coloured crystals (Rickes *et al.* 1948). The fact they could only isolate a few micrograms of the compound at a time initially hindered the experimental progress. Despite the isolation of purified vitamin B_{12}, its characterisation and chemical structure remained elusive as it was a compound quite unlike anything else that had previously been studied. It was, in fact, the application of X-ray crystallography by Dorothy Hodgkin that solved the problem (Hodgkin *et al.* 1955). This was a remarkable achievement to gain structural data on this complicated molecule. At the time she explained that “A great advantage of X-ray analysis as a method of chemical structure analysis is its power to show some totally unexpected and surprising structures with, at the same time, complete certainty” (Battersby 2000).

The total chemical synthesis of vitamin B_{12} was achieved in the 1970’s by two groups headed by Woodward and Eschenmoser (Woodward 1973.; Eschenmoser and Wintner 1977). At the time this represented a massive achievement in organic synthesis.

1.8 Vitamin B_{12}

Vitamin B_{12} is an essential nutrient that is required in mammals but is only produced by bacteria that are found in soil and water. In nature there is a limited number of bacteria which produce vitamin B_{12}. Three of these bacteria are also used for commercial production of this vitamin (*Pseudomonas denitrificans*, *Bacillus megaterium* and *Propionibacterium freudenreichii*). Since this vitamin cannot be produced by the body it imperative that it is acquired from the diet. The B_{12} producing organisms that live in soil are ingested by animals such as cows and other free grazing animals, therefore, providing humans with a source of vitamin $B_{12.}$. Vitamin B_{12} when ingested binds to a protein called haptocorrin (R-factor), which is secreted by the salivary glands. After binding, the complex is then carried to the small intestine where pancreatic enzymes cleave the B_{12}-haptocorrin complex. Intrinsic factor, which is a glycoprotein secreted by the gastric parietal cells, binds B_{12} and the complex then binds receptors in the ileum where B_{12} is absorbed (Gherasim, Lofgren and Banerjee 2013). Poor absorption results in impairment of metabolic processes that have neurological and hematologic function (O'Leary and Samman 2010).

1.9 Cobalamin-dependent enzymes

B12 and other cobalt containing corrins are essential cofactors in numerous biological processes required by both eukaryotic and prokaryotic organisms. The central cobalt atom is responsible for the biological activity. This cobalt ion has the ability to form organo-metallic bonds which are stable (Banerjee and Ragsdale 2003a). There are two different forms of cofactor, firstly where the cobalt is bound to a methyl group (methyl cobalamin), and secondly where the cobalt is bound to 5' -deoxyadenosine (adenosylcobalamin). These two cofactors are utilised by B_{12} dependent enzymes (Ludwig, Drennan and Matthews 1996). The key to the reactivity is this unique Co^{III}-C bond was revealed by x-ray diffraction (Lenhert and Hodgkin 1961). The most studied

of cobalamin is the B_{12} coenzymes, adenosylcobalamin and methylcobalamin. These two coenzymes are the bioactive forms of vitamin B_{12} and are involved in the catalysis of rearrangement reactions. These coenzymes are involved in the rearrangement reactions involving reversible cleavage of the Co – C bond to generate an organic radical Co^{II} which result in the eventual formation of a radical intermediate. This intermediate can then re-bind and reform the bond to Co^{II} resulting in the regeneration of the coenzyme (Broderick 2001).

Adenosylcobalamin is the co-enzyme for the enzyme methylmalonyl-CoA mutase, which is found in the mitochondria and is involved in the conversion of methylmalonyl-CoA to its isomer succinyl-CoA this reaction is catalysed by methylmalonyl-CoA mutase, and results in catabolism of odd chain fatty acids and branched amino acids. The C-Co bond in this molecule is relatively unstable and can result in catalytic cleavage forming and adenosyl radical (E. Neill. Marsh and Gabriel D. Roman Melendez 2012). Accumulation of methylmalonic acid (MMA) is usually observed in patients who are vitamin B_{12} deficient. Excess of MMA can result in neurological damage (Briani *et al.* 2013).

Methylcobalamin is the second organometallic derivative, and is the cofactor of methionine synthase. This biosynthesis is important to both humans and bacteria. The enzyme is involved in the conversion of homocysteine to methionine, and plays an important role in metabolism. This reaction requires methyl-tetrahydrofolate (M-THF) which is cleaved to tetrahydrofolate (Ragsdale 2011). This reaction is linked with folate metabolism, which involves the recycling of methyl-tetrahydrofolate this involves the transfer of a methyl group to cobalamin which results in methylcobalamin

1.10 Biosynthesis of Cobalamin

Tetrapyrroles are synthesised along a branched biosynthetic pathway. The common precursor in the synthesis of all of the above molecules is 5-aminolevulinic acid (ALA)

(Kikuchi *et al.* 1958). This molecule can be synthesised biologically by one of two distinct pathways. The C4 pathway, which involves the condensation of succinyl-CoA and glycine, is typically known as the Shemin pathway (Shemin and Kikuchi 1958). This route is commonly used by mammals, fungi and the σ-group of the proteobacteria. The other route involves the transformation of glutamate into ALA and is referred to as the C5 pathway. The C5 pathway is used by plants, archaea and most bacteria (Beale and Castelfranco 1973).

1.10.1 The C4 pathway

The C4 pathway is also known as the Shemin pathway as it was discovered in the 1940's by David Shemin. Shemin used labelled ^{15}N to follow the uptake of nitrogen into haem. To do this he ingested 66 g of labelled [^{15}N]-glycine over a period of 3 days before extracting and analysing his own blood. He and his co-worker David Rittenberg assessed the ^{15}N content of the haem group by mass spectrometry (Shemin and Kikuchi 1958). These results showed that glycine was incorporated into protoporphyrin. He then went on to look at which of the carbons of glycine were used in porphyrin synthesis. He discovered that 8 of the carbons came from the α carbon of glycine and that the remaining 26 came from succinate. From this work Shemin suggested that ALA was formed from succinyl CoA and glycine, which was confirmed when the enzyme ALA synthase (ALAS) was identified (Shemin and Kikuchi 1958).

The C4 pathway is the simplest of the two pathways for the generation of ALA and represents a condensation between glycine and succinyl-CoA (Figure 1.4). This reaction is a pyridoxyl-5 phosphate (PLP) dependent reaction. ALAS has been purified from many bacteria and eukaryotic sources and has been biochemically characterised (Ferreira and Gong 1995). The full length X-ray crystal structure of ALAS has been solved from *Rhodobacter capsulatus*, allowing a molecular insight into the mechanism of this enzyme (Astner *et al.* 2005). This structure reveals that the

protein exists as a homodimer with PLP bound to the two active sites via a conserved lysine (K_{248}). The PLP forms a covalently bound Schiff base in the absence of substrate or product. A second crystal structure was obtained by soaking crystals of ALAS/PLP with glycine. The structure shows that the glycine undergoes a transaldimination, allowing the PLP to bind directly to the glycine instead of the lysine. A third crystal structure was obtained when ALAS/PLP crystals were soaked with succinyl-CoA. By superimposing the two structures (bound glycine and succinyl-CoA) Astner was able to show that both substrates can bind simultaneously within the active site, without incurring steric clashes. The last step in this process involves the decarboxylation of the glycine moiety, which eventually yields ALA bound to PLP ready for release (Astner *et al.* 2005).

1.10.2 The C5 pathway

In 1973 a second pathway for the synthesis of ALA was discovered (Beale and Castelfranco 1973). This was called the C5 pathway (Beale pathway) (Figure 1.4) and occurs in higher plants, algae, archaea and bacteria (Jahn and Heinz 2009; Murooka *et al.* 2005). In evolutionary terms it has been suggested that the C5 pathway represents the primordial route for ALA synthesis (Figure 1.5). It involves the transformation of glutamate to ALA in a multi-enzyme pathway. The pathway proceeds from glutamate via glutamyl-tRNA (delta-aminolevulinic acid-synthesizing enzymes need an RNA moiety for activity) (Huang *et al.* 1958). This represents one of the few reactions where a tRNA is used in something other than protein biosynthesis. The next step in this reaction is the reduction of the activated glutamate by the NADPH-dependent enzyme glutamyl-$_t$RNA reductase (GluTR). This yields glutamate-1-semialdehyde (GSA). Glutamate-1-semialdehyde aminotransferase transfers an amino group using PLP as a cofactor, which results in the formation of ALA (Moser *et al.* 2001).

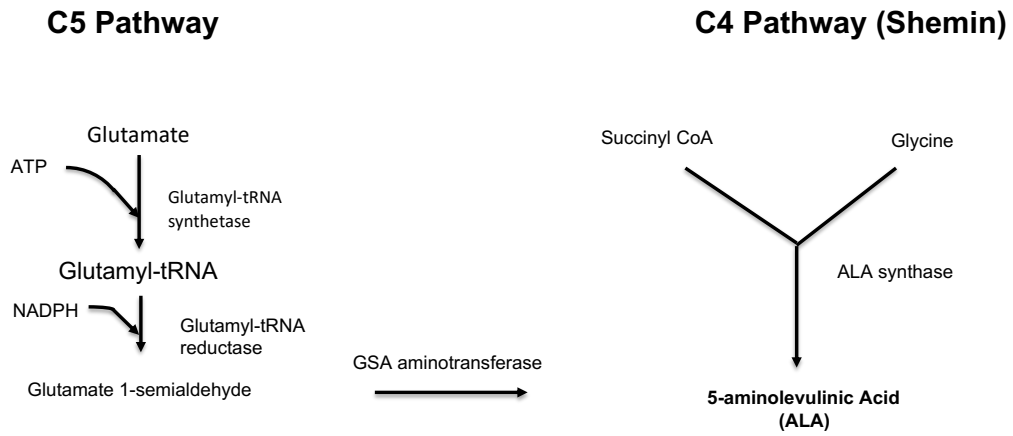

Figure 1.4: Diagram showing the C5 and the C4 (Shemin) pathways. The C5 pathway involves the transformation of the intact glutamate carbon backbone into ALA in three consecutive steps. The C4 pathway involves a single enzyme-mediated step whereby glycine and succinyl CoA are combined to generate ALA with the release of CoA and CO_2.

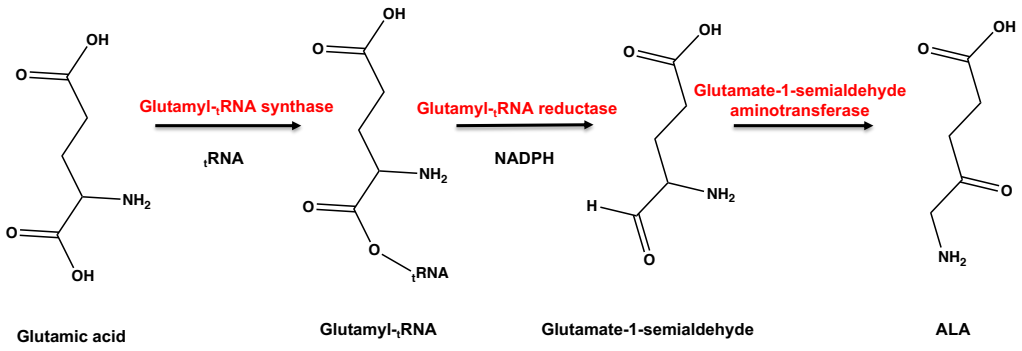

Figure 1.5: Biosynthesis pathway of 5-aminolaevulinic acid (ALA) via the C5 pathway. Three consecutive steps, step (i) the charging of tRNA with glutamate (ii) reduction to semialdehyde in a catalysed reaction of glutamyl-tRNA synthase (iii) transamination to form ALA.

This pathway utilises glutamate, ATP and NADPH as co-substrates. In tetrapyrrole biosynthesis it is believed that the synthesis of ALA is the rate limiting step reflecting the fact that tetrapyrrole biosynthesis is tightly regulated by feedback inhibition (Shin *et al.* 2007).

The structure of the *Methanopyrus kandleri* glutamyl-tRNA reductase has been solved. This structure revealed the enzyme to be a homodimer, which has a unusual V-shaped topology (Moser *et al.* 2001). The X-ray crystal structure of glutamate-1-semialdehyde aminomutase was solved in 1997 (Hennig *et al*. 1997). This structure revealed that the enzyme belongs to the aspartate aminotransferase family. Using the glutamyl-tRNA reductase structure Moser *et al* modelled glutamate-1-semialdehyde aminotransferase into the groove. Based on the model he concluded that a complex was formed which would allow direct metabolite transfer between the two enzymes (Moser *et al.* 2001).

1.11 The synthesis of uroporphyrinogen (uro'gen III)

The biosynthesis of the uro'gen III macrocycle from ALA requires the successive participation of three enzymes, 5-aminolaevulinic acid dehydratase (ALAD), porphobilinogen deaminase (1-hydroxymethylbilane synthase) and uro'gen III synthase. Uro'gen III is the major precursor found in all biological systems that are involved in the synthesis of tetrapyrroles. The first step in this process requires the enzyme catalysed condensation of two molecules of ALA. ALAD is the enzyme which dimerises two ALA molecules to generate porphobilinogen in a Knorr type condensation reaction (Jordan and Berry 1981).

Hydroxymethylbilane synthase then takes four molecules of porphobilinogen and polymerises them into hydroxymethylbilane, a linear tetrapyrrole (bilane) structure (Louie *et al.* 1992). The third enzyme in this pathway is uro'gen III synthase, which cyclises the linear tetrapyrrole and at the same time inverts ring D to generate the type III isomer of uro'gen (Battersby 1978; Mathews *et al.* 2001) (Figure 1.6). This is the last common precursor for all the natural tetrapyrroles. It is at this point that the tetrapyrrole biosynthetic pathway diverges (Leeper 1987).

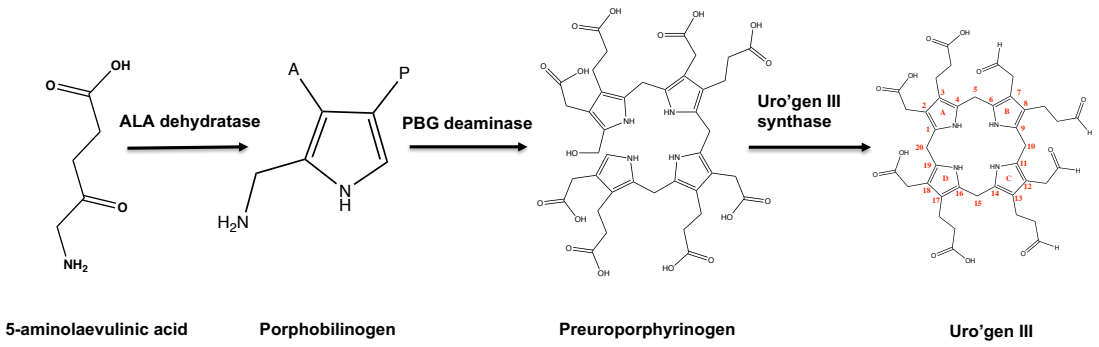

Figure 1.6: Diagram showing formation of uro'gen III from ALA. Porphobilinogen deaminase (PBG deaminase) and Uro'gen III synthase are responsible for the coming together of four molecules of porphobilinogen (PBG), to form uro'gen III. This pathway is common to all modified tetrapyrroles.

1.12 The aerobic biosynthesis of cobalamin

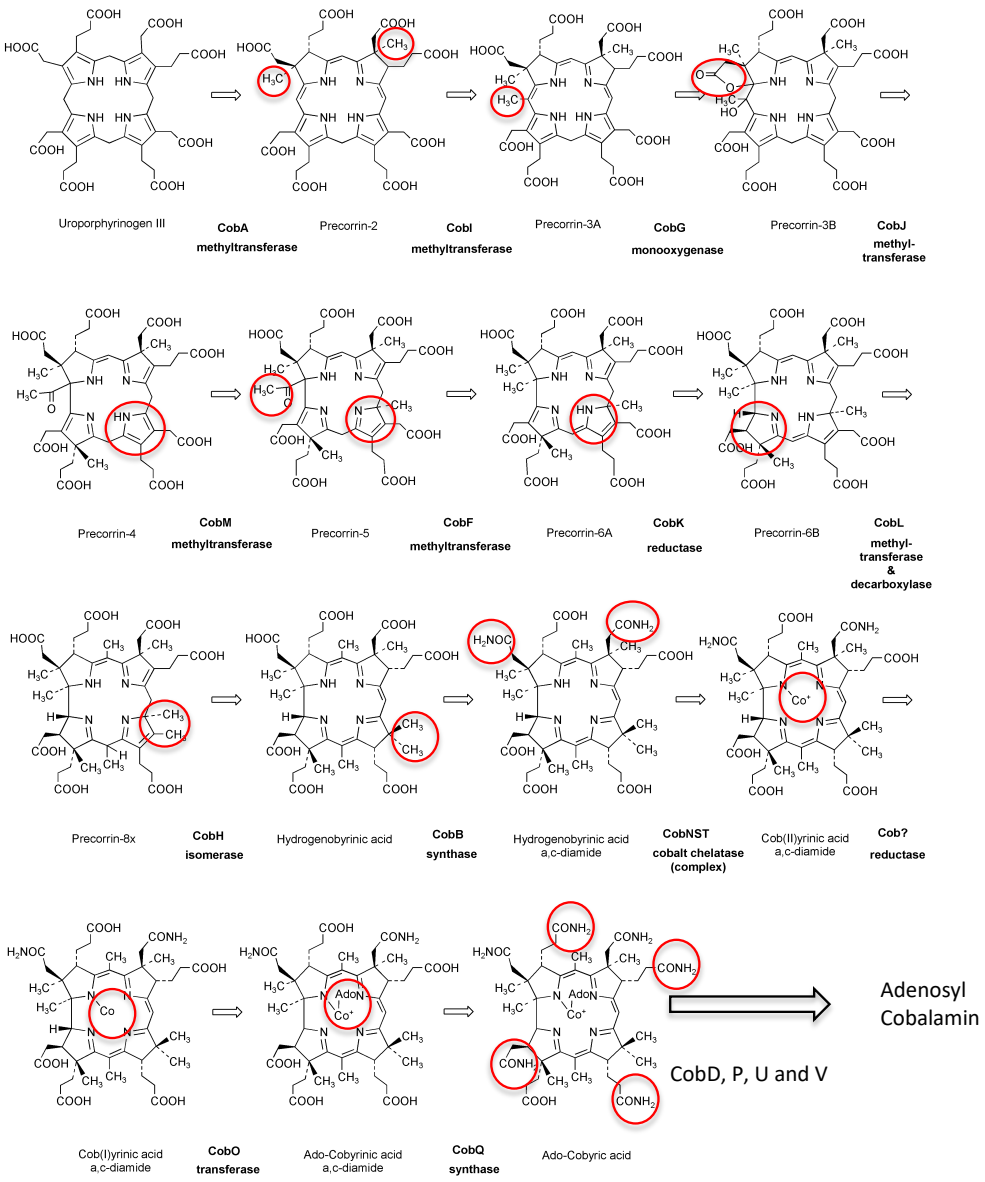

Figure 1.7: Aerobic pathway for the biosynthesis of cobalamin. The steps show the enzymes involved in the biosynthesis of adenosylcobyric acid from uroporphyrinogen III (uro'gen III). (Figure is taken from Warren *et al.* 2002).

There are two known pathways for the biosynthesis of adenosylcobalamin, which differ in their requirement for molecular oxygen and the timing of cobalt insertion. The two routes are referred to as the aerobic and anaerobic pathways (Blanche *et al.* 1993). The aerobic pathway has been studied mostly in *Pseudomonas denitrificans* (Debussche *et al.* 1993), whilst the anaerobic pathway has been studied in

Salmonella typhimurium, *Bacillus megaterium*, and *Propionibacterium shermanii*(Warren *et al.* 2002; Roth *et al.* 1993).

This thesis will focus on the aerobic pathway, however, it is worth mentioning the major differences between the two routes. The anaerobic pathway has no requirement for molecular oxygen and cobalt insertion occurs early on. By way of contrast, the aerobic pathway requires oxygen and cobalt insertion occurs late on. The two pathways diverge after the production of precorrin-2 and then re-join at the level of adeonsylcobyrinic acid *a, c*-diamide (Martens *et al.* 2014).

Uro'gen III is transformed into precorrin-2 by the action of an enzyme called S-adenosylmethionine uroporphyrinogen III methyltransferase (SUMT), which was found to be encoded by *cobA* (Blanche *et al.* 1991). The enzyme is sometimes also referred to as CobA. It methylates uro'gen III at positions C2 and C7 to give the dimethylated intermediate precorrin-2 and requires *S*-adenosyl-L-methionine (SAM) as a co-substrate and source of the methyl groups. The initiation of a methyl group at position C20 on the ring system is the first unique step in the aerobic pathway. This generates the trimethylated intermediate precorrin-3A (Warren *et al.* 1992). The enzyme involved in this is CobI, which was first identified in *P. denitrificans* (Thibaut et al 1990) (Figure 1.7).

1.12.1 Precorrin-3B synthesis

One of the most interesting steps in the biosynthesis of the corrin framework is that associated with the ring contraction process, where a carbon atom is removed from the macrocyclic ring. In the aerobic pathway the ring contraction process is initiated with the enzyme CobG (precorrin-3B synthase), which generates a hydroxylactone intermediate. In this reaction CobG introduces a hydroxyl group at C20, with oxygen coming from molecular oxygen (Spencer *et al.* 1993; Scott *et al.* 1993) (Figure 1.8). The actual ring contraction process is performed by CobJ, which methylates at position C17 and extrudes the C20 carbon to form precorrin-4 (Debussche *et al.* 1993). This reaction is believed to be a concerted process in which it is likely that ring contraction follows methylation (Scott *et al.* 1993; Debussche *et al.* 1993). In order for C20 ring-contraction to occur it was noted that this molecule had to be first converted into a tertiary alcohol (Eschenmoser 1988). This stabilises the molecule and prevents the irreversible tautomerisation to a 20-oxo

1.12.2 Precorrin-5 synthesis

The synthesis of precorrin-5 involves the methylation of the C11 position on the corrin ring. This wasn't discovered till Debussche *et al* took an oxidised form of precorrin-3A and incubated it with cell extract from a *P.denitrificans* strain, that overproduced the enzymes CobG, CobJ and CobM (Debussche *et al.* 1993). This resulted in the production of a new intermediate compound with a newly incorporated methyl group. In cobalamin this methyl group is attached to the C12 position, however, in this intermediate compound it was found attached to C11 (Figure1.7). The positioning of this methyl group was confirmed by NMR of the octamethyl ester derivative of precorrin-5 (Min *et al* 1993). This confirmed that a further enzymatic activity is required to allow the migration of the methyl group from C11 to its final position on C12. The

crystal structure of CobM from *R. capsulatus* was solved in 2010 to high resolution (1 Å) (Seyedarabi *et al.* 2010).

1.12.3 Precorrin-6A and Precorrin-6B synthesis

Precorrin-5 is converted to pecorrin-6A by CobF, a bifunctional enzyme that was first isolated from a *P. denitrificans* strain that overproduced CobF. One of the functions of this enzyme involves the deacetylation of the C1 methyl ketone, which is released as acetic acid. The second function is that of a SAM-dependent methyltransferase that results in the methylation at the C1 position (Debussche *et al.* 1993) (Figure 1.7).

The following enzyme in the pathway converts precorrin-6A to precorrin-6B. This is a NADPH-dependent reaction resulting in a change in the oxidation state of the macrocycle (Blanche *et al.* 1992; Moore *et al.* 2013). The enzyme involved in this transformation is CobK, where the double bond between C18 and C19 is reduced by hydride transfer from the H_R position of the NADPH cofactor onto C19 with the additional proton required at C18 being obtained from the solvent. The crystal structure for this enzyme has been solved (Gu *et al.* 2015) (Figure 1.7). The crystal structure revealed that five conserved basic residues of CobK bind the carboxylates of the tetrapyrrole very tightly (Jahn and Heinz 2009).

1.12.4 Precorrin-8 synthase

The synthesis of precorrin-8 is catalysed by a multifunctional enzyme called CobL. CobL is involved in SAM dependent methylations at C5 and C15, as well as the decarboxylation of the acetic acid side chain at C12 (Blanche *et al.* 1992) (Figure 1.7). The protein is composed of two distinct domains, an N-terminal domain, which has a typical canonical methyl transferase fold and the C-terminal a non-canonical methyl transferase domain. There is crystal structure of the C-terminal of CobL from R. capsulatus which diffracted to 1 Å resolution (Deery *et al.* 2012). It has, however, been

noted that in some organisms CobL is encoded by two separate genes, this implies that *cobL* may have arisen from a gene fusion event (Roth *et al.* 1993). It has now been shown that the C-terminal domain of CobL initially decarboxylates precorrin-6B and methylates at C15 to give precorrin-7. Precorrin-7 is then methylated at C5 by the N-terminal region of CobL to generate precorrin-8 (Deery et al, 2012).

1.12.5 Hydrogenobyrinic acid (HBA) synthesis

The next step in the biosynthesis of the corrin macrocycle produces hydrogenobyrinic acid (HBA) (Thibaut *et al.* 1992). This reaction is catalysed by CobH and involves the migration of the SAM-derived methyl group at C11 to C12 (Figure 1.7). The migration of the methyl group results in a change in the conjugated π – system, which result in a colour change from yellow to pink. CobH is a relatively small homodimeric, protein of ~23 kDa, which contains a highly conserved histidine residue (His-43). This conserved histidine residue is believed to be involved in playing a critical role in the catalytic mechanism of CobH by protonating the nitrogen of ring C. The crystal structure of this molecule has been solved with bound substrate to high resolution (Shipman *et al.* 2001).

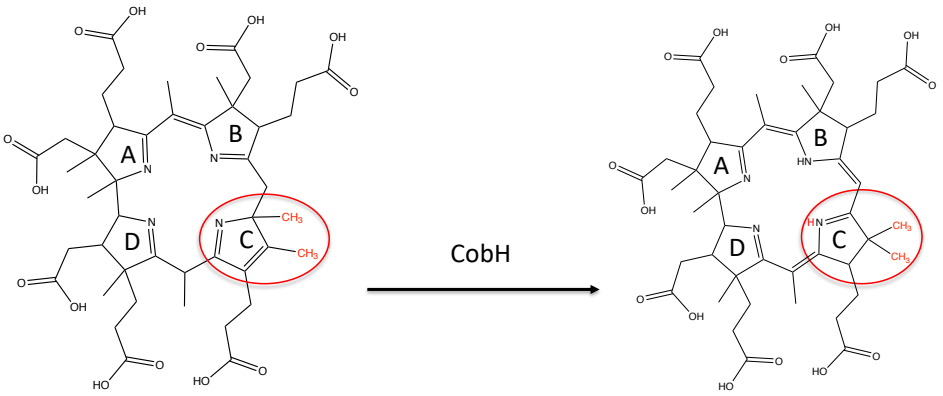

Figure 1.8: Mechanism in which Precorrin 8 is converted to HBA. Showing how the SAM derived methyl group on C11 moves to position C12 on the tetrapyrrole ring.

1.12.6 Hydrogenobyrinic acid *a, c*-diamide (HBAD) synthesis

HBA is next modified to HBA *a, c*-diamide. This represents the first stage in the amidation of the carboxylic acid side chains of the corrin ring. Cobyrinic acid has seven carboxyl groups which are labelled *a, b, c, d, e, f,* and *g*. All of these are amidated with ammonia apart from side chain *f*, which is amidated by (R)-1-amino-2-propanol. The first two amidation steps are catalysed by the enzyme CobB, which is known to amidate positions *a* and *c* on the ring system. The remaining amidations are catalysed by CobQ.

CobB is a multi-functional enzyme in that it is able to deaminate Gln and transfer the released ammonia group for incorporation into another compound (Debuscche *et al.* 1990). The initial report on CobB described how researchers were able to purify the protein and to characterise the reaction products. This involved the development of an HPLC assay that was used to determine the specificity and the order in which the amidations took place. It was found that amidation first took place on the side chain (*c*) attached to C7 of the ring. However, it was not known whether the second amidation reaction involved the dissociation of the substrate or whether the molecule

just rotated 90° within the active site. When evaluating the rate of the reaction it was found that the amidation of the *c* position was 5-7 fold faster than the that of *a* carboxylic acid side chain attached to C2. The activity of this enzyme was also monitored and it was shown that in order to go to completion that ATP/Mg^{2+}/Gln were required (K_m = 30.2 μM), with the preferred amide group donor being Gln (K_m = 20.3 μM). Gln could be replaced by ammonia but the reaction was much weaker with a K_m = 12 mM (Debuscche *et al.* 1990).

CobB is a homodimer with a subunit molecular mass of 47 kDa. CobB contains two distinct binding sites; an N-terminal ATP binding site and a C-terminal Gln binding site. There is no crystal structure of this enzyme, although a model was constructed based on the structure of the dethiobiotin synthetase (PDB entry 1DAK). This model relied on the fact that there is sequence conservation between CobB and CobQ, and that both are related to the MinD family of ATPases. Using the structure of dethiobiotin synthetase active site as a guide, Galperin and Grishin were able to develop a model for the interaction of CobB and CobQ for their respective substrates (Figure 1.8) (Galperin and Grishin 2000).

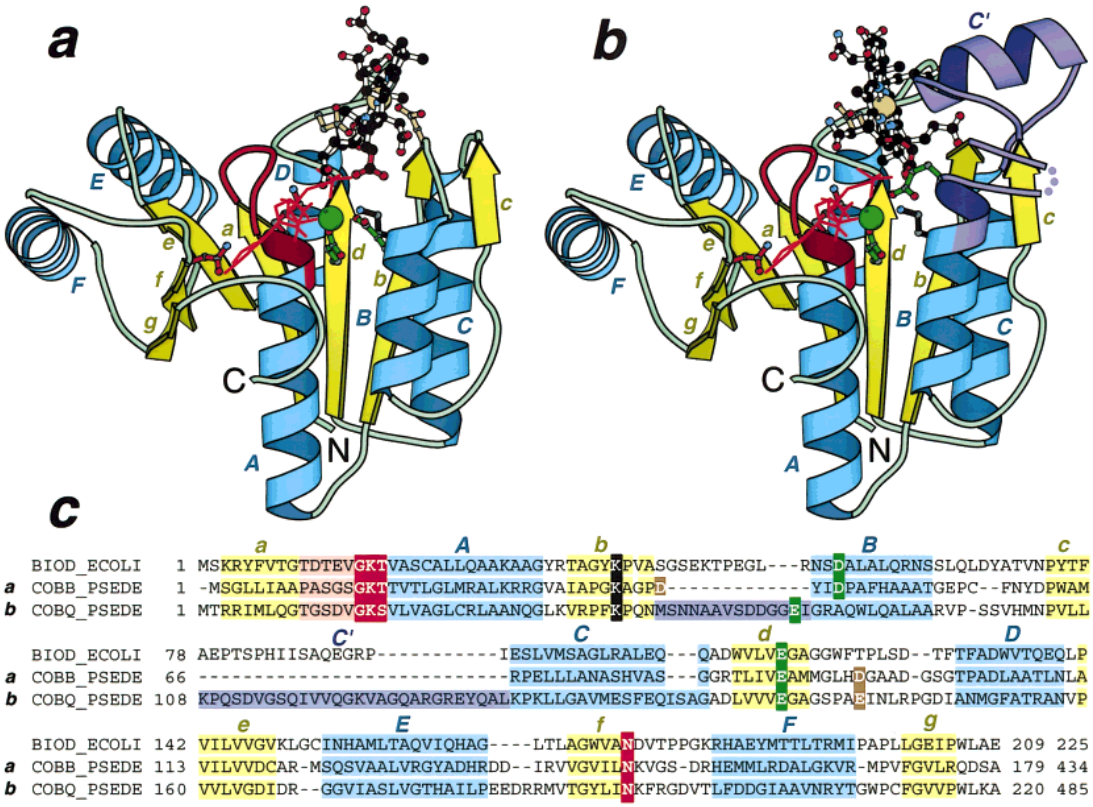

Figure 1.9: Model of CobB and CobQ based on the dethiobiotin synthetase structure . (a) CobB (b) CobQ (c) sequence showing conserved regions (red) for both Cob and CobQ. Yellow and blue show alpha helices and beta sheets respectively. Long insertions in the potential substrate-binding region of CobQ (b) are shown in purple. Mg-binding residues are shown in green. Catalytic lysine residue (Lys37 in dethiobiotin synthetase) is black. The figure was prepared using Bobscript,63 modified version of Molscript. (Galperin and Grishin 2000).

CobB is believed to belong to the Triad family of amidotransferases that contain C-terminal Gln amidotransferase domains. This family of proteins contain three residues which form a catalytic triad, Cys-His-Glu. However, the Glu residue of this triad is missing in CobB.

In all of the aminotransferases studied so far the acceptor substrate is located at a distance from the Gln site, or even on a different domain or polypeptide chain (Raushel, Thoden and Holden 1999). With more and more X-ray crystal structures of these aminotransferases available it has been noted that enzymes that have multiple

active sites utilise molecular tunnels that connect the active sites (Raushel, Thoden and Holden 2003).

1.12.7 Cob(II)yrinic acid *a, c*,-diamide synthesis

Insertion of cobalt into the ring-contracted tetrapyrrole is a complex process requiring chelation of the cobalt atom to generate cob(II)yrinic acid *a, c*-diamide. This reaction is dependent on the presence of ATP and Mg^{2+} and is catalysed by the cobaltochelatase. The enzymes responsible for this reaction forms a large protein complex consisting of CobN, CobS and CobT (Debussche *et al.* 1992b). The largest of these subunits is CobN with a molecular mass of 140 kDa. This domain is believed to contain the binding site for both the hydrogenobyrinic acid *a, c*-diamide and the Co(II) ion. However, it is not clear whether CobN forms a complex with the two other enzymes but it is known that CobS and CobT do interact together. What is clear is that all three subunits are required for activity, and this proceeds in an ATP dependent manor (Debussche *et al.* 1992a; Heldt *et al* 2005).

A low resolution three-dimensional structure of the *Brucella melitensis* CobST complex has been published using single particle electron microscopy. From the structure these enzymes look to form a chaperone type complex, which is similar to a class of proteins called AAA+ (ATPases Associated with a variety of cellular activities) class of proteins (Lundqvist *et al.* 2009). AAA+ proteins often perform chaperone like functions that are involved in the assembly, operation or disassembly of protein complexes. The structure of CobST shows two rings stacked together where each of the individual rings contains six subunits, which form a trimer of dimers. There is an ATP binding domain on the CobS subunit that contains the Walker A and B motifs, which is common to ATP binding motifs (Walker *et al.* 1982). This system of cobalt insertion displays sequence identity to the magnesium chelatase that is involved in

the biosynthesis of chlorophyll (Reid and Hunter 2002; Waker, C. J and Willows, R. D, 1997).

1.12.8 Cobalt reduction

After insertion of the cobalt the next step is the attachment of an upper ligand. Before this bond can be formed it is necessary to reduce the Co(II) to Co(I). This involves a single electron reduction of the cobalt ion to form cob(I)yrinic acid *a, c*-diamide. This reaction is considered energetically unfavourable, however, an enzyme was isolated from *P. denitrificans* which contained a flavin mononucleotide (FMN) cofactor that catalysed the reduction in a range of Co(II)-corrin compounds in an FAD-dependent manor (Blanche *et al.* 1992).

The gene encoding this enzyme (*cob*R) was also identified in *B. melitensis*. This protein was recombinantly overexpressed and purified, which enabled structural analysis and mechanical studies to be carried out. The structure of CobR was solved to 1.6 Å resolution (Figure 1.9). The structure identified a bound flavin cofactor, which was identified as FAD. Kinetic and electron paramagnetic resonance (EPR) spectra analysis provided evidence for the enzyme proceeding via a semiquinone form, proposing that it may react with the adenosyltransferase to overcome the large thermodynamic barrier required for co(II)rrin reduction (Lawrence *et al.* 2008a). It was also noted that CobR shared basic homology with the cobalamin reductase PduS, which is involved in the metabolism of 1, 2-propanediol (Sampson, Johnson and Bobik 2005) (Parsons *et al.* 2010).

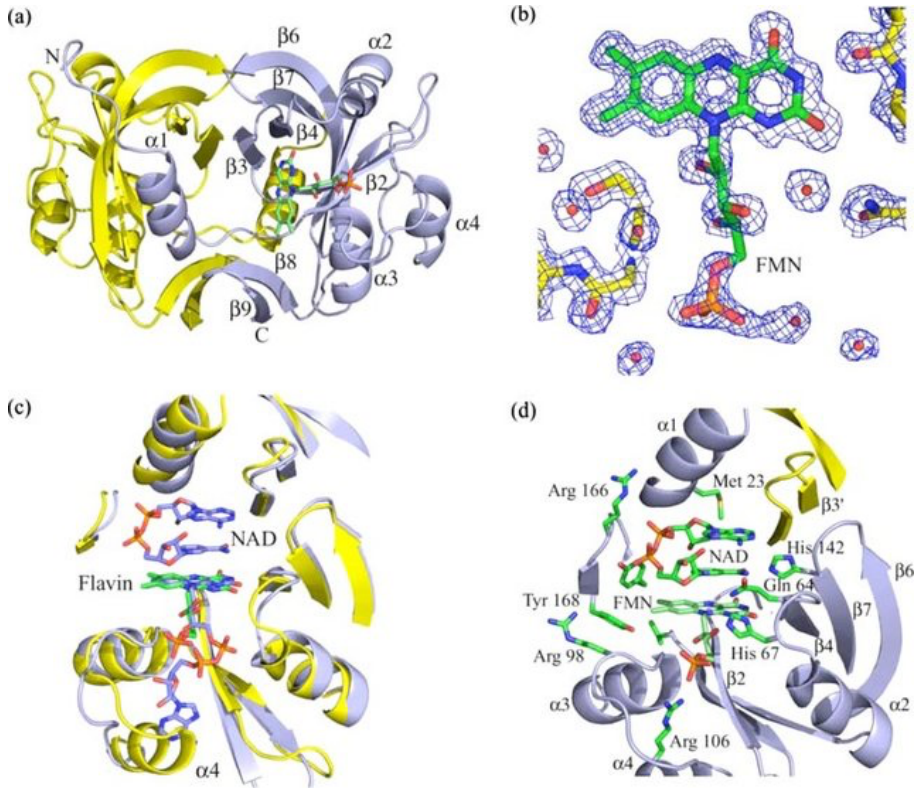

Figure 1.10: Crystal structure of CobR. (a) Stick representation of CobR with FMN. **(b)** electron density showing isoalloxazine ring of the bound FMN **(c)** superimposition of flavin reductase and CobR showing isoalloxazine rings of the flavin shown in stick representation **(d)** FMN and NAD binding in CobR showing key interactions. (Lawrence *et al.* 2008a).

1.12.9 Adenosylcobyrinic acid *a, c*-diamide synthesis

The adenosyltransferase, CobO, is involved in the attachment of the upper ligand to the centrally chelated cobalt ion. This enzyme catalyses the ATP-dependent adenosylation of cob(I)yrinic acid *a, c*-diamide into its co-enzyme form adenosyl cobalamin cob(III)yrinic acid *a, c*-diamide (Figure 1.10). CobO is a homodimer and has a subunit molecular mass of 28 kDa (Crouzet *et al.* 1991). There are three classified groups of adenosyltransferases that have been identified, which are referred to as the CobA type, PduO type and EutT type. The CobA group contains adenosyltransferases CobA, CobO and ButR, all of which have a high degree of sequence identity (Suh and Escalante-Semerena 1993; Johnson *et al.* 2001).

The Co(I) of the cob(I)yrinic acid *a, c*-diamide is a powerful nucleophile. The corrin substrate is in close proximity to the ATP, which is the other substrate. CobO catalyses the transfer of an adenosyl group from the ATP to the cobalt. This allows the Co(I) nucleophile to attack the C5' ribose carbon of ATP, forming the Co(III) adenoslylcob(III)yrinic acid *a, c*-diamide and triphosphate as the only product (Figure 1.10) (Debussche *et al.* 1991).

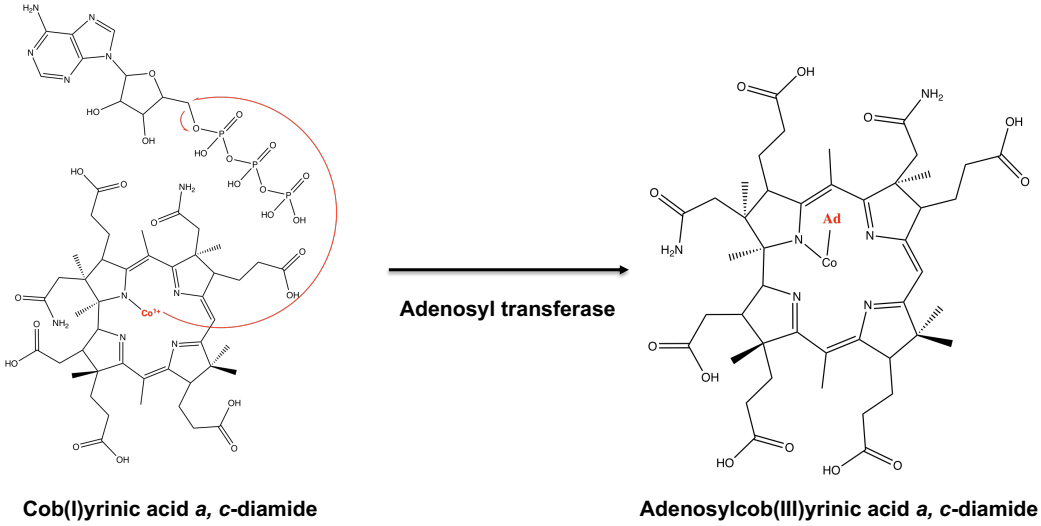

Cob(I)yrinic acid *a, c*-diamide **Adenosylcob(III)yrinic acid *a, c*-diamide**

Figure 1.11: Mechanism of the adenosyl transferase CobA. Adenosylation of Cob(I)yrinic acid *a, c*-diamide occurs via a nucleophilic Co^{1+} species to form adenosylcob(III)yrinic *a, c*-diamide.

1.12.10 Adenosylcobyric acid synthesis

The final amidation step is carried out by the enzyme CobQ, which amidates position *b, d, e and g*, to produce adenosylcobyric acid (Warren *et al.* 2002; F Blanche *et al.* 1991). CobQ is a homodimer, with a subunit molecular mass of 57 kDa. As with the CobB, CobQ requires ATP, Gln and Mg^{2+} for activation (Blanche *et al.* 1991). The reaction is carried out in a stepwise process with the sequential order being *e, d, b* and *g*. Experimental evidence suggested that ATP is used to activate carboxylate groups on the ring system to form a phosphorylated intermediate. This was supported

by labelling the ATP with [γ-$^{18}O_4$] resulting in [γ-$^{18}O_4$]-ATP. The enzyme in this reaction was CbiP from the anaerobic pathway, which is equivalent to CobQ in the aerobic route. This enzyme catalysed the positional isotope exchange of the βγ-bridge oxygen with the two β-nonbridge oxygens (Fresquet, Williams and Raushel 2007). CobQ is a multifunctional enzyme that catalyses four separate reactions on a single substrate. As with CobB it is unknown whether this reaction is dissociative, where at each amidation site the substrate leaves the active site rotating and re-joining, or whether it rotates within the active site (Fresquet, Williams and Raushel 2007). Following the synthesis of adenosylcobyric acid the aerobic and anaerobic pathways then converge. Figure 1.7 shows the vitamin B_{12} pathway starting from the synthesis of uroporphyrin III to adenosylcobyric acid (ado-cobyric acid) synthesized by CobQ.

1.12.11 Synthesis of adenosylcobalamin from adenosylcobyric acid

The final phase in the biosynthesis of cobalamin involves the synthesis and attachment of the lower nucleotide loop. This is initiated with the formation of adenosylcobinamide phosphate, which involves the attachment of an aminopropanol phosphate linker to the propionic side chain (*f*) that is found on ring D (Figure 1.11). The aminopropanol phosphate is derived from threonine. To begin with, threonine is phosphorylated in an ATP-dependent manner to form L-threonine *O-3-phosphate.* This reaction is catalysed by a kinase encoded by the *pduX* gene (Fan and Bobik 2008). Threonine phosphate is converted into aminopropanol phosphate by the action of CobC, which is a PLP-dependent enzyme that mediates the decarboxylation of threonine phosphate. The aminopropanol phosphate is next attached to the corrin framework in a reaction mediated with CobD, generating an amide linkage with the *f* side chain. It seems likely that CobC and CobD form a complex (Figure 1.11) (Blanche *et al.* 1995).

The construction of the lower loop is continued by the action of a GDP transferase called either CobP (*P. denitrificans*) or CobU (*S. enterica*). The enzyme uses GTP as a substrate and results in the formation of adenosylcobinamide GDP (Figure 1.11).

The lower nucleotide within cobalamin contained an unusual base called 5, 6-dimethylbenzimidazole (DMB), which is incorporated into the nucleoside alpha-ribazole 5'-phosphate. This reaction is catalysed by CobU (*P. denitrificans*) (Cameron *et al.* 1991) or CobT (*S. enterica*) (Trzebiatowski *et al* 1994), by the transfer of a phosphoribosyl moiety (Figure 1.11).

The final stage of the lower loop assembly involves the formation of adenosylcobalamin 5' -phosphate (Figure 1.11). The enzyme responsible for this conversion is CobV (*P. denitrifica*ns) or CobS (*S. enterica*). The last enzyme in the pathway is CobC, which removes the 5'-phosphate to generate cobalamin (Figure 1.11) (Zayas and Escalante-semerena 2007).

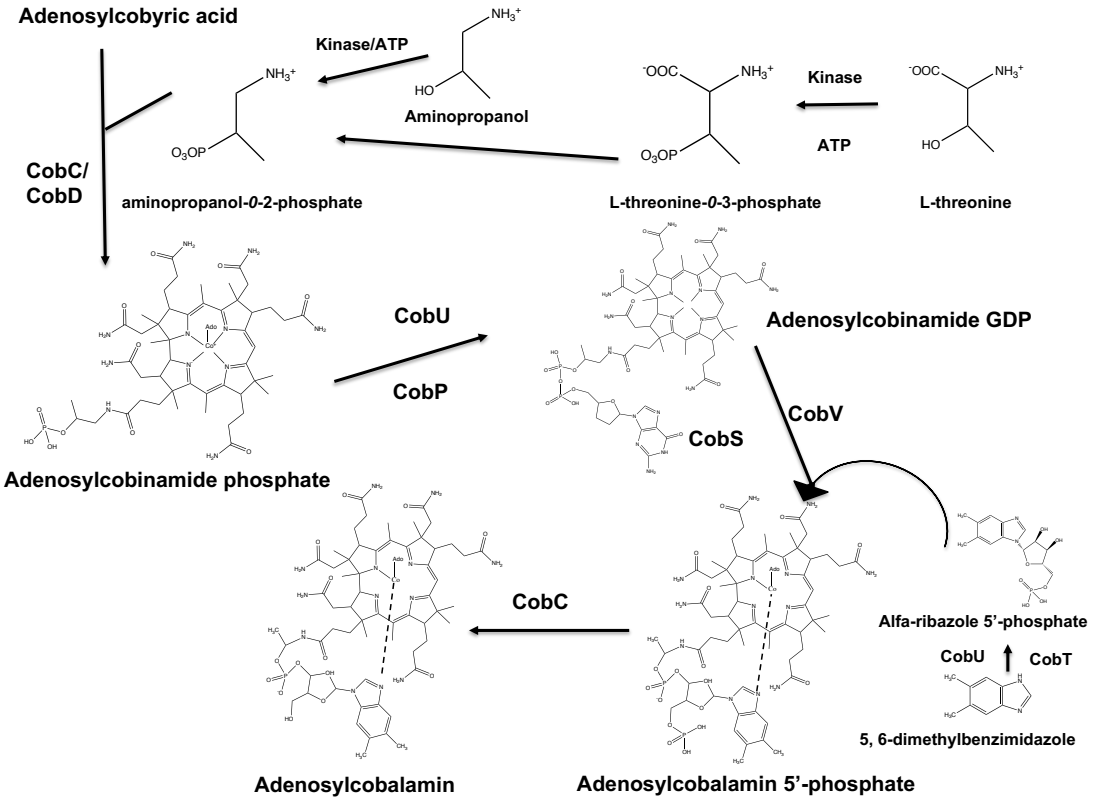

Figure 1.12 Late stage nucleotide assembly of adenosylcobalamin. Amino propanol phosphate is attached to adenosylcobyric acid to form adenosylcobinamide phosphate. Activation of the adenosylcobinamide with GTP results in the formation of adenosylcobinamide GDP. The GDP moiety is replaced with the alpha ribazole nucleoside to give adenosylcobalamin 5' -phosphate. CobC then removes the phosphate to give adenosylcobalamin.

1.13 Objectives

Obtaining structural and biophysical information on both CobB and CobQ was the primary objective. A crystal structure of CobB and CobQ was modelled on the dethiobiotin synthetase structure in the paper from M. Galperin and N. Grishin. However as this was a model it could not be considered as a true representation of the crystal structure (Galperin and Grishin 2000). Specifically, that a crystal structure of CobB could be determined to provide the first insights into this class of enzyme associated with cobalamin biogenesis. Stopped-flow analysis was used to gain kinetic insight into the binding of CobB to its substrates, which are HBA, hydrogenobyrinic

acid *c*-monoamide (HBAM) and HBAD its product. In particular, it was hoped that such an approach would give insights into conformational changes that may take place during substrate binding and catalytic turnover and to relate such findings to the structure of the enzyme.

Finally, it is speculated that a number of the pathway enzymes within the B_{12} pathway operate a form of direct metabolite transfer, where the product of one enzyme is passed directly onto the next enzyme. It is already known that CobH binds it product very tightly. This product, HBA, is the substrate for CobB and it was hoped that a structure for CobB would allow imaging of interaction with CobH. All of these aims and objectives are described in more detail in the main experimental sections of this thesis, chapters 3-6.

Chapter 2

Materials and Methods

2.1 Materials

Genomic DNA of *Brucella melitensis* strain ATCC 23456 was provided by Prof. J. J. Letesson from the Laboratoire d'Immunologie et de Microbiologie, URBM, Facultes Universitaires Notre-Dame de la Paix, Namur, Belgium. For *Rhodobacter capsulatus* genomic DNA strain SB1003 and *Allochromatium vinosum* genomic DNA DSM180 provided by Dr. Evelyne Deery, University of Kent.

All genes were cloned into pET14b (creating a N-terminus His_6 fusion) from genomic DNA using either NdeI or AseI and SpeI restriction enzymes (see Table 2.1). FastStart high fidelity polymerase (Roche) was used for all PCRs. T4 DNA ligase and restriction enzymes were purchased from Promega except AseI, which was purchased from NEB.

Table 2.1 Plasmids used

List of plasmids	Gene product	Source	Restriction enzymes
pET14b		Novogen	
pET14b- Bmei cobH	Precorrin-8 (11-12) methyl-mutase from *Brucella melitensis*	E. Deery	Nde/Spe
pET14b- Bmei cobB	HBA:L-Gln amido-ligase from *Brucella melitensis*	E. Deery	Nde/Spe
pET14b-BmeicobB^{c327A}	HBA:L-Gln amido-ligase, mutation C327A	E. Deery	Spe
pET14b-BmeicobB^{c327A}	HBA:L-Gln amido-ligase, mutation H427A	E. Deery	Spe
pET14b- Bmei cobQ	Ado-cobyrinic acid ac diamide:L-glutatamine amido-ligase from *Brucella melitensis*	E. Deery	Ase
pET14b- Rc cobQ	Ado-cobyrinic acid ac diamide:L-glutatamine amido-ligase from *Rhodobacter capsulatus*	E. Deery	Nde/Spe
pET14b- Alv cobQ	Ado-cobyrinic acid ac diamide:L-glutatamine amido-ligase from. *Allochromatium vinosum*	E. Nemoto-Smith	Nde/Spe

2.1.1 Chemicals

Most of the chemicals, DEAE-sephacel and antibiotics were purchased from Sigma-Aldrich Ltd. Other materials were purchased from manufacturers as follows: IPTG and ampicillin from Melford Laboratories Ltd; chelating fast flow sepharose, disposable PD10 columns from GE Healthcare; Tryptone, yeast and bacterial agar from Oxiod LTD. Crystallisation screens and additive screens were purchased from Molecular dimensions and Hampton Research.

2.1.2 Media and solutions used for bacterial work

Luria-Bertani (LB) broth:

Tryptone (10 %)	10 g/L
Yeast extract (8 %	5 g/L
NaCl	86.2 mM

Made up to 1L with dH_2O and autoclaved.

2YT broth (2 x Yeast/Tryptone)

Tryptone (40 %)	16 g/L
Yeast extract (16 %	10 g/L
NaCl	86.2 mM

Made up to 1L with dH_2O and autoclaved.

2YTNN (2 x Yeast/Tryptone Na/NH_5Cl)

Tryptone (40 %)	16 g
Yeast extract (16 %)	10 g
NaCl	86.2 mM
Na_2HPO_4	50 mM
NaH_2PO_4	20 mM
NH_5C	20 mM

Made up to 1L with dH_2O and autoclaved.

Mg_{2+} stock solution:

$MgCl_2(H2O)$	10 mM
$MgSo_4(H_2O)_6$	10 mM

Made up to 10 mL with H_2O.

For SOC media Tryptone and yeast extract were dissolved in 967.5 mL of H_2O and autoclaved prior to the addition of the other components. All components that were not autoclaved were passed through a sterilised filter (0.2 µm pore size) prior to use.

Luria Bertani agar:

15 g of Bacterial agar was added to 1 L LB broth before autoclaving.

10x M9 salts

KH_2PO	222 mM
Na_2HPO_4	478 mM
NH_4Cl	187 mM
NaCl	86.2 mM

Make up to 1L with dH_2O and autoclaved.

Trace elements solution:

EDT	18 mM
$FeCl_3.6H_2$	0.02 nM
$ZnSO_4.7H_2O$	0.01 nM
CuCl2.2H2O	0.06 nM
$Co(NO_3)_2.6H_2O$	0.03 nM
$(NH_4)_6MO_7O_{24}.4H_2$	0.008 nM

All metals were dissolved separately in a small quantity of dH_2O before being mixed,

pH was adjusted to 7.00 and made up to 1 L. The solution was then autoclaved before use.

Selenomethionine labelling media

10x M9 salt (stock)	100 mL
Trace elements (stock)	10 mL
Glycerol (50% (v/v))	20 mL
$MgSO_4$ (1 M)	1 mL
$CaCl_2$ (1 M	0.4 mL
Biotin (1 mg mL)	1 mL
Thiamine (1 mg mL)	1 mL
Ampicillin (100 mg mL)	1 mL
Selenomethionine	25 mg

Add chemicals to dH_2O 865.6 mL.

All solutions were made up separately and autoclaved (M9 salts, trace elements, glycerol) or filter sterilised ($MgSO_4$, $CaCl_2$, biotin, thiamine, ampicillin; 0.2 µm pore size) prior to mixing.

IPTG solution 1M

2.38 g of IPTG were dissolved in 10 mL dH_2O, filter sterilised (0.2 µm), aliquoted into 0.4 mL and stored at -20 °C. The final working concentration was 0.4 mM.

Table 2.2 Additives and antibiotics

Additives	Stock concentration	Final concentration
IPTG	1 M in dH_2O	100 mM
Ampicillin	100 mg mL in dH_2O	100 µM/mL
Chloramphenicol	34 mg/mL in dH_2O	34 µM/mL

2.1.3 Solutions used for protein work

2.1.3.1 Solutions for nickel affinity chromatography

Binding buffer:

Tris-HCl, pH 8.00	20 mM
NaCl	500 mM
Imidazole	20 mM

Wash buffer: As above

Elution buffer:

Tris-HCl, pH 8.00	20 mM
NaCl	500mM
Imidazole	1 M

2.1.3.2 Solutions for PD10 de-salting column

Transfer buffer:

Tris-HCl, pH 8.00	20 mM
NaCl	150mM

2.1.3.3 Solutions for ion exchange

Binding buffer:

Tris-HCl pH 8.00	20 mM
NaCl	150 mM

Elution buffer:

Tris-HCl pH 8.0	20 mM
NaCl	1 M

Protein elutes at 300 mM.

PBS Buffer:

NaCl	5 mM
KC	30 mM
Na_2HPO_4	100 mM
KH_2PO_4	20 mM

2.1.3.4 Size exclusion chromatography

Tris-HCl pH 8.00	20 mM
NaCl	100 mM

2.1.3.5 Solutions for protein polyacrylamide gel electrophoresis

10 x running buffer:

Tris-HCl	250 mM
Glycine	2 mM

10mL/L 10% (v/v) SDS added to 1 x running buffer for SDS gel.

2 x SDS sample buffer:

Tris-HCl, pH6.80 (0.5M	6 mL
Glycerol (100 %)	4.8mL
SDS 10% (v/v)	9.6 mL
Bromophenol blue 0.05%	1.2 mL(v/v)
dH2O	24 mL

14uL B-mercaptoethanol added per mL 2x SDS sample buffer.

Denaturing molecular weight marker – Pre-stained protein marker, broad range (NewEngland BioLabs):

Protein	Molecular weight (Da)
MBP-B-galactosidse	175,000
MBP-parayosin	72,000
MBP-CBD	55,000
CBD-*Mxe* Intein-2CBD	45,000
CBD-*Mxe* Intein	34,000
CBD-BmFKBP13	24,000
Lysozyme	17,000
Aprotinin	11,000

Coomassie blue stain:

Trichloroacetic acid (100%)	250.00 mL
Coomassie blue R250	0.60 g
SDS (1 M)	0.10 g
Tris-HCl (1 M)	0.25 g
Glycine (1 M)	0.15 g

Make up to 500 mL with dH_2O.

Table 2.3 Running gel SDS Gel

SDS

Running gels	12.5%	15%	Stacking gel	5%
dH_2O	3.4	2.2	dH_2O	3.4
30% Acrylamide (mL) **Acryl/Bis 29:1**	6.3	7.5	30% Acrylamide (mL-1) Acryl/Bis 29:1	1.5
1.5 M Tris-HCl pH8.8 (mL)	3.8	3.8	1.5M Tris-HCl pH6.8 (mL)	1.9
10% (v/v) SDS (mL)	1.5	1.5	10% (v/v) SDS (mL)	0.75
10% APS (v/v) (mL)	0.15	0.15	10% APS (v/v) (mL)	0.075
TEMED (mL)	0.01	0.01	TEMED (mL)	0.01

TAE x 50	**0.2 ml**
dH2O	3.1 mL
30% Acrylamide (mL) **Acryl/Bis 29:1**	6.6 mL
10% APS (v/v) (mL)	0.100 µL
TEMED (mL)	5 µL

2.1.3.6. Solutions for Cobalt insertion and amidation of HBAD and HBAH

Cobalt insertion 0.5 M cobalt acetate ($Co(CH_3CO_2)_2$) pH 6.00

Rhodium insertion (glove box).

23 mg of anhydrous NaCl in acetic acid (2 mL).

2.5 mg of rhodium(1) dicarbonyl chloride ($Rh_2Cl_2(CO)_4$) dimer in 800 µL tertiary butanol.

2.1.3.7 Solutions for gel filtration chromatography (FPLC)

Sample buffer A 1 L:

Tris-HCl, pH 8.0	20 mM
NaCl	150 mM

Sample buffer B 1 L:

Tris-HCl, pH 8.0	20 mM
NaCl	1 M

All solutions were filtered before use.

2.1.3.8 Solutions for HPLC-MS

Tetrapyrrole HPLC-MS analysis:

Solution A:	Triflouroacetic acid(v/v)	0.1%
Solution B:	Acetonitrile	100%

Protein HPLC-MS analysis.

Solution A:	Trifluoroacetic acid (v/v)	0.05%
Solution B:	Acetonitrile (v/v)	80%
	Trifluoroacetic acid (v/v)	0.045%

All solution were filtered prior to use.

2.1.3.9 Solutions for crystallisation

Table 2.4 Molecular dimension screen 1: Screen contains common salts, precipitants and buffers used for initial screening of all proteins. This screen was used in an attempt to crystallise CobB.

Condition	Salt	Precipitant	Buffer
1	0.02 M Calcium chloride dihydrate	30% (v/v) 2-methyl 2,4 pentanediol	0.1 M Na Acetate trihydrate pH 4.6
2	0.2 M Ammonium acetate	30% (v/v) PEG-4000	0.1 M Na Acetate trihydrate pH 4.6
3	0.2 M Ammonium sulphate	25% (v/v) PEG-4000	0.1 M Na Acetate trihydrate pH 4.6
4		2.0 M Sodium formate	0.1 M Na Acetate trihydrate pH 4.6
5		2.0 M Ammonium sulphate	0.1 M Na Acetate trihydrate pH 4.6
6		8% (v/v) PEG-4000	0.1 M Na Acetate trihydrate pH 4.6
7	0.2 M Ammonium acetate	30% (v/v) PEG-4000	0.1 M tri-sodium citrate dihydrate pH 5.6
8	0.2 M Ammonium acetate	30% (v/v) 2-methyl 2,4 pentanediol	0.1 M tri-sodium citrate dihydrate pH 5.6

9		20% (v/v) 2-propanaol, 20% (v/v) PEG 4000	0.1 M tri-sodium citrate dihydrate pH 5.6
10		1.0 M Ammonium dihydrogen phosphate	0.1 M Na citrate pH 5.6
11	0.2 M Calcium chloride dihydrate	20% (v/v) 2.propanol	0.1 M Na acetate pH 4.6
12		1.4 M Na acetate trihydrate	0.1 M Na Cacodylate pH 6.5
13	0.2 M tri-sodium citrate dihydrate	30% (v/v) 2-propanol	0.1 M Na Cacodylate pH 6.5
14	0.2 M Ammonium sulphate	30% (v/v) PEG-8000	0.1 M Na Cacodylate pH 6.5
15	0.2 M Magnesium acetate tetrahydrate	20% PEG 8000	0.1 M Na Cacodylate pH 6.5
16	0.2 M Magnesium acetate tetrahydrate	30% (v/v) 2-methyl 2,4 pentanediol	0.1 M Na Cacodylate pH 6.5

17		1.0 Sodium acetate trihydrate	0.1 M Imidazole pH 6.5
18	0.2 M Sodium acetate trihydrate	30% (v/v) PEG-8000	0.1 M Na Cacodylate pH 6.5
19	0.2 M Zinc acetate dihydrate	18% (v/v) PEG-8000	0.1 M Na Cacodylate pH 6.5
20	0.2 M Calcium acetate hydrate	18% (v/v) PEG-8000	0.1 M Na HEPES pH 7.5
21	0.2 M tri-sodium citrate dihydrate	30% (v/v) 2-methyl 2,4 pentanediol	0.1 M Na HEPES pH 7.5
22	0.2 MgCl2 hexahydrate	30% (v/v) 2-propanol	0.1 M Na HEPES pH 7.5
23	0.2 M Calcium chloride dihydrate	28% PEG 400	0.1 M Na HEPES pH 7.5
24	0.2 M MgCl2 hexahydrate	28% PEG 400	0.1 M Na HEPES pH 7.5
25	0.2 M tri-sodium citrate dihydrate	20% (v/v) 2-propanol	0.1 M Na HEPES pH 7.5

26		0.8 M K, Na tartrate tetrahydrate	0.1 M Na HEPES pH 7.5
27		1.5 M Lithium sulphate monohydrate	0.1 M Na HEPES pH 7.5
28		0.8 M Na Phosphate monobasic monohydrate/0.8 M Potassium phosphate monobasic	0.1 M Na HEPES pH 7.5
29		1.4 M tri-sodium citrate dihydrate	0.1 M Na HEPES pH 7.5
30		2% (v/v) PEG 400/2.0 M Ammonium sulphate	0.1 M Na HEPES pH 7.5
31		10% (v/v) 2-propanol, 20% (v/v) PEG 4000	0.1 M Na HEPES pH 7.5

32		2. M Ammonium sulphate	0.1 M Tris HCl pH 8.5
33	0.2 M MgCl2 hexahydrate	30% (v/v) PEG-4000	0.1 M Tris HCl pH 8.5
34	0.2 M tri-sodium citrate dihydrate	30% (v/v) PEG-400	0.1 M Tris HCl pH 8.5
35	0.2 M Lithium sulphate monohydrate	30% (v/v) PEG-4000	0.1 M Tris HCl pH 8.5
36	0.2 M Ammonium acetate	30% (v/v) 2-propanol	0.1 M Tris HCl pH 8.5
37	0.2 M Sodium acetate trihydrate	30% (v/v) PEG-4000	0.1 M Tris HCl pH 8.5
38		8% (v/v) PEG-8000	0.1 M Tris HCl pH 8.5
39		2.0 M Ammonium dihydrogen phosphate	0.1 M Tris HCl pH 8.5
40		0.4 M K, Na Tartrate	
41		0.4 M Ammonium dihydrogen phosphate	

42	0.2 M Ammonium sulphate	30% (v/v) PEG-8000	
43	0.2 M Ammonium sulphate	30% (v/v) PEG-4000	
44		2.0 M Ammonium sulphate	
45		4 M Sodium formate	
46	0.05 M Potassium dihydrogen phosphate	20% (v/v) PEG-8000	
47		30% (v/v) PEG 1500	
48		0.2 M Magnesium formate	

Table 2.5 Molecular Dimension Additive used in crystallisation: This screen contains all of the necessary additives that can be used to improve initial crystals obtained from Molecular dimensions screen 1.

Well	Chemical name	known as/for	Concentration	
A1	Water	control	-	
A2	PEG 20000	precipitant	20.00	% v/v
A3	PEG 500 MME	precipitant	40.00	% v/v
A4	PEG 8000	precipitant	20.00	% v/v
A5	Ethylene glycol	cryoprotectant	40.00	% v/v
A6	PEG 4000	precipitant	20.00	% v/v
A7	Glycerol	cryoprotectant	40.00	% v/v
A8	MPD	cryoprotectant	25.00	% v/v
A9	PEG 1000	precipitant	25.00	% v/v
A10	PEG 3350	precipitant	25.00	% v/v
A11	MES monohydrate	buffer (acid)	0.50	M
A12	Imidazole	buffer (base)	0.50	M
B1	MOPS	buffer (acid)	0.50	M
B2	Sodium HEPES	buffer (base)	0.50	M
B3	BICINE	buffer (acid)	0.50	M

B4	Trizma® base	buffer (base)	0.50	M
B5	MgCl2 hexahydrate	nucleant	0.60	M
B6	Calcium chloride dihydrate	nucleant	0.60	M
B7	Sodium fluoride	phasing	0.60	M
B8	Sodium bromide	phasing	0.60	M
B9	Sodium iodide	phasing	0.60	M
B10	Sodium nitrate	precipitant	0.60	M
B11	Sodium phosphate dibasic dihydrate	precipitant	0.30	M
B12	Ammonium sulphate	precipitant	0.60	M
C1	1-Butanol	precipitant	0.40	M
C2	1,4-Butanediol	precipitant	0.40	M
C3	1,2-Propanediol	precipitant	0.40	M
C4	1,3-Propanediol	precipitant	0.40	M
C5	2-Propanol	precipitant	0.40	M
C6	1,6-Hexanediol	precipitant	0.40	M
C7	Diethylene glycol	precipitant	0.60	M

C8	Triethylene glycol	precipitant	0.60	M
C9	Tetraethylene glycol	precipitant	0.60	M
C11	N-Acetyl-D-glucosamine	stabiliser	0.40	M
C12	Fucose	stabiliser	0.40	M
D1	D-Galactose	stabiliser	0.40	M
D2	D-Glucose	stabiliser	0.40	M
D3	D-Xylose	stabiliser	0.40	M
D4	D-Mannose	stabiliser	0.40	M
D5	Ammonium acetate	precipitant	0.40	M
D6	Sodium oxamate	precipitant	0.40	M
D7	Sodium formate	precipitant	0.40	M
D8	Potassium sodium tartrate tetrahydrate	precipitant	0.40	M
D9	Sodium citrate tribasic dihydrate	precipitant	0.40	M
D10	DL-Glutamic acid monohydrate	stabiliser	0.40	M

D11	DL-Lysine monohydrochloride	stabiliser	0.40	M
D12	DL-Alanine	stabiliser	0.40	M

Table 2.6 Molecular Dimension Additive screen 2: This screen contains all of the necessary additives that can be used to improve initial crystals obtained from Molecular dimensions screen 1.

Well	Chemical name	known as/for	Concentration	
E1	Glycine	stabiliser	0.40	M
E2	DL-Serine	stabiliser	0.40	M
E3	PEG 3000	precipitant	30.00	% v/v
E4	1,2,4-Butanetriol	cryoprotectant	40.00	% v/v
E5	NDSB 256	surfactant	4.00	% v/v
E6	1,2,6-Hexanetriol	cryoprotectant	40.00	% v/v
E7	1,5-Pentanediol	cryoprotectant	40.00	% v/v
E8	Trimethylolpropane	cryoprotectant	50.00	% v/v
E9	NDSB 195	surfactant	4.00	% v/v
E10	MOPSO	buffer (acid)	0.50	M
E11	Bis-Tris	buffer (base)	0.50	M
E12	BES	buffer (acid)	0.50	M

F1	TEA	buffer (base)	0.50	M
F2	Gly-Gly	buffer (acid)	0.50	M
F3	AMPD	buffer (base)	0.50	M
F4	Lithium sulphate	precipitant	0.60	M
F5	Sodium sulphate	precipitant	0.60	M
F6	Potassium sulphate	precipitant	0.60	M
F7	Manganese(II) chloride tetrahydrate	nucleant	0.02	M
F8	Cobalt(II) chloride hexahydrate	nucleant	0.02	M
F9	Nickel(II) chloride hexahydrate	nucleant	0.02	M
F10	Zinc acetate dihydrate	nucleant	0.02	M
F11	Barium acetate	phasing	0.02	M
F12	Cesium acetate	phasing	0.02	M
G1	Rubidium chloride	phasing	0.02	M
G2	Strontium acetate	phasing	0.02	M
G3	Sodium chromate tetrahydrate	phasing	0.01	M

G4	Sodium molybdate dihydrate	phasing	0.01	M
G5	Sodium orthovanadate	phasing	0.01	M
G6	Sodium tungstate dihydrate	phasing	0.01	M
G7	Erbium(III) chloride hexahydrate†	phasing	0.01	M
G8	Terbium(III) chloride hexahydrate†	phasing	0.01	M
G9	Ytterbium(III) chloride hexahydrate†	phasing	0.01	M
G10	Yttrium(III) chloride hexahydrate†	phasing	0.01	M
G11	Xylitol	cryoprotectant	0.40	M
G12	D-Fructose	cryoprotectant	0.40	M
H1	D-Sorbitol	cryoprotectant	0.40	M
H2	L-Rhamnose monohydrate	cryoprotectant	0.40	M
H3	myo -Inositol	cryoprotectant	0.40	M
H4	DL-Arginine hydrochloride	stabiliser	0.40	M
H5	DL-5-Hydroxylysine hydrochloride	stabiliser	0.40	M

H6	DL-Threonine	stabiliser	0.40	M
H7	trans -4-Hydroxy-L-proline	stabiliser	0.40	M
H8	DL-Histidine monohydrochloride monohydrate	stabiliser	0.40	M
H9	Spermine tetrahydrochloride	stabiliser	0.20	M
H10	Spermidine trihydrochloride	stabiliser	0.20	M
H11	1,4-Diaminobutane dihydrochloride	stabiliser	0.20	M
H12	DL-Ornithine monohydrochloride	stabiliser	0.20	M

2.1.3.10 Heavy Atom Derivatives

Table 2.7 Heavy atoms

Heavy atom	Stock concentration
Mercury Chloride	1 M
Mercury nitrate	1 M
Potassium tetrachloplatanate	1 M
Iodine-dATP	100 mM
Silver nitrate	1 M

2.2 Microbiological methods

2.2.1 Sterilisation

Unless stated otherwise storage media and buffers were sterilised for 15 min at 121 °C and 1 bar pressure in an autoclave. Temperature sterilised substances were filtered through a 0.2 µm pore size filter.

2.2.2 Preparation of *E. coli* competent cells

Competent *E. coli* cells were prepared based on a method previously described by Sambrook *et al* (1989). A bacterial overnight starter culture derived from a single colony was incubated in 10 mL of fresh LB broth and grown to an OD_{600} of 0.3. The cells were cooled on ice for 15 minutes on ice then centrifuged at 1,252 x *g* temperature of 4 °C. The pellet was gently resuspended in 25 mL of ice cold 0.1 M $CaCl_2$ and incubated on ice for 30 min. Cells were centrifuged for a second time and resuspended in 0.25 mL of 0.1 M $CaCl_2$ containing 26% glycerol v/v. Aliquots of 30 µL were frozen rapidly using nitrogen and stored at -80 °C.

2.2.3 Transformation of *E. coli* competent cells

Compotent cells were defrosted on ice for 20 min before addition of 1 µL of plasmid DNA. The mixture was incubated on ice for 30 min and then heat shocked at 4 °C for 90 sec, the mixture was then placed on ice for a further 30 min. After the addition of 200 µL of NTY broth the cells were incubated at 37 °C for 2 hr to allow antibiotic resistance expression. The mixture was then spread on an LB plate containing the required antibiotics and incubated over night at 37 °C.

2.2.4 Storage of bacteria

For long time storage of bacteria, glycerol stocks were prepared. Glycerol was added to an overnight bacterial culture to a final concentration of 25 % (v/v). The culture was then frozen at -80 °C

2.2.5 Liquid cultures

Liquid cultures were incubated at 28 °C for CobB and 37 °C for CobQ, overnight. A scraping of bacteria from glycerol stock at -80 °C was transferred to a 50 mL falcon tube containing 2 x 2YT with antibiotics and glucose. The liquid cultures were shaken at 160 rpm.

2.2.6 Transformation of *E. coli* competent cells

Compotent cells were placed on ice and allowed to thaw for 15 min before adding 1 µL of plasmid DNA. The mixture was incubated on ice for 20 min and then heat shocked for 90 sec at 42 °C, before being transferred to ice and left for a further 10 min. SOC media (200 µL) was added to the cells and depending on protein, was left at 28 °C or 37 °C . The mixture was then spread onto an agar plate containing the appropriate antibiotics and incubated at the appropriate temperature.

2.2.7 Recombinant protein overproduction in *E. coli*

The *E. coli* strain BL21 (DE3) pLysS was transformed with a vector containing the gene of interest cloned in frame. The recombinant strain was grown overnight in 10 mL of LB plus ampicillin (100 µg/L), chloramphenicol (100 µg/L) and glucose (0.4 % v/v). The 10 mL culture was then seeded into 2YT (2 x yeast/tryptone) broth containing anti-biotics and glucose. CobB was grown at 28 °C for 24 hours no induction with IPTG. CobQ was grown at 37 °C till an OD_{600} of 1.2 was reached. Protein production

was induced using 0.4 mM IPTG and the bevelled flasks were left shaking at 160 rpm overnight at 19 °C. The cells were then collected the following day by centrifugation at 8,765 x *g* for 20 min at 4 °C. The pellet was then re-suspended in 30 mL of Ni Buffer A (20 mM Tris-HCl pH 8.0,150 mM NaCl, 20 mM imidazole, and frozen at -20 °C.

2.2.8 Production of selenomethionine (Se-Met) labelled protein

Brucella CobB was transformed using KRX_pET14b-*cobB* cells and plated onto LB agar plates which were left overnight at 37 °C. A single cell was incubated with 10 mL of LB plus 0.4% glucose (v/v) and 100 µg/L of ampicillin and incubated at 37 °C for 8 hr until an OD_{600} of 0.2.

The above starter culture was then added to 2 L of LB plus ampicillin and glucose and grew overnight at 37 °C . The overnight culture was spun down and resuspended in induction media. Cells were incubated for 1 hr and then induced using 0.2 % Rhamnose for 24 hr at 25 °C.

Induction media: 100 mL of M9 salt x 10, 9 mL $CaCl_2$, 2mL $MgCl_2$, 100mL trace elements, 10% glycerol (v/v), 1 mL thiamine, 1 mL ampicillin and 125 mg/L of SeMet.

After 24 hours the sample was centrifuged at 1,252 x *g* for 20 min, pellet was resuspended in Ni Buffer A (20 mM Tris pH 8.00, 500 mM NaCl, 2 mM $MgCl_2$ and 20 mM imidazole), the same method as native protein.

2.2.9 Lysis of cells by sonication

Harvested cells were lysed by sonication using a Sonics Vibracell Ultrasonic VCX 150 processor (VWR), with an out watt of between 20 and 30 in 30 sec bursts with 20 sec break repeated 5 times. The sonicated cells were centrifuged at 8,765 x *g* for 20 min, at 4 °C to remove the cell debris.

2.3 Biochemical methods

2.3.1 Protein purification by immobilised metal ion affinity chromatography

The His_6-tag sequence of the fused protein has affinity for transition metals such as Co^{2+}, Ni^{2+}, Zn^{2+} and Fe^{3+}. Chelating Sepharose^{TM} Fast resin loaded with Zn^{2+} selectively retains proteins with exposed histidine, which will form a complex with the resin enabling purification of the protein of interest. The protein can then be eluted by washing with an imidazole gradient.

Protein was purified at room temperature using an Acta P-920 FPLC system (Amersham Biosciences). The pre-packed column was washed with 5 column volumes of water, and equilibrated using Ni^{2+} buffer A.

The lysate was clarified by centrifugation at 8,765 x *g* for 20 min, and run through a Ni^{2+} NTA column, protein was eluted using an imidazole gradient (Ni buffer B: 20 mM Tris-HCl pH 8.0, 150 mM NaCl and 1 M imidazole), CobB elutes at around 300 mM imidazole.

2.3.2 Buffer exchange

Purified protein was desalted on a pre-packed disposable Sephadex G25 column (PD-10, bed volume 8.3 mL; GE Healthcare). The column was equilibrated with 3 column volumes of MonoQ buffer A (desired exchange buffer), 2.5 mL of protein solution was applied to the column, and the protein was then washed through with 3.5 mL of buffer A.

2.3.3 Ion exchange chromatography

Ion exchange was performed using an Äkta P-920 FPLC system (Amersham

Biosciences). MonoQ column was washed in buffer and then equilibrated using 20 mM Tris-HCl pH 8.0, 150 mM $NaCl_2$ and 2 mM MgCl. The sample was loaded to the equilibrated column and then removed from the column using a salt gradient (buffer B: 20 mM Tris-HCl pH 8.0, 1 M $Nacl_2$ and 2 mM MgCl.

2.3.4 Gel filtration

An Äkta FPLC chromatography system was used for gel filtration purification. A Superdex™ 200 HiLoad™ 16/600 column (Sigma/Aldrich) was pre-equilibrated with 2 column volumes of buffer A (20 mM Tris-HCl, 150 mM $NaCl_2$ and 2 mM MgCl). Concentrated purified protein (1 mL) was loaded onto the column. The protein was eluted at a flow rate of 0.5 mL/min into 1 mL fractions with buffer A. Fractions were analysed by SDS-PAGE and the purest fractions pulled. The column was recovered with 1 column volume of buffer A and stored in water.

2.3.5 Production and purification of HBA and HBAD

HBA and HBAD was produced using a strain containing all of the enzymes necessary to produce the substrate (HBA) and product (HBAD) (Glycerol stock of strain supplied by Evelyne Deery). A scraping of cells from the glycerol stock was incubated in 10 mL of 2YTNN (see 2.1.2) media for 4 hrs, this was then added to 1 L of the same media. The protein media was incubated for 6 hrs, then induced using IPTG (0.4 mM), after induction the flask was moved to a 28 °C incubator for 24 hrs. The following day the lysate was centrifuged (8,765 x *g* for 20 min) and the pellet re-suspended in 10 mL of water and 30 mL methanol (v/v). The mixture was then placed in a water bath at 60 °C for 20 min, after 20 min the sample was again centrifuged to remove the denatured protein. The supernatant contained the substrate and product HBA and HBAD.

DEAE-Sepharose column (diethylaminoethyl) (Sigma-Aldrich) was equilibrated with 10 mL of 20 mM Tris-HCL pH 7.5, the HBA/HBAD sample was applied, a small

amount of HBAH was in the sample which did not bind the column (this sample was not used). HBAD was still bound, and was washed from column with 20 mM Tris-HCL pH 7.5 and 200 mM $NaCl_2$.

LiChroprep RP18 column (20-40 µM), beads activated with hexane and then washed with ethanol 3 times. A small amount of activated resin was poured into the column, and washed with 3 column volumes of acetonitrile. Column was then equilibrated with 5 column volumes of water. HBAD (pH to 4.5 with acetic acid) sample was applied to column and a further wash of 3 column volumes. Samples were separated using 5%, 10%, 20% and 30% methanol.

2.3.6 Preparation of crosslinkers DMS, DMP and DFDNB

Each of the crosslinkers were resuspended in water to a concentration of 100 µM (stock solution). Using a PD10 column the enzymes were exchanged into phosphate buffer saline (PBS). The concentration of CobB and CobH were adjusted to a concentration of 0.7 mg/mL. HBA was added to a final concentration of 100 mg/mL to the dilute CobH. CobB and CobH/HBA were combined and 50 μL of the crosslinker was added to the dilute complex. The complex was then left rotating at room temperature for 2 hr. To stop the reaction the buffer was changed using a PD10 column back into the original 20 mM Tris/HCl buffer, pH 8.0, containing 150 mM $NaCl_2$.

2.3.7 A280 protein concentration estimation

Protein concentration was estimated using a nanolitre spectrophotometer. The OD_{280} was recorded and the concentration estimated from the calculated extinction coefficient for the protein using the following equation. The absorbance and the extinction coefficient were derived from ProtoParam on the ExPASy server.

A_{280} = Concentration x Extinction coefficient x Path length

To convert to mg mL:

Protein concentration (mg/mL) = Molecular mass x Concentration.

2.3.8 Polyacrylamide gel electrophoresis

2.3.8.1 SDS-PAGE precast gels

Pre-cast polyacrylamide gels NuPAGE Novex 4-12 % Bis-Tris Gels (1.0 mm thick, 12 or 15 well) were used to check protein purity after purification.

Sample buffer (5x) containing 2-mercaptoethanol was added to samples and heated at 95 °C for 10 mins before loading. The gels were run in MOPS buffer (50 mL of NuPAGE/MOPS running buffer (20x) (Life Technologies) mixed with 950 mL dH_2O) at 200 V for 45 mins. The gels were then incubated in Coomassie blue staining solution (1 g Coomassie brilliant blue dissolved in 1 L of: 50 % (v/v) methanol, 10 % (v/v) glacial acetic acid, 40 % (v/v) dH_2O). The gels were then transferred to a de-staining solution (7% (v/v) glacial acetic acid, 25 % (v/v) methanol, 68 % (v/v) dH_2O) 2-3 times to reveal the protein bands.

2.3.8.2 SDS-PAGE

The composition of the gel, buffers and stain were previously described in Section 2.1.3.1.4.

Polyacrylamide gels were run according to Laemmli (Laemmli 1970). The sample was denatured by 1:1 addition of protein and SDS sample buffer and boiling for 5 min. Between 10 to 20 µL denatured sample was loaded into each well and 7 µL of molecular mass marker was run on each gel to estimate the relative molecular mass of the protein of interest. Electrophoresis was performed at a constant voltage of 200 V using an Atto Dual Mini Slab AE6450 electrophoresis apparatus and an Atto Mini

Power electrophoresis power supply Sj1082, both obtained from GRI Ltd. The gel was stained using Coomassie blue stain (2 hours) and de-stained by washing in water.

2.3.8.3 Native PAGE

A standard 12.5% (v/v) acrylamide gel was run as described in Section 2.3.5.1. Instead of staining with coomassie blue, the gel was fixed and stained using the following protocol. The acrylamide gel was washed in 200 mL 12.5% (v/v) TCA for 30 min and then for a further 20 min in dH_2O. Bands were developed using staining solution and appeared within 5 to 10 minutes.

2.3.9 Anaerobic techniques

Anaerobic work was carried out under nitrogen using an anaerobic chamber (glove box), containing less than 4 ppm oxygen. Liquids such as water and buffers stocks were degassed under argon prior transfer into the glove box. Chemicals were taken into the glove box as powders and were made up with degassed water once inside.

2.3.10 UV/visible spectrophotometry

All UV/visible spectra were recorded on a Varian Cary 50 Bio UV/visible spectrophotometer over a range of 300 -700 nm.

Intrinsic and extrinsic fluorescence were used to measure the kinetics of the reactions.

2.3.11 HPLC-MS

Mass spectroscopic data were obtained on an Agilent 1100 liquid chromatography (LC) system connected to a Agilent 1100 LC/MSD Trap, using electro-spray ionization technique in the positive mode. Spectra were monitored by DAD-UV detection.

2.4 Biophysical analysis

2.4.1 Fluorescence-emission spectra

Fluorescence spectrophotometry of the binding of substrate to the enzyme was performed in 20 mM Tris pH 8.0 and 150 mM NaCl, at room temperature, using a Perkin-Elmer LS-50 fluorometer. The excitation was fixed at 280 nm (recorded from 300-650) and 330 nm (recorded from 360-650), and the excitation slits were fixed at 2.5 nm each. Two samples of CobB (1 μM) was mixed with HBA (10 μM) and the emission spectra was collected with and without AMPPNP (5 mM) present.

2.4.2 Stopped Flow experiments

Stopped-flow is a method employed to allow the measurement of fast reaction kinetics on very short time scales (Toseland and Geeves 2014). The stopped-flow spectrometer used throughout this thesis was a SF-61 DX2 manufactured by HiTech Scientific which was capable of double mixing but only used for single mixing. The stopped-flow contains two 700 μL sample syringes driven by air-pressure from an external air pressure pump (concentration can vary depending on sample). Both syringes were triggered simultaneously pushing the reactants into an observation cell which is in the optical light path of a high intensity light source. The light source used for these experiments was a Xenon-Mercury lamp. The fluorescence of the sample was detected via a photomultiplier placed at a right-angle to the incoming light. When the samples reached the observation cell they were mixed in a 1:1 ratio resulting in the concentration of both reactants being halved. As the solution leaves the observation cell it fills the empty stop syringe which forces the syringe to hit a back-stop which immediately ceases the flow. The samples syringes are temperature controlled by an external water bath.

Intrinsic fluorescence originates from naturally fluorescent groups like certain amino acids within a protein such as tryptophan or tyrosine (Eccleston, Martin and Schilstra 2008). Tryptophan/tyrosine fluorescence is very commonly used as it can respond to changes in the local environment. In the case of the CobB there are a number of tyrosine residue located around the hydrogenobyrinic acid (HBA) binding site. This can be observed by an decrease in fluorescence when HBA binds, The tyrosine molecule was excited at a wavelength of 295 nm with the emission signal detected above 320 nm via a WG320 cut- off filter.

Extrinsic fluorescence derives from an external fluorophore being attached to a ligand of interest. In this study HBA, HBAM and HBAD with CobB, was excited at a wavelength of 360 nm and the emission detected above 450 nm.

2.4.3 Thermal shift assay

CobB in 20 mM Tris pH 8.00, 300 mM NaCl and 2 mM MgCl at a concentration of 5 µM was run with and without substrates. The assay was run on a Bio-Rad qPCR machine (real time PCR), 45 µL of enzyme and enzymes with substrates, was added to a 96 well plate. To each sample 1 µL (final concentration 5 mM) of a 5,000 times concentrated SYPRO Orange dye was added to the samples. This assay uses a temperature gradient to determine stability of the complex, as the temperature increases the protein starts to unfold, SYPRO orange will then bind to the hydrophobic core of the protein emitting a fluorescence signal (Santos *et al.* 2012).

2.5 MicroScale Thermophoresis (MST)

2.5.1 His_6-tag MST protocol

To 73.5 µL of protein (10 µM) in PBS buffer (concentration of 200 mM) 1.5 µL of concentrated dye solution (RED-tris-NTA) was added. This dye binds to the histidine

tag of the protein giving a fluorescence signal enabling any changes in the molecule when binding to be observed. A further 25 µL of PBS was added to the sample (100 µL), and the sample was incubated at room temperature for 30 min. After incubation the mixture was centrifuged at 15,000 x *g* at 4 °C for 10 min.

2.5.2 MST assay

MicroScale Thermophoresis (MST) is a method commonly used for the characterisation of intermolecular reactions. The instrument used was a Monolith NT.115. This instrument has a number of advantages over other technologies, mainly only very small amounts of protein are required to give accurate readings. For this assay a Tris-NTA with an oligohistidine tag was used, this gives a high fluorescence signal and an optimal signal to noise ratio in MST. The RED-tris-NTA binds to the histidine tag of one of the samples and enables the binding reaction to be monitored (Bartoschik *et al.* 2018).

In total 16 eppendorf samples are labelled 1 to 16, in sample 1: 20 µL of the ligand solution is added. To the remaining 15 samples: 10 µL of PBS is added to each eppendorph. Serial dilutions are then employed, taking 10 µL from sample 1 and mixing with sample 2, removing 10 µL from sample 2 and mixing with sample 3 this is continued until all of the 16 samples have protein. The labelled samples are then loaded into glass capillaries using capillary action. Overview of the procedure is shown in Figure 2.1.

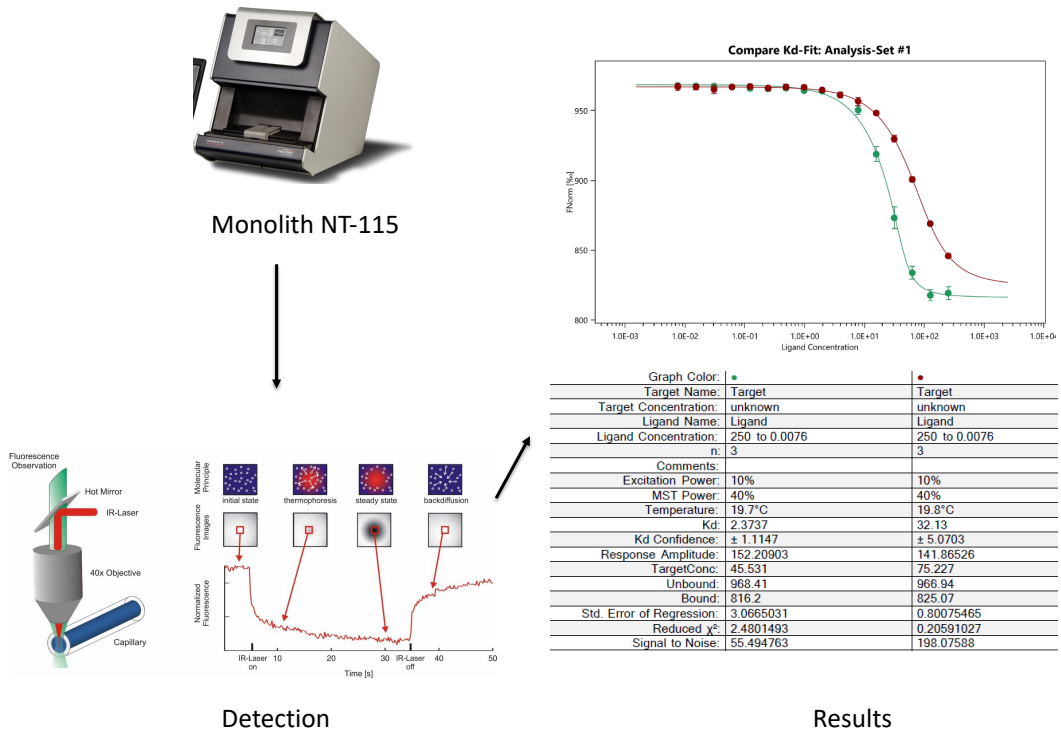

Graph Color:	●	●
Target Name:	Target	Target
Target Concentration:	unknown	unknown
Ligand Name:	Ligand	Ligand
Ligand Concentration:	250 to 0.0076	250 to 0.0076
n:	3	3
Comments:		
Excitation Power:	10%	10%
MST Power:	40%	40%
Temperature:	19.7°C	19.8°C
Kd:	2.3737	32.13
Kd Confidence:	± 1.1147	± 5.0703
Response Amplitude:	152.20903	141.86526
TargetConc:	45.531	75.227
Unbound:	968.41	966.94
Bound:	816.2	825.07
Std. Error of Regression:	3.0665031	0.80075465
Reduced χ^2:	2.4801493	0.20591027
Signal to Noise:	55.494763	198.07588

Figure 2.1 Monolith NT-115. Showing instrument Monolith NT-115, detection method and example of results. Results show a typical graph of two proteins binding to a ligand. Green is sample 1 and red is sample 2. The table shows the conditions used in the experiment and the Kd values obtained for each sample. Green sample has a Kd of 2.3 μM and red 32 μM.

2.6 Crystallisation and X-ray crystallography

2.6.1 Initial Crystallisation using hanging drop vapour diffusion method

The hanging drop vapour diffusion method was used for the screening of the proteins of interest (Figure 2.2). As previously described protein was purified using Ni^{2+} chromatography, de-salting column and ion exchange chromatography. Protein was then run on an SDS PAGE gel to determine the purity of the protein. Fractions of the purified protein were then collected. The protein was then tested for stability over a range on concentrations and temperature for storing, protein was found to be stable at low concentration and stored at -20 °C, aliquots of 1 mL were frozen at this temperature The protein for crystallisation (1 mL) was then concentrated to a final concentration of 4 mg/mL using an Amicon Ultra-15 centrifugal filter unit (Merck Millipore) with a molecular weight of 10,000 Da.

Initial screening was carried out using Molecular Dimensions screen 1 and 2 (total of 96 conditions), the trays were set up using greased 24 well plates, and 18 inch round siliconised cover slips (Hampton Research).

A 100 µL sample of the Molecular Dimension screen 1 ad 2 was placed in each well (total of 96 wells), and a protein sample of 2 µL was placed on each glass cover slip, 1µL from the well solution was then placed over the top of the protein drop. The cover slip was then inverted over the well solution, the grease seal on the top of the well plates enabled the sealing of the wells. The pates were then placed at both 4 °C and room temperature (20 °C)..

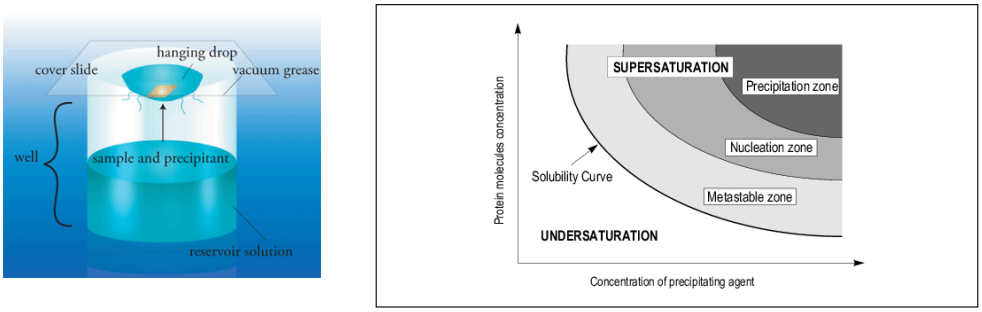

Initial crystallisation trials were set up using Molecular Dimensions screen 1 and 2.
Optimisation produced crystals which were good enough to send to the synchrotron.

Figure 2.2. Vapour Diffusion in the hanging drop. Showing vapour diffusion crystallisation drop and phase diagram.

2.6.2 Heavy atom soaks

As there was no previous structure molecular replacement could not be used to solve the structure, so to solve the phase problem heavy atom derivatives of the structure was required. Native protein was selected and soaked in a range of heavy atom derivatives (Table 2.7). The crystals were soaked for a period ranging from 15 min to 24 hrs, determined by the stability of the crystals. Crystals were then frozen and archived for diffraction purposes.

2.6.3 SeMet crystals

SeMet labelled CobB was expressed and purified as already described (2.2.8). A crystallisation tray was prepared using the same conditions as the unlabelled CobB (0.2 M ammonium acetate, 0.1 M Na citrate, pH 5.6, 30% PEG 4K). This produced crystals similar to the native crystals. The first crystal appeared four days after set up, but took about a week to be of a size for x-ray diffraction.

2.6.4 Archiving and storage of crystals

The most commonly used cryoprotectants include glycerol, ethylene glycol, PEG 400 and propylene glycol. A good cryoprotectant will provide protection and prevent damage caused by freezing and at the same time will not hinder the diffraction potential of the crystal (McFerrin and Snell 2002). Crystals were removed from the protein drop using a Hampton Cryo-Loop, the loop was slowly passed through a cryo-protectant solution. The cryo-protectant solution was 5 µL of well solution and 5 µL of a 50 % glycerol (v/v) solution (final concentration 25 % glycerol v/v). This seemed to give a glacial freeze and did not destroy the crystals. The crystals were then flash frozen in liquid nitrogen and stored until required for data collection.

2.6.5 X-ray diffraction

Crystals were mounted onto a goniometer where a constant cold stream of nitrogen gas at 100 K was applied, this was to keep the crystal vitrified. The data was processed using MOSFLM (Leslie 2006) and reduced using SCALA (Evans 2006). Processing refers to the indexing of the diffraction pattern and the integration of the intensities, image by image. Reduction is the process whereby reflections, are measured twice in order to obtain crystallographically equivalent reflections. These reflections are merged together to form the unique data set. At this stage the intensities are converted to structure factor amplitudes.

The SeMet crystals, native crystals, ADP bound, CobB with mutation at position C327A and CobB/ATP/HBA were collected on beamline I03 at the DIAMOND Light Source (Oxfordshire). CobB/HBA crystals and CobB/HBA/AMPPNP crystals were collected at beamline Proxima 2 (Soleil, France).

2.6.6 Refinement and model building

Successive cycles of refinement and model building were carried out using REFMAC (refinement package which includes refinement against anomalous data set this program is supported by the CCP4 data suite) (Vagin *et al.* 2004) and COOT (molecular graphics model building program supported by CCP4 data suite) (Emsley and Cowtan 2004) to improve the agreement of the model and experimentally derived structure factor amplitudes. Agreement was measured as the Rfactor and along with this value Rfree was also calculated as a control, using the 5 % of reflections consistently left out of the refinement. After refinement the resultant electron density map was examined to see if there are any parts of the structure that could be improved manually using COOT (Emsley and Cowtan 2004). The Rfree and Rfactor indicate the quality of the refined data. Pymol was used to draw structure figures throughout (The Pymol Molecular Graphics System, Version 0.99, Schrödinger, LLC).

Chapter 3

Biochemical and structural analysis of

Brucella melitensis CobB

3.1 Introduction

The production of adenosylcobalamin involves a highly complex intricate biological pathway comprising more than 30 enzymes-mediated steps. In order to gain insight into the mechanism into how cobalamin is produced, researchers have tried to study each of the individual enzymes to determine their role in the formation of this valuable molecule (Raux, Lanois and Levillayer 1996).

There are two distinct routes for the production of cobalamin, which are referred to as the aerobic and the anaerobic pathways (Figure 3.1). These two pathways diverge at the level of precorrin-2 and then re-converge after the synthesis of adenosylcobyric acid. Overall, the biosynthesis of cobalamin involves methylations, macrocyclic ring contraction, a decarboxylation, amidations, cobalt insertion, adenosylation and the construction and attachment of a lower nucleotide loop (Warren *et al.* 2002).

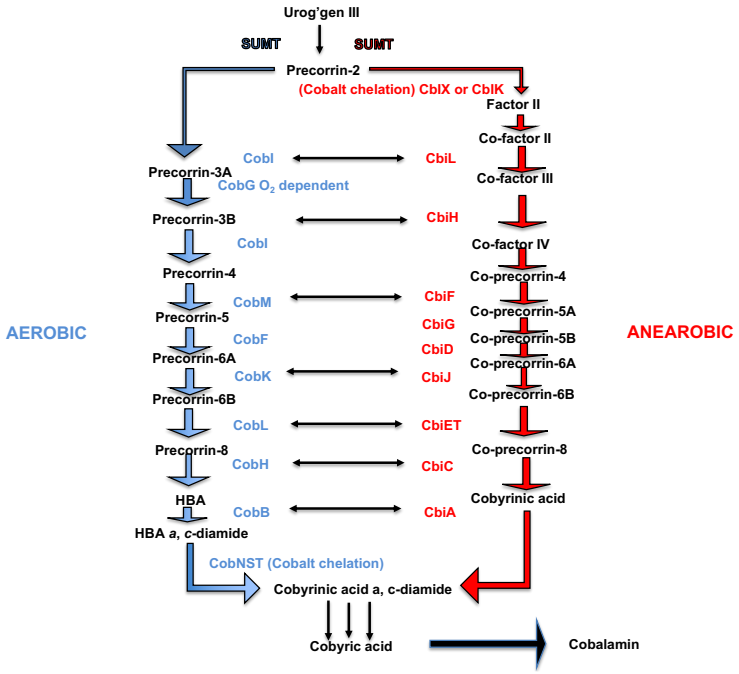

Figure 3.1: Aerobic and anaerobic pathway of the production of cobalamin. Diagram shows where the aerobic and anaerobic pathways diverge, after the production of precorrin-2, and re-converge, after the production of cobyrinic acid *a, c*-diamide.

The differences between the two pathways are in the requirement for molecular oxygen and the timing of cobalt insertion. For the anaerobic pathway cobalt insertion takes place early on whereas the aerobic pathway requires molecular oxygen and involves the late insertion of cobalt (Battersby 1994; Raux 1996; Scott 2003).

In this chapter the structure of cobyrinic acid *a, c*-diamide synthase, CobB, from *Brucella melitensis* is described. This enzyme is involved in the aerobic pathway and amidates hydrogenobyrinic acid (HBA) to give firstly hydrogenobyrinic acid *c*-monoamide (HBAM) and then hydrogenobyrinic acid *a,c*-diamide (HBAD) (Debussche *et al.* 1990). The homologous enzyme in the anaerobic pathway is called CbiA, which amidates cobyrinic acid to cobyrinic acid *a,c*-diamide. The enzymes require Gln/ATP/Mg^{2+} together with their corrin substrates to mediate the reaction (Fresquet, Williams and Raushel 2004). In both the aerobic and anaerobic pathways there are a total of six amidation steps, which are carried out by two separate enzymes called CobB and CobQ (Galperin and Grishin 2000). CobB from *P. denitrificans* has been shown to catalyse the amidation of the C2 and C7 carboxylates of hydrogenobyrinic acid (Figure 3.2). This enzyme will also use cobyrinic acid as a substrate, although the affinity for cobyrinic acid is significantly weaker (a *K*m of 160 μM versus 0.41 μM for hydrogenobyrinic acid) (Fresquet, Williams and Raushel 2004), (Debuscche *et al.* 1990).

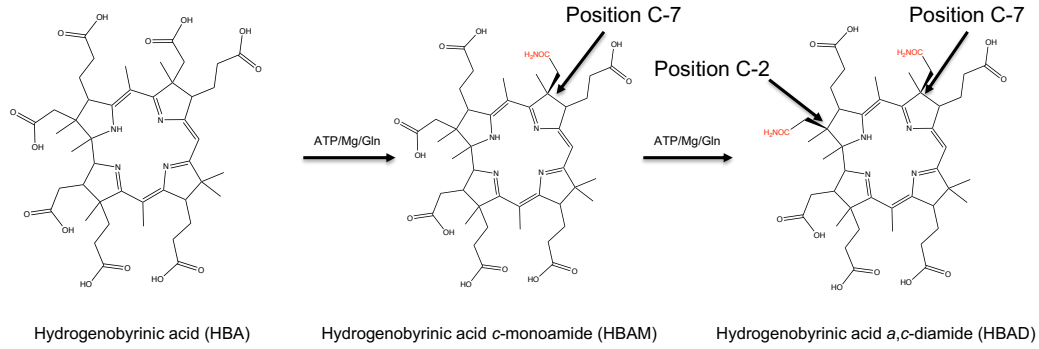

Figure 3.2: Amidation of HBA to HBAD. Diagram shows the amidation of firstly the C7 position on the ring to form HBAM, and then the amidation of C2 to form the product HBAD. In order for this reaction to proceed ATP, Mg^{2+} and Gln are required.

In the aerobic pathway cobalt insertion occurs at hydrogenobyrinic acid *a,c*-diamide in a reaction catalysed by the cobalt chelatase. The chelatase is a three component system composed of CobN, S and T and generates cob(II)yrinic *a,c*-diamide (Blanche 1993). It is at this point that the aerobic and anaerobic pathways re-converge. The cobalt is then reduced to cob(I)yrinic *a, c*-diamide and adenosylated.

CobQ (CbiP), the second amidase in the pathway, amidates adenosylcobyrinic acid *a,c*-diamide at positions *b, d, e* and *g,* on the tetrapyrrole ring to yield adenosylcobyrinic acid. The fifth carboxyl at the side chain *f* in the corrin ring is amidated using (R) – 1 amino-2-propanol in the aerobic pathway (Debuscche *et al.* 1990; Warren et al 2002).

In order to provide molecular detail on the mechanism of CobB the *B. melitensis* enzyme was produced recombinantly in *E. coli. B. melitensis* is a Gram negative coccobacillus bacterium from the Brucellaceae family, which is heterotrophic and can carry out either aerobic or anaerobic respiration. *B. melitensis* has all the necessary genes required for the aerobic biogenesis of B_{12}.

3.2. Results

3.2.1 Expression and purification of His tagged *Brucella melitensis* CobB

E. coli strain BL-21 (DE3) pLys*S* was transformed with pET14b carrying the *cobB* gene (Dr. Evelyne Deery), which allowed for the production of recombinant N-terminus His_6-tagged CobB. The cells were grown in 2YT broth supplemented with ampicillin and chloramphenicol overnight at 18 °C. (described in Section 2.2.7). After harvesting by centrifugation the cell pellet was resuspended in Tris-HCl buffer, pH 8.0, containing 500 mM NaCl and 20 mM imidazole. The cells were then lysed by sonication and centrifuged for a second time to remove the cell debris.

His tagged native CobB was purified using a Ni chelate column (Figure 3.3) followed by ion exchange chromatography. From 1 L of culture ~10 mg of protein was reproducibly produced. The purified CobB was run on a 12% SDS PAGE gel and appeared as a single band of 47 kDa, which is in close agreement to the expected molecular mass of 47.02 kDa (Figure 3.4).

The protein was observed to be highly soluble and could be concentrated to 20 mg/mL. However, the stability of the protein over time was problematic as it tended to precipitate at concentrations of greater than 2 mg/mL when stored at -20 ˚C. By lowering the salt concentration and keeping the concentration of the enzyme below 1 mg/mL this problem was overcome. The enzyme could be stored for periods of up to 6 months without any degradation.

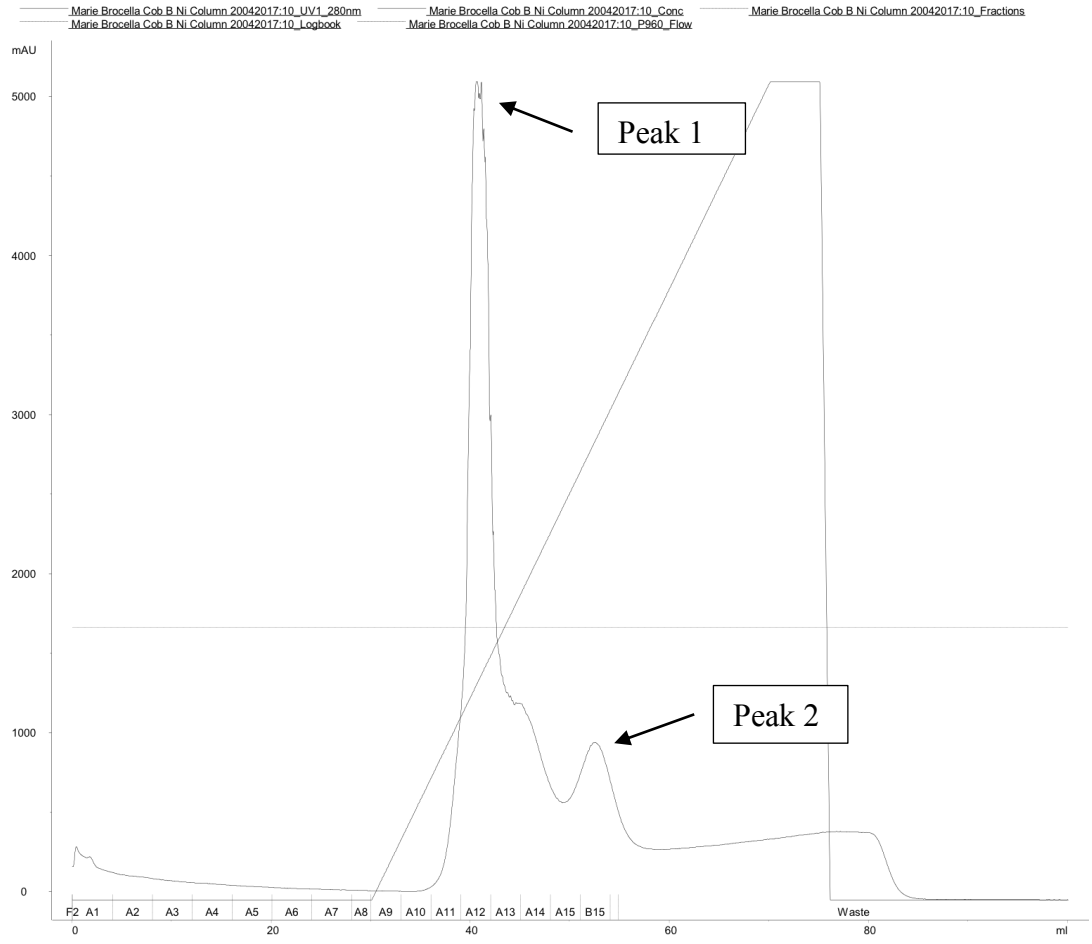

Figure 3.3: Chromatogram of Ni column showing elution of CobB. The large peak was collected in fractions A11 to A13, whilst the smaller peak was collected in fractions A15 and B15. The imidazole gradient, from 20 mM to 1 M.

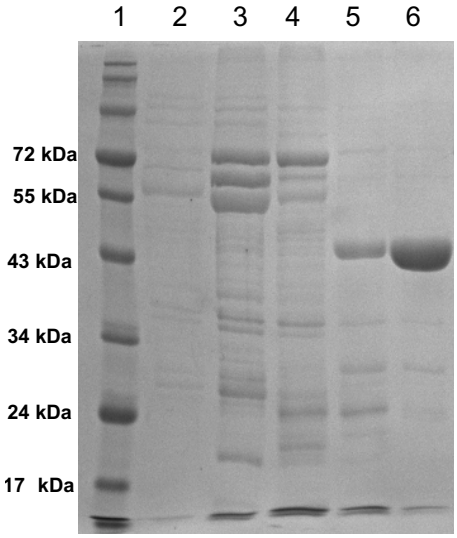

Figure 3.4: 12 % SDS-PAGE of fractions from CobB purification from IMAC. Lane 1 contains the protein ladder of known molecular masses as shown. Lanes 2, 3 and 4 contain samples taken from peak 1 from the chromatogram in Fig 3.3 and correspond to fractions A11-A13 (Fig 3.3). Lanes 5 and 6 contain samples from peak 2 from chromatogram in Fig 3.3 and correspond to peaks A15 and B15 (Fig 3.3). CobB was found to elute in peak 2, eluting at a concentration of ~250 mM imidazole. Over expressed CobB was not run on gel.

Protein fractions corresponding to lanes 5 and 6 on the SDS gel were pooled and the enzyme was run through a PD10 column to remove the imidazole (PD10 buffer, 20mM Tris/HCl, pH8.0, containing 150 mM NaCl and 2 mM MgCl). The protein was then applied to a MonoQ ion exchange column. The fractions from peak one were run on an SDS-PAGE gel (Figure 3.5).

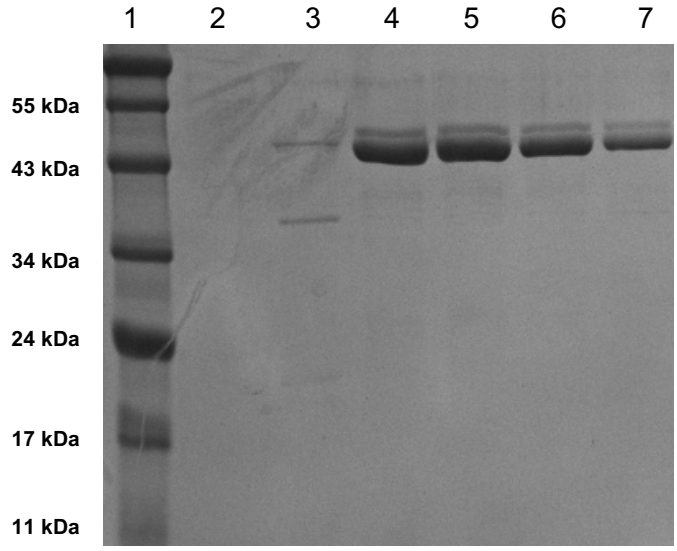

Figure 3.5: 12 % SDS gel of *B. melitensis* CobB showing fractions collected during purification. Lane 1: contains protein markers of known molecular mass, as shown. Lanes 2 & 3 contain the flow through from the MonoQ column. Lanes 4-7 contain the peak fractions from the chromatogram. Higher molecular weight band could be a proteolytic fragment.

3.2.1 Production and purification of HBA and HBAD

Hydrogenobyrinic acid (HBA) is the corrin substrate for CobB, amidating the carboxylate on the *a* and *c* side chains of the macrocycle resulting in the production of hydrogenobyrinic acid *a, c*-diamide (Debuscche *et al.* 1990). To investigate the structure and function of CobB, ready access to the corrin substrate and product is required. Both of these compounds have to be isolated from a genetically engineered strain of *E. coli*. A strain containing all the necessary enzymes to produce both substrate and product was obtained from Dr. Evelyne Deery, University of Kent. The recombinant *E. coli* strain contains *cobA-cobI-cobG-cobJ-cobM-cobF-cobK-cobL-cobH-cobB*, which encodes for all the enzymes required to convert uro'gen (III) into HBAD, although it also accumulates HBA too. The strain was grown in 2YTNN broth and expression of HBA and HBAD is described in Section 2.3.5. After overnight expression the mixture was spun at 13148 x *g* and the pellet resuspended in 30 mL of ethanol. The supernatant was then boiled for 30 minutes to denature the protein, and spun again at 18,000 rpm to remove the debris. The samples were then vacuum

dried to remove ethanol and frozen at -20 °C until required. In order to separate HBA from HBAD, the sample was run on a DEAE column. The first to elute from the anion exchange column was HBAD in 100 mM NaCl, followed by HBAD in 300 mM NaCl (Figure 3.6). Further purification of each sample was carried out using a reverse phase column (RP18), where pure material was removed from the column in 30 % (v/v) methanol.

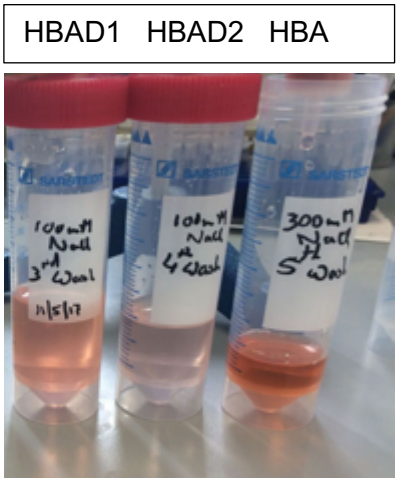

Figure 3.6: Samples of HBA and HBAD eluted from a DEAE column. HBAD (labelled wash 3 and 4) eluted from the column by washing with 100 mM NaCl. HBA, in the tube marked wash 5, was removed from the column with 300 mM NaCl.

The purified samples of HBA and HBAD were then run on a 20 % polyacrylamide gel to determine their purity (Figure 3.7). As shown in Fig 3.7, the purified material run as single fluorescent bands when viewed under UV light.

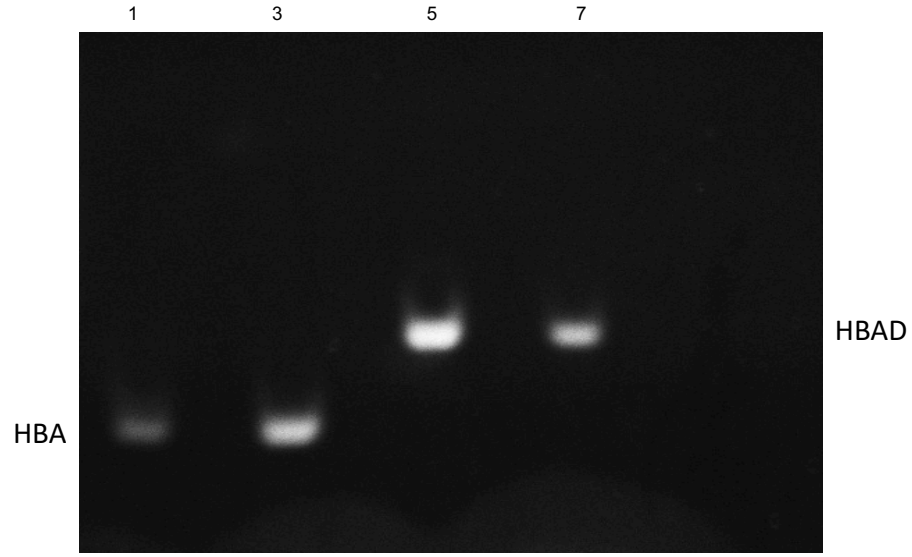

Figure 3.7: 20 % polyacrylamide gel. Standards of HBA and HBAD are shown in lanes 1 and 7, respectively, and were supplied by Dr. Evelyne Deery. The purified HBA and HBAD samples are in lanes 3 and 5, respectively, from the gel HBA and HBAD look to be pure running at the same rate as the standards.

3.2.3: UV/visible spectra of substrate and product

A UV/visible spectrum of each sample was recorded over the range of 300 nM to 700 nM. It is not possible to determine the difference between HBA and HBAD using this method but it does give information on the purity of the samples. HBA and HBAD have distinct absorbance maxima at 330 nm, 495 nm and 522 nm. With an extinction co-efficient of 20,000 M^{-1} cm^{-1} for the peak at 330 nm and 50,000 M^{-1} cm^{-1} for peaks 495 and 522 (Figure 3.8), it was determined that the purified batches contained ~300 µg/L of HBAD and ~150 µg/L of HBA.

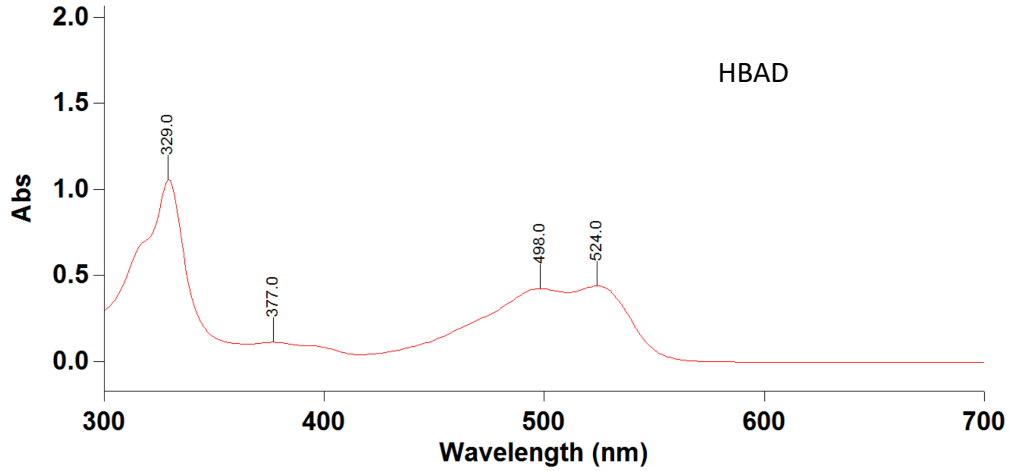

Figure 3.8: **UV/visible spectrum of HBAD**. HBAD has typical absorption maxima at 329 nm, 498 nm and 524 nm as shown in the spectrum.

3.2.4: Chromatography-mass spec analysis (LC-MS)

In order to verify that there was HBA and HBAD in each of the samples and to determine the purity of the samples they were analysed by LC-MS (Dr. Andrew Lawrence, University of Kent). LC-MS revealed the presence of one major compound that had a mass of 881.426 g/mol for HBA and 879.465 g/mol for HBAD (Figure 3.9). These results were very similar to the published mass for each compound 880.989 g/mol (HBA) and 879.021 g/mol (HBAD).

(a)

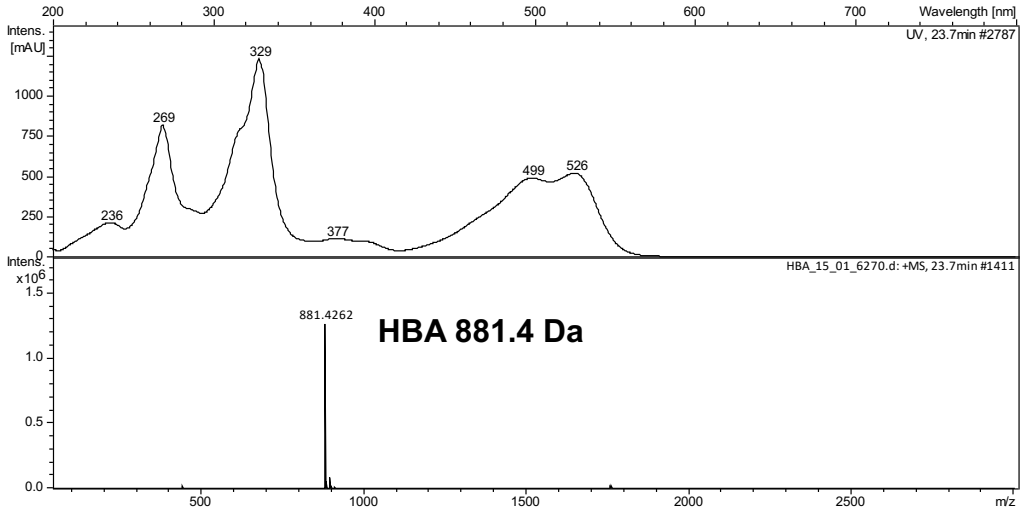

(b)

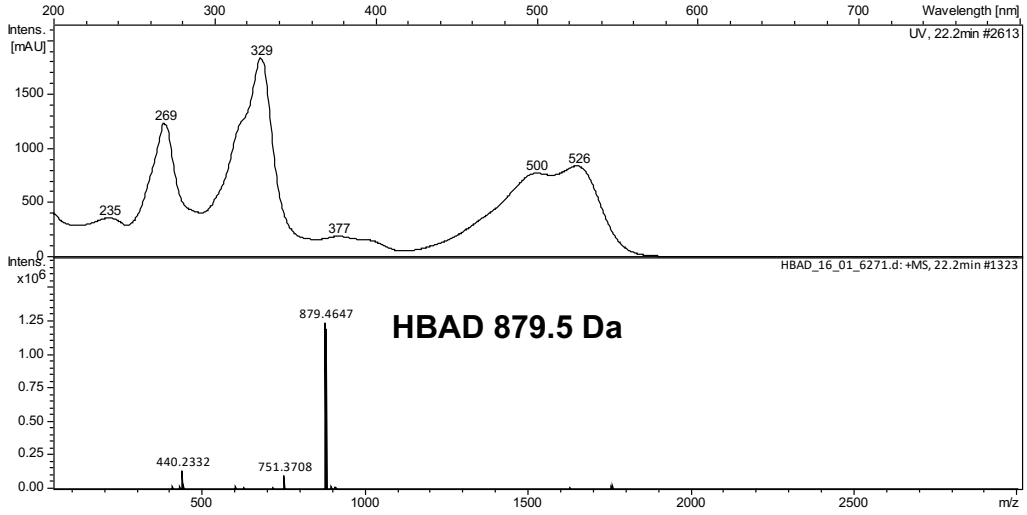

Figure 3.9: **LC-MS analysis of HBA and HBAD.** The spectra of (a) HBA shows a molecular mass of 881.4 Da and (b) HBAD shows a molecular mass of 879.5 Da, which is consistent with their molecular formulae.

3.4: Thermal stability measurement of *B.melitensis CobB*

In crystallisation experiments it is important to have a stable homogenous protein. One way to investigate the stability of the protein is to use a thermal shift assay. This assay is a technique that enables the determination of the stability of the protein under a range of conditions by, for example, monitoring the change in fluorescence of the binding of a dye over a temperature range. This techniques allows for an investigation into the suitability of buffers, binding partners or additives (Santos *et al.* 2012). For CobB this assay was performed in order to determine if the binding of substrates or cofactors increased the stability of CobB.

A number of samples were run with and without substrates and product, and the interaction monitored. The samples were run over a temperature gradient from 25 °C to 80 °C, at which point the protein starts to unfold and the dye (sypro orange) binds to the hydrophobic core of the enzyme resulting in a fluorescent signal (Figure 3.10, Table 3.1).

(a)

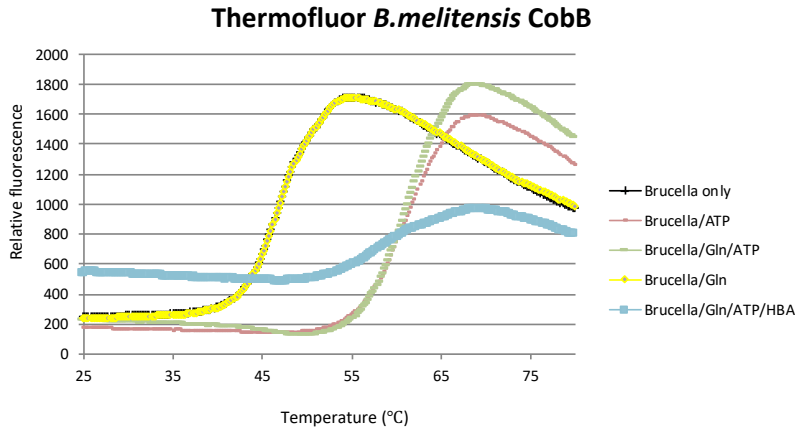

(b)

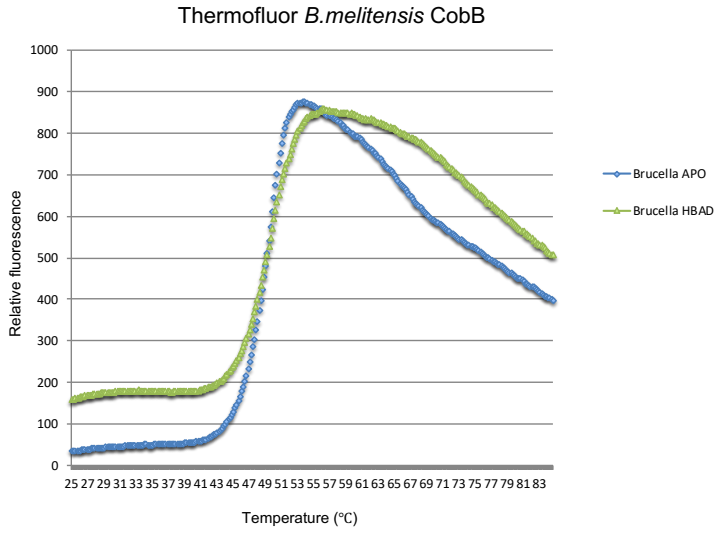

Figure 3.10: Melting curves of *B. melitensis* CobB. Curves showing change in relative fluorescence of either CobB alone or with substrates against temperature. (a) CobB only (black), CobB/ATP (pink), CobB/Gln/ATP (green), CobB/Gln (yellow), CobB/ATP/Gln/HBA (pale blue). (b) CobB (blue) and CobB/HBAD (green).

Table 3.1: Thermal melting temperature for *B. melitensis* CobB. CobB only has a thermal melting temperature of 47°C. The presence of ATP increases the binding stability of CobB/ATP by 14.2°C, CobB/Gln/ATP stabilisation of 14.4 °C, *Brucella*/Gln no change, *Brucella*/Gln/ATP/HBA stabilisation 12 °C and CobB/HBAD no change.

Enzyme	**Tm(Thermalmelting temperature)**	**Δ** ℃
CobB only	47 °C	0 °C
CobB/ATP	61.2 °C	14.2 °C
CobB/Gln/ATP	61.4 °C	14.4 °C
CobB/Gln	47 °C	0 °C
CobB/Gln/ATP/HBA	59 °C	12 °C
CobB/HBAD	48 °C	1 °C

B. melitensis CobB, in the absence of any substrates, has a Tm value of 47 °C. The addition of ATP to CobB results in an increase of 14 °C, this is a significant change in the stability of this enzyme. This indicates that when CobB binds ATP the active site of the enzyme is stabilised in the presence of ATP. The addition of Gln or HBAD does not change the thermal melting temperature this suggests they may not be binding or if they do their presence does not induce stabolisation in the active site. The thermal melting temperature when all cofactors are present is 59 °C this is 2 °C lower than the CobB/ATP, as 1 to 2 °C is considered within error this is not a significant decrease.

3.5: Crystallisation of *Brucella* CobB

His-tagged *B. melitensis* CobB was purified by metal affinity chromatography and ion exchange chromatography. The purified protein was run through a PD10 column to remove the excess salt from the ion exchange buffer. CobB was concentrated to 4 mg/mL and 24 well crystallisation trays were set up using the Molecular Dimension crystal screens 1 and 2. The method used was vapour diffusion with hanging drops, with a 2:1 ratio of protein to well solution. Initial screening conditions (0.2 M ammonium acetate, 0.1 M sodium citrate, pH 6.5, and 30% PEG 4K) produced crystals, of less than 1 micron (Figure 3.11).

(a) (b)

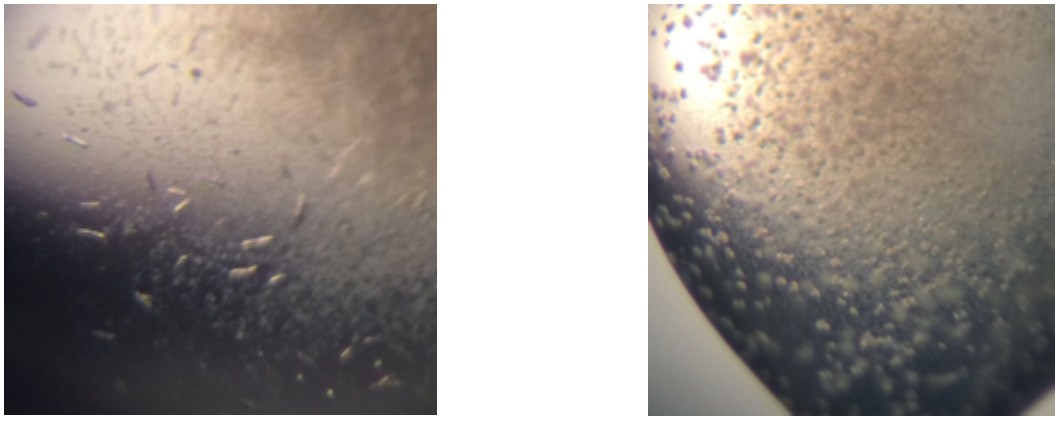

Figure 3.11: Initial crystals of *B. melitensis* CobB. Crystals (a) grown from 0.2 M ammonia acetate, 0.1 M Na citrate, pH 5.6, 30% PEG 4K and (b) crystals grown from 0.1 M Na citrate, pH 5.6, PEG 4K, 20% propanol.

In order to improve the quality and size of the crystals screening around the initial conditions by changing factors such as the pH, protein concentration and precipitant concentration. However, as these initial experiments did not improve the crystal quality, the use of an additive screen was also tried. An additive screen contains a number of small molecule compounds that are believed to stabilise proteins and improve morphology or diffraction. In this case the Molecular Dimensions Morpheus® Additive screen was used (Chapter 2). This library is comprised of 96 conditions

containing low molecular weight components that were found in many solved structures. Other components of the screen include compounds that are known to alter protein stability and solubility, such as heavy metals, polyamines, monosaccharides and amino acids.

From this approach crystals of CobB were obtained in a screen that contained rubidium as an additive (Figure 3.12).

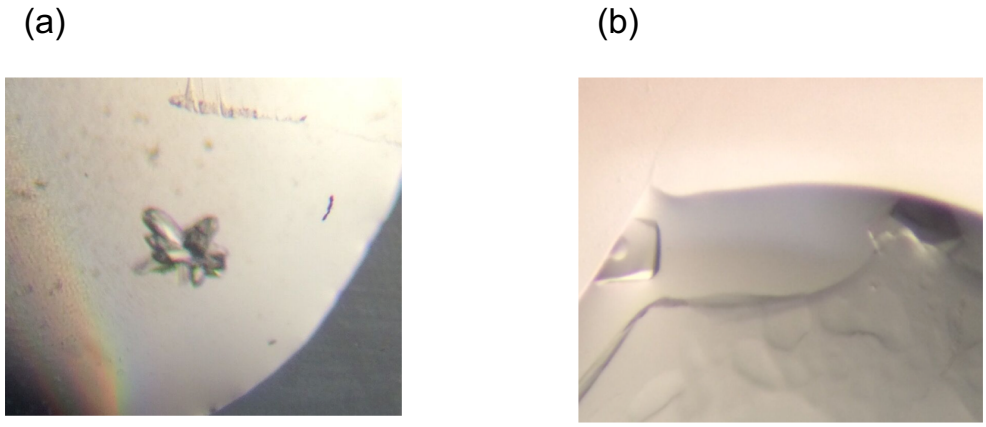

Figure 3.12: *B. melitensis* CobB crystals. (a) Crystals were grown from 0.2 M ammonium acetate, 0.1 M Na citrate, pH 5.6, 30% PEG 4K, with a 2:1 protein to well ratio plus 0.5 µL of rubidium. (b) Crystals were also obtained in a well containing 0.2 M ammonium sulphate, 0.1 M MES, pH 6.5, 30% PEG 5K and MME.

The crystals were sent to the Diamond Light Source (DLS), Oxford for data collection. The crystals diffracted to 1.9 Å, with a space group of P1 and cell dimensions of 55.39 Å, 57.12 Å and 74.23 Å and $\alpha = 82.61$, $\beta = 68.75$ and $\gamma = 72.94$. As there were no previous structures in the Protein Data Bank with sufficient sequence homology to CobB, experimental phasing approaches were investigated. Two approaches were initially employed to obtain the necessary X-ray diffraction data to solve the crystal structure; isomorphous replacement (using heavy atom derivatives) and single wavelength anomalous dispersion (SAD), using selenomethionine (Se-met) labelled protein. As there are 15 methionine residues in CobB, the selenomethionine route

would produce enough phasing power to enable structure determination if heavy atom route failed.

3.5.1: Heavy atom derivatives

As there is no data set available for CobB in the protein data bank CobB native crystals were grown from 0.2 M ammonium acetate, 0.1 M sodium citrate, pH 5.6, 30 % PEG 4K, with a 2:1 protein to well ratio plus 0.5 µL of rubidium. These crystals were soaked in solution containing 1 mM to 60 mM of a range of heavy atoms, over a time scale ranging from 15 minutes to 24 hours (Table 3.2). Most of the crystals survived the soak, even at high concentrations of the heavy atom. The crystals were then cryoprotected using 20 % v/v glycerol and flash frozen in liquid nitrogen. These crystals were taken to the DLS for data collection. Data was collected on all of the crystals but none had the heavy atom incorporated.

Table 3.2: CobB crystals soaked with heavy atom derivatives: Table shows the range of heavy atoms used, how long the crystals were soaked for and how the crystals diffracted at the synchrotron.

Heavy atom	Soak time	Diffraction analysis
Mercury chloride	5 minute soak	Data collected to 2 Å no heavy atom present
Mercury chloride	1 week soak	Crystal isomorphous no data set collected
Mercury nitrate	5 minute soak	Data collected to 3 Å no heavy atom bound
Potassium tetrachloplatanate	5 minute soak	Data collected to 2.5 Å no heavy tom bound
Potassium tetrachloplatanate	15 minute soak	Data collected to 2.6 Å no heavy atom bound
Potassium tetrachloplatanate	1 hour soak	Crystal quality poor no data collected
Iodine-dATP	Co-crystallisation	Data collected to 2 Å no heavy atom bound
Silver nitrate	24 hour soak	Crystal quality poor no data collected

3.6: Production of selenomethionine enriched *B. melitensis* CobB

Another method used for solving the phase problem is incorporation of selenium methionine in the protein of interest, this is a common method used in crystallography. It was the work of Cowie and Cohen in 1957, that demonstrated that *E. coli* during synthesis had the ability to incorporate selenium instead of sulphur during biosynthesis (Cowtan 2006). The production of SeMet labelled protein involves growing a methionine-auxotrophic strain of *E. coli* in LB which was supplemented with amino acids and SeMet (Zhoo, Hartnett and Slater 2007).

In order to produce Se-met enriched CobB for crystallisation, the plasmid encoding the protein was transformed into *E. coli* KRX cells and plated onto LB agar plates. The following day a single colony was picked and incubated with 10 mL of LB broth plus 0.4 % glucose and 100 µg/L of ampicillin and incubated at 37 °C for 8 hours. This starter culture was added to 2 L of LB plus ampicillin and glucose and grown overnight at 37 °C. After centrifugation the pellet was resuspended in induction media, incubated for 1 hour and then induced using 0.2 % rhamnose for 24 hours at 25 °C. The T7 RNA polymerase gene in the KRX strain is under the control of the *rhaPBAD* promoter and is positively activated by rhamnose and catabolically repressed by glucose (Zhoo, Hartnett and Slater 2007).

The protein was purified by use of nickel affinity resin and anion exchange chromatography, and the protein purity was verified by SDS PAGE gel (Figure 3.13).

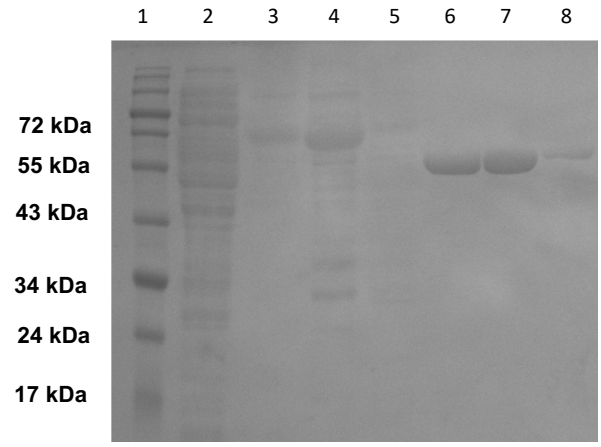

Figure 3.13: 12 % SDS-PAGE gel. Lane 1 contains protein the markers of known molecular mass. Lane 2 contains a sample of the flow through from the column, lanes 3, 4 and 5 represent impurities. Lanes 6, 7 and 8 contain the purified Se-met enriched CobB.

Se-met enriched CobB was crystallised using the same condition as the native protein (0.2 M ammonium acetate, 0.1M sodium citrate, pH 5.6, 30% PEG 4K, with a 2:1 protein to well ratio plus 0.5 µL of rubidium. The crystals were then cryoprotected using 25 % v/v ethylene glycol and flash frozen for data collection.

Electrospray mass spectrometry was used to estimate the level of incorporation of Se-met into CobB (Figures 3.14 and 3.15). The sample proved to be difficult to work with but by mixing in a 1:3 ratio of 8 M urea and EDTA to a final concentration of 1 mg/mL, the level could be calculated (Kevin Howland, University of Kent).

The presence of Se-met in the protein results in an increased mass of 46.89 Da per residue in comparison to methionine. By comparing the mass of the native protein with that of the labelled the incorporation efficiency can be determined.

$$\% \text{ incorporation} = 100 \times \frac{(MW_{labelled\_experiment} - MW_{unlabelled\_experiment})}{(MW_{labelled\_theoretical} - MW_{unlabelled\_theoretical})}$$

His-CobB from the MS trace has a molecular mass of 49066.30 Da whilst the Se-met enriched material has a mass of 49768.9 Da. The theoretical molecular mass for unlabelled CobB is 48498.69 Da whilst the theoretical mass of the Se-met protein is 49202.04. By using the above equation it was determined that a high level of incorporation (>90 %) had been achieved.

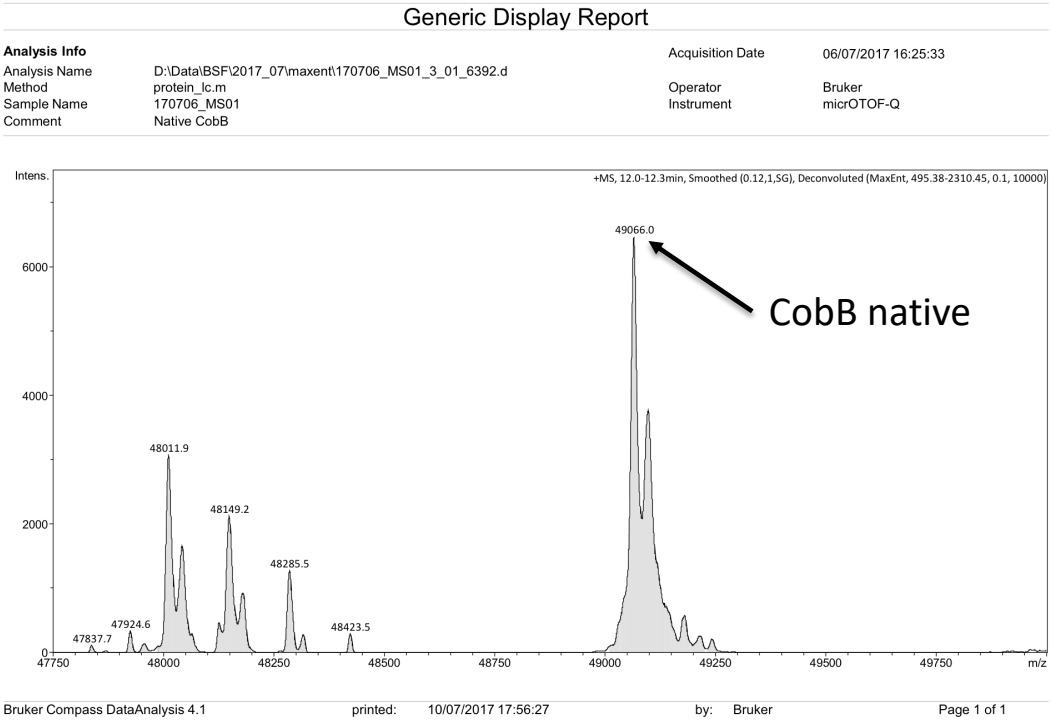

Figure 3.14: LC-MS trace of native CobB. The trace shows a molecular mass of 49066.30 Da for CobB.

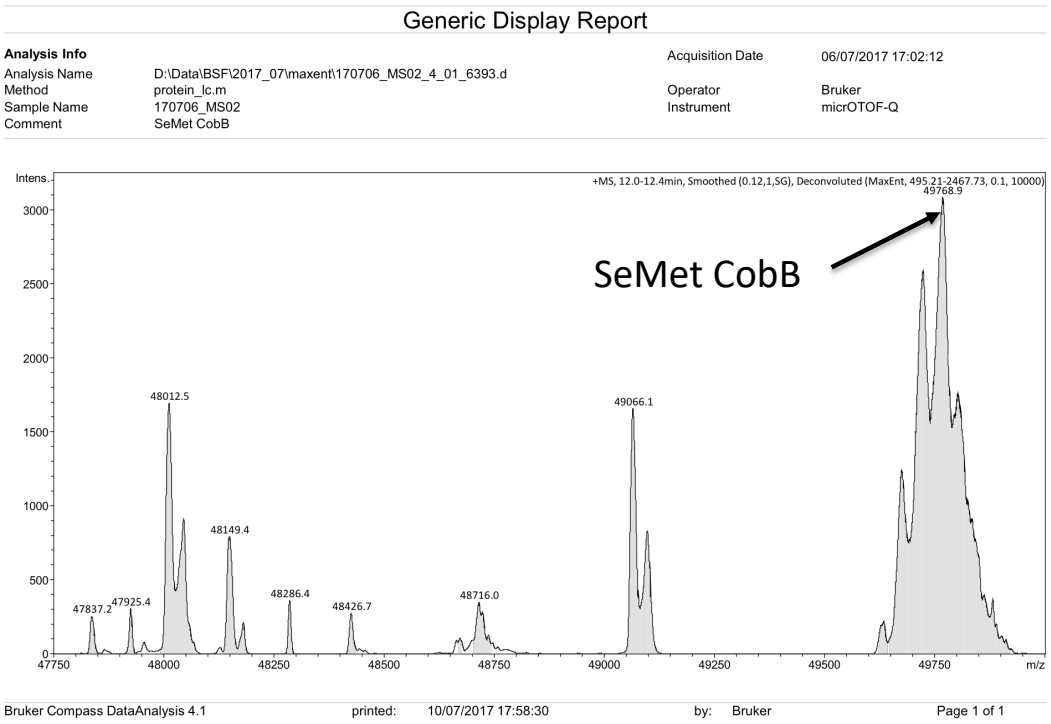

Figure 3.15. LC-MS trace of Se-met enriched CobB. The trace shows the molecular mass of Se-met enriched CobB as 49768.9 Da.

3.6.1 Purification and crystallisation of Se-met CobB

Se-met enriched CobB (Chapter 2) was produced and purified for crystallisation using a combination of metal affinity and ion exchange chromatography. The purified protein was run through a PD10 column to remove the excess salt from the ion exchange buffer. Se-met enriched CobB was concentrated to 4 mg/mL and a crystal tray was prepared using the same conditions as the native protein (Figure 3.16).

Figure 3.16: Se-met labelled CobB crystals. Picture showing crystals of Se-met enriched CobB. Although twinned these crystals were of a suitable size and quality for X-ray diffraction data collection.

Crystals were flash frozen in liquid nitrogen using 25 % (v/v) ethylene glycol and sent to DLS. Data sets were collected using single-wavelength anomalous diffraction (SAD) at the K-absorption edge of selenium. These crystals diffracted to 1.7 Å resolution with two molecules of CobB in the asymmetric unit.

3.7 Crystallographic data collection and refinement

Both native and Se-met crystal data were collected on beam line I03 at the DLS, in collaboration of Prof. Dave Brown (University of Kent). Se-met data was collected to 1.7 Å, which allowed phasing using SAD (single anomalous diffraction) This method is favoured as only one crystal is required to obtain all of the necessary data. Fortunately, the native and the Se-met structures belonged to the same space group $P1_1$ with a Matthews coefficient of 2 molecules of the dimer in the asymmetric unit. SHELX was used to find the initial Se-met sites, this program was designed by George Sheldrick (Cowtan 2006). The anomalous data from this experiment was then fed into this program, enabling the electron density for the CobB structure to be calculated. Bucaneer is a software program that is used for automatic model building (Cowtan 2006) this program was used to trace the initial backbone of the protein.

The initial model was built and refined against the data from the Se-met crystals, however, the native data, which diffracted to higher resolution, was used to refine the first structure of CobB. The resolution of these two data sets are similar but the overall quality of the native data is better.

The native structure was built with molecular replacement of the Se-met model using Refmac for sequential refinement of the data and manually rebuilt using COOT (Emsley 2004).

3.7.1: Structure of *Brucella melitensis* CobB

The structure of CobB confirms that the enzyme is a homodimer with each subunit composed of two globular α/β domains. The crystal has two molecules of CobB in the asymmetric unit (AU). Each subunit consists of an N-terminal and C-terminal domain joined by a linker region. The crystals were grown without removing the histidine tag but this feature is not present in the final structure (Figure 3.17 and 3.18).

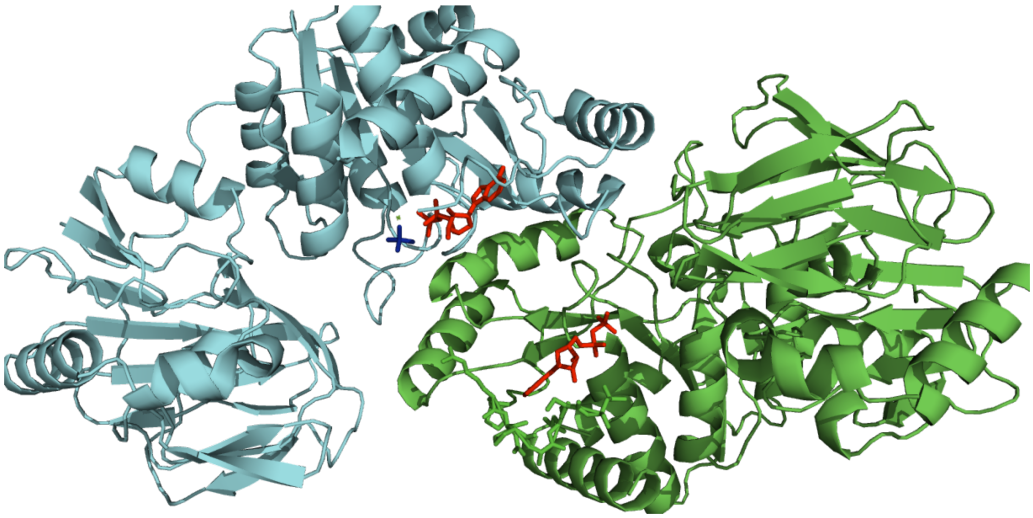

Figure 3.17: Crystal structure of *B. melitensis* CobB. Cartoon diagram of CobB showing molecule A (green) with ADP (red) in the active site and molecule B (cyan) with ADP (red) and phosphate (blue) also present.

(a) (b)

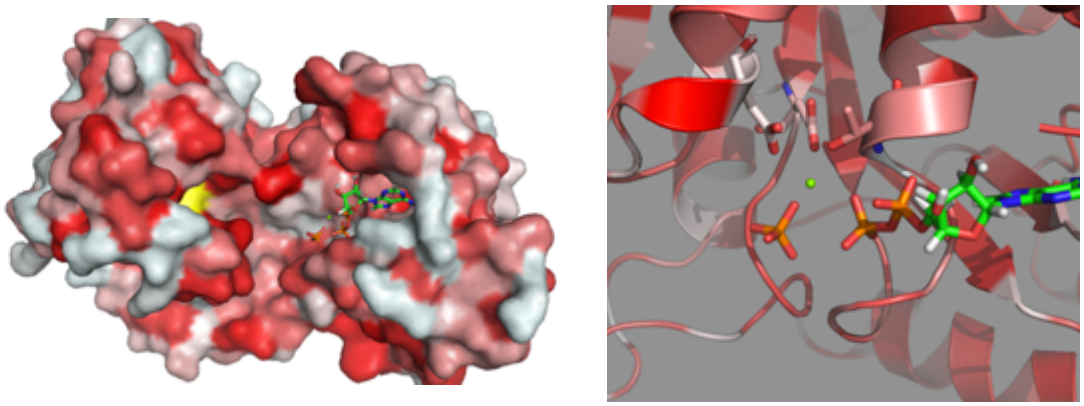

Figure 3.18: Structure of *B. melitensis* CobB. Molecule B alone shows evidence of ATP turnover, as it has a free phosphate and Mg in the active site, whereas molecule A has only ADP.

From sequence analysis the structure of CobB is said to be related to a family of ATPases which are involved in the regulation of cell division in bacteria and archaea. The paper by Michael Galperin and Nick Grishin (Galperin and Grishin 2000), used the crystal structure of Dethiobiotin synthetase (DTBS) to look at the likely mechanism of CobB and CobQ the second enzyme in the amidation process.

(a)

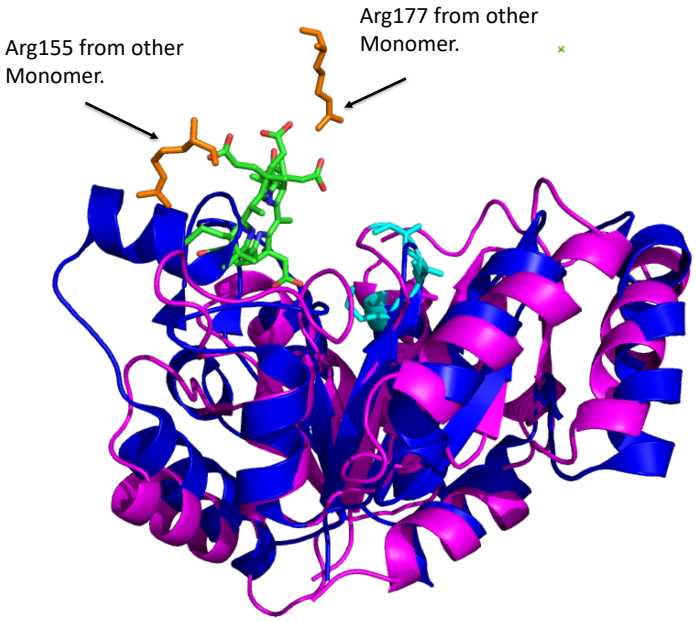

(b)

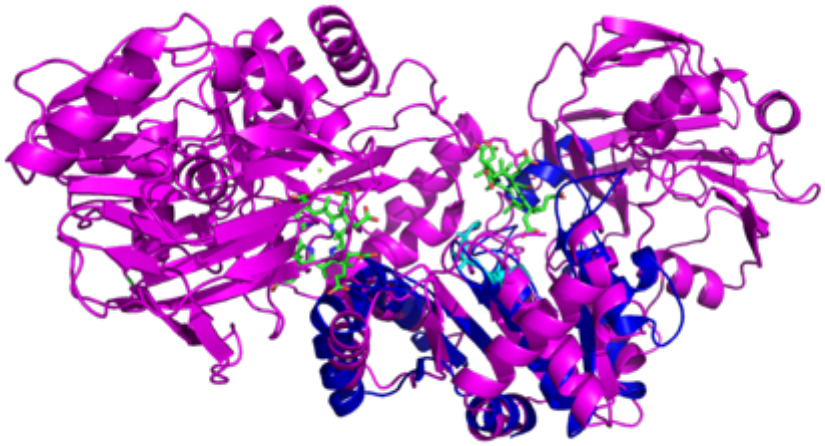

Figure 3.19: **Cartoon representation of the overlaid structure of CobB and dethiobiotin synthetase:** (a) shows the N-terminal binding site with HBA bound to CobB (cyan) and dethiobiotin synthetase (blue). ATP binding site (pale blue). (b) shows a representation of the dimer of CobB binding HBA (cyan), overlaid with the dethiobiotin synthetase monomer domain (blue).

Figure 3.19 shows the importance of the formation of the dimer in the binding of HBA. The main contact when binding substrate is the contribution of Arg155 and Arg177

from the other monomer. Due to this fact dethiobiotin synthetase. Is not a truly represent CobB binding to HBA.

The N-terminal domain of CobB is composed of 8 alpha helices and 6 parallel beta sheets. Amino acids 184-198 are missing from the crystal structure, most likely due to this region being unstructured and flexible. The N-terminal contains a typical ATP binding domain (Walker *et al.* 1982), composed of Gly12, Ser13, Gly14, Lys15 and Thr16. This constitutes a Walker A motif (P loop) which is a typical ATP binding domain present in all ATPase family of proteins, the lysine side chain in this family of proteins is essential for binding ATP. The lysine residue forms a hydrogen bond with the oxygen atoms of the phosphate groups within ATP, thereby creating proximity and orientation for ATP in the binding site. This is also a short loop (Walkers motif) fold over the ATP binding site, and is preceded by a beta strand ($\beta 1$) and followed by an alpha helix ($\alpha 1$) in the crystal structure (Figure 3.20).

The C-terminal domain of CobB contains 4 alpha helices and 15 beta sheets. Three of the helices sit on the surface of the protein ($\alpha 1, \alpha 2$ and $\alpha 3$) where $\alpha 4$ is buried in the active site. The 15 beta sheets form a beta barrel type structure with 10 parallel ($\beta 1$, $\beta 2$, $\beta 3$, $\beta 4$, $\beta 5$, $\beta 7$, $\beta 9$, $\beta 11$, $\beta 12$ and $\beta 15$) ($\beta 6$, $\beta 8$, $\beta 10$, $\beta 13$ and $\beta 14$) and 5 anti-parallel beta sheets ($\beta 6$, $\beta 8$, $\beta 10$, $\beta 13$ and $\beta 14$) (Figure 3.19).

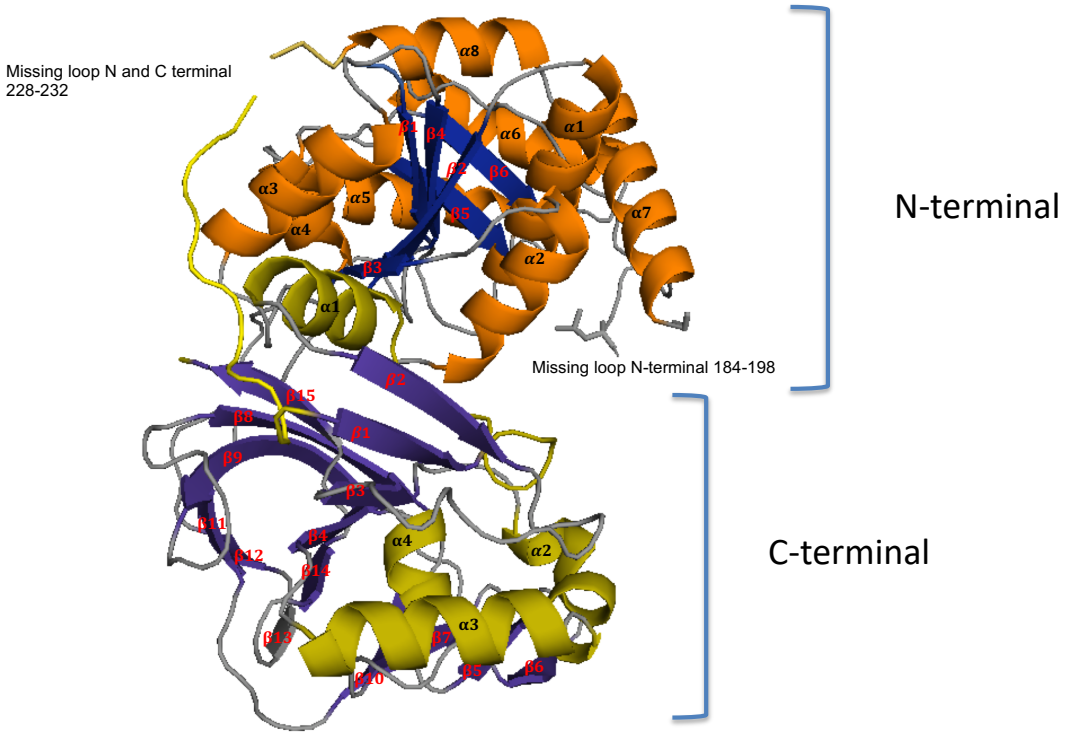

Figure 3.20: Ribbon diagram of CobB with labelled N- and C-terminal domains. The N- and C-domains of CobB are highlighted, showing alpha helices (orange and mustard) and beta sheets (purple) joined by a long flexible loop (yellow). Missing loop region on N-terminal 184 to 196 and N and C terminal 228 to 232, this region looks to be flexible.

The C-terminal domain, known as the GATase domain binds Gln and converts it to ammonia, this domain has a conserved cysteine and histidine residues (Cys327 and His427 in the *B.melitensis* CobB) but lacks the typical Glu residue seen in other class 1 Gln amidotransferases (Raushel, Thoden and Holden 2003; Raushel, Thoden and Holden 1999; Holden, Thoden and Raushel 1998; Galperin and Grishin 2000). The nucleophile of this catalytic triad is generally located in a very sharp turn of the protein backbone structure, called the nucleophilic elbow, and is identified by the consensus sequence GXSXG and the oxyanion hole formed by the residues next to the catalytic cysteine (Figure 3.21) (Leisico *et al.* 2018). In the CobB structure this group of residues is $GEC_{327}GG$.

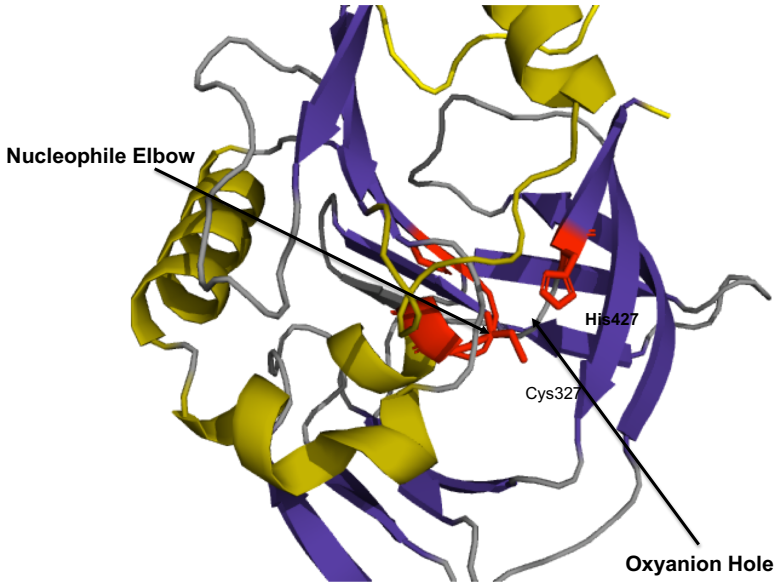

Figure 3.21: C-terminal domain of CobB. showing nucleophile elbow (identified by consensus structure GXCXG) and oxyanion hole. The conserved residues are highlighted in red.

Table 3.3 Summary of crystallographic data and refinement statistics for Se-met CobB. RMSD – root mean squared deviation.

Data collection		**Refinement**	
Source	DIAMOND I03	Resolution	1.73
Wavelength	0.97971	No. reflections	84604 (6260)
Oscillation range	0.1	R_{work} / R_{free}	0.159/0.183
Space group	P1	**No. atoms**	
Number of frames	7200	**Beam Intensity**	50m 5% transmission
Molecules/a.s.u	2	Protein	5260
Cell dimensions *a, b, c* (Å)	55.85, 57.34, 74.55	Ligand/ion	86/83
Cell dimensions α, β, γ (°)	82.61, 68.75, 72.94	Water	496
Resolution (Å)	43.53 – 1.71 (1.75 – 1.71) *	*Average B factors*	
R_{merge}	0.158 (1.602)	Protein	32.32
$I / \sigma I$	8.7 (1.0)	Ligand (s)	37.55
CC 1/2	0.992 (0.656)	Water	496
Total number of observations	734460	R.m.s deviations	
Total number of unique	79307	Bond length (Å)	0.013
Completeness (%)	9.3 (8.1)	Bond length (°)	1.493
Redundancy	2.9 (2.5)	PDB ligand code	ADP

Table 3.4 Summary of crystallographic data and refinement statistics for CobB. RMSD – root mean squared deviation.

Data collection		**Refinement**	
Source	DIAMOND I03	Resolution	1.5
Wavelength	0.9763	No. reflections	37322 (2740)
Oscillation range	0.1	R_{work} / R_{free}	0.184/0.234
Space group	P2	**No. atoms**	
Number of frames	360	**Beam Intensity**	50m 5% transmission
Molecules/a.s.u	2	Protein	5282
Cell dimensions *a, b, c* (Å)	55.83, 57.61, 74.71	Ligand/ion	72/8
Cell dimensions α, β, γ (°)	82.10, 68.67, 73.24	Water	180
Resolution (Å)	55.00 – 1.47 (1.49 – 1.47) *	***Average B factors***	
R_{merge}	0.087 (0.853)	Protein	59.91
I / □*I*	6.2 (1.5)	Ligand (s)	95.19/69.93
CC 1/2	0.925 (0.581)	Water	53.10
Total number of observations	44270 (22848)	***R.m.s deviations***	
Total number of unique	134120 (8283)	Bond length (Å)	0.013
Completeness (%)	95.1 (74.6)	Bond length (°)	1.572
Redundancy	3.3 (2.8)	PDB ligand code	ADP

3.7.2: Crystal structure of CobB co-crystallised with HBA and HBA/AMPPNP

In order to determine the structure of CobB bound with HBA, 1 mL of HBA (200 μM) was added to 3.5 mL of CobB (0.8 mg/mL). The complex was diluted and concentrated 3 times with Tris-HCl buffer, pH 8.0, (3 X 15 mL) using a 30 kDa cut off centricon. This process enables unbound substrate to be removed from the enzyme. Removal of unbound substrate or small molecular weight aggregates can aid in crystallisation.

Crystallisation trays were set up at a protein concentration of 4 mg/mL and Molecular Dimension screens 1 and 2 were prepared, with two drops on each cover slip. Drop one contained CobB with HBA only whilst the second drop contained HBA and AMPPNP, AMPPNP is a non-hydrolysable form of ATP, so its presence will not result in the turnover of substrate (HBA) to product (HBAD). A structure of AMPPNP bound would enable information to be obtained about the binding of ATP in N-terminal binding site. Crystals appeared after 2 days with condition 0.1 M Na cacodylate, pH 6.5, Mg acetate and PEG 8K for the CobB/HBA drop whilst crystals of the CobB/ HBA/AMPPNP complex were observed in 0.01 M Fe(II)Cl, 0.5 M ammonium sulphate and 0.1 M sodium citrate, pH 5.6.

The crystals were archived and stored in liquid nitrogen using the same protocol as described previously. The crystals were sent to SOLEIL, France, for data collection, on beamline Proxima 2. The HBA bound crystals diffracted to 2 Å resolution with a, space group P1 and cell dimensions of 56.05 Å, 57.77 Å, 75.40 Å, α = 82.48, β = 68.58 and γ = 73.24 with 2 molecules in the AU (Figure 3.21, Table 3.4).

The HBA/AMPPNP structures diffracted to 2 Å, with a space group $P2_1$ and cell dimensions of 55.62 Å, 186.47 Å, 89.39 Å, $\alpha = 90$, $\beta = 90.22$, $\gamma = 90$, with 2 molecules in the AU.

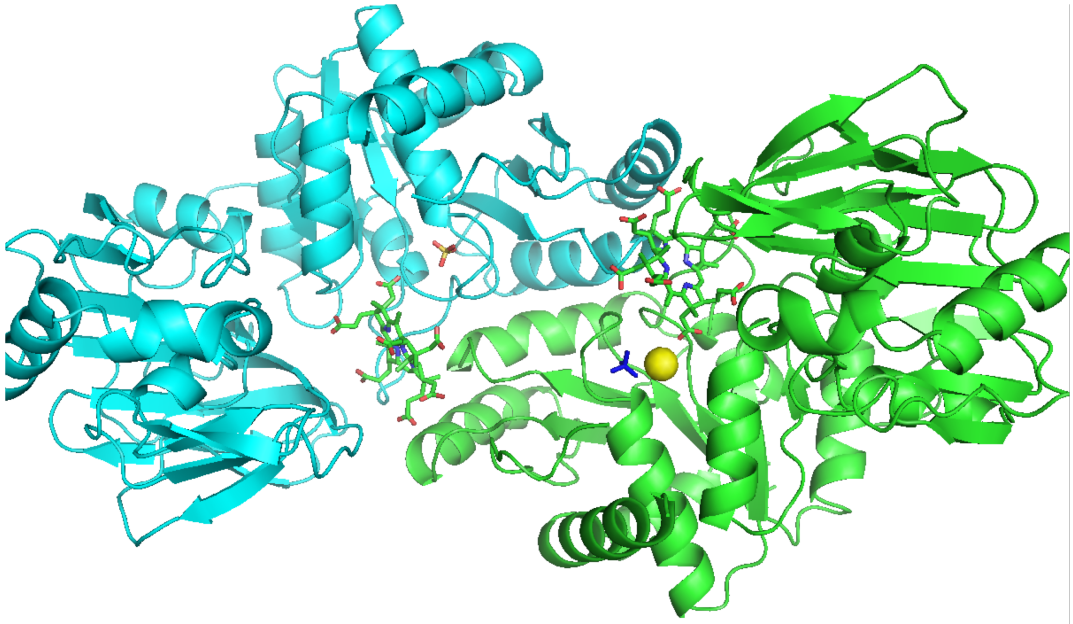

Figure 3.22: Crystal structure of *B. melitensis* CobB/HBA. Cartoon structure of the CobB dimer showing HBA (stick) bound in both subunits. The phosphate (blue) and magnesium (yellow) ions are also shown.

A comparison of the apo structure to the HBA bound structure indicates that no major conformational change has taken place with the binding of HBA to CobB. In the CobB/HBA structure each monomer of the dimer has a HBA molecule bound (Fig 3.22). The molecule is positioned with C2 and C7 of the ring facing into the active site and the other 5 carboxylates facing towards the C-terminal. There is also evidence of the presence of phosphate in both molecule A and molecule B and magnesium in molecule A. As magnesium is present in the purification buffers this was not surprising. However, the presence of phosphate was unexpected as there is no free phosphate present in the buffers or the crystallisation condition. The phosphate is located in close proximity to C7, and aligned in a way that it indicated the site was

primed for amidation. Addition of AMPPNP did not alter the structure of CobB in any way from that of the HBA-only structure. The presence of AMPPNP confirmed that C7 was amidated before C2 as the phosphate from the AMPPNP directly faces the corrin substrate (Figure 3.22, Table 3.5).

The CobB active site contained a number of residues that are observed to be conserved from protein sequence alignments, including Gly39, Pro40, Asp41, Tyr42, Asp44 and Pro45, which are believed to be involved with anchoring the HBA in place.

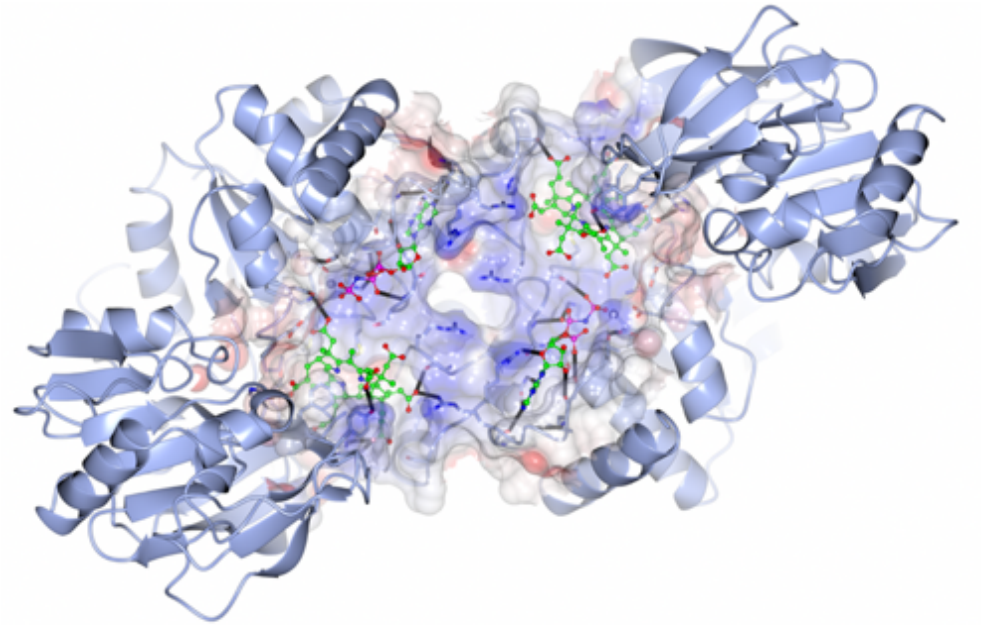

3.23: *B. melitensis* CobB/AMPPNP/HBA. Ribbon diagram highlighting the binding of HBA and AMPPMP (ball and stick representation) to CobB.

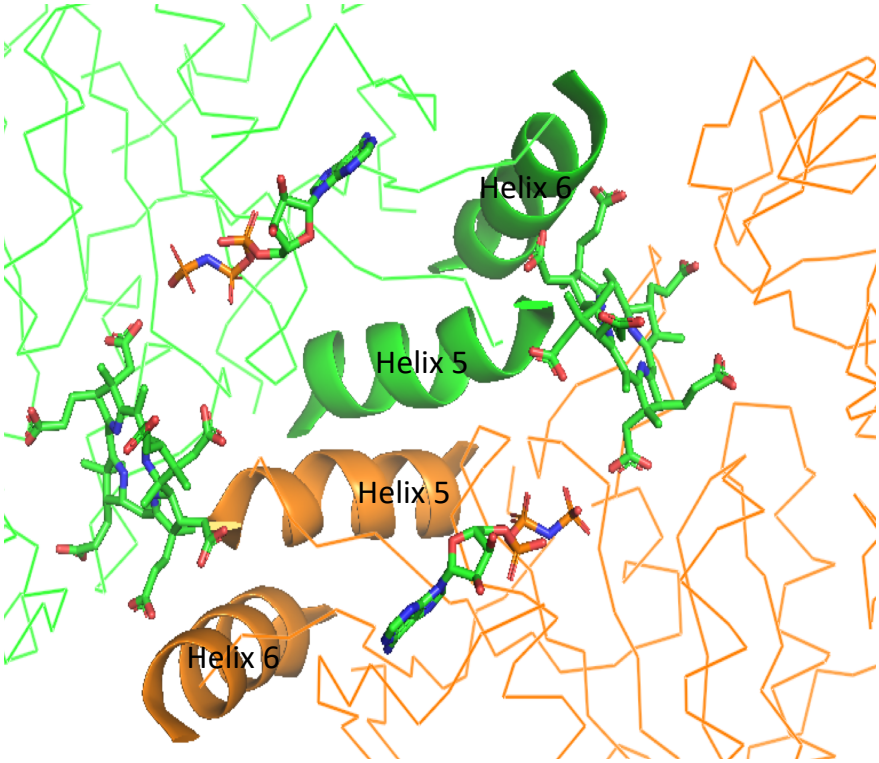

Figure 3.24: Active site of CobB showing the binding of ATP and HBA. The figure shows how helices 5 and 6 of the opposite monomer are involved in binding of HBA to the active site. This shows how dimer formation is necessary for HBA binding.

From the crystal structures the alpha 5 and alpha 6 helices in the N-terminus of each monomer contribute to the binding of HBA. This explains why dimer formation is necessary for binding of the substrate (Figure 3.24).

Table 3.5 Summary of crystallographic data and refinement statistics for CobB/HBA. RMSD – root mean squared deviation.

Data collection		**Refinement**	
Source	SOLEIL Proxima2	Resolution	1.83
Wavelength	0.98397	No. reflections	69149 (5134)
Oscillation range	0.1	R_{work} / R_{free}	0.183/0.220
Space group	P1	**No. atoms**	
Number of frames	360	**Beam Intensity**	50m 5% transmission
Molecules/a.s.u	2	Protein	5260
Cell dimensions *a, b, c* (Å)	56.05, 57.77, 75.40	Ligand/ion	78/31
Cell dimensions α, β, γ (°)	82.48, 68.58, 73.24	Water	383
Resolution (Å)	44.05-1.95	***Average B factors***	
R_{merge}	0.076 (1.168)	Protein	39.44
I / σI	9.7 (1.0)	Ligand (s)	47.94/46.74
CC 1/2	0.9654 (0.463)	Water	43.81
Total number of observations		***R.m.s deviations***	
Total number of unique		Bond length (Å)	0.016
Completeness (%)	98.0 (98.4)	Bond length (°)	1.770
Redundancy	3.3 (3.5)	PDB ligand code	HBA

Table 3.6 Summary of crystallographic data and refinement statistics for CobB/HBA/AMPPNP. RMSD – root mean squared deviation.

Data collection		**Refinement**	
Source	SOLEIL Proxima2	Resolution	2.01
Wavelength	0.98397	No. reflections	53212 (3925)
Oscillation range	0.1	R_{work} / R_{free}	0.195/0.237
Space group	$P2_1$	**No. atoms**	
Number of frames	600	**Beam Intensity**	
Molecules/a.s.u	4	Protein	5260
Cell dimensions *a, b, c* (Å)	55.62, 186.47, 89.39	Ligand/ion	70/52
Cell dimensions α, β, γ (°)	90, 90.22, 90	Water	335
Resolution (Å)	53.31-2.79 (2.90-2.79)	***Average B factors***	
R_{merge}	0.222 (1.158)	Protein	48.58
I / σI	5.3 (1.4)	Ligand (s)	81.17/60.84
CC 1/2	0.972 (0.393)	Water	48.6
Total number of observations	152516 (15305)	***R.m.s deviations***	
Total number of unique	44751 (4589)	Bond length (Å)	0.013
Completeness (%)	97 (95.6)	Bond length (°)	1.523
Redundancy	3.5 (3.1)	PDB ligand code	HBA

3.7.3 Structure of C327A CobB

The essential catalytic residues within the C-terminal domain of CobB include C327 and H427, In order to determine the importance of these residues in the *B. melitensis* CobB two variants of the enzyme were cloned with mutations at these position C327A and position H427A. The same protocol as previously used for CobB expression and purification was employed. The C327A variant expressed and behaved well producing 10 mg/L of enzyme. However, the H427A variant yielded very little enzyme and was not used in crystallisation trials. Initial crystal trials were set up using protein from the C327A variant. The protein produced crystals, including crystals grown in the presence of either Gln or with HBA/ATP/Mg^{2+}/Gln. Unfortunately, the crystals obtained with Gln did not show the presence of this substrate molecule in the crystal structure. However, the crystals grown with HBA/ATP/Mg^{2+}/Gln gave data to 1.6 Å. There was no turnover of HBA to HBAD, which confirms that the cysteine residue is necessary for CobB activity (Table 3.7).

Table 3.7 Summary of crystallographic data and refinement statistics for CobB mutated. RMSD – root mean squared deviation.

Data collection		**Refinement**	
Source	Diamond I03 Mx16207-13	Resolution	1.6
Wavelength	0.91587	No. reflections	106816
Oscillation range	0.1	R_{work} / R_{free}	0.23/0.267
Space group	P_1	**No. atoms**	
Number of frames	360	**Beam Intensity**	50m 5% transmission
Molecules/a.s.u	2	Protein	6720
Cell dimensions *a, b, c* (Å)	55.7 57.9 74.6	Ligand/ion	137
Cell dimensions α, β, γ (°)	82.88 68.99 73.04	Water	291
Resolution (Å)	55.06-1.56 (1.59 – 1.56)	***Average B factors***	
R_{merge}	0.0453 (0.4376)	Protein	16.77
I / σI	6.63 (1.07)	Ligand (s)	53.85
CC 1/2	0.9971 (0.5290)	Water	29.99
Total number of observations	15169	***R.m.s deviations***	
Total number of unique	7600	Bond length (Å)	0.020
Completeness (%)	95.46	Bond length (°)	1.985
Redundancy	3.3 (2.8)	PDB ligand code	-

3.7.4: Crystal structure of *B. melitensis* with HBAM (hydrogenobyrinic acid *c*-monoamide)

CobB is a multi-functional enzyme that amidates firstly at the C7 position of HBA and then the C2 position to give the product HBAD. The mono-amidated intermediate is HBAM. Attempts were made to obtain crystals of CobB with HBAM bound. To achieve this 1 mL of 200 µM HBAM (supplied by Joe Baker, University of Kent) and 5 mM AMPPMP were added to 3.5 mL of 0.8 mg/mL CobB. The complex was diluted 3 times in Tris-HCl buffer, pH 8.0, (3 x 15 ml) using a 30 kDa cut off centricon, a process which helps to remove any unbound substrate from the enzyme.

Crystallisation trials were initiated with Molecular Dimension screens 1 and 2 at a protein concentration of 4 mg/mL. Small crystals appeared in a number of the drops but were not of a high enough quality required for X-ray diffraction. Optimisation of the most promising condition (1.8 M ammonium sulphate) produced slightly larger crystals (Figure 3.25). The crystals grew with ammonium sulphate as precipitant and took about 4 days to grow to a size suitable for X-ray diffraction. The golden colour of the crystals suggested that HBAM had bound to the active site of CobB. The crystals were cryogenically frozen using 25 % (v/v) ethylene glycol and were found subsequently to diffract to high resolution.

The crystals diffracted to 1.5 Å resolution, with a space group of P1 and, cell dimensions of 55.9 Å x 58.04 Å x 75.156 Å, $\alpha = 82.190, , \beta = 68.61$ and $\gamma = 73.11$ with 2 molecules in the AU (Table 3.8)

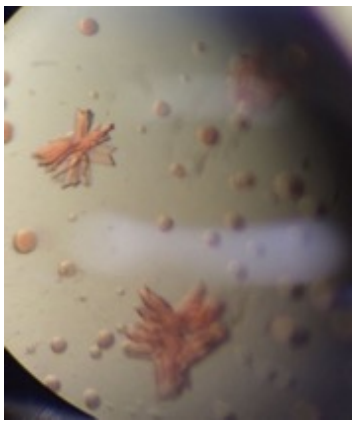

Figure 3.25: Crystals of CobB grown in the presence of HBAM. The picture shows a number of orange-coloured clumped crystals together with some orange-coloured spheres.

The HBAM crystal structure showed that, in comparison to HBA, the HBAM had rotated 90° in relation to the previously obtained position of HBA, consistent with it being in a conformation that allows C2 to be amidated (Figure 3.26). The question arises as to how this reaction takes place in the enzyme, it is possible that the enzyme simply rotates in the active site, allowing C2 to be in the position for amidation. Another possibility is that the molecule leaves the active site, rotates and then returns in the correct orientation.

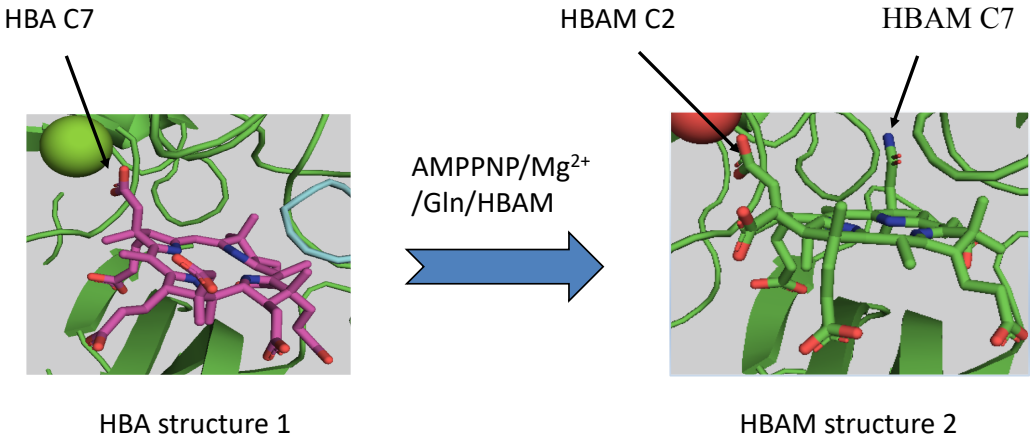

Figure 3.26: Active site of CobB bound to HBA and HBAM. (a) The carboxylate at C7 is positioned close to AMPPNP. There is also a magnesium ion (green) that sits between the AMPPNP and the HBA. (b) The structure with HBAM reveals the macrocycle has rotated so that C2 is now in the correct orientation for amidation.

Table 3.8 Summary of crystallographic data and refinement statistics for CobB/HBAM. RMSD – root mean squared deviation.

Data collection		**Refinement**	
Source	Diamond I03	Resolution	1.53
Wavelength	0.91587	No. reflections	
Oscillation range	0.1	R_{work} / R_{free}	0.20/0.23
Space group	P2	**No. atoms**	
Number of frames	360	**Beam Intensity**	50m 5% transmission
Molecules/a.s.u	2	Protein	6275
Cell dimensions *a, b, c* (Å)	55.9 58.04 75.156	Ligand/ion	136
Cell dimensions α, β, γ (°)	82.190 68.61 73.11	Water	144
Resolution (Å)	55.06-1.56 (1.59 – 1.53)	***Average B factors***	
R_{merge}	0.0462 (0.4668)	Protein	6253
I / σI	6.85 (1.01)	Ligand (s)	41.86
CC 1/2	0.995 (0.5844)	Water	43.15
Total number of observations	117409	***R.m.s deviations***	
Total number of unique	30421	Bond length (Å)	0.0318
Completeness (%)	93.84 (80.89)	Bond length (°)	1.5
Redundancy	3.1 (2.8)	PDB ligand code	-

3.7.5 Structure of an incomplete HBAD phosphorylated Intermediate

From the previous structures it seems likely that ATP binds CobB first followed by HBA, prior to the generation of a phosphorylated intermediate (Figure 3.27). Ammonia

is transported from the C-terminal active site via a molecular tunnel to the ATP/HBA binding site (Huang, Holden and Raushel 2001) (Raushel, Thoden and Holden 2003) where the phosphorylated carboxylate intermediate is then amidated by ammonia at the C7 position. This is followed by a second amidation step at C2 resulting in the product HBAD.

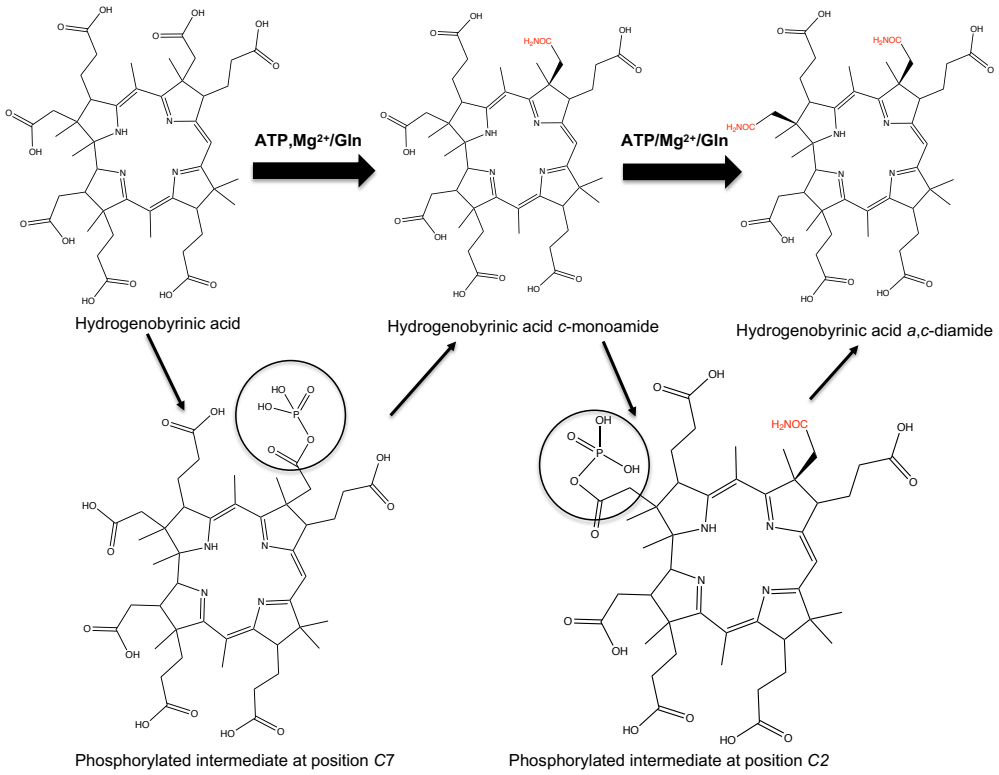

Figure 3.27: **CobB stepwise conversion of HBA into HBAD.** CobB binds HBA in the presence of ATP, Mg^{2+} and Gln. This activates the enzyme for turnover of HBA to producing firstly HBAM and then HBAD the product. Diagram showing the phosphorylated intermediates formed at each stage of the transformation of HBA into HBAD.

Crystal trays were set up in the presence of CobB/HBA/ATP/Mg^{2+}/Gln in the hope of obtaining CobB bound to its product HBAD. A number of small crystals appeared after a couple of days. The crystals were archived for data collection at the DLS using the same cryo conditions employed for all of the crystals. Although these crystals were small and looked to be twinned, they did diffract to a high resolution. Diffraction data was collected to 1.59 Å with cell dimensions of 55.76 Å x 55.76 Å x 58.09 Å, α =

82.260, β = 68.650 and γ = 72.920 with 2 molecules in the AU (Table 3.9). The structure was solved by molecular replacement. Surprisingly the structure showed a phosphorylated intermediate (Figure 3.28) with the phosphate attached to the carboxylic acid of the acetic acid side chain on C2. This was obvious from the electron density where the C2 position is clearly extended (Figure 3.29). Within the enzyme structure the C2 position of the corrin is in closer proximity to the resultant ADP molecule.

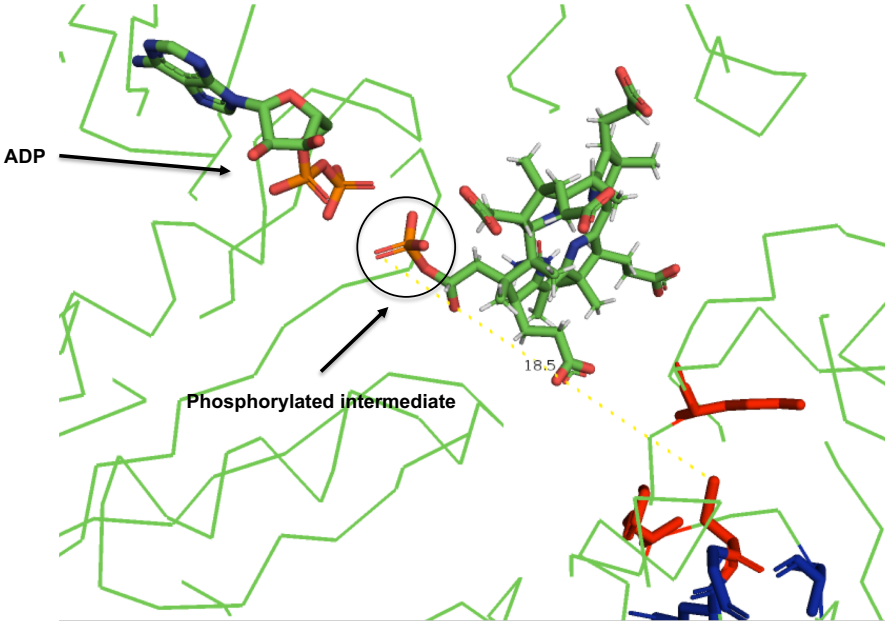

Figure 3.28: Trace of CobB with the phosphorylated intermediate of HBAMP. Ball and stick showing the backbone of CobB binding HBAMP (C2) binding in the active site close to a molecule of ADP (does not show side chains).

Although there is no evidence of a conformational change, when the structure of HBAM is overlaid with the position of the phosphorylated intermediate some distortion of the corrin ring appears to have taken place. On closer inspection it looks like that on phosphorylation HBAM is pulled closer to the ATP molecule (Figure 3.30).

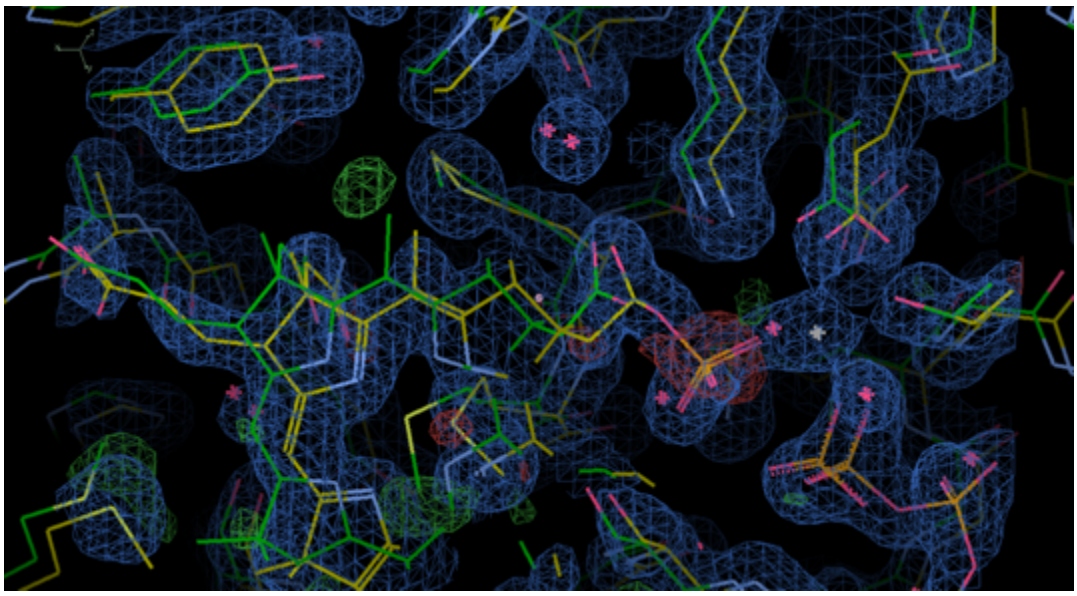

Figure 3.29: Electron density map of CobB monoamide structure overlaid with CobB diamide phosphate intermediate. CobB/monoamide structure (green) shows C2 positioned for amidation, and CobB phosphorylated intermediate (yellow) picture shows C2 which is phosphorylated. The residues around the active site (green) for HBAM and HBAM-phosphorylated (yellow) show the differences between the two structures.

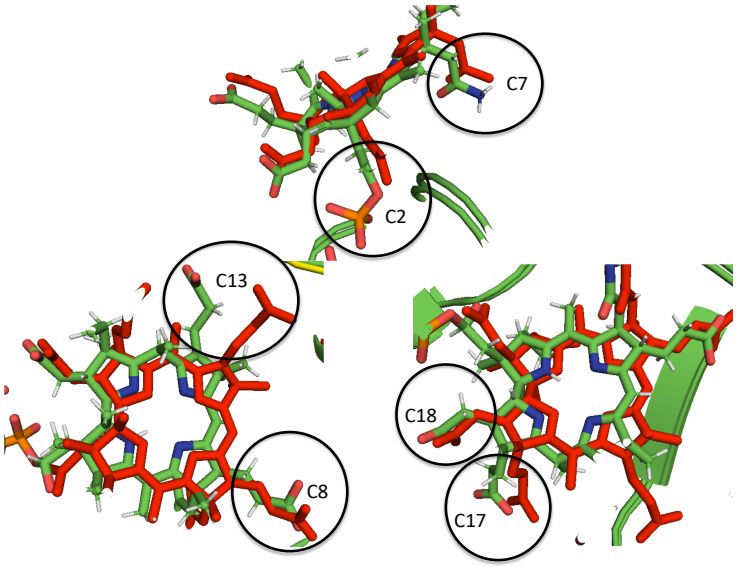

Figure 3.30: HBAM and HBAMP overlaid. Close up of the individual carboxylates C2, C7, C8, C13, C17 and C18 showing distortion in the ring. The phosphorylated intermediate is shown in green whilst HBAM is shown in red.

Table 3.9 Summary of crystallographic data and refinement statistics for CobB/HBAM phosphorylated intermediate. RMSD – root mean squared deviation.

Data collection		**Refinement**	
Source	Diamond I03	Resolution	1.59
Wavelength	0.91587	No. reflections	102986
Oscillation range	0.1	R_{work} / R_{free}	0.20/0.24
Space group	P1	**No. atoms**	
Number of frames		**Beam Intensity**	
Molecules/a.s.u	2	Protein	6309
Cell dimensions *a, b, c* (Å)	55.760 58.090 74.780	Ligand/ion	190
Cell dimensions α, β, γ (°)	82.260 68.650 72.920	Water	318
Resolution (Å)	69.61-1.59	***Average B factors***	
R_{merge}	0.0761 (0.7554)	Protein	24.3
I / σI	9.78 (1.00)	Ligand (s)	35.44
CC 1/2	0.9756 (0.4501)	Water	31.2410
Total number of observations	108234	***R.m.s deviations***	
Total number of unique	45000	Bond length (Å)	0.018
Completeness (%)	96.4 (95.00)	Bond length (°)	1.990
Redundancy	3.4 (3.1)	PDB ligand code	-

3.7.6: Crystal structure of CobB/HBAD

In order to try and obtain a crystal structure with HBAD bound, crystal trays were prepared using CobB/HBAD and ADP. From the initial screen tiny crystals were obtained, although the crystals appeared to be badly twinned. Nonetheless, these crystals were sent to the DLS for data collection. The crystals diffracted to 2.5 Å with a space group P1 and cell dimensions of 56.05 Å, 57.77 Å, 75.4 Å, α = 82.26 β = 68.65, γ = 72.92. with 2 molecules in the AU.

The structure was solved by molecular replacement. HBAD was docked into the active site but the orientation of the molecule did not fit with the density. On closer inspection, the molecule in the active site appeared to be HBA with the C7 carboxylate where the C2 should be. The reason for this is unclear and further investigation would be required. No further work was carried out to solve this structure.

3.8. Discussion

The *B. melitensis* CobB is the first amidase of the vitamin B_{12} pathway to have its structure determined at high resolution. Initial heavy atom soaks with this enzyme were unsuccessful, however, Se-met crystals of the *B. melitensis* CobB were obtained which enabled determination of the first structure of this enzyme. The structure was partially solved with these crystals whilst molecular replacement was used to complete the structure. The initial crystal diffracted to 1.7 Å resolution and was solved using single anomalous diffraction (SAD). The crystals grew in bunches (Figure 3.18) but once separated the crystals diffracted to high resolution.

All of the crystal structures of CobB show that the protein is composed of two globular domains: An N-terminal amidotransferase domain that binds ATP, Mg^{2+} and HBA and a C-terminal domain that binds Gln. These domains are connected by a long flexible region. For this reaction to go to completion, ATP, Gln and Mg^{2+} must be present to allow the formation of the product (HBAD). In the initial structure of CobB no ATP was added to the enzyme prior to crystallisation. However, the structure of the enzyme revealed the presence of ADP in one of the monomers whilst the other monomer contained ADP and a free phosphate. The presence of ADP reflects that it must be carried by the enzyme during the purification process.

From the structural information ATP binds in the N-terminal binding site, Mg^{2+} activates the ATP (Ko, Hong and Pedersen 1999) ATP is then hydrolysed to ADP, the free phosphate forms a phosphorylated carboxylate at positions C7 on the HBA macrocycle, ready for amidation.

The GAT domain is divided into two subfamilies, which are termed type I and II. CobB resembles the class 1 of GAT domain enzymes although it lacks the third residue (Glu) in the catalytic triad associated with this family of enzymes (Cys, His and Glu).

The oxyanion hole in the class 1 type enzymes is believed to stabilise the negative charge on the oxygen atom on the tetrahedral intermediate that results from attack of the cysteine residue on Gln (Trotta *et al.* 1974).

The crystal structure of *B. melitensis* CobB shows that the active sites of the α and β subunits are 17.7 Å apart (Figure 3.31). For the two domains in the catalytic sites to come together would require a major conformational change. However, no such major conformational change is observed in any of the CobB crystal structures.

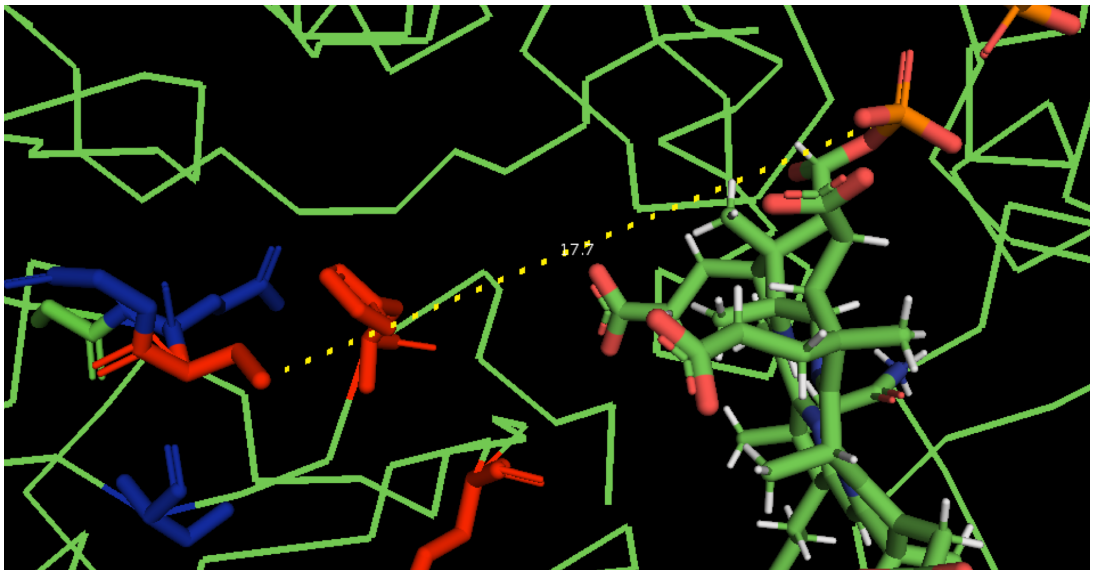

Figure 3.31: Distance between the two distinct actives sites in CobB. The distance between the conserved cysteine (Cys327 in C-terminal domain) and the phosphorylated intermediate in the N-terminal domain is highlighted as a dotted line 1 reveals a largely hydrophobic area surrounding the Gln binding site, which is similar to other enzymes containing molecular tunnels (Miles, Rhee and Davies. 1999). It is therefore plausible that *B. melitensis* CobB also uses substrate channelling to transport ammonia from the GATase domain to the amidotransferase domain by a molecular tunnel.

This suggests that CobB uses substrate channelling in order to transport ammonia from the C-terminal domain to the N-terminal domain. A research article by Lucas Pravda *et al* analysed the active site of 4,306 enzymes, which all had channels of greater than 15 Å long. They showed that 64 % of enzymes contained two or more long channels. On the whole, the channel tends to have more aromatic residues such as His, Trp, Tyr and Cys. CobB has a tunnel of 17.7 Å long, and the channel has Tyr, Pro, His and Asp the length of the tunnel (Pravda *et al.* 2014).

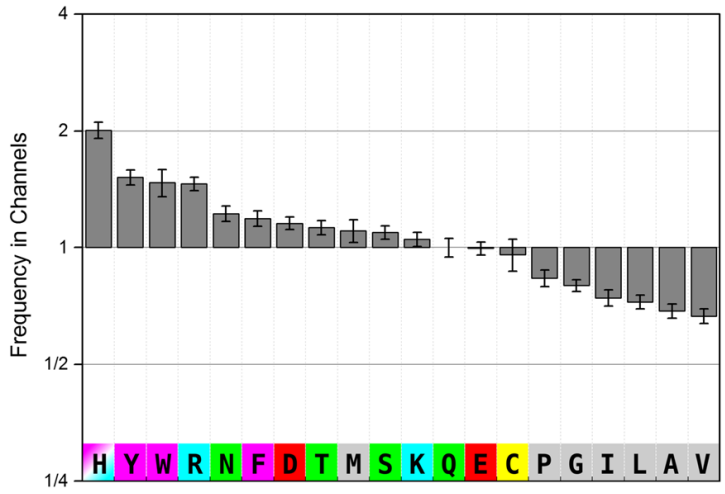

Figure 3.32: Channel frequency of amino acids. Enhancement of frequencies of individual amino acids in channels indicates which amino acids are more likely to occur in the channel walls than anywhere else in the protein structure. Hydrophobic aliphatic residues are shown in grey, aromatic amino acids in magenta, polar residues in green, negatively charged in red, positively charged in blue and cysteine in yellow (Pravda *et al.* 2014).

Site directed mutagenesis of the CobB to generate a Cys327Ala variant allowed an investigation into the role played by this amino acid for activation. This structure was solved in the presence of HBA/ATP/Mg^{2+}/Gln. If the variant was active it would result in the production of HBAD when supplied with HBA, ATP and Gln. As this did not happen it confirmed that the Cys327 is essential for enzyme activity.

The class 1 Triad family of GAT enzymes normally contain a conserved His-Cys-Glu motif in their active site. However, although CobB is considered part of this family it does not have the conserved Glu. Nonetheless, there is a conserved Glu in the CobB family of proteins, which given its position within the active site, suggests that this

alternative Glu likely forms the third member of this Triad family (Figure 3.33).

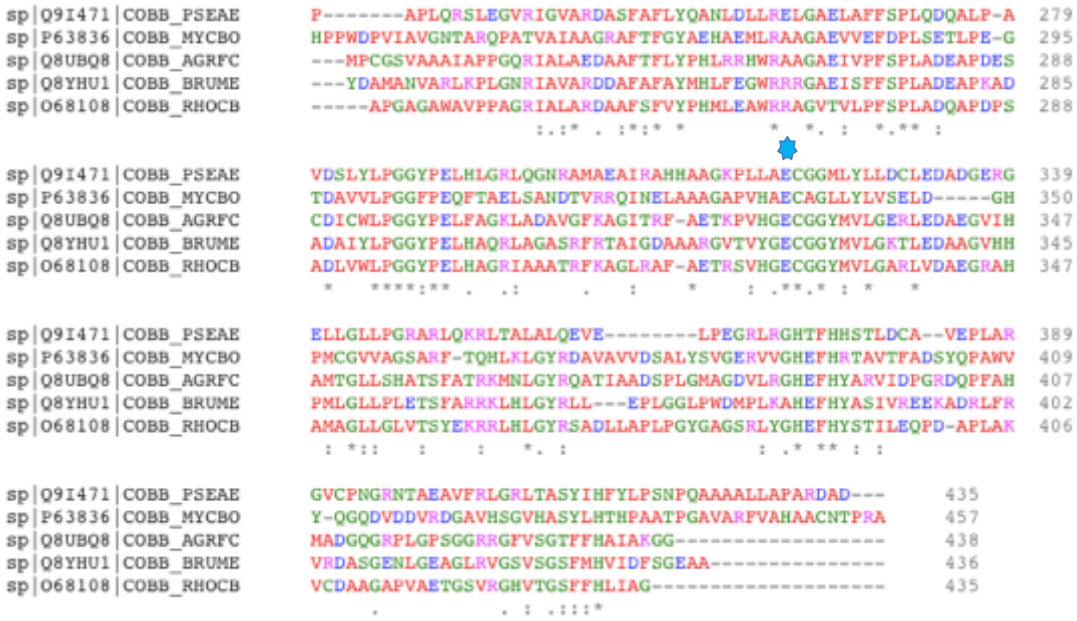

Figure 3.33: Amino acid sequence alignment of CobB proteins. Q91471 (*Pseudomonas aeruginosa*), P63836 (*Mycobacterium bovis*), Q8UBQ8 (*Agrobacterium fabrum*), Q8YHU1(*Brucella melitensis*) and 068108 (*Rhodobacter capsulatus*). Conserved Glu residue shown with blue star. (Figure generated by Clustal Omega, EMBL-EBI).

Chapter 4

Stopped Flow analysis of binding of *Brucella melitensis* CobB with substrates and product

4.1 Introduction

The X-ray crystal structures discussed in Chapter 3 of the *B. melitensis* CobB represent the first molecular description of this enzyme. These structures have helped in understanding the mechanism underpinning the amidation process of this enzyme. CobB is a multifunctional enzyme that employs two distinct active sites to catalyse firstly the deamidation of Gln and then secondly the amidation of HBA. Moreover, it repeats the same amidation chemistry at two sites on the corrin substrate, initially at position C7 where HBA is amidated to HBAM and subsequently at C2 to produce HBAD (Fresquet, Williams and Raushel 2004).

Debussche *et al* looked at CobB from *Pseudomonas denitrificans* and determined the catalytic properties and substrate specificity of this enzyme using steady state kinetic analysis. By this approach they determined K_m values of CobB for HBA (0.41 μM), HBAM (K_m = 0.21 μM), Gln (K_m = 20.3 μM) and ATP (K_m = 30.2 μM) (Debussche *et al.* 1990).

Cobyrinic acid *a, c*-diamide synthetase from *Salmonella typhimurium* (CbiA) is the equivalent enzyme to CobB from the anaerobic pathway. Fresquet *et al* determined the kinetic data for this enzyme (Fresquet, Williams and Raushel 2004). CobB and CbiA share a reasonable degree of identity (40%) and perform the same amidations albeit on slightly different corrin substrates. For CbiA, the activity of the C-terminal and N-terminal domains of the protein were studied separately. They showed that

CbiA was able to hydrolyse Gln (K_m = 49 μM) in the absence of cobyrinic acid or ATP, which suggests there is no crosstalk between the two domains. However, V. Fresquet *et al* 2004 noted that when ATP or glutamic acid was added there was an enhanced rate of Gln hydrolysis. This was enabled by a two-fold lowering of the K_m for Gln in the presence of ATP (K_m = 2.5 μM) and a 20 x fold decrease with glutamic acid present (K_m = 25 μM) (Fresquet, Williams and Raushel 2004).

However, the decrease in the K_m for Gln is substantially larger (200-fold) when both ATP and cobyrinic acid (K_m = 0.2 μM) are present in solution. They surmised that the reduction in the *Km* for Gln must originate from conformational changes in the binding site for Gln that are allosterically induced by the binding of substrates to the synthetase domain (Fresquet, Williams and Raushel 2004).

Fresquet *et al* also went on to hypothesise that the conformational change could be induced by the formation of a phosphorylated intermediate of cobyrinic acid, before amidation to cobyrinic acid *c*-monoamide. The X-ray crystal structure of *B. melitensis* CobB is a dimer and shows both monomers occupied by a phosphorylated intermediate of hydrogenobyrinic acid *c*-monoamide after amidation (see Chapter 3). Interestingly, when the structures of the HBAM-bound enzyme and the form containing a phosphorylated intermediate are superimposed, there appears to be a slight distortion of the substrate, resulting in change in conformation of the propionic acid attached to the C13 position (Figure 4.1). However, there did not seem to be any conformational change in the enzyme itself.

Gln binds at a separate site in the C-terminal domain, whereas HBA/ATP binds in the N-terminal domain. As there is no X-ray crystal structure of Gln bound at the C-terminal domain, it is not possible to say if Gln induces a conformational change in the enzyme.

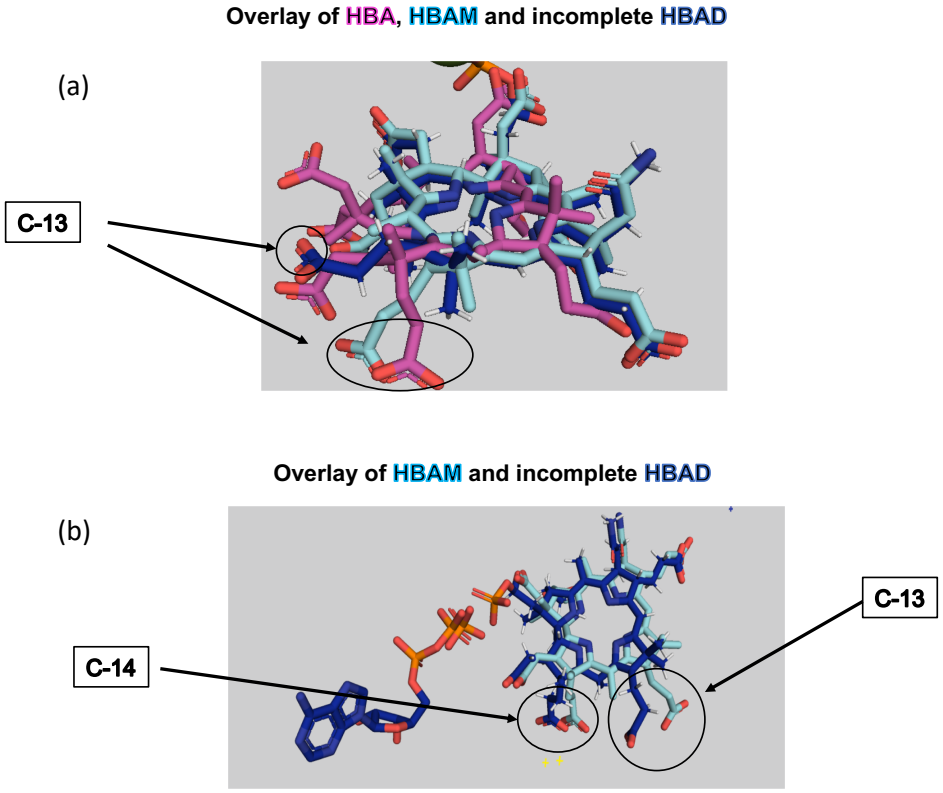

Figure 4.1: Overlay of substrates HBA, HBAM and HBAD when bound to CobB. (a) Shows all three substrates overlaid, where the side chain attached to C-13 on the corrin ring has a different conformational. (b) The binding of HBAM and HBAD show that the side chain attached to C-13 has undergone a conformational change with a slight movement in the side chain attached to C-14.

In order to obtain kinetic information that would complement the structural data, stopped flow analysis was undertaken (Toseland and Geeves 2014). This method is mostly commonly employed for transient type reactions where the reaction occurs at a very fast rate. It can be coupled with fluorimeters and spectrophotometers to look at changes in the fluorescence or the absorbance of a protein on binding of a substrate. Fluorescence signals can be attributed to the protein if it contains tryptophan or tyrosine residues as they are known to have inherent fluorescence properties (Rehms and Callis 1993). However, if the substrate also has strong absorbance or fluorescence properties, then these can also be measured.

From the crystal structure of CobB it can be seen that there are a number of tyrosine residues in the HBA binding site. In addition to the aromatic residues at the binding site, the substrate, HBA, also has a conjugated π system, which gives it fluorescence properties. With this in mind it was envisioned that fluorescence emission spectroscopy and stopped flow analysis could be performed to monitor binding to the protein. This would provide kinetic data for this reaction, and complement the recently determined structural information. Using stopped-flow spectroscopy to look at the individual steps of this reaction could give valuable information on reaction rates, identifying rate limiting steps and substrate and product binding (Woalder Xiwe *et ali* Zheng, Cong Bi, Zhao Li, Maria Podariu 2017) (Toseland and Geeves 2014).

In order to identify the optimal reporter system to monitor binding, fluorescence emission spectra were run. This involved two separate experiments, firstly looking at the intrinsic properties of the protein and secondly looking at the emission spectra for he substrate. Once optimum conditions were identified stopped flow analysis of the *B. melitensis* CobB was performed in order to gain insight into the reaction catalysed by the enzyme.

4.2 Results

4.2.1 Fluorescence-emission spectra measuring protein fluorescence

The basis of stopped flow analysis relies on significant changes in absorbance or fluorescence emission when the enzyme and substrate interact. Therefore, it is important to know the optimum wavelength to be monitored during the reaction.

It was predicted that as the ATP/substrate binding site of CobB has a number of tyrosine residues (Y257, Y295, Y366 and Y388) present it may be possible to measure the binding affinity of HBA using the protein's intrinsic fluorescence (Eccleston, Martin and Schilstra 2008). This was investigated by monitoring the fluorescence-emission spectra from 300 nm to 700 nm after excitation of the protein at a wavelength of 280 nm. CobB, by itself, has fluorescence emission peaks at 350 nm and another at 650 nm. HBA by itself shows no fluorescence when excited at the same wavelength. When CobB (1 μM) was mixed with a sample of HBA (10 μM) and was excited at 280 nm the fluorescence emission spectra showed a reduction in the peak at 330 nm together with a new emission peak at 540 nm and 600 nm. This confirmed that when CobB binds HBA there is a significant change in the fluorescence emission spectrum reflecting the binding of the corrin substrate. These results suggested that protein fluorescence could be used for stopped flow analysis (Figure 4.2).

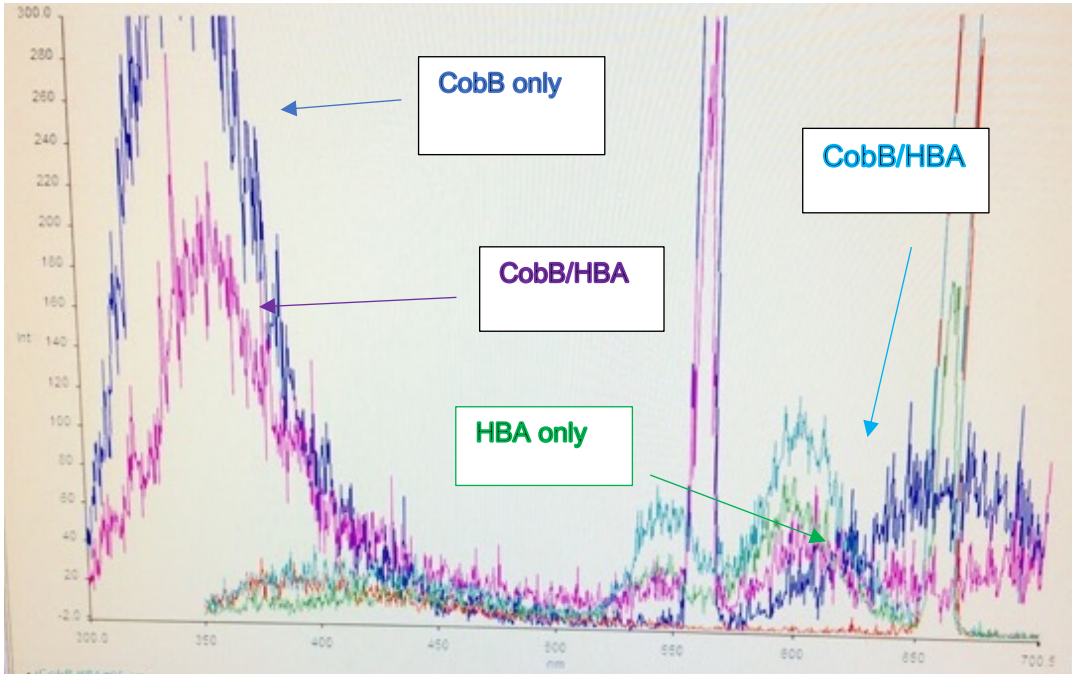

Figure 4.2: Measurement of protein fluorescence emission of CobB binding HBA. Excitation at 280 nm shows CobB by itself (dark blue) has a large peak at 350 nm and small peak at 650 nm, whereas excitation at 280 nm of CobB with HBA (pink) sees a reduction in the size of the peak at 350 nm and new peaks at 540 nm and 600 nm (intrinsic protein fluorescence). Excitation at 330 nm of CobB alone (orange) shows no peak. Excitation at 330 nm of HBA alone (green) shows peaks at 540 nm and 600 nm, whilst excitation of CobB with HBA (pale blue) at 330 nm shows an increase in the size of the peaks at 540 nm and 600 nm (corrin fluorescence).

4.2.2: Fluorescence-emission spectra measuring substrate fluorescence

Changes in the emission spectrum of the corrin substrates and product were also monitored on binding to CobB. In this case the florescence emission spectra were recorded over a range of 360 nm to 700 nm after excitation at 330 nm. When CobB (1 μM) was mixed with HBA (10 μM) and was excited at 330 nm the fluorescence emission spectrum showed peaks at 400 nm, 550 nm and 600 nm. The same conditions were used to measure the fluorescence spectrum for CobB binding HBAM. This gave the same spectrum as CobB binding HBA. However, again keeping

conditions constant, CobB in the presence of HBAD showed an increase in the peak size at 540 nm and 600 nm, with a new emission peak at 440 nm (Figure 4.3).

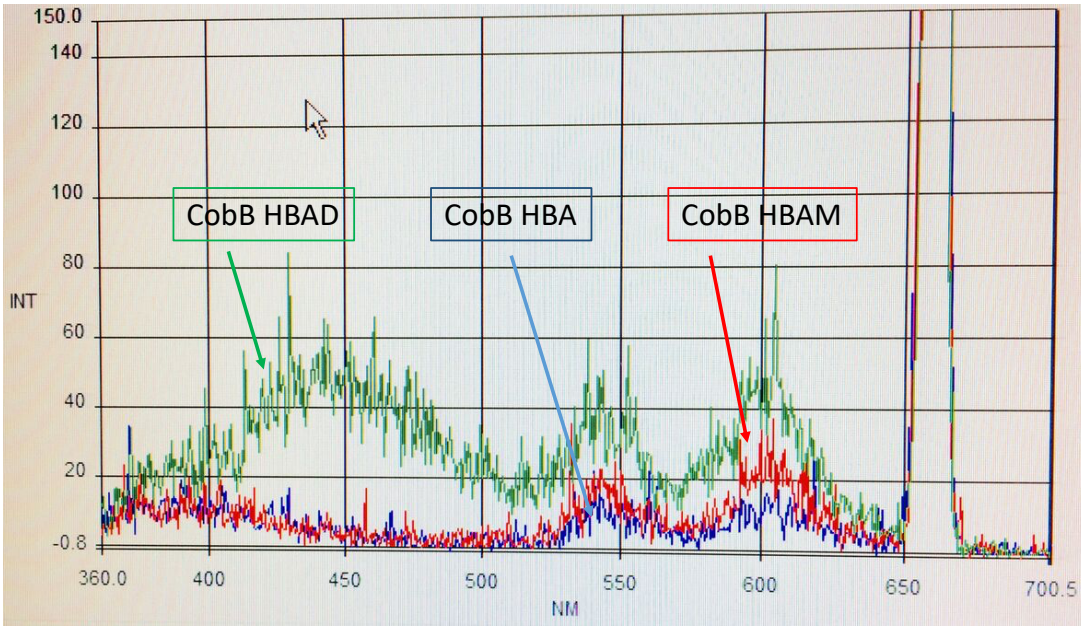

Figure 4.3: Fluorescence from HBA, HBAM and HBAD binding to CobB. Samples were excited with a wavelength of 330 nm. CobB/HBA peaks (dark blue) are observed at 400 nm, 540 nm and 600 nm, CobB/HBAM peaks (red) are observed at 400, 540 nm and 600 nm and HBAD peaks (green) are observed at 440 nm, 540 nm and 600 nm.

4.2.3: Stopped-Flow analysis using substrate fluorescence

4.2.3.1 Stopped flow experimental parameters

The fluorescence emission spectra gave a clear indication of binding using both the intrinsic protein fluorescence and substrate fluorescence. Although either approach could have been used it was decided to use the substrate fluorescence for monitoring its binding to CobB.

Stopped flow was performed with CobB (1 μM) in one of the two syringes on the stopped flow apparatus. The other syringe contained HBA, and the concentration was increased for each data collection from 1 μM to 5 μM. At the start of the experiment

each syringe injects 100 µL of sample into the cell where the two samples are mixed. The stop flow syringe enables data to be collected instantaneously, and usually about six samples are run at a single concentration. The average from these runs is used to give the final data for each concentration of ligand. This experiment was used to measure the fluorescence change from HBA on binding CobB by exciting at 330 nm.

4.2.3.2 Stopped-Flow analysis of CobB binding HBA

Stopped-flow fluorescence spectroscopy was used to determine the dissociation constant (K_d) associated with the binding of CobB to HBA. This experiment was carried out using a constant concentration of CobB (1 µM) and varying the concentration of HBA (between 1 µM and 10 µM). Excitation was carried out at 330 nm and fluorescence emission was measured at 450 nm. The reaction was then monitored by recording fluorescence emission changes resulting from the substrate binding to the enzyme (Figure 4.5).

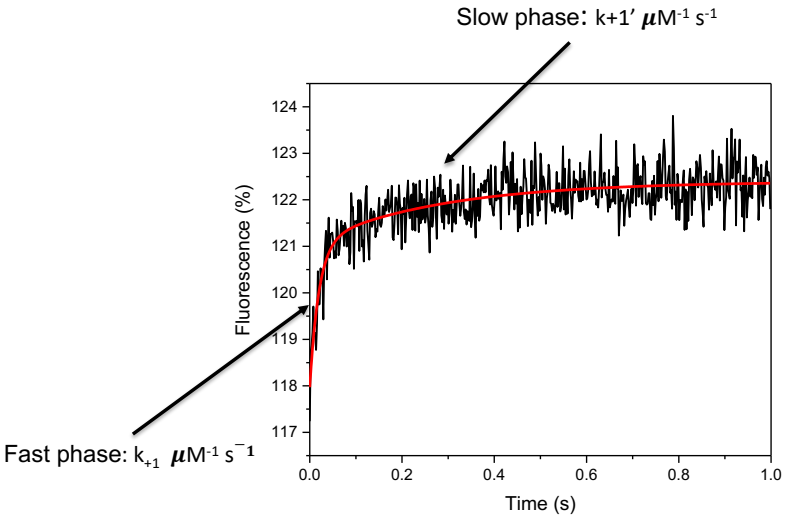

Figure 4.4: Stopped-flow trace. An example trace of the fluorescence change upon 1 µM HBA binding to 1 µM CobB. The trace shows the biphasic nature of the binding of HBA to CobB.

Figure 4.4 shows a trace taken from the stopped-flow experiment highlighting the binding of HBA to CobB. The binding of HBA to CobB shows a two phase reaction, an initial fast rate followed by a slower rate. The initial fast (burst) phase is termed R1 and is complete after 0.05 seconds. The second phase is termed R2, and lasts approximately one second. There are several possible explanations for this biphasic binding. As a homodimer, the enzyme has two active sites that bind HBA and it could be that R1 represents fast binding to one site and that R2 represents the binding of HBA to the second site. This would require that the binding of HBA to the first site leads to a change in the conformation of the second site so that it binds at a slower rate. Alternatively, the different rates could reflect an initial fast binding phase followed by a slower change in the conformation of the protein that affects the binding of HBA. It is more likely that the bi-phasic binding mode reflects the former rather than the latter.

The process of reversible binding is described in the equations in Scheme 1.

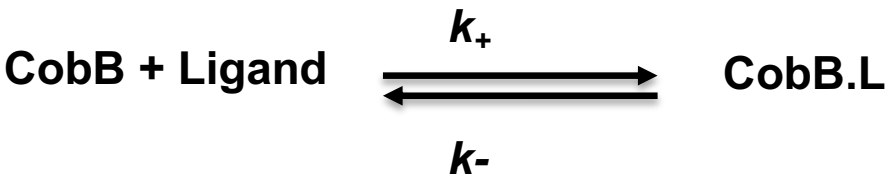

$$K_d = k_-/k_+ = [CobB]\,[L]/[CobB.L]$$

For reversible association reactions a plot of the observed rate (k_{obs}) versus concentration of protein will be a straight line. As the observed rate of reaction is a combination of both the forward and reverse reactions, $k_{obs} = k_{+1}[CobB] + k_{-1}$, when [CobB] is zero then k_{obs} will equal k_{-1}. Hence the *y*-intercept gives a value for k_{-1}.

For the interaction between CobB and HBA the initial rate data from Figure 4.4 can be determined by the use of non-linear regression to generate the k_{obs} at different CobB concentrations. The observed rates of either R1 or R2 can then be plotted against the concentration of CobB, which generate straight line graphs demonstrating that the observed rate constants are a linear function of CobB concentration. The gradient of these plots, as shown in Figure 4.5, represents k_{+1} whilst the y intercept represents k_{-1}.

(a)

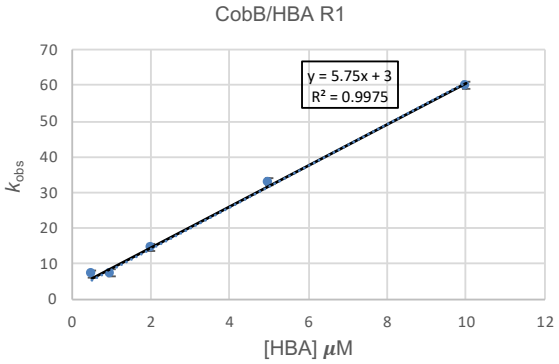

K_{d1} = 3/5.75
= 0.52 ± 0.16

(b)

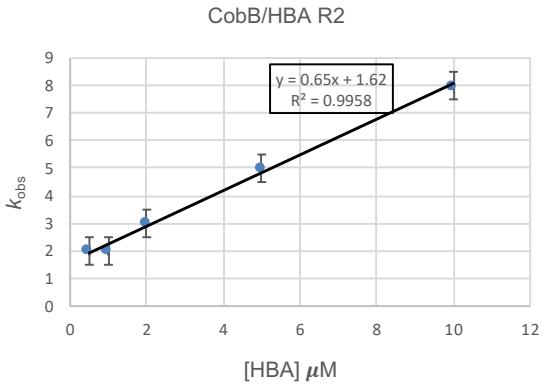

K_{d2} = 1.62/0.65
= 2.48 ± 1.01

Figure 4.5: Dependence of k_{obs} versus [HBA]. Calculation of rate constants k_{+1} (line gradient) and k_{-1} (y intercept) from stopped-flow measurements of k_{obs} at different concentrations of HBA (1-10 μM) and constant concentration of CobB (1 μM) a) the initial phase of reaction (R1), with calculated k_{+1} = 5.76 μM^{-1} s^{-1}, k_{-1} = 3 s^{-1} and K_{d1} = 0.52 μM and b) the second phase of reaction (R2) with k_{+1}' = 0.65 μM^{-1} s^{-1}, k_{-1}' = 1.61 s^{-1} and K_{d2} = 2.48 μM. Values are averages of 3 biological repeats (from three different HBA preparations) ± SEM**.** By knowing the values of k_{+1} and k_{-1} it is possible to determine K_d (Scheme 1). Thus, from Figure 4.5 it is possible to say that HBA binds to CobB relatively tightly with a K_{d1} = 0.52 μM with a rate constant of 5.76 μM^{-1} s^{-1}. This is 9 fold faster than the second step of the reaction (R2), which has an association rate of 0.65 μM^{-1} s^{-1} and a K_{d2} of 2.48 μM.

4.2.3.3 Effects of ATP on the binding of HBA to CobB

Figures 4.4 and 4.5 demonstrated that it was possible to determine the K_d for values for the binding of HBA to CobB in the absence of any other substrates. However, we wanted to know if the presence of the other substrates had an effect on either the rates of association or the K_d values. Therefore, the binding of HBA to CobB was repeated in the presence of the other substrates, the first of which was ATP. In this case the k_{obs} was monitored at a fixed concentration of CobB and ATP but with variable [HBA] (1 μM to 5 μM). The addition of ATP to the CobB/HBA sample did not appear to change the K_{d1} value, but did slow the rate at which HBA binds to CobB (R1) by 3 fold (k_{+1} = 5.76 μM^{-1} s^{-1} value without ATP and k_{+1} = 1.78 μM^{-1} s^{-1} with ATP) (Figure 4.6). This suggests that, most likely, ATP binds first to CobB, inducing a slight change in the conformation of the active site. This could hinder the binding of HBA, resulting in a slower rate of binding.

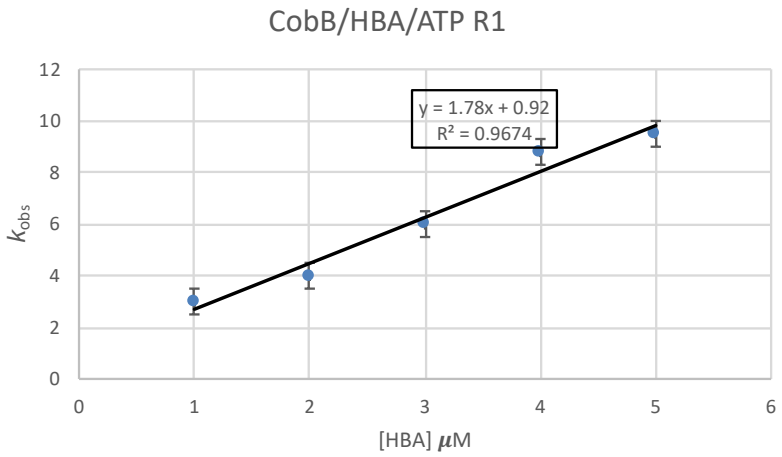

K_{d1} = 0.92/1.78
= 0.52 μM ±0.10

(b)

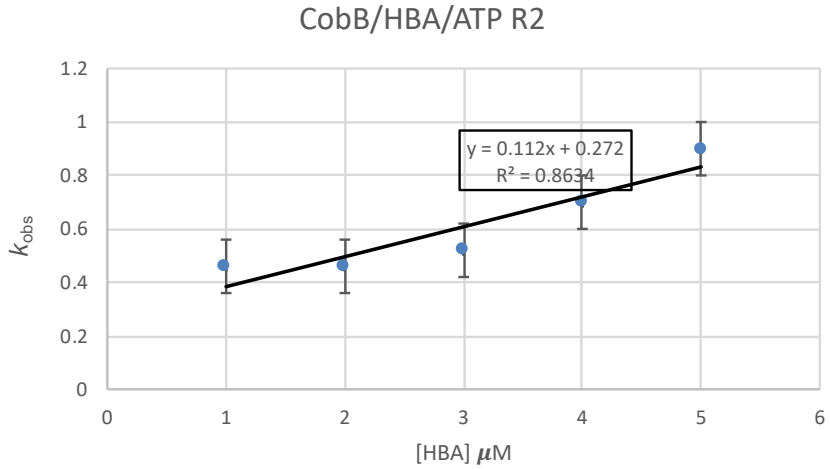

K_{d2} = 0.272/0.122
= 2.23 μM ±1.01

Figure 4.6: Dependence of k_{obs} versus [HBA] and ATP. Calculation of rate constants k_{+1}(line gradient) and k_{-1} (y intercept) from stopped-flow measurements of k_{obs} at different concentrations of HBA (1 μM – 5 μM)/ATP (5 mM) and constant concentration of CobB (1 μM). a) the initial phase of reaction (R1), with calculated k_{+1} = 1.78 μM^{-1} s^{-1}, k_{-1} = 0.92 s^{-1} and K_{d1} = 0.52 μM and b) the second phase of reaction (R2) with k_{+1}' = 0.12 μM^{-1} s^{-1}, k_{-1}' = 0.27 s^{-1} and K_{d2} = 2.23 μM. Values are averages of 3 biological repeats (from three different HBA preparations) ± SEM.

4.2.3.4 Effects of Gln on the binding of HBA to CobB

To determine the effects of Gln on the kinetics of HBA binding to CobB, the stopped-flow assay was repeated as in the previous experiments. Gln was added to CobB at a concentration of 5 mM and the concentration of the enzyme was kept constant (1 μM) and HBA was varied between 1 μM and 5 μM refer to Figure 4.7 at end of section 4.2,3,4.

(a)

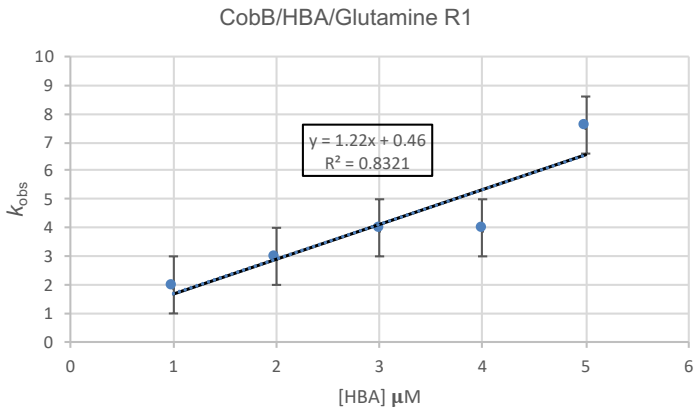

K_{d1} = 0.46/1.22
= 0.38 μM $\pm$0.33

(b)

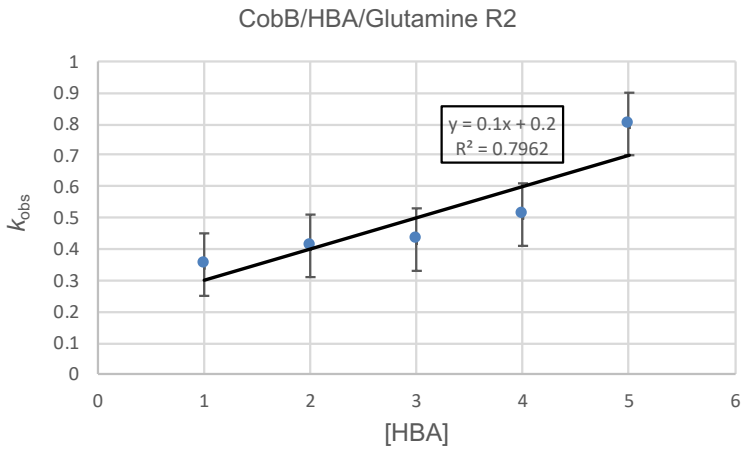

K_{d2} = 0.2/0.1
= 2 μM $\pm$1.5

Figure 4.7: Dependence of k_{obs} versus [HBA] in the presence of Gln. Calculation of rate constants k_{+1} and k_{-1} from stopped-flow measurements of k_{obs} at different concentrations of HBA (1 µM 5 µM) in the presence of CobB (1 µM)/Gln (5 mM) for a) the initial phase of reaction (R1) with CobB, with calculated k_{+1}= 1.22 µM^{-1} s^{-1}, k_{-1} = 0.46 s^{-1} and K_{d1}= 0.38 µM and b) the second phase of reaction (R2) with CobB, with k_{+1}' = 0.10 µM^{-1} s^{-1}, k_{-1}' = 0.2 s^{-1} and K_{d2} = 2 µM. Values are averages of 3 biological repeats (from three different HBA preparations) ± SEM.

The results show that the addition of Gln slightly increases the affinity of HBA binding to CobB (K_{d1} = 0.38 μM with and 0.52 μM without). The second phase K_{d2} was very similar to K_{d2} without Gln (2.00 μM and 2.48 μM respectively). The results are summarized in Table 4.1.

4.2.3.5 Effects of ATP and Gln on the binding of HBA to CobB

To complete the data set, the binding of HBA with CobB was investigated in the presence of ATP and Gln. This was accomplished by keeping a fixed concentration of CobB, ATP and Gln and varying the concentration of HBA. The results of this are shown in Figure 4.8.

(a)

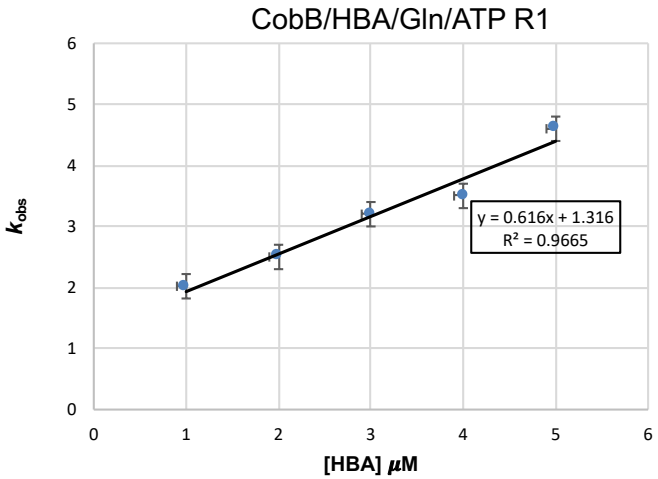

Kd_1 = 1.36/0.616
= 2.12 μM± 0.71

(b)

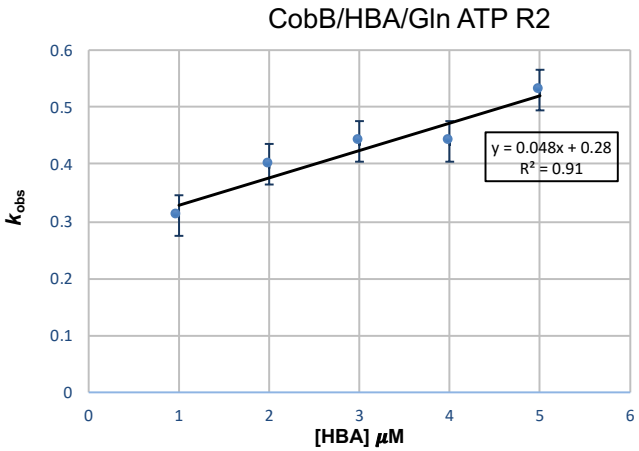

Kd_2 = 0.28/0.048
= 5.83 μM ±4.53

Figure 4.8: **Dependence of k_{obs} versus [HBA] in the presence of Gln and ATP.** Calculation of rate constants k_{+1} and k_{-1} from stopped-flow measurements of k_{obs} at different concentrations of HBA (1 μM – 5 μM) in the presence of Gln (5 mM) and ATP (5 mM) for a) the initial phase of reaction (R1) with CobB (1 μM), with calculated k_{+1} = 0.62 μM^{-1} s^{-1}, k_{-1} = 1.36 s^{-1} and K_{d1} = 2.12 and b) the second phase of reaction (R2) with CobB, with k_{+1}' = 0.05 μM^{-1} s^{-1}, k_{-1}' = 0.28 s^{-1} and K_{d2} = 5.83 μM. Values are averages of 3 biological repeats (from three different HBA preparations) ± SEM.

The largest change in the rate of binding and the affinity of HBA to CobB was the addition of both ATP and Gln. The reaction, in the presence of both Gln and ATP, had a lower affinity of binding (K_d = 2.14 μM) and a much slower reaction rate of both k_{+1} and k_{+2}', which was approximately 10 fold slower (k_{+1} = 0.62 μM^{-1} s^{-1} and k_{+1}' = 0.05 s^{1}) than binding of HBA alone. The results are summarized in Table 4.1.

Table 4.1 Rate and binding constants of HBA, HBA/ATP, HBA/Gln and HBA/ATP/Gln binding CobB.

Brucella CobB	R^2	Kd μM R1	Kd μM R2	k_{+1} $\mu M^{-1} s^{-1}$	k-1 s^{-1}	k+1' $\mu M^{-1} s^{-1}$	k-1' s^{-1}
HBA	0.998	0.52	2.48	5.76	3.00	0.65	1.60
HBA/ATP	0.959	0.52	2.23	1.78	0.90	0.12	0.27
HBA/Gln	0.832	0.38	2.00	1.22	0.46	0.10	0.20
HBA/ATP/Gln	0.967	2.14	5.83	0.62	1.36	0.05	0.28

4.2.3.6 Stopped-Flow analysis of CobB binding HBAM

Stopped-flow was used to monitor the binding of HBAM to CobB. The parameters of the experiment were the same as used in the binding of HBA, where the concentration of HBA was varied between 1 µM to 5 µM with a fixed concentration of CobB (1 µM).As with the binding of HBA to CobB, the binding of HBAM was also found to be biphasic (Figure 4.9).

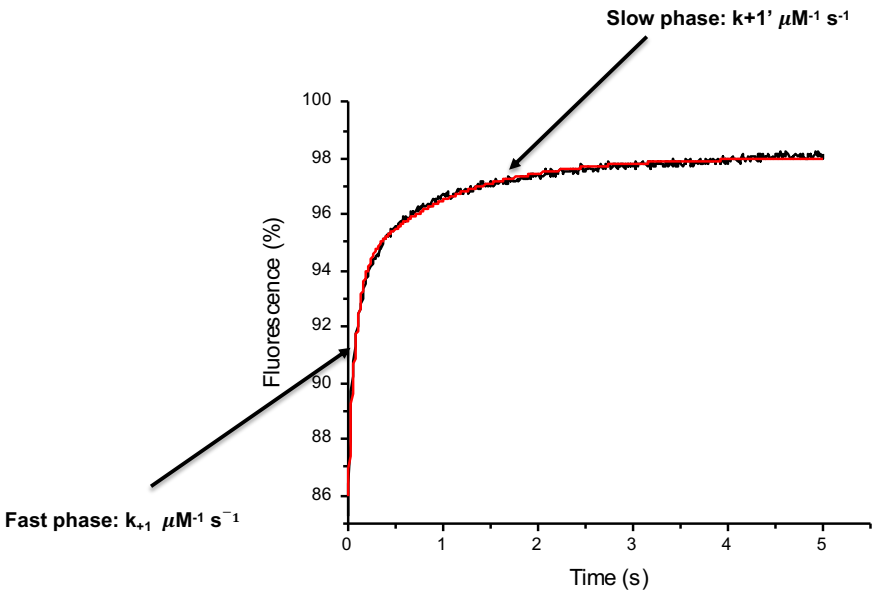

Figure 4.9: An example trace of the fluorescence change upon 1 µM HBAM binding to 1 µM CobB. The trace shows the biphasic nature of the binding of HBAM to CobB.

(a)

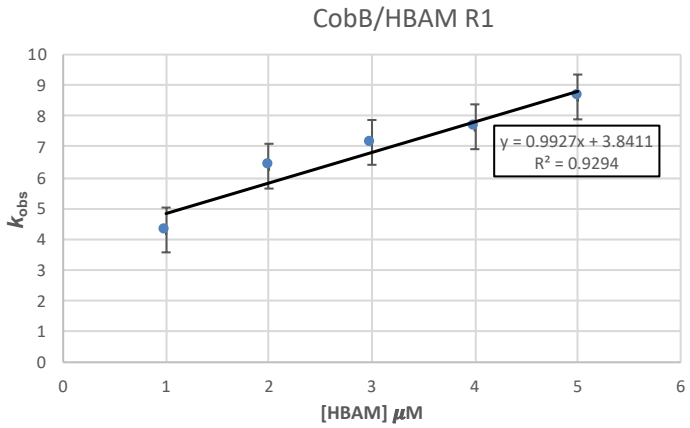

Kd_1 = 3.85/0.992
= 3.88 μM $\pm$2

(b)

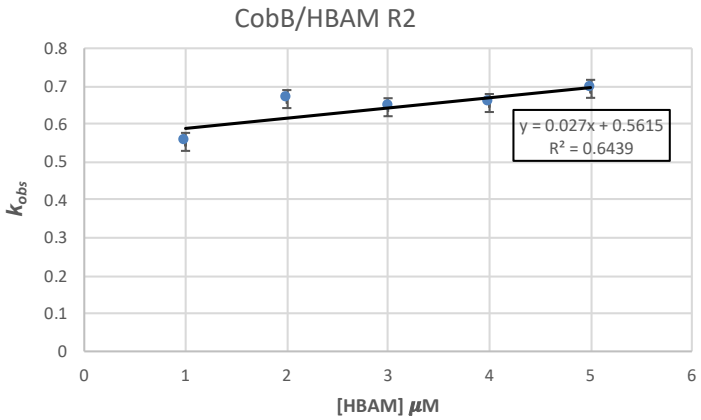

Kd_2 = 0.565/0.027
= 21 μM

Figure 4.10: Dependence of k_{obs} versus [HBAM]. For R1, the rate constants k_{+1} and k_{-1} were determined from the line gradient and y intercept. (a) Shows the initial phase of reaction (R1), with calculated k_{+1} = 0.99 μM^{-1} s^{-1}, k_{-1} = 3.85 μM^{-1} s^{-1} and K_{d1} = 3.88 whilst (b) shows the second phase of reaction (R2) with k_{+1}' = 0.03 μM^{-1} s^{-1}, k_{-1}' = 0.56 s^{-1} and K_{d2} = 21 µM. Values are averages of 3 biological repeats (from three different HBA preparations) ± SEM.

A comparison of k_{obs} for both the fast (R1) and slow (R2) binding of HBAM with CobB revealed a linear relationship with the concentration of HBAM, as shown in Figure 4.10. From these data it was determined for the R1 reaction that HBAM binds with a K_d of 3.89 μM with a rate constant of 0.99 μM^{-1} s^{-1}. In contrast, for the second binding event (R2) HBAM binds with a higher K_{d2} of 20.7 μM and a slower rate constant of 0.03 μM^{-1} s^{-1} (Table 4.2).

4.2.3.7 Effect of ATP on the binding of HBAM to CobB

The stopped-flow experiment was repeated in the presence of the other substrates (ATP, Gln and then both ATP with Gln) to determine the effects of these substrates would have on HBAM binding CobB. In the presence of a fixed concentration of ATP and CobB the k_{obs} was monitored against variable HBAM concentrations (Figure 4.11). For the binding of the first HBAM molecule (R1) the presence of ATP did not appear to change the K_d value, but did slow the rate at which HBAM binds to CobB by nearly 3 fold (k_{+1} = 0.99 μM^{-1} s^{-1} value without ATP and k_{+1} = 0.35 μM^{-1} s^{-1} with ATP, respectively) (Figure 4.10, Figure 4.11, Table 4.2). For the second binding event, R2, there was a significant, five-fold, drop in the K_{d2} from 20.7 to 4.2 μM (Table 4.2). However, the data generated for the R2 binding is of variable quality (Figure 4.11) and the R2 value is low.

(a)

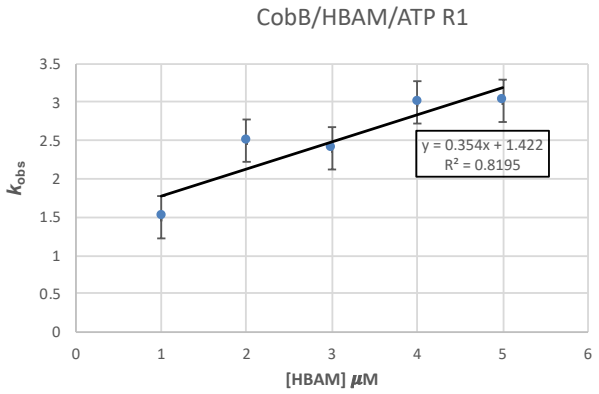

Kd_1 = 1.422/0.354
= 4.0μM±5

(b)

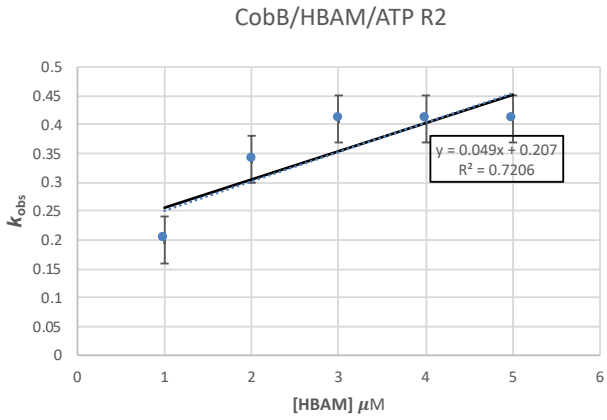

Kd_2 = 0.207/0.049
= 4.22 μM

Figure 4.11: Dependence of k_{obs} versus [HBAM] and ATP. Calculation of rate constants k_{+1} (line gradient) and k_{-1} (y intercept) from stopped-flow measurements of k_{obs} at different concentrations of [HBAM] and constant concentration of CobB/ATP for a) the initial phase of reaction (R1), with calculated k_{+1} = 0.35 μM^{-1} s^{-1}, k_{-1} = 1.42 s^{-1} and K_{d1} = 4 μM and b) the second phase of reaction (R2) with k_{+1}' = 0.21 μM^{-1} s^{-1}, k_{-1}' = 0.05 s^{-1} and K_{d2} = 4.22 μM. These values have very high errors and the data is poor, so the accuracy of these results is questionable. Values are averages of 3 biological repeats (from three different HBA preparations) ± SEM..

4.2.3.8 Effect of Gln on the binding of HBAM to CobB

To determine if Gln has any effect on the binding of HBAM to CobB, the stopped-flow assay was repeated but in the presence of a fixed concentration of Gln. Gln was added to CobB at a concentration of 5 mM and the concentration of CobB was kept constant (1 μM) and HBAM was varied between 1 μM and 5 μM. The results are shown in Figure 4.12

(a)

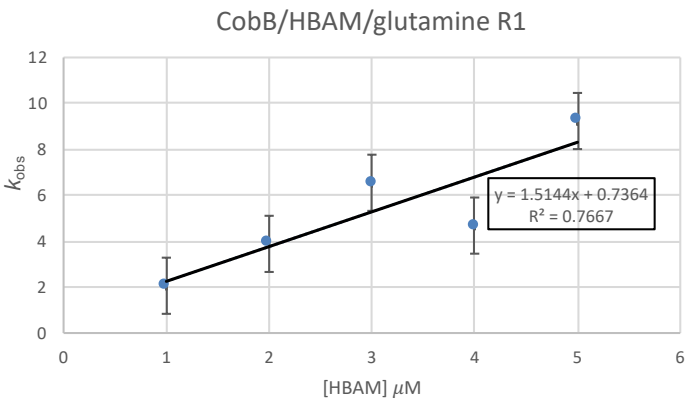

Kd_1 = 0.736/1.514
= 0.49 μM $\pm$0.3

(b)

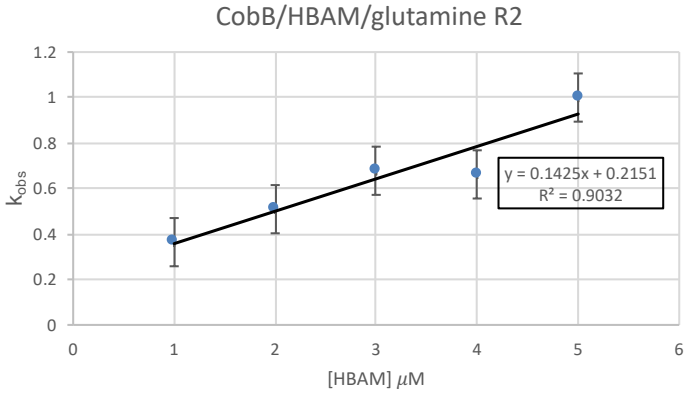

Kd_2 = 0.215/0.142
= 1.5μM $\pm$1

Figure 4.12: Dependence of k_{obs} versus [HBAM] and Gln. Calculation of rate constants k_{+1} (line gradient) and k_{-1} (*y* intercept) from stopped-flow measurements of k_{obs} at different concentrations of HBAM and constant concentration of CobB/Gln for a) the initial phase of reaction (R1), with calculated k_{+1} = 1.51 μM^{-1} s^{1}, k_{-1} = 0.74 s^{-1} and K_{d1} = 0.49 and b) the second phase of reaction (R2) with k_{+1}' = 0.14 μM^{-1} s^{-1}, k_{-1}' = 0.22 s^{-1} and K_{d2} = 1.5 µM. Values are averages of 3 biological repeats (from three different HBA preparations) ± SEM.

For the R1 binding event, the effect of Gln was significant (Figure 4.12). The K_{d1} reduced to 0.49 µM, which is nearly an order of magnitude lower than that observed

in the absence of Gln. In particular, the rate describing the dissociation of the CobB-HBAM complex, k_{-1}, was much slower (Table 4.2). For the second binding event, R2, there was also a reduction in the K_{d2} although in this case the reaction was linked with a faster association (k_{+1}') of the CobB-HBAM complex

4.2.3.9 Effect of ATP and Gln on the binding of HBAM to CobB

To complete the data set, the binding of HBAM with CobB was investigated in the presence of both ATP and Gln. This was accomplished by keeping a fixed concentration of CobB, ATP (5mM) and Gln (5 mM) and varying the concentration of HBAM. The results of this are shown in Figure 4.13.

(a)

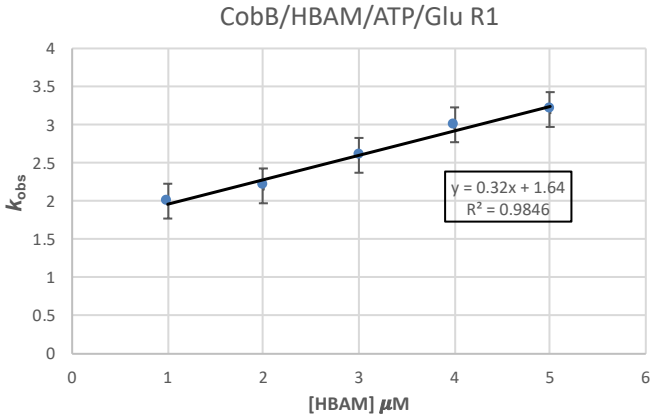

Kd_1 = 1.64/0.32
= 5.12 μM± 1.8

(b)

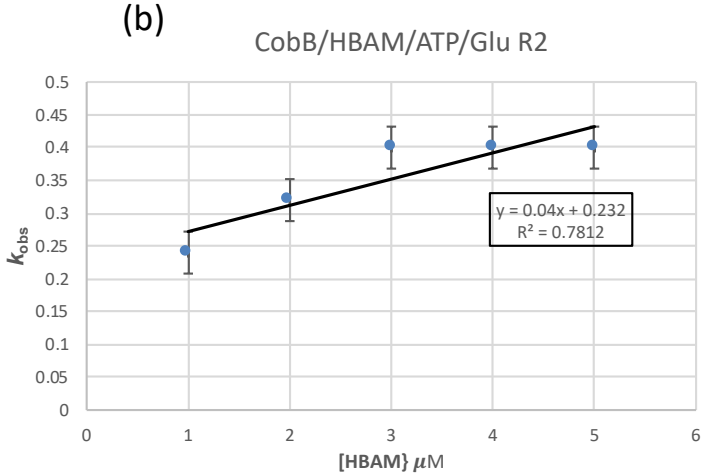

Kd_2 = 0.232/0.04
= 5.80 μM ±4

Figure 4.13: Dependence of k_{obs} versus [HBAM], ATP and Gln. For R1 the rate constants k_{+1} (line gradient) and k_{-1} (y intercept) from stopped-flow measurements of k_{obs} at different concentrations of HBAM and constant concentration of CobB/ATP/Gln for a) the initial phase of reaction (R1), with calculated k_{+1} = 0.32 μM^{-1} s^{-1}, k_{-1} = 1.64 s^{-1} and K_{d1} = 5.13 and b) the second phase of reaction (R2) with k_{+1}' = 0.04 μM^{-1} s^{-1}, k_{-1}' = 0.23 s^{-1} and K_{d2}' = 5.8 µM. Values are averages of 3 biological repeats (from three different HBA preparations) ± SEM.

When all the substrates (HBAM, ATP and Gln) are present the binding of CobB to HBAM mirrors the binding that is observed in the presence of ATP alone. Thus, for both R1 and R2, the reduction that was observed in the presence of Gln is lost when both Gln and ATP are present (Table 4.2).

Table 4.2: Reaction rates and binding constants of amidation reaction of HBAM, HBAM/ATP, HBAM/Gln and HBAM/ATP/Gln/ binding to CobB

Brucella CobB	R^2	Kd μM R1	Kd μM R2	k_{+1} $\mu M^{-1} s^{-1}$	k-1 s^{-1}	k+1' $\mu M^{-1} s^{-1}$	k-1' s^{-1}
HBAM	0.929	3.88	20.70	0.99	3.80	0.03	0.56
HBAM/ATP	0.819	4.01	4.22	0.35	1.42	0.05	0.21
HBAM/Gln	0.809	0.53	5.86	1.50	0.80	0.07	0.41
HBAM/ATP/Gln	0.985	5.13	5.80	0.32	1.64	0.04	0.23

R^2 is an indication of the accuracy of the data, the closer this value is to 1 the more accurate the data is considered to be. With CobB/HBAM/ATP and HBAM/Gln having R^2 values of 0.819 and 0.809 respectively the validity of these results is questionable.

4.2.3.10 Binding of HBAD to CobB

HBAD is the final product of the enzymatic reaction of CobB, which is generated after amidation of both the C2 and the C7 side chains of HBA. HBAD was produced and purified from a recombinant strain of *E. coli* as described in Chapter 2. The binding of HBAD to HBAD was investigated in the same way as the binding of HBA and HBAM.

Stopped-flow was again used to determine the binding of HBAD to CobB, where CobB was maintained at 1 µM whilst the concentration of HBAD was varied between 1 µM and 5 µM (Figure 4.14).

(a)

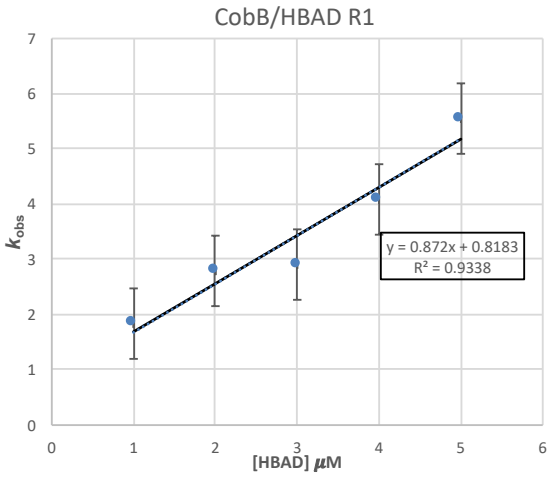

Kd_1 = 0.183/0.872
= 0.94 μM $\pm$0.808

(b)

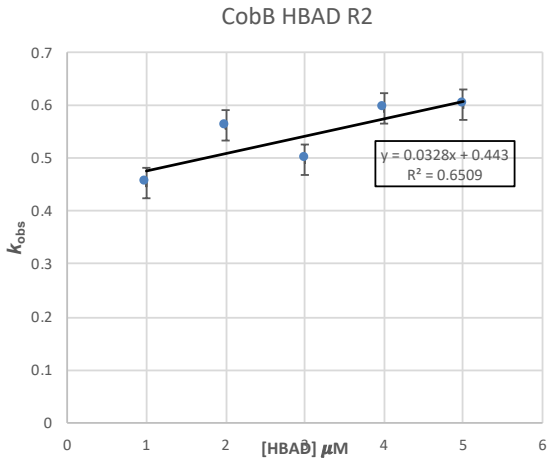

Kd_2 = 0.443/0.032
= 13.20 μM $\pm$15.5

Figure 4.14: Dependence of k_{obs} versus [HBAD]. Dependence of k_{obs} versus [HBAD]. For R1 the rate constants k_{+1} (line gradient) and k_{-1} (y intercept) from stopped-flow measurements of k_{obs} at different concentrations of HBAD and constant concentration of CobB for a) the initial phase of reaction (R1), with calculated k_{+1} = 0.87 μM^{-1} s^{-1}, k_{-1} = 0.18 s^{-1} and Kd_1 = 0.94 and b) the second phase of reaction (R2) with k_{+1}' = 0.03 μM^{-1} s^{-1}, k_{-1}' = 0.4 s^{-1} and K_{d2} = 13.2 μM, this data is poor and is not considered to be accurate. Values are averages of 3 biological repeats (from three different HBA preparations) ± SEM.

From Figure 4.14 it can be seen that for the first binding event (R1) that HBAD binds CobB with a K_{d1} of 0.94 µM whilst the second binding event (R2) has a K_{d2} of 13.2 µM indicating that the second HBAD molecule binds much less tightly (Figure 4.14 and Table 4.3). However, the binding rates for the formation of the $CobB_2$-HBAD and $CobB_2$-$HBAD_2$ complexes are relatively slow, with k_{+1} = 0.87 μM^{-1} s^{-1} and k_{+1}' = 0.03 s^{-1} respectively (Figure 4.14 and Table 4.3).

4.2.3.11 Binding of HBAD to CobB in the presence of ATP

Stopped-flow was used to monitor the binding of HBAD to CobB in the presence of ATP. The parameters of the assay were as described previously, with CobB fixed at 1 µM, ATP at 5 mM and with variable concentrations of HBAD between 1 µM and 5 µM (Figure 4.15).

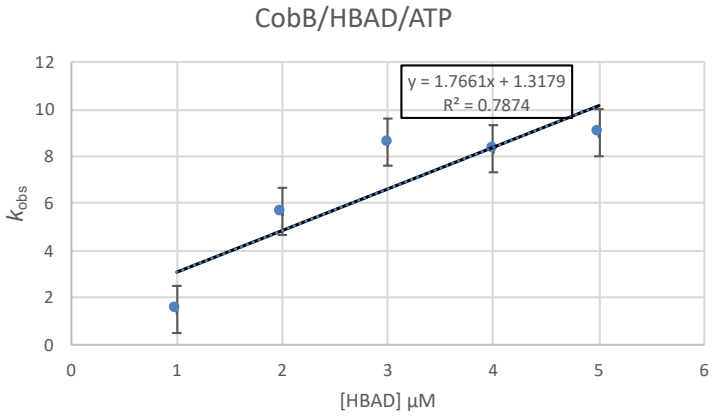

K_{d1} = 1.318/1.766
= 0.75 μM $\pm$1.92

Figure 4.15: Dependence of k_{obs} versus [HBAD] and ATP. Dependence of k_{obs} versus [HBAD]. For R1 the rate constants k_{+1} (line gradient) and k_{-1} (y intercept) from stopped-flow measurements of k_{obs} at different concentrations of HBAD and constant concentration of CobB/ATP for a) the initial phase of reaction (R1), with calculated k_{+1} = 1.77 μM^{-1} s^{-1}, k_{-1} = 1.32 s^{-1} and K_{d1} = 0.75 µM. This data is poor and not considered to be accurate. Values are averages of 3 biological repeats (from three different HBA preparations) ± SEM.

In the presence of a fixed concentration of ATP and CobB the k_{obs} was monitored against variable HBAD concentrations (Figure 4.18). For the binding of the first HBAD molecule (R1) the presence of ATP changed the affinity of HBAD only, binding CobB by almost 6 fold tighter in the presence of ATP (K_d = 0.17 and 0.94 respectively), however, slowed the rate at which HBAD binds to CobB by nearly 3 fold (k_{+1} = 0.87 μM^{-1} s^{-1} value without ATP and k_{+1} = 2.4 μM^{-1} s^{-1} with ATP, respectively) (Figure 4.14, Figure 4.15, Table 4.3).

4.2.3.12 Binding of HBAD to CobB in the presence of Gln

To determine if Gln has any effect on the binding of HBAD to CobB, the stopped-flow assay was repeated in the presence of a fixed concentration of Gln. Gln was added to CobB at a concentration of 5 mM and the concentration of CobB was kept constant (1 µM) and HBAD was varied between 1 µM and 5 µM. The results are shown in Figure 4.16.

(a)

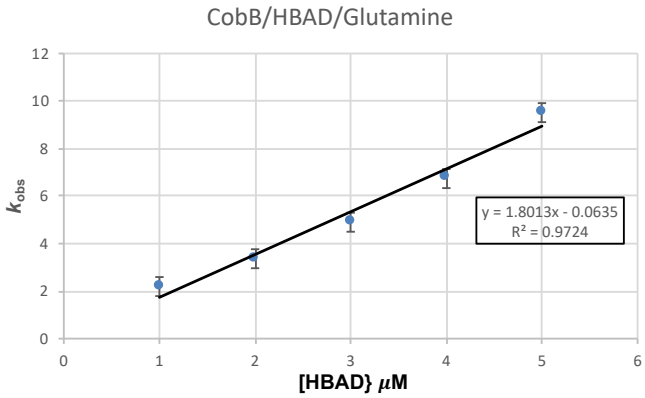

K_{d1} = 0.0635/1.801
= 0.04 μM ±0.01

(b)

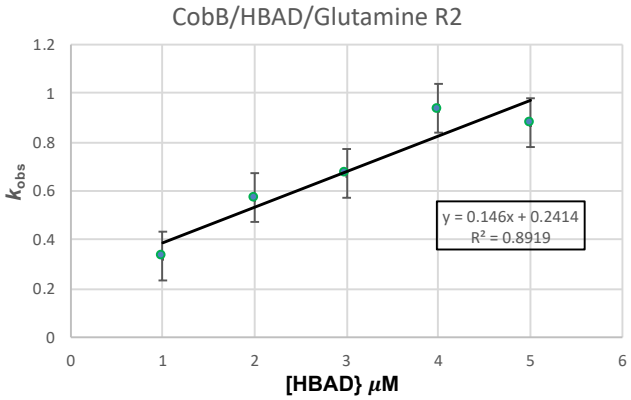

K_{d2} = 0.241/0.146
= 1.65 μM ±1

Figure 4.16: **Dependence of k_{obs} versus [HBAD] and Gln.** For R1 the rate constants k_{+1} (line gradient) and k_{-1} (*y* intercept) from stopped-flow measurements of k_{obs} at different concentrations of HBAD and constant concentration of CobB/Gln for a) the initial phase of reaction (R1), with calculated k_{+1} = 1.80 μM^{-1} s^{-1}, k_{-1} = 0.06 s^{-1} and K_{d1} = 0.04 and b) the second phase of reaction (R2) with k_{+1}' = 0.15 μM^{-1} s^{-1}, k_{-1}' = 0.24 s^{-1} and K_{d2} = 1.65 μM. Values are averages of 3 biological repeats (from three different HBA preparations) ± SEM.

Figure 4.16 shows that in the presence of a fixed concentration of Gln and CobB where the K_{obs} was monitored against variable HBAD concentrations, that Gln has a striking effect on the binding of HBAD to CobB (Figure 4.16). For the binding of the first HBAD molecule (R1) the presence of Gln changed the affinity of HBAD by 27 fold compared to that of CobB binding HBAD only, and 5 fold CobB-ATP (K_{d1} = 0.04, K_{d1} = 0.94 and K_{d1} = 0.17 respectively) (Table 4.3).

4.2.3.13 Binding of HBAD to CobB in the presence of Gln and ATP

To complete the data set, the binding of HBAD with CobB was investigated in the presence of ATP and Gln. This was accomplished by keeping a fixed concentration of CobB (1 μM), ATP (5 mM) and Gln (5 mM) and varying the concentration of HBAD. The results of this are shown in Figure 4.17.

(a)

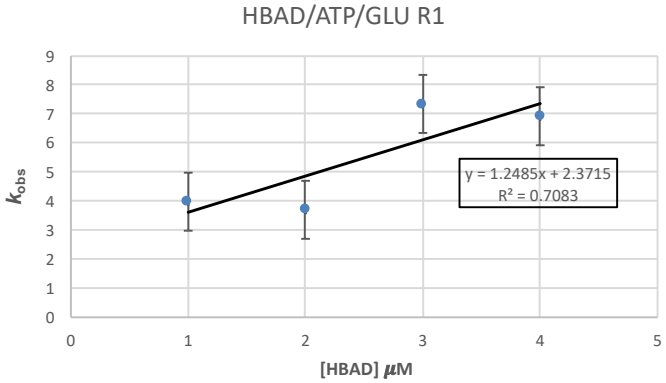

K_{d1} = 2.371/1.248
= 2μM ±1

(b)

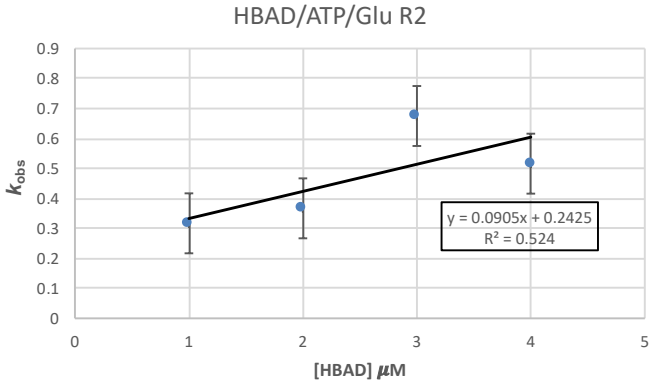

K_{d2} = 0.242/0.095
= 3μM ±2.8

Figure 4.17: Dependence of k_{obs} versus [HBAD], ATP and Gln. For R1 the rate constants k_{+1} (line gradient) and k_{-1} (y intercept) from stopped-flow measurements of k_{obs} at different concentrations of HBAD and constant concentration of CobB/ATP/Gln for a) the initial phase of reaction (R1), with calculated k_{+1} = 1.25 μM^{-1} s^{-1}; k_{-1} = 2.37 s^{-1} and K_{d1} = 2 μM and b) the second phase of reaction (R2) with k_{+1}' = 0.09 μM^{-1} s^{-1}; k_{-1}' = 0.24 s^{-1} and K_{d2} = 3 μM. Values are averages of 3 biological repeats (from three different HBA preparations) ± SEM.

When all the substrates (HBAD, ATP and Gln) are present the binding affinity of CobB for HBAD is decreased by 2 fold (K_{d1} = 2.0 and K_{d1} = 0.94 respectively). Thus, for both R1 and R2, reduction that was observed in the presence of Gln is lost when both Gln and ATP are present. The first order rate constants however, are very similar to HBAD binding CobB/Gln and CobB/ATP/Gln (k_{+1} = 1.80 μM^{-1} s^{-1} and k_{+1} = 1.25 μM^{-1} s^{-1} respectively) (Table 4.3). Whereas, the rate describing the dissociation of the CobB-HBAD in the presence of Gln was 38 fold slower than that of CobB-HBAD in the presence of ATP and Gln (k_{-1} = 0.06 s^{-1} and k_{-1} = 2.37 s^{-1} respectively) (Table 4.3).

Table 4.3 Reaction rates and binding constants of CobB binding to HBAD in the presence and absence of cofactors ATP and Gln.

Brucella CobB	R^2	Kd μM R1	Kd μM R2	k+1 μM^{-1} s^{-1}	k-1 s^{-1}	k+1' μM^{-1} s^{-1}	k-1' s^{-1}
HBAD	0.934	0.94	13.20	0.87	0.81	0.03	0.44
HBAD/ATP	0.813	0.17	-------	2.51	0.41	------	------
HBAD/Gln	0.972	0.04	1.65	1.80	0.06	0.15	0.24
HBAD/ATP/Gln	0.709	2.00	3.00	1.25	2.31	0.09	0.24

To conclude the results show that CobB binds HBA/ATP/Mg^{2+}/Gln with a K_d = 2 µM, HBAM/ ATP/Mg^{2+}/Gln K_d = 5 µM and HBAD/ ATP/Mg^{2+}/Gln K_d = 2 µM. These results are a representation of the enzyme being active, as all of the necessary cofactors are present. For HBA and HBAM do not bind CobB to high affinity as HBA will be turned over to HBAD you would not expect tight binding as the product has to tunover quickly for the production of more product. The fact that HBAM binds 2.5 fold weeker could represent the theory that once amidated at possition C7 the molecule leaves the active site and rebinds at possition C2. The K_d value obtained for HBAD/ ATP/Mg^{2+}/Gln binding, can be considered speculative as the R^2 value is 0.709, for an accurate result the R^2 value should be close to 1.

4.3 Discussion

In this chapter stopped-flow was used to measure the binding of CobB with its corrin substrates and product in the presence and absence of co-substrates ATP and Gln.

The binding profile indicate that CobB and HBA interact in a two phase process. The first 0.05 seconds signifies the fast phase of the reaction representing the initial formation of a CobB.HBA (monomer A) complex. The second binding phase is much slower and is presumed to represent monomer B. The crystal structures of CobB looks to confirm this as there is differences between the active site in each monomer. When there is no substrate in the active site, Arg177 in the unstructured region moves away from the HBA binding site of the opposite monomer and the other residues looks to fold round the ATP binding site of their own monomer. However, when HBA is present in the active site, Arg177 from the opposite monomer (B) interacts with the side chain attached to C18 of the corrin ring present in monomer A, whilst the other residues from Ala180 to Leu183 in monomer B flip away from the ATP binding site. This scissor like mechanism explains the difference in affinity and binding rate between the two monomers.

The K_d of HBA binding in the first phase is 0.52 μM, whilst in the second phase it is 2.48 μM. CobB seems to exhibit negative cooperativity, in that binding of a substrate molecule to one active site decreases the affinity of the enzyme for the second substrate molecule. The negative cooperativity of substrate binding suggests that the enzyme follows a sequential model in which binding of substrate to one monomer induces a change in the other monomer. The X-ray crystal structure of CobB binding HBA looks to confirm this theory. On examination of the two monomers (A and B), residues V171 to G184 show weak electron density. This suggests that the region is disordered, on examination of the B-factors (Mura 2014) between the two monomers we see a difference in the stability of each. Monomer A with HBA bound looks to be

slightly more stable than monomer B which is empty (Figure 4.18).

(a) (b)

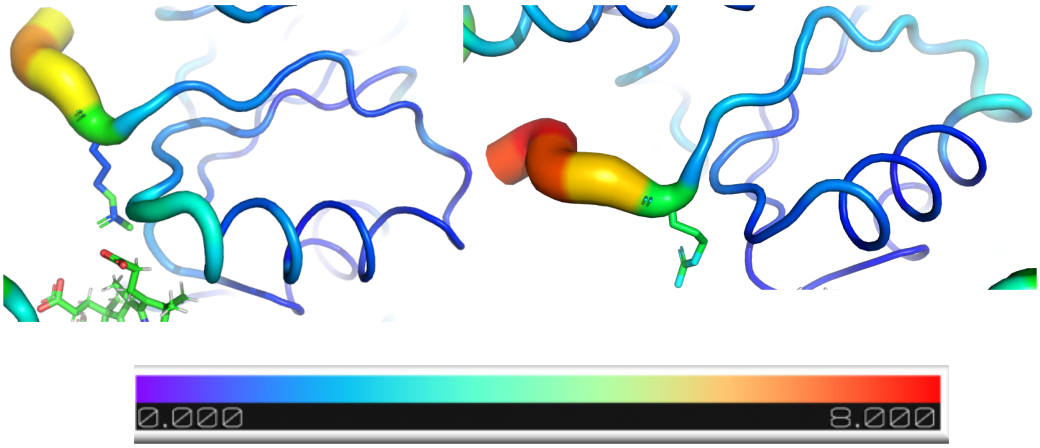

Figure 4.18: Crystal structure of monomer A and B for *B. melitensis* CobB/HBA (B-factors). Structure shows B-factors (corresponding to flexible regions), where blue represents low flexibility and red indicates high flexibility. (a) Monomer A appears slightly less flexible than (b) monomer B. Image created using B-factor Putty in PyMol.

In the crystal structure the unstructured region (Phe176 to Leu183) from each monomer is involved in substrate binding to the opposite monomer. One of the main contributors to binding in this unstructured region is Arg177 (Figure 4.19). When HBA binds to monomer A the unstructured loop region containing Arg177 of monomer B binds to HBA in the active site of monomer A. This pools the unstructured loop further away from the HBA binding site (monomer B) shortening the distance between Leu183 to the Gly198 (6.8 Å) in monomer A, and increasing the distance in these two residues from the other monomer (11.4 Å) (Figure 4.20). This changes the active site of the second monomer, which could account for the different binding affinity and binding rates.

(a) (b)

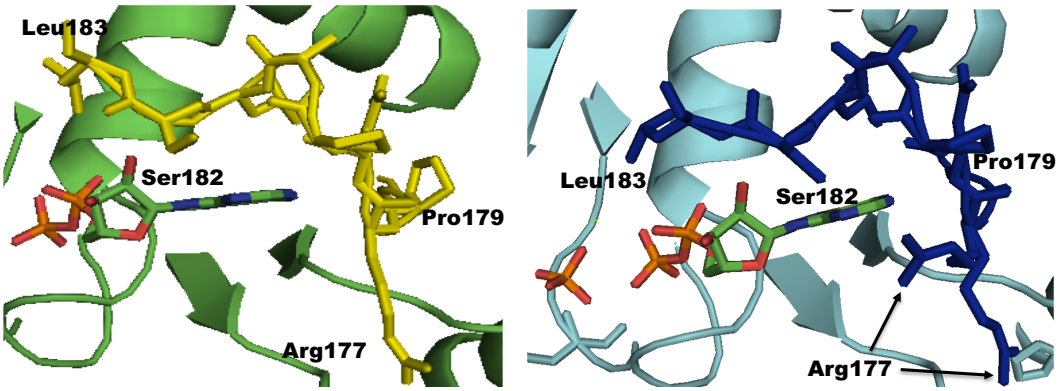

Figure 4.19: Monomer A binding ADP and Monomer B binding ADP plus free phosphate. (a) Monomer A showing the unstructured region of B (yellow) that spans the ATP binding site. Leu183 has flipped outwards away from the ADP binding site. Arg177 is positioned into the HBA binding site. (b) Monomer B showing where the unstructured region of A (blue) spans the ATP binding site. Ser182 and Leu183 look to be interacting with ADP, whilst Arg177 is shown in two positions and appears to flip between the two states.

(a) (b)

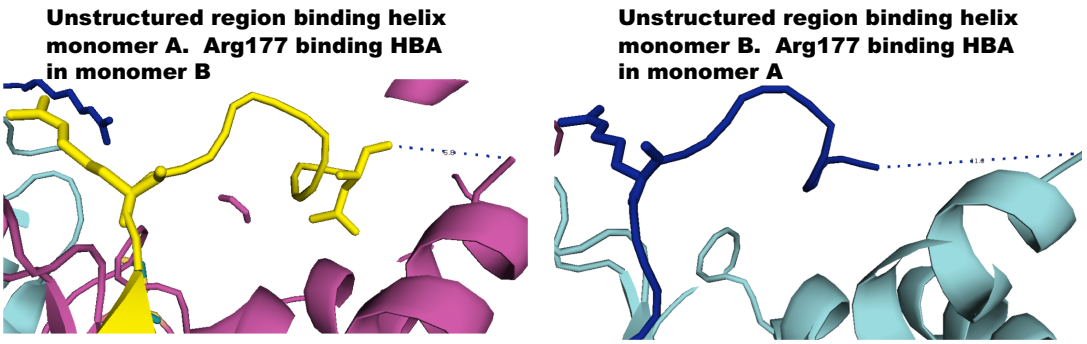

Figure 4.20: *B. melitensis* CobB binding HBA structure. (a) Unstructured region (yellow) of monomer A (with beta sheet) showing the distance 6.8 Å to alpha helix. (b) Unstructured region of monomer B (no beta sheet) showing distance 11.4 Å to alpha helix.

When ATP binds CobB the affinity for HBA binding remains the same as when no ATP is present (K_d = 0.52 µM with ATP and K_d = 0.52 µM without). However, the rate of the binding of the two reaction was three fold slower when ATP was present. This signifies that ATP binds first and restricts binding of HBA. This is attributed to this

unstructured region (Phe176 to Leu183) of the CobB. As already stated, the crystal structure shows that on binding ATP Arg177 flips into the HBA binding site (Figure 4.19). When binding ATP, part of the loop is pulled closer to the ATP binding site, thus moving the other part further away from HBA binding site. Overall, this may have the effect of restricting the binding of HBA to the second monomer.

When Gln, but not ATP, is present, the Kd = 0.38 μM and with ATP/Gln Kd = 2.14 μM this is not surprising as in the presence of all the cofactors HBA will be turned over to HBAD the product which is expected to not bind as tightly (see Table 4.1). The rate of the reaction is two-fold slower when all the cofactors are present which suggests that Gln influences the rate of binding, suggesting that cooperation between the two binding sites. This could infer that Gln binds first and that this binding is relayed to the HBA active site, perhaps causing a slight conformational change that obstructs the binding of HBA. However, Fresquet *et al* surmised that the reduction in the K_m for Gln must originate from conformational changes in the binding site for Gln, which are allosterically transmitted by the binding of substrates to the synthetase domain (Fresquet, Williams and Raushel 2004). This would only be correct if HBA bound first. The stopped flow analysis does infer that there is some sort of communication between the two domains.

The binding of HBAM to CobB is a lot weaker than HBA, and occurs at a much slower rate (11 fold slower) in the fast phase of the reaction. HBAM, once formed, most likely leaves the active site and rebinds to position itself in an orientation that allows amidation at the second position, producing the final product (HBAD). It would be unusual for the enzyme to want to bind tightly and hold onto to a partially amidated product, therefore, it is expected that binding to CobB should be weaker.

As with HBA binding to CobB in the presence of ATP, there is very little difference in the fast phase (R1) of HBAM binding to CobB/ATP, (K_d = 4.01 μM with ATP and K_d =

3.88 μM without). However, for the slower phase R2, the K_{d2} has 5 fold weaker affinity for HBAM/ATP binding (K_{d2} = 4.22 μM with ATP and K_{d2} = 20.6 μM without).

Another issue that could affect the binding affinity and rate of the reaction of HBAM with or without cofactors is the formation of the phosphorylated intermediate. From the X-ray crystal structure of HBAM with a phosphorylated intermediate at the C2 position there is a clear difference between the two monomers. Arg177 of monomer B has moved away from the HBAM active site (13.6 Å), whereas monomer A is still very much in the HBAM binding site (4.1 Å). In the monomer A structure the unstructured region looks to be more stable than monomer B (Figure 4.21).

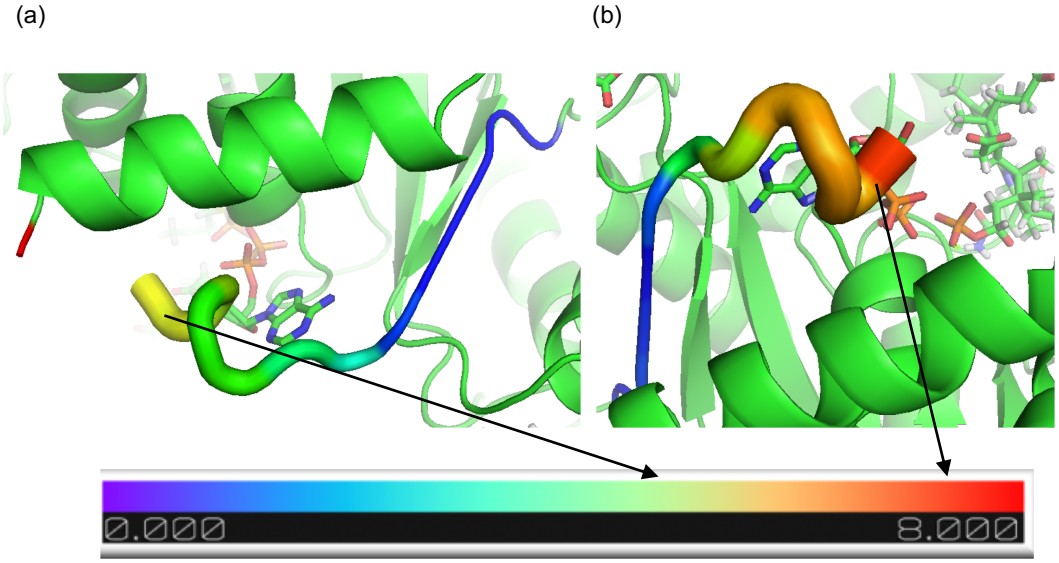

Figure 4.21: Crystal structure of monomer A and B of *B. melitensis* CobB binding HBAMP (B-factors). Structure shows B-factors (corresponding to flexible regions), where blue represents low flexibility and red indicates high flexibility. (a) monomer A to be slightly more stable than monomer B when binding HBAM as a phosphorylated intermediate. Figure was generated using B-factor Putty in PyMol.

In the presence of Gln but not ATP, HBAD binding to CobB shows a 2 fold increase in the rate of reaction, compared to HBAD on its own. It is possible this is caused by a conformational change in the enzyme that is not observed in the crystal structure.

There is no crystal structure of CobB with Gln or products of this partial reaction (ammonia or Gln). However, the mechanism for this part of the reaction has been previously well established.

The production of HBAD is the final step in the enzyme reaction. In the presence of ATP and Gln it would normally be expected for the product HBAD to leave the active site at a faster rate than that of HBA and HBAM. However, HBAD/ATP/Gln (K_{d1} = 2 μM) has the same binding affinity as that of HBA/ATP/Gln ($K1_d$ = 2.14 μM).This slow release reflects the general tight binding of products to the B_{12} biosynthetic enzymes, where evidence suggest the enzymes operate a form of substrate channelling. Indeed, the rate for the dissociation of the CobB.HBAD complex is significantly slower than that for either the CobB.HBA or CobB.HBAM complexes.

To summarise, in the presence of ATP, HBA binds tightly (0.52 μM) to CobB at monomer A, a binding that induces a conformational change in monomer B. ATP binds monomer B at a slower rate than binding of monomer A, by what looks to be a scissor type mechanism, as one monomer opens up after binding ATP the other monomer becomes more closed (see Figure 4.19). In Figure 4.19, Arg177 looks to be in two positions with one pointing into the ADP binding site and the other flipping outwards to bind in the HBA binding site. From the crystal structures it could be assumed that monomer B is preparing to bind HBA. At this point monomer A has most likely bound at the C7 position on the corrin ring and has started the process of amidation, by forming a phosphorylated intermediate. This intermediate is then amidated to produce HBAM.

The crystal structure of CobB binding HBAM shows the unstructured region in monomer A to be more structured with the formation of a beta sheet, whilst in monomer B this region remains unstructured. Another difference between the two monomers is that Arg177 no longer binds to the corrin ring, but has flipped back

allowing the active site to open up. In monomer B, however, Arg177 still remains bound (Figure 4.22).

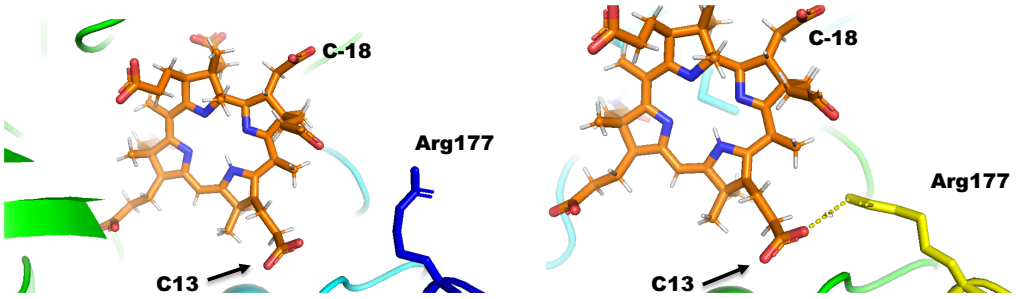

Figure 4.22: HBAM binding CobB. Monomer A shows Arg177 (blue) moving away from the active site, whereas in monomer B Arg177 (yellow) interacts with the side chain attached to C13 on the corrin ring.

Once amidated at position C7, HBAM then leaves the active site, repositioning itself for amidation of the side chain attached to C2. HBAM binding to CobB /ATP has a similar affinity for binding as HBAM alone. After amidation of the C2 position the final product is achieved (HBAD). From the stopped-flow assay and the X-ray crystal structures, it seems that this scissor type mechanism may be the method in which amidation is achieved.

Chapter 5

Evidence for an interaction between *Brucella melitensis* CobB and CobH to mediate metabolic transfer

5.1 Introduction

CobH and CobB are two enzymes involved in sequential steps in the cobalamin pathway. CobH is the enzyme that mediates the migration of a methyl group from position C11 to C12 on the corrin ring system of its substrate, precorrin-8x, resulting in the production of product hydrogenobyrinic acid (HBA) (Thibaut *et al.* 1992; Blanche *et al.* 1992; Shipman *et al.* 2001).

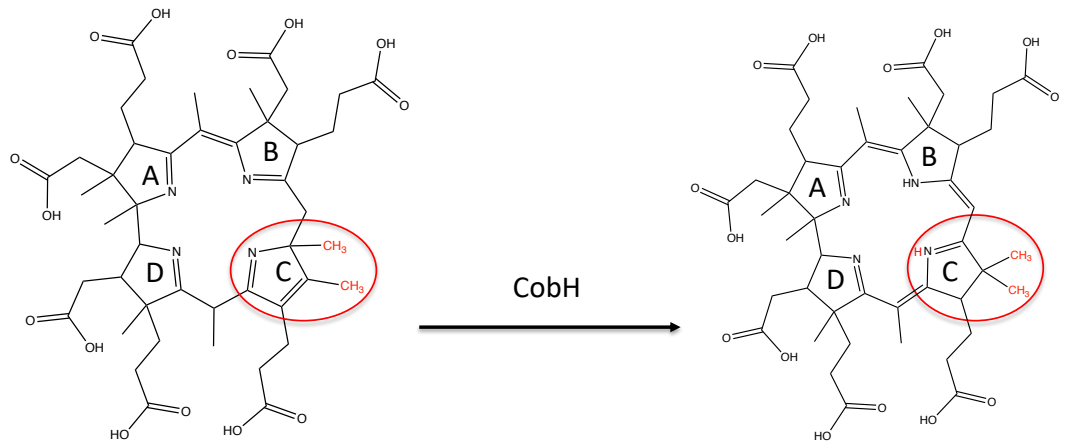

Figure 5.1: **CobH binding its substrate precorrin-8 to produce product HBA.** Precorrin-8 binds CobH where the nitrogen of pyrrole ring C is protonated, this triggers a suprafacial [1,5]-sigmatropic rearrangement; the methyl group then passes from C-11 to C-12 in a single concerted step, with the double bonds in the ring shifting position, to give the product precorrin 8.

The next enzyme in the pathway is catalysed by CobB, which is involved in the amidation of the carboxylic acid side chains attached to C2 and C7 of HBA on the corrin ring (Debuscche *et al.* 1990). CobH is known to bind its product (HBA) very tightly and hence the question arises as to how this product is released so that it can be used as a substrate by CobB (Thibaut *et al.* 1992). The focus of this chapter is to

determine the mechanism by which HBA is transferred from CobH to the active site of CobB for the amidation reactions to take place.

The crystal structure of *Rhodobacter capsulatus* CobH shows that its product HBA is encapsulated within the active site of the enzyme (Figure 5.2). CobH forms a homodimer and contains two active sites, which are composed of amino acid residues from both subunits. The homo-dimer forms a ball-shape conformation (Deery *et al.* 2012).

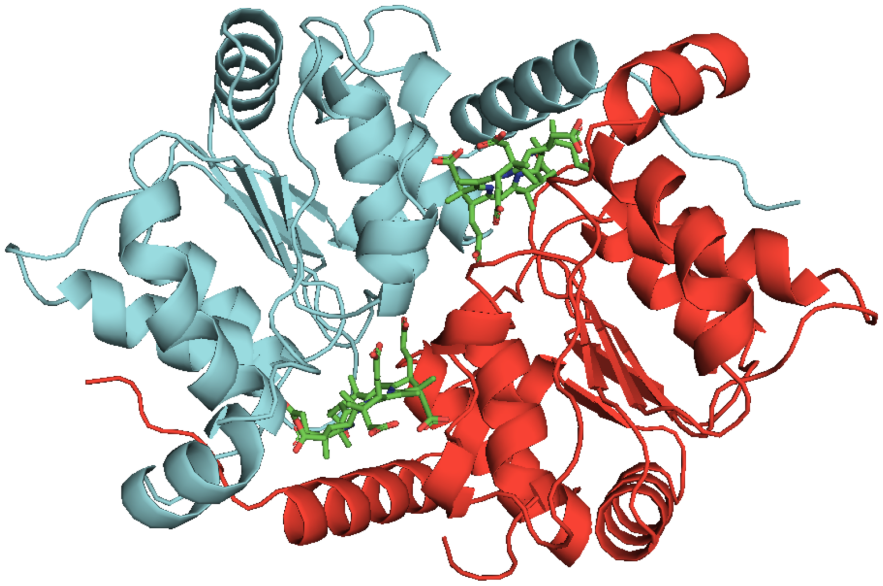

Figure 5.2: Cartoon representation of *R. capsulatus* CobH. The diagram shows the presence of two molecules of HBA encapsulated within the active site of the homodimeric structure (PDB 4AU1).

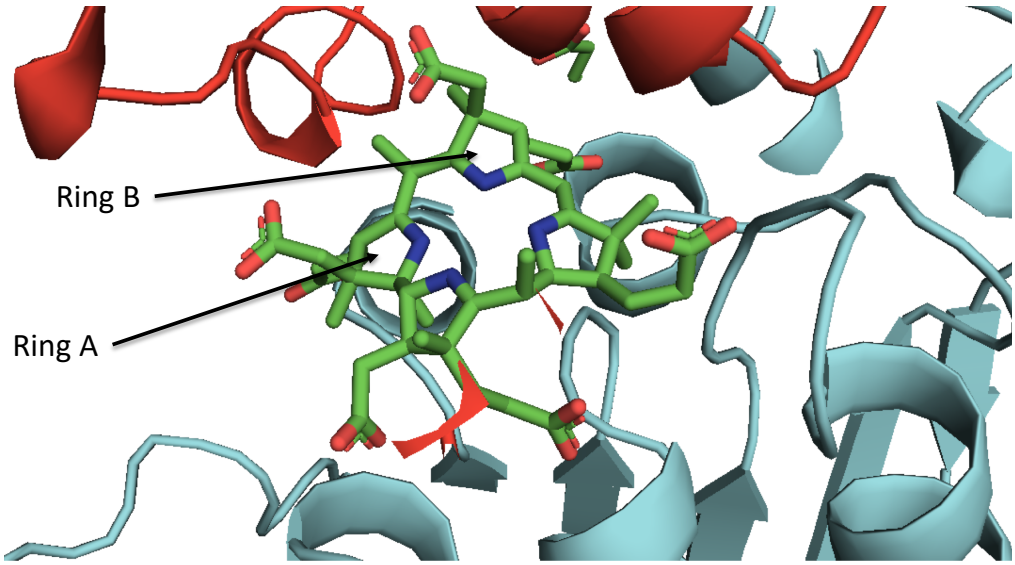

Figure 5.3: Cartoon representation of *R. capsulatus* CobH. The diagram shows HBA binding the monomer, where ring A and B of the corrin substrate are positioned near the opening of the active site.

In the crystal structure rings A and B of HBA are positioned near the opening of the active site and are exposed to solvent, whereas rings C and D are encapsulated more deeply within the cavity, with many of the hydrophobic residues making hydrogen bonds with the macrocycle (Figure 5.3) (Deery *et al.* 2012). The complex between HBA and CobH suggests that free movement of HBA from this pocket would be hindered. This infers that a conformational change in the enzyme is required in order to release the product. Weak density is observed for residues 79-102 of the CobH structure, residues that contribute to a flexible C-terminal loop region, which may swing open to allow the free movement of HBA (Shipman *et al.* 2001).

The kinetic parameters for the *P. denitrificans* CobH reveal that the enzyme has a high affinity and low turnover for its product HBA. This means that HBA binds very tightly to CobH and is very slow to leave the active site. This was determined by measuring the k_{cat} (which is the number of substrate molecules converted to product per unit time) of the enzymatic reaction, which was found to be extremely slow at 5.1

h^{-1}. The V_{max} for the reaction is 230 nmol h^{-1} mg^{-1}. It was concluded from this research that HBA competitively inhibits CobH (Thibaut *et al.* 1992).

Due to the tight binding and the build-up of HBA in the active site of CobH, it is not clear how this molecule is released from the active site and transferred to the next enzyme in the pathway (CobB). One possibility is that CobH and CobB interact, whereby CobB encourages CobH to release its product directly into the active site of CobB. This would represent a form of direct metabolite transfer. In order to determine the mechanism by which CobH and CobB communicate with each other, structural and biophysical analyses were employed. For the purposes of this study the *B. melitensis* CobB and CobH were used since interactions between sequential enzymes in a pathway are more likely to be conserved between enzymes from the same species.

5.2 Results

5.2.1 Expression and purification of His_6- tagged *B.melitensis* CobH

E. coli strain BL-21 (DE3) pLysS was transformed with pET14b carrying the *B. melitensis cobH* gene, provided by Dr. Evelyne Deery, which allowed for the production of recombinant N-terminus His_6-tagged CobH. The cells were grown in 2YT broth supplemented with ampicillin and chloramphenicol overnight at 37 °C, as described in Chapter 2.4. After harvesting the bacteria by centrifugation the cell pellet was resuspended in Tris-HCl buffer, pH 8.0, containing 500 mM NaCl and 20 mM imidazole. The cells were then lysed by sonication and centrifuged for a second time to remove the cell debris.

His_6-tagged native CobH was purified using a Ni-chelate column followed by ion

exchange chromatography. From 1L of culture ~20 mg of protein was reproducibly purified. The protein ran as a single band, with a molecular mass of 24 kDa, which is in close agreement to the gene predicted molecular mass (Figure 5.4).

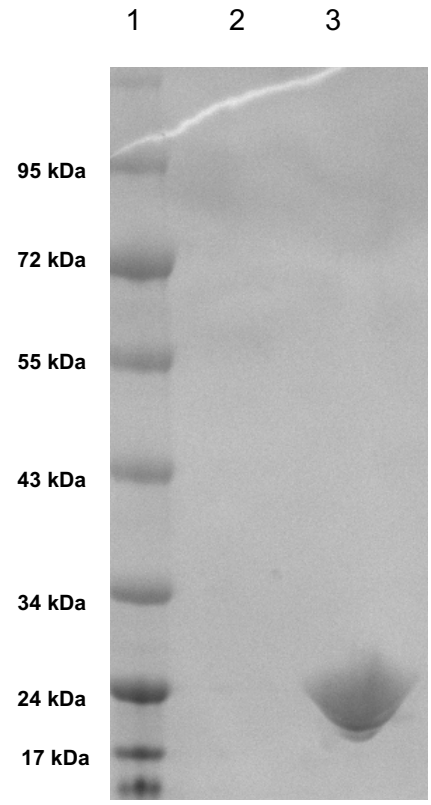

Figure 5.4: **12.5% SDS PAGE gel of purified *B. melitensis* CobH**. Sample of CobH from Ni+ affinity column. Lane 1 contains protein markers of known molecular mass, as shown. Lane 2 is empty. Lane 3 contains purified *B. melitensis* CobH (24 kDa).

5.2.2 Expression and purification of His_6-tagged *B. melitensis* CobB

E. coli strain BL-21 (DE3) pLysS was transformed with a pET14b plasmid carrying the *B. melitensis cobB* gene, which allowed for the production of recombinant N-terminus His_6-tagged CobB. The cells were again grown in 2YT broth supplemented with ampicillin and chloramphenicol overnight at 18 °C, as described in Section 2.2.7. After harvesting a 1 L culture by centrifugation the cell pellet was resuspended in Tris-HCl

buffer, pH 8.0, containing 500 mM NaCl and 20 mM imidazole. The cells were then lysed by sonication and centrifuged for a second time to remove the cell debris. His_6 tagged native CobB was purified using a Ni-chelate column followed by ion exchange chromatography. From a 1 L culture ~10 mg of protein was reproducibly produced. The purified CobB was run on a SDS gel, which migrated as a single band, as previously reported in Chapter 3 (see Figure 3.6).

5.2.3 Co-crystallisation of CobH/HBA with CobB/HBA

In order to determine if CobH and CobB form a complex co-crystallisation of the two proteins was attempted. HBA was added stochiometrically to each of the proteins (100 μM) and then the two proteins were mixed in an equi-molar ratio. The sample was left at room temperature for one hour before being concentrated using a 30 kDa cut off centricon. The complex was diluted into 20 mM Tris-HCl buffer, pH 8.0, containing 150 mM NaCl, and repeatedly concentrated and diluted in buffer in order to help remove any unbound HBA. The final concentration for crystallisation was 4 mg/mL. Molecular Dimensions crystal screens 1 and 2 were used for crystallisation with a protein to well ratio of 2:1 by using the hanging drop vapour diffusion method. Initial screening produced a number of crystals of a quality suitable for initial X-ray diffraction (Figure 5.5).

Crystals were flash frozen in liquid nitrogen using 2 μL of well solution with 2 μL of 50% v/v ethylene glycol (cryo-protectant). X-ray data were collected on four of the crystals at the DIAMOND Synchrotron Radiation Centre. These structures were solved using molecular replacement.

(a) (b) (c) (d)

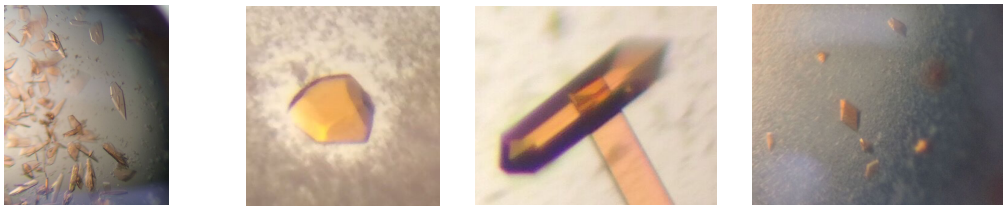

Figure 5.5: Crystals of CobH/CobB were grown from Molecular Dimensions screen 1 and 2: (a) 10 % PEG 1K (v/v) +10 % PEG 8K (v/v), crystals 2: 0.2 M magnesium acetate, 0.1 M cacodylate pH 6.5 and 30% PEG 8K v/v,(b) 0.2 M lithium sulphate, 0.1 M Tris-HCl pH 8.5 and 30% PEG 8K, (c): 0.2 M ammonium sulphate, 0.1 M sodium cacodylate pH 6.5, 30%(v/v) PEG 8K (d) 30% (v/v) ethylene glycol.

The CobH/HBA/CobB crystallisation trials produced 4 crystals that were subject to X-ray diffraction. Unfortunately, the data revealed that these crystals contained only CobH, with no density for CobB in any of the structures.

The three published X-ray crystal structures of *P. denitrificans* (HBA bound), *R. capsulatus* (HBA bound) and *B. melitensis* all have similar structures. However, the in-house structure of *B. melitensis*, although similar to the published structures, has HBA bound in only one molecule of the dimer (Figure 5.6). This crystal diffracted to 2 Å resolution, with a space group $P2_1\ 2_1\ 2$, and cell dimensions of 68.282 Å, 126.51 Å, 51.177 Å, $\alpha = 90$, $\beta = 90$ and $\gamma = 90$ with 2 molecules in the AU. The sequence of *B. melitensis*, *P. denitrificans*, *R. capsulatus* CobH are highly conserved, so it is expected that the crystal structures will be very similar (Figure 5.7).

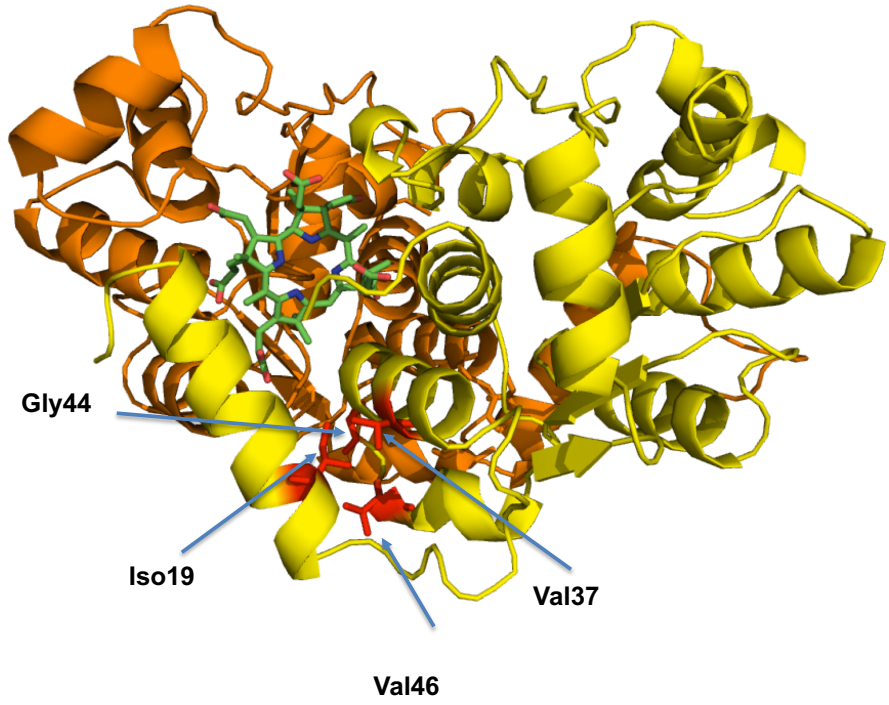

Figure 5.6: X-ray crystal structure of *Brucella melitensis* CobH. Ribbon diagram of CobH, with one molecule of HBA bound in one of the monomers. Conserved residues in red, and HBA in green.

```
           1                                                                  80
tr|A0A2X1C   MTDYIRDG QAIYDRSFAI IRAEADLRHI PADLEKLAVR VIHACGMVDV ANDLAFSEGA GKAGRNALLA GAPILCDARM
sp|P21638|  MPEYDYIRDG NAIYERSFAI IRAEADLSRF SEEEADLAVR MVHACGSVEA TRQFVFSPDF VSSARAALKA GAPILCDAEM
tr|D5AV08|  MP-HEYEKDG AKIYVQSFAT IRAEADLARF TPEEEVVVVR MIHAAGMVGL ENHVRFAPGM AIAARAALEA GAPILCDARM

           81                                                                160
tr|A0A2X1C  VAEGITRSRL PADNRVIYTL GDPSVPELAK KIGNTRSAAA LDLWLPHIEG SIVAIGNAPT ALFRLFELLD AGA-PKPALI
sp|P21638|  VAHGVTRARL PAGNEVICTL RDPRTPALAA EIGNTRSAAA LKLWSERLAG SVVAIGNAPT ALFFLLEMLR DGA-PKPAAI
tr|D5AV08|  VSEGITRARL PAKNEVICTL QDPRVPALAQ EMGNTRSAAA LELWRPKLEG AVVAIGNAPT ALFHLLNMLE DPACPRPAAI

           161                                                 211
tr|A0A2X1C  IGMPVGFVGA AESKDELAAN SRGVPYVIVR GRRGGSAMTA AAVNALASER E
sp|P21638|  LGMPVGFVGA AESKDALAEN SYGVPFAIVR GRLGGSAMTA AALNSLARPG L
tr|D5AV08|  IGCPVGFIGA AESKAALAV- ANPVPWVIVE GRLGGSAITV AAVNALACRK E
```

Figure 5.7: **Sequence alignment of the *B. melitensis* (A0A2X1C*)*, *P. denitrificans* P21638, *R. capsulatus* (D5AVO8*)* CobH**. Conserved residues highlighted in red.

5.3. Model to hypothesise interaction between CobH and CobB

Under steady state conditions CobH shows a high affinity for its product HBA (K_d = 0.91 μM and a K_i = 0.7 μM respectively) (Thibaut *et al.* 1992), slightly higher than that of its substrate, which was evident by the inhibitory effect of HBA (Shipman *et al.* 2001). Therefore, the mechanism by which CobH releases its product to CobB, the next enzyme in the pathway, is of importance. The crystal structure of CobH shows a globular protein, whereas the structure of CobB is more elongated (Figure 5.8 and 5.9). The general shape of these two enzymes indicates that it may be possible for them to form a complex, resulting in the transfer of HBA from CobH to CobB. With this in mind, a model of CobH binding to CobB was produced. Although the fit of CobH into CobB from the model looks to be tight, it is conceivable that there is a conformational change on binding. Both enzymes have flexible regions, Arg78 to Arg103 in CobH and Arg226 to Asn243 in CobB which could allow for the conformational change required. Until the structure of the complex is determined the nature of how these two proteins interact will remain conjecture.

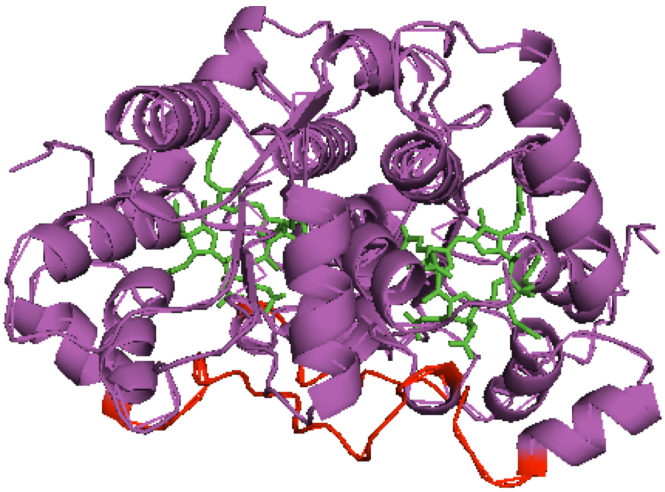

Figure 5.8: ***R. capsulatus* CobH.** Flexible region spanning Arg78 to Arg103 (red), CobH (purple) with HBA bound in each site (green).

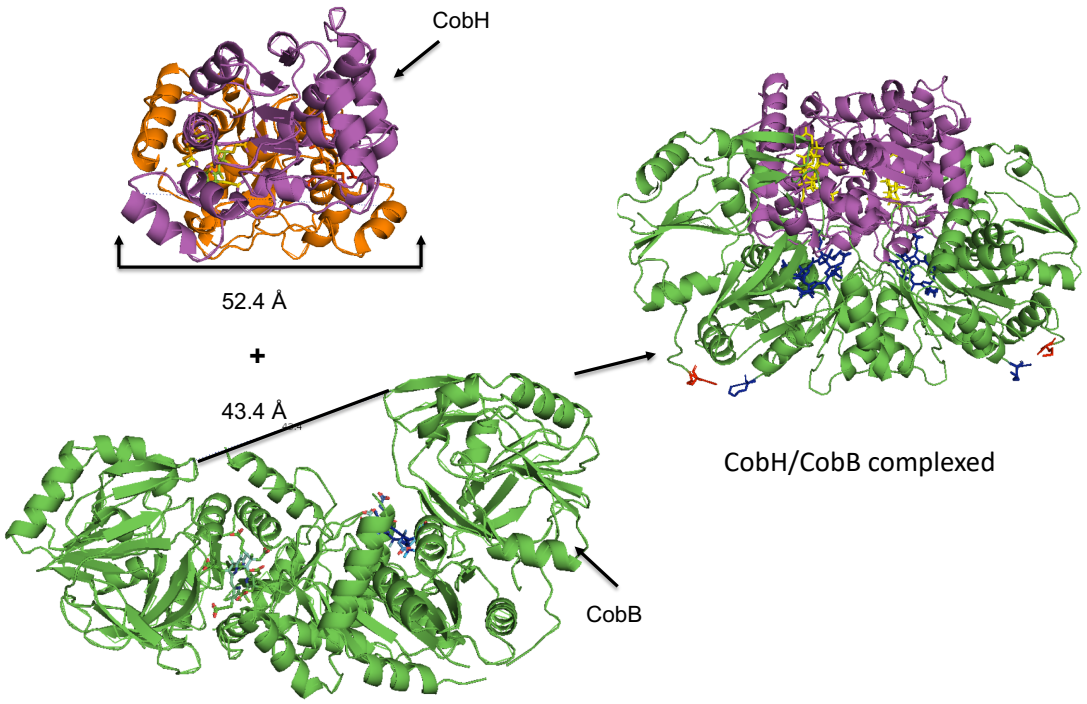

Figure 5.9: Hypothetical docking of CobB binding with CobH. Cartoon representation of CobH (purple and gold), which at the widest point of the enzyme has a width of 52.4 Å, together with CobB (green), which has an opening of 43.4 Å for binding of CobH. Complex shows CobH (purple) binding CobB (green) where HBA (blue and yellow) are present in both enzymes. Flexible regions in both enzyme could allow for an improved fit upon conformational change (Dave Brown).

There is, however, no experimental evidence for the formation of a complex between CobH and CobB, or the transfer of HBA directly from one enzyme to the other. In order to obtain experimental data to support this hypothesis stopped-flow was employed as a technique to monitor the binding of CobH and CobB. In order to do stopped-flow analysis it is first important to determine if there are any significant changes in either the absorbance or fluorescence spectra of these proteins when they come together. Such changes would be expected to occur, for instance, if CobH releases HBA to CobB.

5.4 Fluorescence-emission spectra measuring substrate fluorescence

5.4.1 Measurement of fluorescence emission spectra for CobH/HBA and CobB/HBA.

To monitor changes associated with the transfer of HBA from CobH to CobB, fluorescence emission spectra of CobH/HBA and CobB/HBA were initially recorded before a study was made of any reaction between CobH/HBA and CobB. The florescence emission spectra were recorded over 360 nm to 700 nm after excitation at 330 nm. It was found that the fluorescence associated with HBA when bound to CobB ((λ_{max} = 410 nm) is quite distinct to that observed when HBA is bound to CobH (λ_{max} = 450 nm) (Figure 5.10). Therefore, the transfer of HBA from CobH to CobB can be followed by looking for an increase in the fluorescence emission at 410 nm.

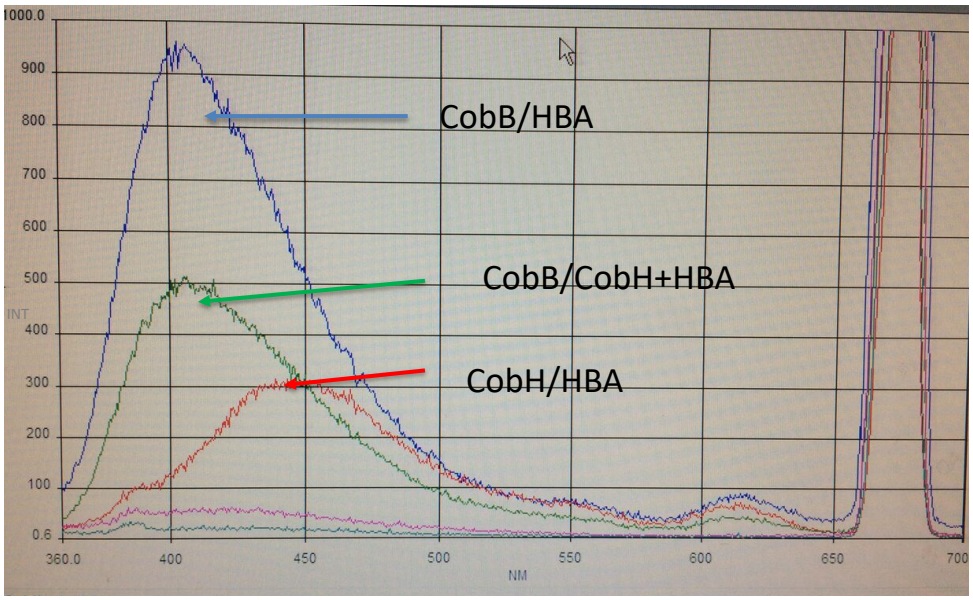

Figure 5.10: Fluorometer showing binding of CobB/HBA, CobH/HBA and CobB/CobH/HBA. Excitation at 330 nm shows CobB/HBA has a large peak at 410 nm and small peaks at 555 nm and 625 nm. CobH/HBA has a unique peak at 450 nm and two small peaks at 550 nm and 635 nm. CobH/HBA peak moves from 450 nm to 410 nm in the presence of CobB.

5.5: Stopped-Flow analysis using substrate fluorescence

5.5.1 Effect of CobH on the binding of HBA to CobB

In order to obtain kinetic data on the mechanism by which HBA is transferred from CobH to CobB, stopped-flow fluorescence spectroscopy was employed. In this stopped-flow experiment the concentration of CobH and CobB (1 μM) was kept constant and the concentration of HBA was varied (1 μM to 5 μM). Excitation was performed at 330 nm to measure fluorescence emission from HBA binding CobB. A GG455 filter was used to remove scattered light from the excitation.

Stopped flow was performed with the CobB mixture in one of the two syringes on the stopped flow apparatus (Eccleston *et al* 2008). The other syringe contained CobH mixed with the HBA whose concentration was varied from 1 μM to 5 μM. At the start of the experiment each syringe injects 100 μL of sample into the cell where the two samples are mixed. The stop flow syringe enables data to be collected

instantaneously, and usually about six samples are run at a single concentration. The average from these runs is used to give the final data for each concentration of ligand. The reaction was followed by monitoring the fluorescence emission at 410 nm from HBA on binding to CobB after excitation at 330 nm.

5.5.2 Stopped-Flow analysis of CobB/ATP/Gln plus CobH/HBA/ATP/Gln where HBA is varied

In order to determine the dissociation constant (K_d) associated with the binding of HBA to CobB stopped-flow fluorescence spectroscopy was used. An example of the fluorescence change is shown in Figure 5.10. This experiment was carried out using a constant concentration of CobB (1 μM) and CobH (1 μM). Both of the enzymes were initially mixed with 5 mM ATP and 10 mM Gln. HBA was mixed with CobH only and the concentration of the substrate was varied between 1 μM and 5 μM (HBA). Excitation was carried out at 330nm and fluorescence emission was measured at 410 nm. The reaction was then monitored by recording fluorescence emission changes resulting from the substrate binding to the enzyme (Figure 5.12).

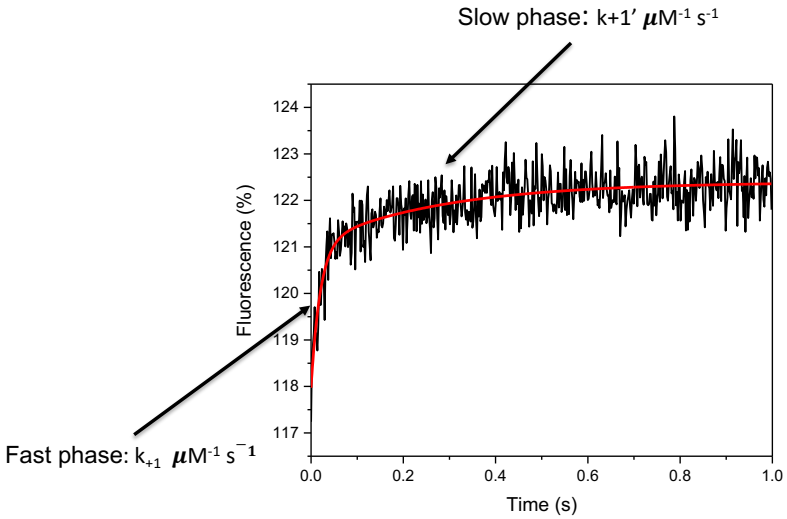

Figure 5.11: An example trace of the fluorescence change upon 1 µM HBA binding to 1 µM CobB. Trace shows a biphasic reaction with a fast and slow phase, with HBA binding monomer A and then monomer B of CobB. Where k_{obs} = 3.3 s^{-1} with fluorescence increase = 4 %.

As already shown in Chapter 4.2.2.2 the binding of HBA to CobB shows a biphasic reaction. This is also the case when the binding of HBA to CobB is followed in the presence of CobH. There is an initial fast rate (R1) followed by a slower rate (R2).

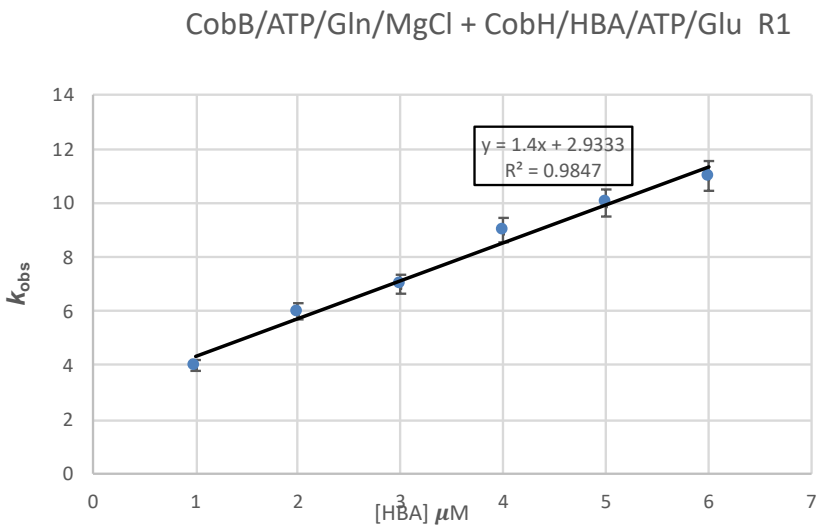

Kd = 2.9/1.4
= 2 μM ± 0.63

Figure 5.12: Dependence of k_{obs} versus [HBA], ATP and Gln. Calculation of rate constants k_{+1} (line gradient) and k_{-1} (y intercept) from stopped-flow measurements of k_{obs} at different concentrations of HBA and constant concentration of CobB/ATP/Gln/Mg^+ and CobH/ATP/Gln/Mg^+ for a) the initial phase of reaction (R1), with calculated k_{+1} = 1.4 μM^{-1} s^{-1}, k_{-1} = 2.9 s^{-1} and K_{d1} = 2 μM. Values are averages of 3 biological repeats (from three different HBA preparations) ± SEM.

For the interaction between CobB and HBA the initial rate data from Figure 5.12 can be determined by the use of non-linear regression to generate the k_{obs} at different HBA concentrations. The gradient of these plots, as shown in Figure 5.12, represents k_{+1} whilst the y intercept represents k_{-1}. The data indicate that the binding of HBA to CobB (K_d = 2 μM) is relatively weak, with a rate constant of k_{+1} = 1.4 μM^{-1} s^{-1}. Data for R1 was produced but the quality of the data for R2 was poor and hence could not be used.

5.5.3 Effect of ATP and Gln on the transfer of HBA from CobH.HBA to CobB

In order to determine if ATP and Gln have an effect on the binding of HBA to CobB in the presence of CobH, the experimental parameters of the stopped flow assay were adjusted, where ATP and Gln were removed from both enzymes. The experiment was run keeping CobB and CobH constant (1 μM), and again varying the concentration of HBA (1– 6 μM) (Figure 5.13). Excitation was again at 330 nm with a GG455 filter.

(a)

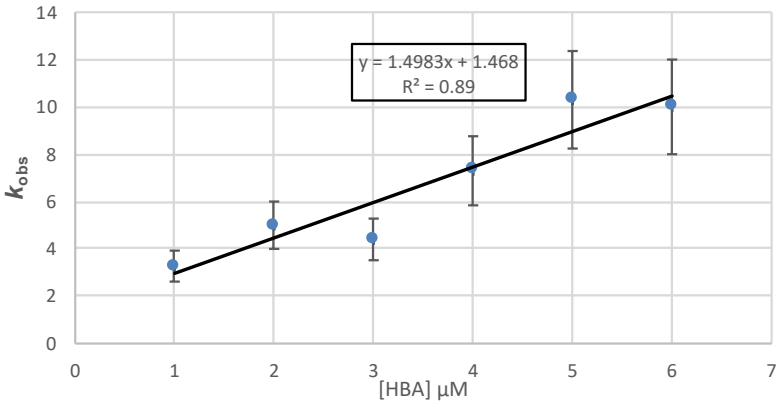

Kd = 1.468/1.493
= 1 μM ±0.414

(b)

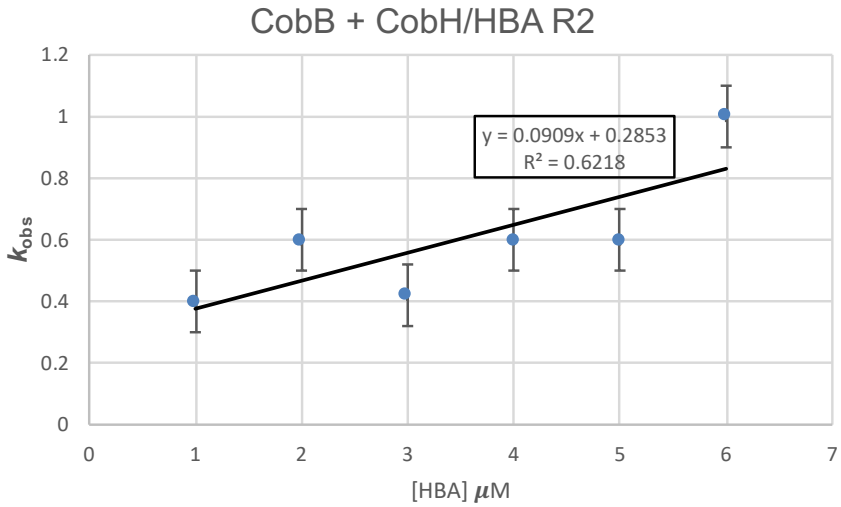

Kd = 0.285/0.091
= 3.17μM ±1.395

Figure 5.13: **Dependence of k_{obs} versus [HBA] CobB and CobH constant.** Calculation of rate constants k_{+1} (line gradient) and k_{-1} (y intercept) from stopped-flow measurements of k_{obs} at different concentrations of HBA and constant concentration of CobB and CobH for a) the initial phase of reaction (R1), with calculated k_{+1} = 1.49 µM^{-1} s^{-1}, k_{-1} = 1.47 s^{-1} and K_{d1} = 1 µM and b) the second phase of reaction (R2) with k_{+1}' = 0.09 µM^{-1} s^{-1}, k_{-1}' = 0.28 s^{-1} and K_{d2} = 3.17 µM.

The removal of ATP and Gln from the stopped-flow had very little effect on the initial binding of HBA to CobB (R1). The reaction was found to have a K_{d1} = 1 μM with a rate of k_{+1} 1.49 μM^{-1} s^{-1}. The affinity of substrate binding was much weaker (~3 fold) K_{d2} = 3.2 μM (Table 5.1). Values are averages of 3 biological repeats (from three different HBA preparations) ± SEM.

5.5.4 Effects of removing ATP and Gln from CobB keeping CobH/ATP/Gln/Mg/ HBA varied

To look at the effects of having ATP and Gln with CobH only, the stopped flow assay was run again. ATP (5 mM) and Gln (10 mM) were added to CobH/HBA, where the HBA concentration was varied. The concentration of CobB and CobH were kept constant (1 mM) and the concentration of HBA was varied from 1 μM to 5 μM (Figure 5.13). Excitation was again at 330 nm with a GG455 filter.

(a)

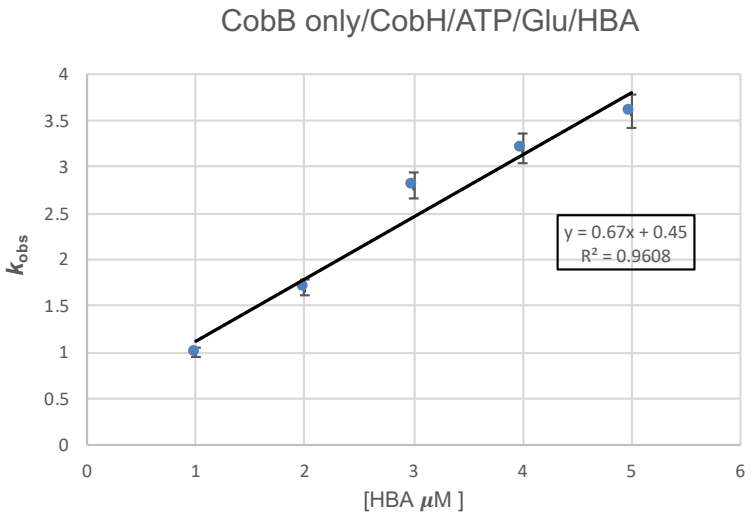

Kd = 0.45/0.67
= 0.67 $\boldsymbol{\mu}$M ± 0.264

(b)

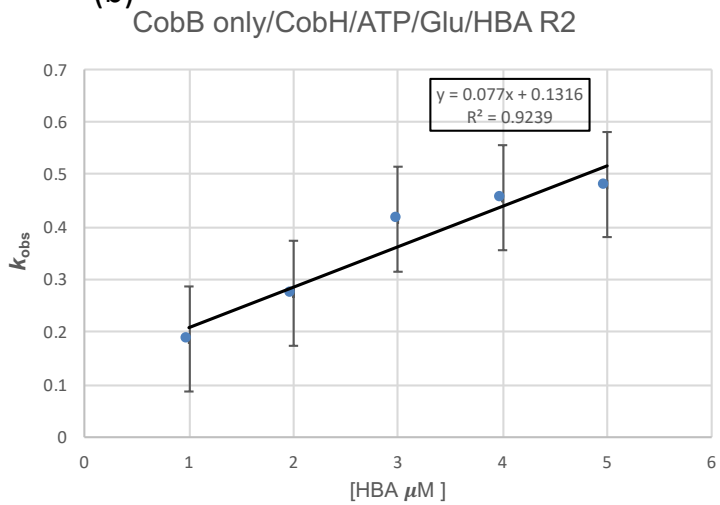

Kd = 0.1316/0.077
= 2 $\boldsymbol{\mu}$M ± 1.205

Figure 5.14: Dependence of k_{obs} versus [HBA] CobB and CobH/ATP/Gln. Calculation of rate constants k_{+1} (line gradient) and k_{-1} (y intercept) from stopped-flow measurements of k_{obs} at different concentrations of HBA and constant concentration of CobB and CobH/ATP/Gln for a) the initial phase of reaction (R1), with calculated k_{+1} = 0.67 μM^{-1} s^{-1}, k_{-1} = 0.45 s^{-1} and K_{d1} = 0.67 μM and b) the second phase of reaction (R2) with k_{+1}' = 0.08 μM^{-1} s^{-1}, k_{-1}' = 0.13 s^{-1} and K_{d2} = 2 µM. Values are averages of 3 biological repeats (from three different HBA preparations) ± SEM.

When ATP/Gln are present with CobH only, HBA binds CobB relatively tightly with a K_{d1} of 0.67 µM but the rate is 3 fold slower than with HBA present only, and 2 fold slower (R1 and R2) than HBA/ATP/Gln present in both enzymes (Table 5.1).

Table 5.1: Rate and binding constants of HBA binding CobB where HBA concentration has been varied:

	R^2	Kd μM R1	k_{+1} μM^{-1} s^{-1}	k-1 s^{-1}	Kd μM R2	k_{+1}' μM^{-1} s^{-1}	k-1' s^{-1}
CobB/ATP/Mg/Gln + CobH/ATP/Gln/Mg/HBA varied	0.981	2.00	1.4	2.9	----------	----------	--------
CobB/Mg + CobH/Mg/HBA varied	0.956	1.00	1.5	1.5	3.2	0.091	0.285
CobB/Mg + CobH/ATP/Gln/Mg/HBA varied	0.957	0.672	0.67	0.45	2	0.077	0.13

From the above table, R^2 is a statistical measure of the fit of the linear regression line, where a value as close to 1 signifies a good fit for the data collected. The weakest binding (K_d = 2 µM) value is the binding of HBA to CobB when all cofactors are present. This reaction showed two phases although the data for the second phase was of very poor quality and was not determined.

These values are very similar to CobB/HBA/ATP/Gln in Chapter 4, Table 4.1, where the K_d is very similar (K_d = 2 µM). However, the rate of the reaction (k_{+1} = 0.62 μM^{-1} s^{-1}) was two-fold slower. Again comparing the binding and rate of reaction with CobB/HBA only (Chapter 4, Table 4.1) to CobB only with CobH/HBA/Gln the K_d looks to be two-fold weaker, and R1 the rate of the fast reaction eight-fold slower.

Strangely, in the absence of ATP and Gln, CobB appears to have a greater affinity for HBA in the presence of CobH. CobB with CobH/HBA shows HBA binds CobB two-

fold tighter than when CobH/HBA has all the cofactors present. Not only does the absence of cofactors increase the binding affinity it also increases the rate of the reaction, which is nine-fold faster (5.70 μM^{-1} s^{-1} and 0.62 μM^{-1} s^{-1}).

5.5.5 Effects of varying the concentration of CobB and keeping CobH.HBA constant

To look at the effects of having excess CobB in the transfer of HBA from CobH to CobB, CobB was varied from 1 µM to 5 µM. The ratio of CobH and HBA was 1:1 and kept at a concentration of 1 µM (Figure 5.15). Fluorescence was monitored at 410 nm after excitation at 330 nm with a GG455 filter.

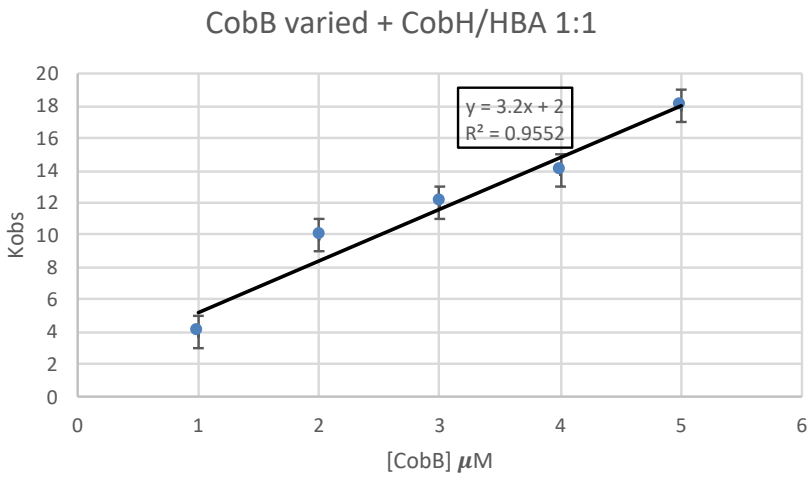

Kd =2/3.2
= 0.625 μM $\pm$0.607

Figure 5.15: Dependence of k_{obs} versus [CobB]. Calculation of rate constants k_{+1} (line gradient) and k_{-1} (y intercept) from stopped-flow measurements of k_{obs} at different concentrations of CobB and a constant concentration of CobH/HBA. This is a single phase reaction with calculated k_{+1} = 3.2 μM^{-1} s^{-1}, k_{-1} = 2 s^{-1} and K_d = 0.62 µM. (Table 5.2). Values are averages of 3 biological repeats (from three different HBA preparations) ± SEM.

All the stopped flow data to date had shown a bi-phasic reaction. Initially there is a fast reaction which signified binding of HBA to the N-terminal active site of one of the monomers and then a much slower rate of binding to the second monomer. However, when excess CobB is present there is a single phase reaction consistent with the transfer of a single HBA to the CobB dimer. The single reaction, equivalent to R1, had a K_d of 0.62 μM, and a relatively fast phase of k_{+1} = 3.2 μM^{-1} s^{-1} and a k_{-1} = 2 s^{-1}. As both k_{+1} and k_{-1} are relatively fast reactions (3.2 μM^{-1} s^{-1} and 2 s^{-1} respectively) it suggests preferential binding to one monomer.

5.5.6 Effects of varying the concentration of CobB and keeping CobH.HBA constant with the addition of ATP and Gln

To determine if having ATP and Gln mixed in with the CobH and HBA would change the binding of HBA to CobB, the assay was adjusted by the addition of ATP (5 μM) and Gln (10 μM) to the CobH/HBA mix. The concentration of CobB (1 μM to 5 μM) was again varied (Figure 5.16). The fluorescence was monitored at 410 nm after excitation at 330 nm with a GG455 filter.

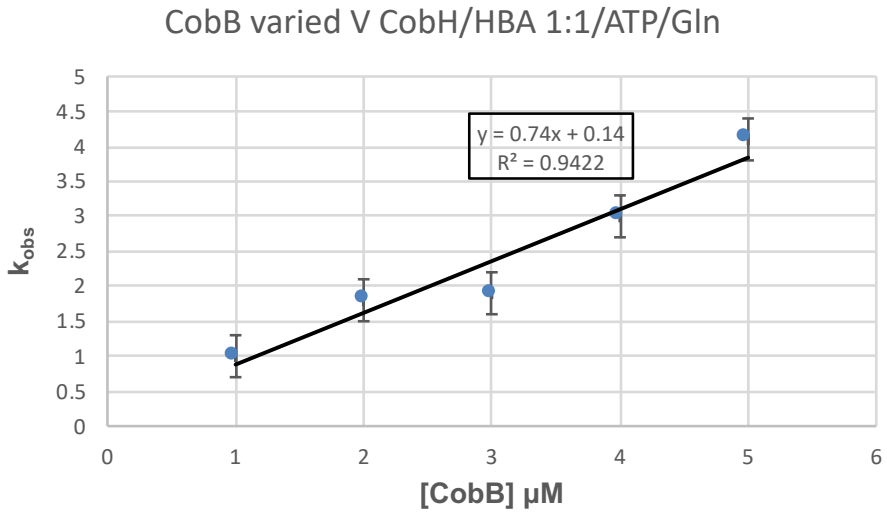

Kd = 0.14/0.74
= 0.19 ±0.21

Figure 5.16: Dependence of k_{obs} versus [CobB] constant concentration of CobH/HBA 1:1 ATP/Gln/Mg. Calculation of rate constants k_{+1} (line gradient) and k_{-1} (y intercept) from stopped-flow measurements of k_{obs} at different concentrations of CobB and constant concentration of CobH/HBA 1:1 ATP/Gln/Mg. The rates were calculated as k_{+1} = 0.74 μM^{-1} s^{-1}, k_{-1} = 0.14 s^{-1} and K_d = 0.189 µM. Values are averages of 3 biological repeats (from three different HBA preparations) ± SEM.

Again the results indicate a single phase reaction (Figure 5.16). However, the addition of ATP and Gln changed the affinity with which HBA binds to CobB three-fold. This tighter binding results from a 4 fold decrease in k_{+1} and a 14 fold decrease in k_{-1} (0.74 μM^{-1} s^{-1} and 0.14 s^{-1} respectively) (Table 5.2).

Table 5.2: Rate and binding constants of HBA binding CobB where CobB concentration has been varied

	R^2	Kd μM R1	k_{+1} μM^{-1} s^{-1}	k-1 s^{-1}
CobB varied/Mg Vs CobH/Mg/HBA	0.914	0.625	3.2	2
CobB varied/Mg Vs CobH/ATP/Mg/Gln	0.940	0.4	0.714	0.286

The presence of ATP and Gln in the above reaction increase the affinity of HBA binding to CobB, which results in a slower association and dissociation rate.

5.5.7 Effects of varying the concentration of CobH/HBA 1:1 and keeping CobB constant

A third assay was run this time varying the concentration of CobH and HBA (1:1) keeping CobB constant. The experimental parameters varied were carried out firstly using a constant concentration of CobB (1 μM), and varying the concentration of CobH and HBA (1 μM, 2 μM, 3 μM, 4 μM and 5 μM) (Figure 5.17). Fluorescence emission at 410 nm was monitored after excitation at 330 nm with a GG455 filter.

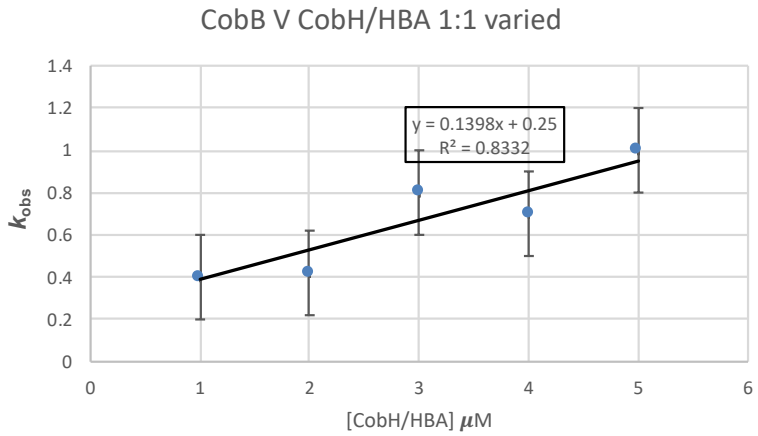

Kd = 0.25/0.14
= 2 μM$\pm$1.75

Figure 5.17: Dependence of k_{obs} versus [CobH/HBA]. Calculation of rate constants k_{+1} (line gradient) and k_{-1} (*y* intercept) from stopped-flow measurements of k_{obs} at different concentrations of CobH/HBA with a constant concentration of CobB. The calculated rates were k_{+1} = 0.14 μM^{-1} s^{-1}, k_{-1} = 0.25 s^{-1} with a K_{d1} = 2 μM (Table 5.3). Values are averages of 3 biological repeats (from three different HBA preparations) ± SEM.

5.5.8 Effects of varying the concentration of CobH in presence of constant HBA and CobB

Stopped flow was run by varying the concentration of CobH and keeping the concentration of CobB at 1 μM. CobH concentration was varied at 1 μM, 2 μM, 3 μM, 4 μM and 5 μM and to each sample 1 μM of HBA was added (Figure 5.18). The fluorescence emission was recorded at 410 nm with excitation at 330 nm with a GG455 filter.

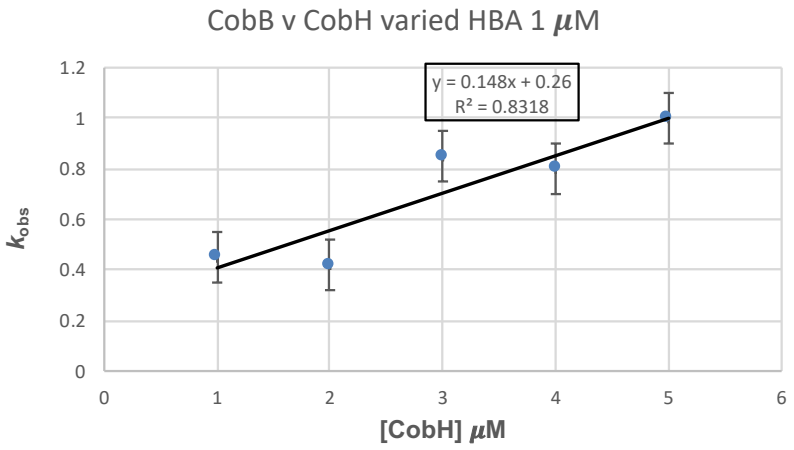

Kd = 0.26/0.15
= 2 μM±1.5

Figure 5.18: Dependence of k_{obs} versus [CobH] constant concentration of CobB, HBA/ATP/Gln/Mg. Calculation of rate constants k_{+1} (line gradient) and k_{-1} (y intercept) from stopped-flow measurements of k_{obs} at different concentrations of CobH and constant concentration of CobB, HBA/ATP/Gln/Mg. The reaction rates were k_{+1} = 0.15 μM^{-1} s^{-1}, k_{-1} = 0.26 s^{-1} with a K_d = 2 μM. Values are averages of 3 biological repeats (from three different CobH preparations) ± SEM.

In this assay CobH is in excess but HBA is constant at the same level as CobB. As the HBA level does not exceed the concentration of CobB this binding event is also observed to be a single phase reaction. However, what is interesting here is that the increasing concentration of CobH results in an increase in k_{obs}, indicating that CobH appears to help promote the binding of HBA to CobB (Table 5.3).

Table 5.3: Rate and binding constants of HBA binding CobB where CobH and HBA concentration has been varied

	R^2	Kd μM R1	k_{+1} μM^{-1} s^{-1}	k-1 s^{-1}
CobB/Mg Vs CobH/HBA 1:1 varied 100sec	0.833	2.00	0.14	0.25
CobB/Mg Vs CobH/varied/HBA 1μM	0.832	2.00	0.15	0.26

5.6 Crosslinking of CobB and CobH

To understand protein-protein interactions at an atomic level X-ray crystallography and NMR spectroscopy are the most common methods employed (Acuner Ozbabacan *et al.* 2011). However, capturing these interactions in order to obtain structural information has proven difficult due to the nature of their life time in this complexed state. Crystallisation of the complex was unsuccessful. This was not unexpected due to the likely transient nature of the interactions between CobB and CobH. At this point two methods were considered, either engineering a fussed construct of CobH/CobB or trying to crosslink the two enzymes. Due to time restrictions it was decided to crosslink the two enzymes, to try and overcome this transient problem (Vishnu *et al.* 2013).

Three crosslinkers were chosen that differed in the length of their spacer arm; DMS (dimethyl suberimidate) which has an 11 Å spacer arm, DMP (dimethyl pimelimidate) which has a 9.2 Å spacer arm and DFDNB (1, 5-difluoro-2, 4-dinitrobenzene) which has a 3.0 Å spacer arm (Figure 5.19). Both DMS and DMP have reactive imidoester groups at either end of the molecule whilst DFDNB contains reactive aryl halide groups. All three of these protein cross-linking reagents are reactive to primary amines at alkaline pH (pH 8-10) and form amidine derivatives. Due to the functional groups in proteins, primary amines are typically nucleophilic which makes them easy to target for conjugation.

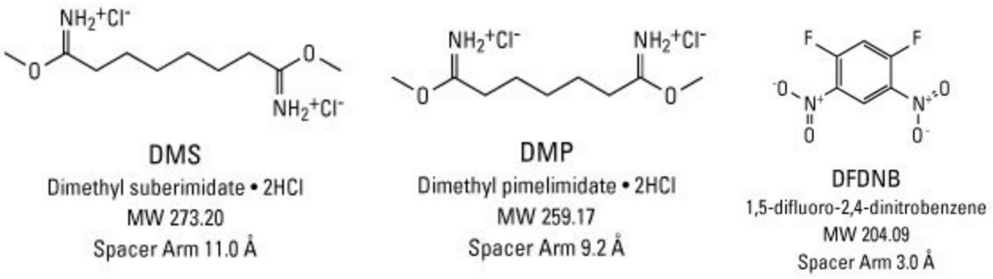

Figure 5.19: Chemical crosslinkers. Structure of the chemical crosslinking reagents used to link CobH and CobB. These crosslinkers react with primary amines at alkaline pH to form amidine derivatives.

5.6.1 Preparation of crosslinkers DMS, DMP and DFDNB

Each of the crosslinkers were resuspended in water to a concentration of 100 µM (stock solution). Using a PD10 column the enzymes were exchanged into phosphate buffer saline (PBS). The concentration of CobB and CobH were adjusted to a concentration of 0.7 mg/mL. HBA was added to a final concentration of 100 mg/mL to the dilute CobH. CobB and CobH/HBA were combined and 50 μL of the crosslinker was added to the dilute complex. The complex was then left rotating at room temperature for 2 hours. To stop the reaction the buffer was changed using a PD10 column back into the original 20 mM Tris/HCl buffer, pH 8.0, containing 150 mM NaCl.

5.6.1.1 Gel Filtration column CobH, CobB and crosslinked CobH.CobB

In order to determine where the individual proteins would elute on a gel filtration column the proteins were run individually. CobH has a molecular mass of 24 kDa, and as a dimer should run at around 48 kDa. The protein was applied to a Superdex S20016/600 column and eluted in 20 mM Tris-HCl, pH 8.0, containing 150 mM NaCl and 2 mM MgCl2 (Figure 5.20).

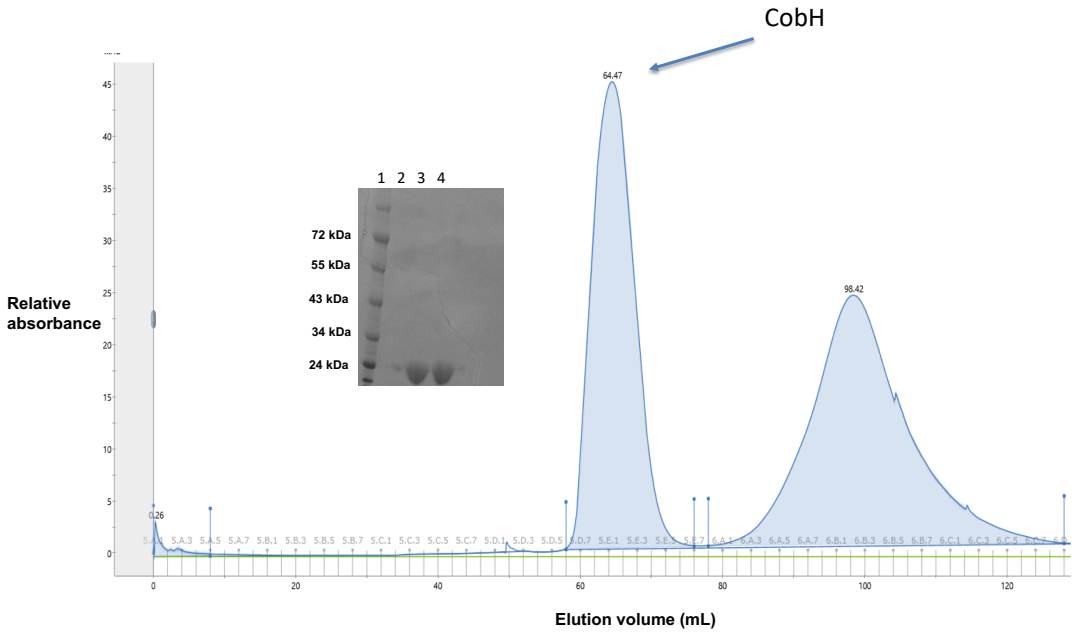

Figure 5.20: CobH gel filtration and resultant SDS PAGE analysis. Gel filtration chromatogram is shown with large peak at 64 mL and smaller second peak at 98 mL. SDS PAGE, lane 1 contains protein markers of molecular masses as shown. Lanes 3 and 4 represent samples taken from the main peak at 64 mL. The second peak did not show on an SDS PAGE gel. As this represents something with a molecular weight of less than 24 kDa on this gel it would not be visible. Second peek most likely a small contaminant.

The large peak at 64.47 mL was analysed by SDS PAGE gel. The major protein was assumed to be CobH as it had a molecular mass of 26 kDa (Figure 5.19).

5.6.1.2 CobB Gel filtration column

CobB has a molecular mass of 47 kDa and as a dimer should run at 114 kDa. The protein was applied to a Superdex S200 16/600 column and eluted in buffer containing 20 mM Tris-HCl, pH 8.0, 150 mM NaCl and 2 mM MgCl2 (Figure 5.21).

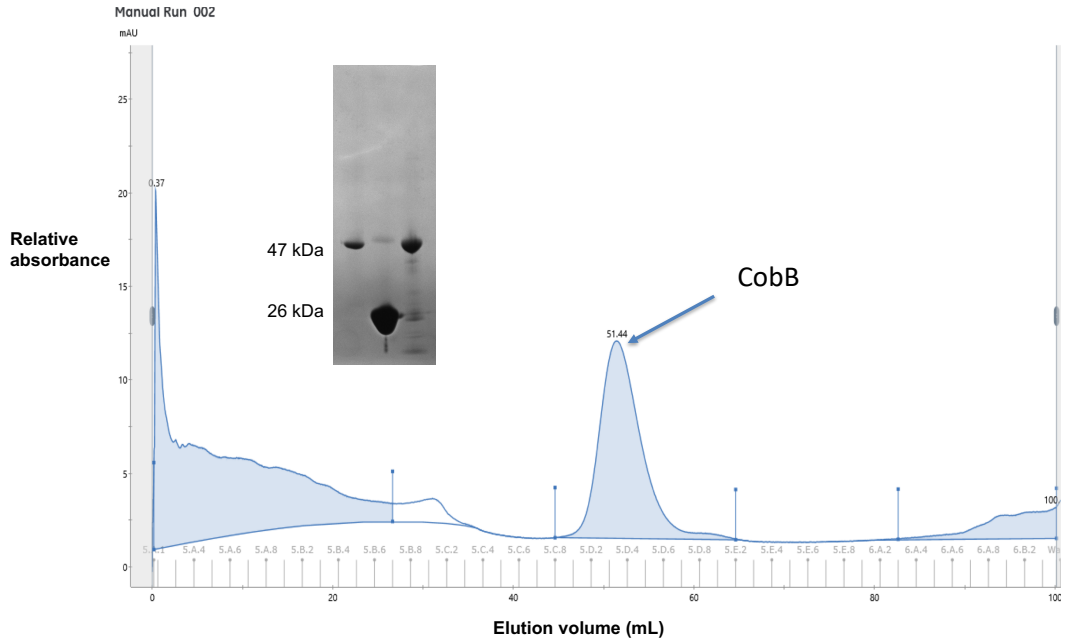

Figure 5.21: CobB gel filtration. Peak at 51.4 mL was run on 10% SDS PAGE gel. Lane 1: main peak, Lane 2: CobH, Lane 3: CobB before gel filtration. Lane 1 shows protein at a molecular mass of 47 kDa. This corresponds to the molecular mass expected for CobB.

The large peak at 51.4 mL was analysed by SDS PAGE gel and the major protein was assumed to be CobB as it had a molecular mass of 47 kDa (Figure 5.21).

5.6.1.3 CobH.CobB crosslinked with DMS and DMP run on gel filtration column

DMS and DMP were used to crosslink CobH and CobB using the method described in Section 5.3.1. However, both of these crosslinkers did not appear to give any cross-linked material. Small peaks were seen on the gel filtration chromatograph but when run on an SDS gel no protein was visible.

5.6.1.4 CobH.CobB crosslinked with DFDNB run on gel filtration column

The third crosslinker to be used was DFDNB using the same method as described in Section 5.3.1.

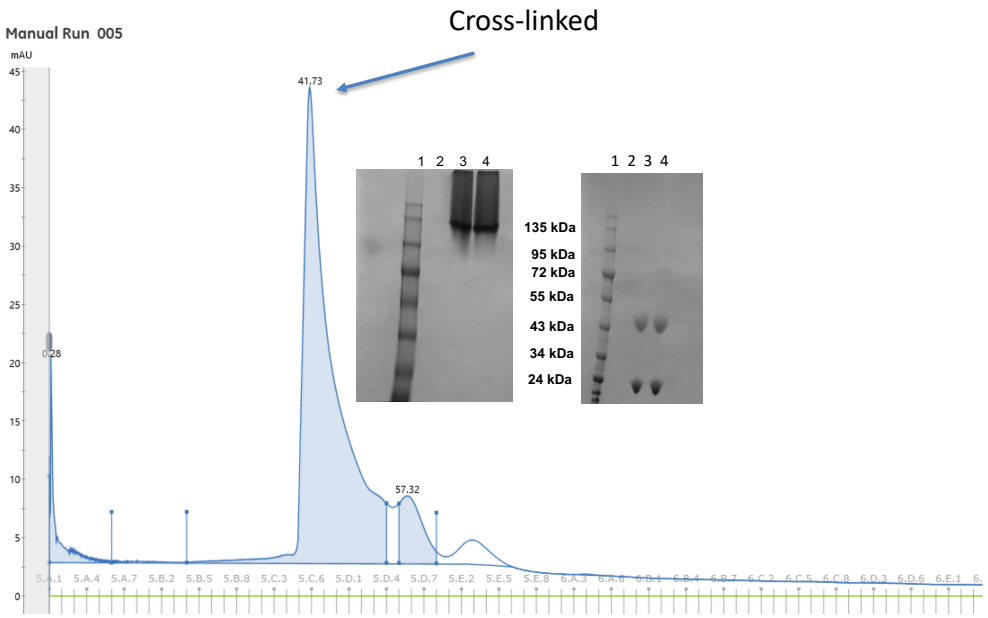

Figure 5.22: CobH.CobB crosslinked with DFDNB gel filtration. Large peak shows elution at 41.73 mL. Peak run initially on a native gel, shows molecular mass of around 135 kDa. Analysis by SDS PAGE gel, lane 1 contains protein markers of known molecular mass, as shown, lane 2 blank, lane 3 and 4 reveals bands at 47 kDa and 24 kDa. These bands correspond to the molecular mass of CobH (24 kDa) and CobB (47 kDa).

DFDNB was incubated with a mixture of CobH and CobB and run on a gel filtration column (Fig 5.22). A large peak was observed at 41.73 mL, which appeared promising as there was also a smaller peak at 57.22 mL, which could suggest free CobB. The samples were run on a native gel and also a 10% SDS gel. From the native gel a band was observed at about 135 kDa, which is close to what would be expected for the complex between a CobH dimer and a CobB dimer. However, the SDS gel revealed two bands, one at 26 kDa and the other at 47 kDa (same molecular mass

as native CobH and CobB respectively). As DFDNB is a covalent crosslinker it would not be expected to see the individual enzymes on denaturing gel.

5.7 Crystallisation of crosslinked CobH and CobB

The crosslinked protein from the gel filtration column was, however, run in crystallisation trials. The protein had a concentration of 0.7 mg/mL and HBA was added to the dilute protein at a concentration of 100 mg/mL. The complex was then diluted and concentrated in a 30 kDa concentrator 3 times using 20 mM Tris-HCl buffer, pH 8.0, containing 150 mM NaCl and 2 mM MgCl2 and concentrated to 4 mg/mL.

Crystallisation trays were then prepared using Molecular Dimensions screens 1 and 2. A 24 well plate was used and 500 μL of screen was added to each well, the drop ratio was 2:1. Small crystals appeared after 2 to 3 days, these crystals were less than 1 micron in length and were badly twinned (Figure 5.23).

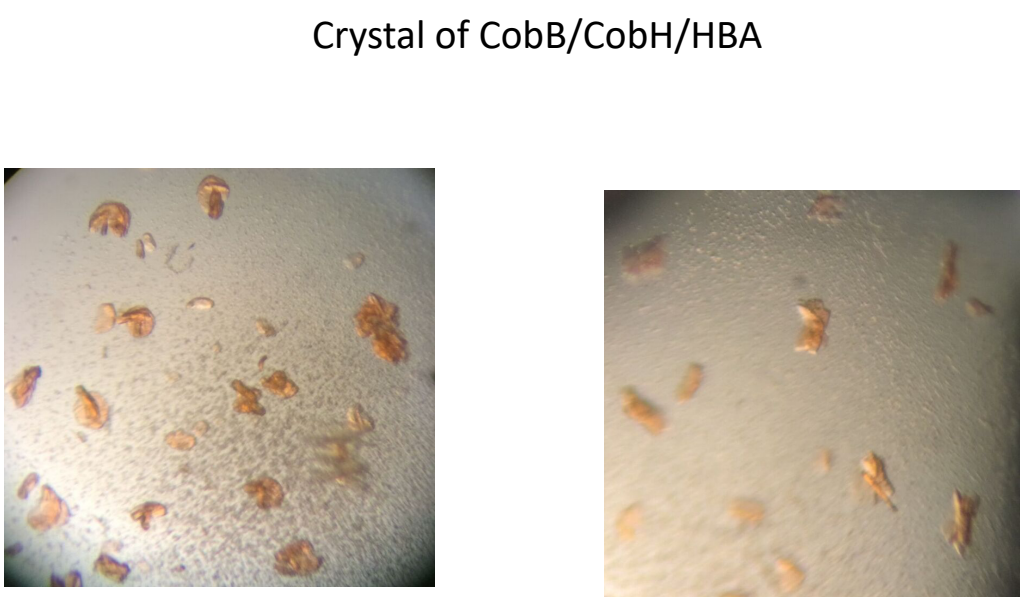

Figure 5.23: Crystals of crosslinked CobH-CobB with HBA. Condition (a), 0.2 M ammonium acetate, 0.1 M sodium citrate pH 5.6 and 30% PEG 4K, condition (b) 0.2 M sodium acetate, 0.1 M sodium cacodylate, pH 6.5, and 30% PEG 4K.

The crystals were archived by freezing in liquid nitrogen and sent to DLS for data collection. The crystals diffracted to 2.5 Å and 2.6 Å and were predicted to have two molecules in the AU. Molecular replacement using the maps from both CobB and CobH were used to try to solve the structures. However, the data collected was of poor quality and it was not possible to solve the structure. Further optimisation of this whole process is required.

5.8 Discussion

The crystal structures of CobH, an enzyme involved in methyl rearrangement of precorrin 8 to HBA, have previously been solved from a number of bacterial systems including *P. denitrificans (*Shipman *et al* 2001*), R. capsulatus (*Deery *et al* 2012*)* and *B. melitensis* (Seattle Structural Genomics PBS. 3E7D not published, no HBA bound). CobH catalyses the methyl group migration from C11 to C12 of the corrin ring (Shipman *et al.* 2001; Deery *et al.* 2012).

CobH crystallises as a homodimer with two molecules in the asymmetric unit, where one molecule of each forms the interphase to complete the dimer. The structure of CobH shows a highly conserved region of amino acids that project into the active site of each monomer. These polar residues generate an extensive hydrogen bonding network between the side chains and the carboxylates on the corrin ring (Shipman *et al.* 2001) (Deery *et al.* 2012).

In the *B. melitensis* structure of CobH there is one molecule of HBA bound to monomer A leaving monomer B empty. However, in the *R. capsulatis* structure with HBA bound both sites have HBA present. The lack of full occupancy in the *B. melitensis* structure may represent an artefact of the crystallisation process.

An overview of the *B. melitensis* apo structure with the *R. capuslatus* CobH (two HBA molecules bound) structure shows that there are pronounced changes in the side chains within the active site when HBA is bound between the two species. In the bound structure Arg115 flips between two conformations where it folds into the active site binding to HBA and moving away from the active site in its absence (Figure 5.24 and 5.25). Overall it looks as if most of the side chains within the active site change conformation in the bound structure, forming a more closed configuration.

Overlay of *Brucella* CobH with *Rhodobacter* CobH

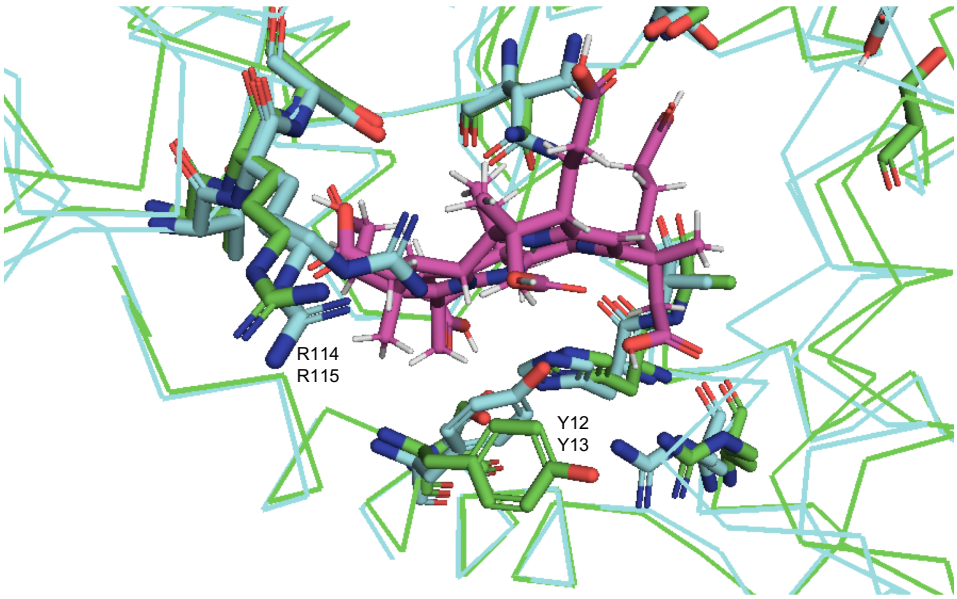

Figure 5.24: Ribbon diagram of *B. melitensis* CobH apo structure (green) overlaid with *R. capsulatus* CobH HBA bound (cyan). R114 from *B. melitensis* and R115 *R. capsulatus* show movement of this residue in the bound structure and unbound. Y12 from *B. melitensis* and R13 from *R. capsulatus* also show a change in conformation.

Overlay of *Brucella* CobH with *Rhodobacter* CobH

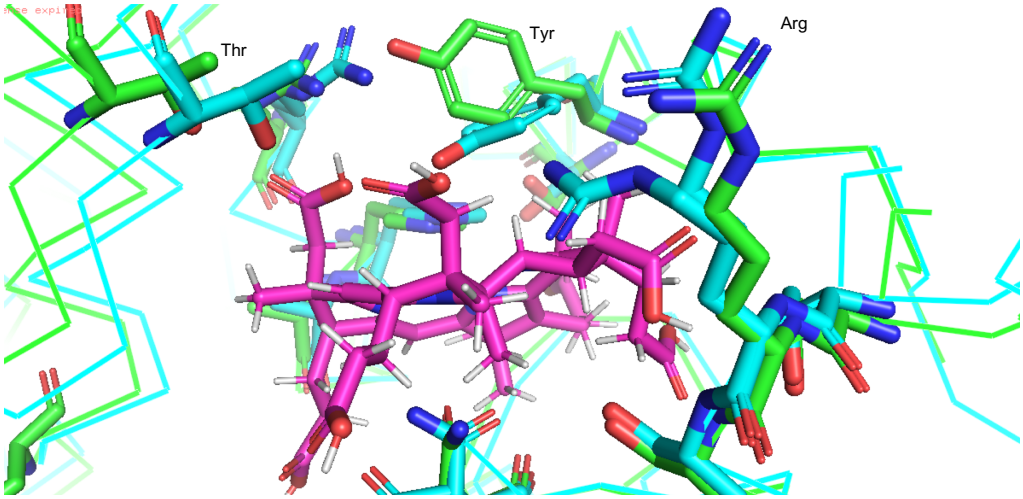

Figure 5.25: Ribbon diagram of *B. melitensis* CobH native structure (green) overlaid with *R. capsulatus* CobH HBA bound (cyan) (2). Different view of the changes in bound and unbound residues.

Due to the transient nature of the CobH.CobB reaction, crystals of the complex were not generated. In order to try and obtain structural data of the complex a technique involving crosslinking of the two enzymes was employed. Three crosslinkers were used varying in the length of their spacer arm. The most promising results came from the shortest spacer arm of 3 Å (DFDNB), however, SDS PAGE did show two separate bands, which corresponded to the same molecular weight as the two enzymes (CobH and CobB). This was not what would be expected, as DFDNB is a covalent crosslinker. Therefore, under denaturing conditions you should still expect to see the complexed protein. This sample was put into crystallisation trials, and very small crystals were obtained. The crystals were sent to the DLS for data collection. One data set was collected but the diffraction data was too low resolution, anisotropic and had ice rings, so no structure was obtained.

The binding of HBA to CobB was investigated in the presence of CobH in order to determine whether CobH has an effect on mediating the direct metabolite transfer of

HBA from CobH to CobB. Three separate Stopped flow experiments were used to investigate this reaction. Firstly varying the concentration of HBA, secondly CobB and thirdly CobH.

The initial results where CobH is present and HBA is varied show a two phase reaction which is identical to CobB binding HBA when HBA s varied (Chapter 4). When CobB has ATP/Mg^{2+}/Gln present the K_d is the same as HBA binding CobB, when no CobH is present (2.0 μM for both). However there is a difference in the rate of the reaction, with CobH present, this reaction is two-fold faster than without (CobB/ATP/Gln/Mg^{2+} + CobH/ ATP/Gln/Mg/HBA = 1.4 μM^{-1} s^{-1} compared to CobB + ATP/Gln/Mg/HBA = 0.62 μM^{-1} s^{-1}). This suggests that the presence of CobH in this interacting with CobB induces a conformational change in the active site of CobB. This more open conformation results in a quicker rate of binding. When the reaction is carried out again this time with no ATP or Gln present in CobB or CobH the K_d is two-fold weaker (1 μM), however the rate of the reaction is almost the same (1.5 μM^{-1} s^{-1}). The next reaction was with CobB/Mg only + CobH/ATP/Gln/Mg/HBA, the Kd for this reaction was 0.672 μM. CobH has Gln present, as this is not required for enzyme activity the free molecule of Gln may have passed from CobH to CobB, this would account for the slightly tighter binding affinity of HBA to CobB. In all of the previous reaction in Chapter 4 the binding affinity of HBA was always tighter when Gln was present with CobB. As there is no crystal structure with Gln bound it is inconclusive regarding the effects Gln has on the enzyme.

The second experiment was carried out, this time varying the concentration of CobB and keeping CobH/HBA at a constant concentration (1 μM:1 μM). This resulted in a single phase reaction which is consistent with the transfer of a single HBA molecule to the CobB dimer. This is not surprising as there is an excess of CobB and a limited number of HBA molecules present to fully occupy the enzyme. The experiment was run again this time CobH/HBA (1 μM:1 μM) was in the presence of ATP/Mg/Gln. As

expected this was again a single phase reaction. However the addition of ATP and Gln change the K_d values from K_d = 0.625 μM to 0.189 μM, which is 3 fold tighter binding and a four-fold decrease in the rate of the reaction (3.2 μM^{-1} s^{-1} and 0.189 μM^{-1} s^{-1} respectively). This results are consistent with what we are seeing in all of the Stopped flow reactions where the presence of Gln increases the affinity for HBA binding CobB. The increased affinity in these two reactions could also be the fact that there is no turnover of HBA to HBAD as there is no ATP present in the CobB sample.

The third assay to be run was this time varying the concentration off CobH/HBA and keeping the concentration of CobB constant (1 µM). This experiment was problematic and did not initially give usable data. The experiment was run for over 100 sec (normal exposure 10 sec) in order to obtain a result. A second experiment was carried out this time by varying CobH only and keeping CobB and HBA at a concentration of 1 µM. This reaction as less problematic and gave the exact same result as CobB + CobH/HBA (1 µM:1 µM) with K_d = 2 µM. The most interesting fact is by increasing the concentration of CobH results in an increase of k_{obs} in both reactions (0.25 s^{-1} and 0.26 s^{-1}). This indicates that CobH appears to help promote the binding of HBA to CobB.

In summary the binding of HBA to CobB is dependent upon the concentration of CobH. As expected, the binding of HBA to CobB is not as fast with free HBA as reported in Chapter 4, but as outlined in Chapter 4 the CobB.HBA complex is stabilised in the presence of Gln. Given the tight association of HBA with CobH, the fact that CobB is able to obtain HBA from the CobH.HBA complex indicates that the two proteins interact in a productive manner. Further work is required to investigate this interaction, including a study of the kinetics of HBA binding to CobH.

Chapter 6

Production, purification and crystallisation of the CobQ enzymes from *Allochromatium vinosum*, *Brucella melitensis* and *Rhodobacter capsulatus*.

6.1 Introduction

Adenosylcobyrinic acid *a,c*-diamide acts as the substrate for the second amidase enzyme in the pathway, CobQ (Debuscche *et al.* 1990). In a similar reaction to that catalysed by CobB, CobQ amidates the carboxylic acids found on side chains *b, d, e* and *g*. These series of four amidations transform adenosylcobyrinic acid *a,c*-diamide into adenosylcobyric acid (Figure 6.1).

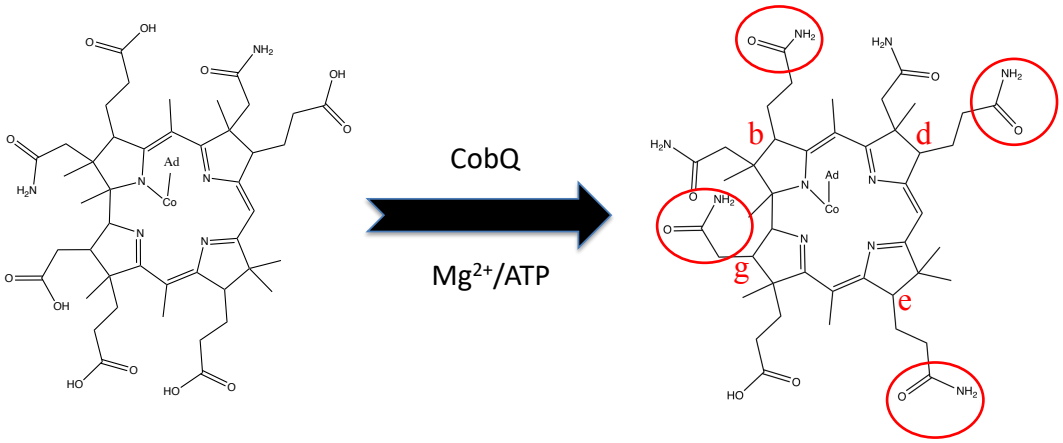

Figure 6.1: Amidation of adenosylcobyrinic acid *a, c*-diamide to adenosylcobyric acid.

Figure shows the amidation at positions *b, d, e* and *g* on the corrin ring.

CobQ firstly amidates the carboxylate acid side chain at position *e*, followed by positions *d, b* and *g*. It is believed that on partial amidation of *e* the intermediate dissociates from the active site and re-orientates at position *b, d and g* sequentially (Fresquet, Williams and Raushel 2007). Interestingly, CobQ amidates three propionate side chains and one acetic acid side chain, so the enzyme displays a level of variability in terms of its regio-specificity. The aim of this chapter was to learn more about the structure of CobQ and understand how the enzyme affords its regio-specificity given that it amidates side chains on different poles of the substrate. The structure would also allow a direct comparison with CobB and would thus give an insight into how CobQ evolved to accommodate its broader specificity. From the

primary sequence in relation to CobB and CobQ (Chapter 4, Figure 4.), both enzymes have a typical ATP binding site and GAT domain binding site, and belong to a family of proteins termed Gln dependent amidotransferses. These enzymes share typical features such as a Gln deaminase (GAT) domain and an ATP hydrolysing synthetase domain where it is attached to phosphorylated carboxyl group of the substrate that is to be amidated. Both enzymes have conserved residues in the N-terminal domain which show a walker motif (p-loop) which is typical for this family of proteins. There are a number of conserved residues with regard to secondary structure between the two enzymes see Figure 1.8 (Galperin and Grishin 2000). In this family of proteins the ATP binding domain shows little homology other than the motifs involved in ATP binding.

The C-terminal domain classified as the GAT domain falls into two groups, both CobB and CobQ although not officially classified as type 1 Gln amidotransferses, homology wise fall into this class. This is due to the presence of a catalytic triad (C366, 425E and H468 CobQ and C327, 326E and H427 CobB).

6.2 Results

6.2.1 Recombinant production of *A. vinosum, B. melitensis* and *R. capsulatus* CobQ

In order to overproduce the various CobQ enzymes *E. coli* strain BL-21 (DE3) pLys*S* was transformed with pET14b vectors harboring the various *cobQ* genes (from *A. vinosum, B. melitensis* and *R. capsulatus*) (Dr. Evelyne Deery). The encoded gene products allow for the production of the various recombinant CobQs with an N-terminal His_6-tag.

The 3 *E.coli* strains each harbouring a cobQ gene from a different organism *(A. vinosum*, *B. melitensis* and *R. capsulatus*) were streaked on agar plates containing chloramphenicol and ampicillin and grown overnight at 37 °C. A single colony was removed from each plate and inoculated into 3 separate 10 mL cultures of LB, containing antibiotics and grown overnight at 37 °C (see Chapter 2.2.7 for protocol).

The following day the overnight cultures were transferred into 3 x 1 L flasks containing 2YT broth with antibiotics and glucose. When the OD_{600} reached around 0.7 the cultures were induced with IPTG and left to grow for a further 3 hours. The cells were harvested and the pellet resuspended in 50 mL of 20 mM Tris-HCl buffer, pH 8.0, containing 500 mM NaCl and 20 mM imidazole, and frozen at -20 °C. When required the cells were lysed by sonication and centrifuged for a second time to remove the cell debris.

6.2.2 Purification of His_6-tagged *Allochromatium vinosum* CobQ

Approximately, 60 mL of supernatant from the *E. coli* strain overproducing the *A. vinosum* CobQ was loaded to a Ni-sepharose column. Fractions from the elution buffer containing 300 mM imidazole were collected (Figure 6.2). The collected samples were run through a PD10 column into ion exchange buffer (Buffer A: 20 mm Tris-HCl, pH 8.0, containing 150 mM NaCl and 2 mM $MgCl_2$) in order to remove the imidazole as the protein was found to be unstable if left overnight in the elution buffer. The final purification step was carried out using an ion exchange column (MonoQ) and the protein eluted by running a gradient between buffer A and buffer B (Buffer B: 20 mM Tris-HCl, pH 8.0, containing 1 M NaCl and 2 mM $MgCl_2$). The purified protein eluted from the column in ~ 250 mM NaCl. The peak fractions were run on an SDS PAGE gel (Figure 6.3) and the protein fractions that contained protein were collected and the dilute protein was aliquoted and stored at -20 °C.

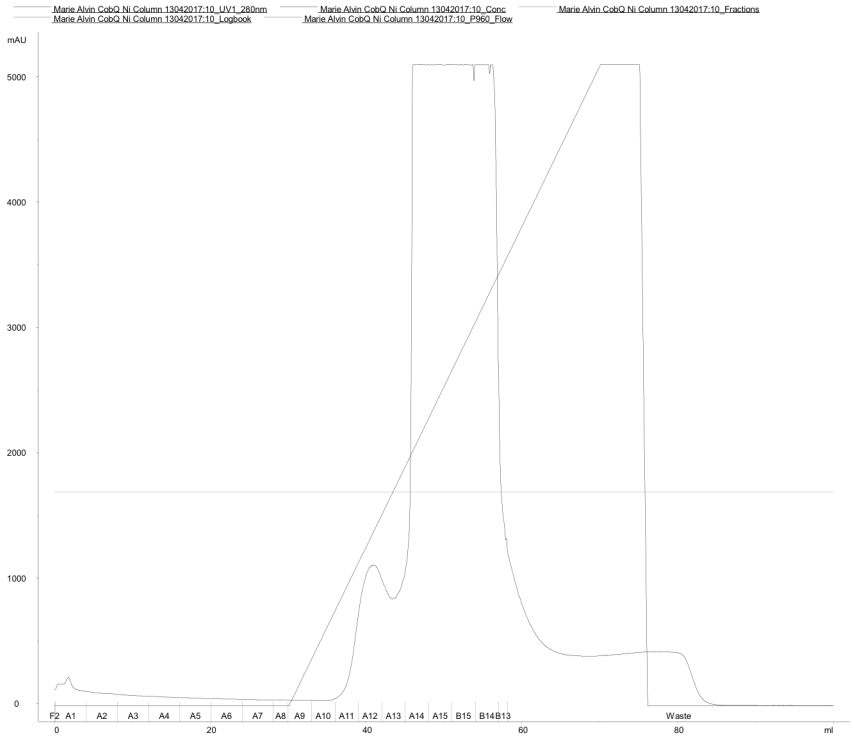

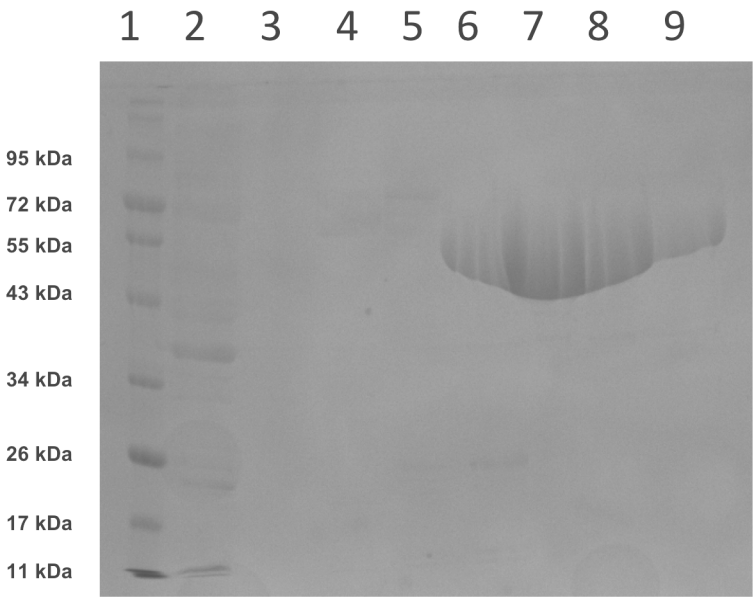

Figure 6.2: 10% SDS PAGE gel of *A. vinosum* CobQ from Ni column. Lane 1 contains protein markers of known molecular mass, as shown, Lane 2 Supernatant pre-column, Samples 3, 4 and 5. Peak 1 from chromatograph, Lane 6, 7, 8 and 9, 2 mL samples collected from position A11 to A15 from peak 2 of chromatograph. Protein in peak 2, A14 and A15.

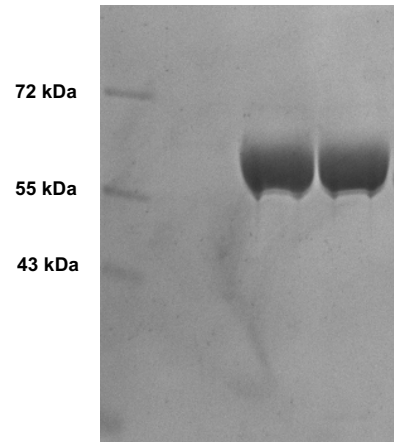

Figure 6.3: *A. vinosum* CobQ from Ion exchange column. 10% SDS PAGE gel showing purified CobQ, from ion exchange column. Two large bands are CobQ

6.2.3 Purification of His_6-tagged *Brucella melitensis* CobQ

The recombinant *E. coli* cell extract containing the overproduced His_6-tagged *B. melitensis* CobQ (~60 mL supernatant) was loaded onto a Ni-sepharose column. The protein was eluted from the column in elution buffer containing 250 mL imidazole and the CobQ-containing fractions were pooled (Figure 6.4). Following this the CobQ was run through a PD 10 column to remove imidazole and the same protocol applied as described in Section 6.1.2. This enzyme eluted from the ion exchange column in 350 mM NaCl. The purified protein, determined from SDS PAGE (Figure 6.5) was aliquoted and stored at -20 °C.

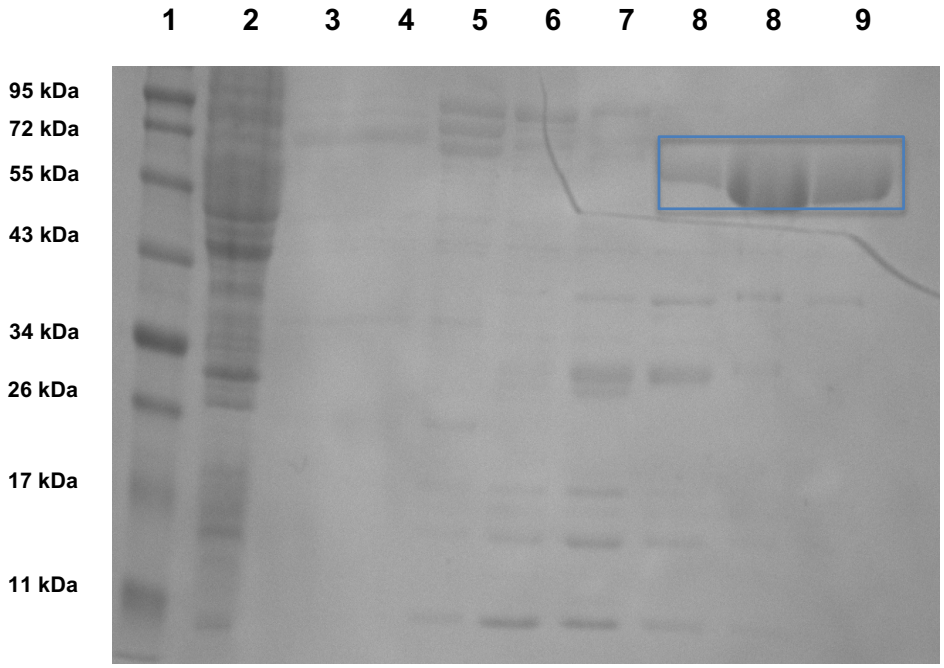

Figure 6.4: *B. melitensis* CobQ SDS PAGE gel from Ni column. Lane 1. contains protein markers of known molecular mass, as shown, Lane 2. Pre-column *A. vinosum* CobQ, Lane 3, 4, 5, 6 and 7 peak 1. Lane 8, 9 and 10 peak 2. Purified *B. melitensis* CobQ in peak 2.

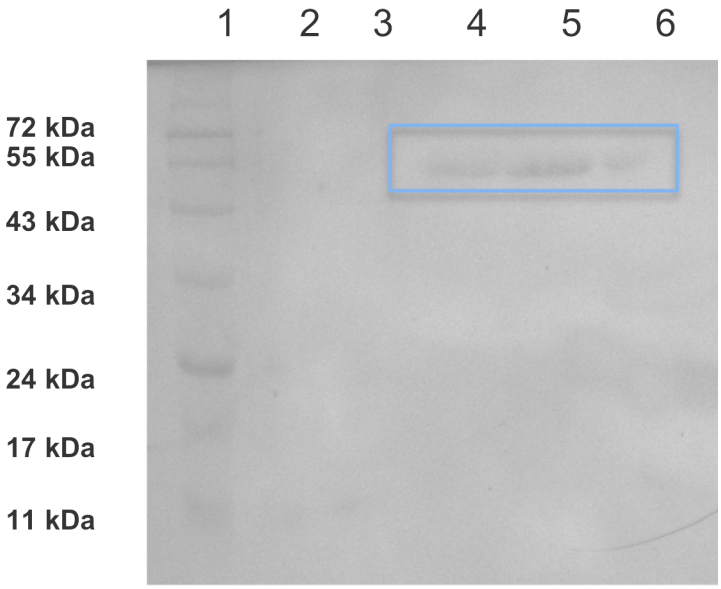

Figure 6.5: *B. melitensis* CobQ SDS PAGE gel from ion exchange. Lane 1, contains protein markers of known molecular mass, as shown, Lane 2 and 3 (A12 to B13). No sample, Lane 4-6. CobQ in samples 4, 5 and 6.

6.2.4 Purification of His-tagged *R. capsulatus* CobQ

A cell extract from the *E. coli* strain overproducing recombinant His_6-tagged *R. capsulatus* CobQ was applied to a Ni-sepharose column (~60 mL of supernatant). The protein was found to elute from the column in elution buffer containing 300 mM imidazole. CobQ-containing fractions were identified by SDS-PAGE and were pooled (Figure 6.6).

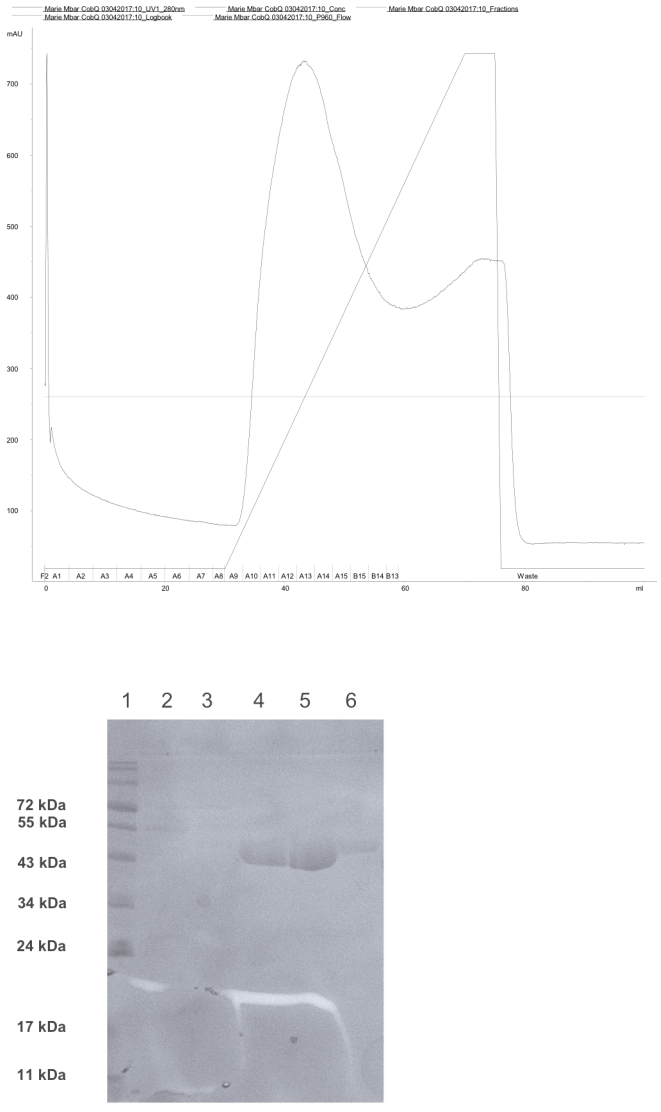

Figure 6.6: *R. capsulatus* CobQ from Ni column. (a) Chromatogram showing large protein peak of *R. capsulatus* CobQ (samples A9 to B15). These samples were collected and run on an SDS gel. (b) SDS PAGE gel Lane 1: contains protein markers of known molecular mass, as shown, Lane 2 & 3: contains flow through from the column, Lane 4: A9, A10 and A11, Lane 5: A12, A13 and A14, Lane 6: A15, B15 and B14. Fractions from samples 4, 5 and 6 were collected .

The collected fractions were run through a PD10 column and applied to an ion exchange column, where the protein eluted at around 300 mM NaCl (Figure 6.7).

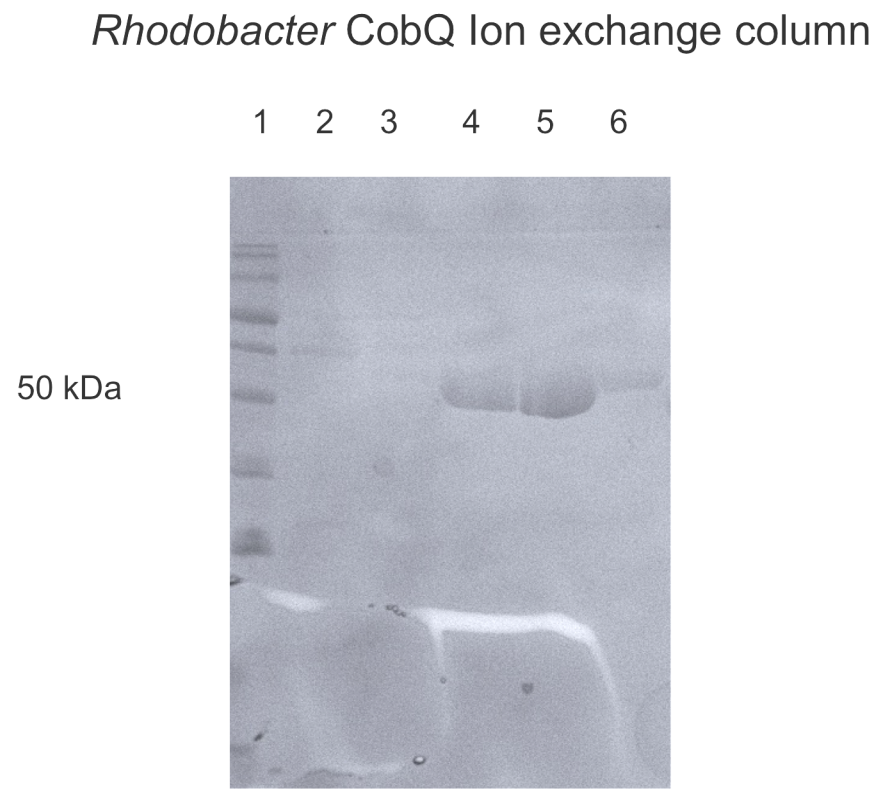

Figure 6.7: *R. capsulatus* CobQ from ion exchange column. Lane 1, contains protein markers of known molecular mass, as shown, Lane 2-6 A13 to B14. Protein was found to be in samples A15, B15 and B14.

6.3 Thermostability measurement of *A. vinosum* CobQ

For most CobQ enzymes, their corrin substrate is adenosylcobyrinic acid a,c-diamide, However, as *A. vinosum* is able to produce cobalt-free corrinoids it seems likely that the *A. vinosum* CobQ is able to amidate HBAD directly and must therefore be able to bind HBAD. In order to determine if the *A. vinosum* can bind HBAD, and also to identify the conditions under which CobQ is most stable, a thermostability assay of the reaction was generated. Here, the protein was subject to a temperature gradient from 25°C to 80°C, as the protein starts to unfold the dye (sypro orange) binds to the hydrophobic core of the enzyme resulting in a fluorescent signal (Santos *et al.* 2012).

A change in Tm value will give a good indication of whether there is a stabling effect on binding ligand, anything over 2 °C can be considered relevant. The other techniques that can be used to measure protein stability is Dynamic Light Scattering (DLS), but this method was unavailable.

The *A. vinosum* CobQ sample was analyzed in this way in the presence and absence of substrates in order to determine if HBAD-binding had a monitorable effect on the protein (Figure 6.8). Results are shown in Table 6.1.

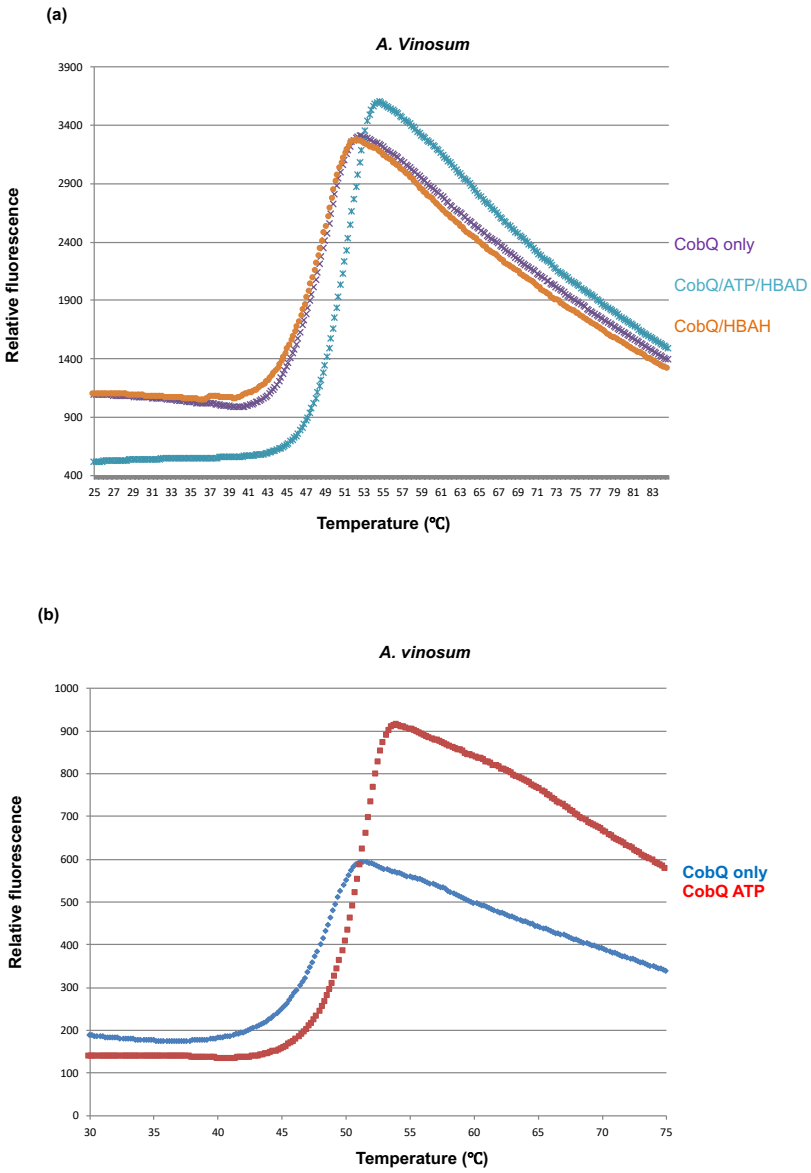

Figure 6.8: Melting temperatures for *A. vinosum* CobQ. (a) CobQ only (purple), CobQ/ATP/HBAD (blue) and CobQ HBAH (orange). (b) CobQ only (blue) and CobQ/ATP (red).

Table 6.1 Showing change in melting temperatures for *A. vinosum* CobQ.

Enzyme	**Tm (Temperature melt)**	**ΔTm**
A. vinosum CobQ only	47 °C	0°C
A. vinosum CobQ with ATP/Gln/HBAD	51 °C	4°C
A. vinosum CobQ/HBAH	47 °C	0°C
A. vinosum CobQ/ATP	51 °C	4°C

From the thermofluor results there is a clear 4 °C increase in the thermal stability of CobQ when it binds ATP and HBAD/ATP/Mg^{2+}. This indicates that CobQ from *A. vinosum* has increased stability in the presence of ATP.

6.4 MicroScale Thermophoresis (MST)

6.4.1 MST analysis of *A. vinosum* binding HBAD

To look more closely at binding of the *A. vinosum* CobQ with HBAD a MicroScale Thermophoresis (MST) assay was employed. This is a method commonly used for the characterisation of intermolecular reactions. It has a number of advantages over other technologies, including the use of very small amounts of protein to give accurate readings. For this assay a Tris-NTA (Tris-nitrilotriacetic acid) with an oligohistidine tag (Figure 6.9) was used to bind the His-tag of CobQ. This gives a high fluorescence signal and an optimal signal to noise ratio in microscale thermophoresis (MST). The RED-tris-NTA was found to be the optimal dye conjugate, this molecule has a high affinity towards histidine tags. Red-tris-NTA has emission in the red region of the

spectrum, and enables reliable measurements of complex biological matrices. By binding to the histidine tag of CobQ the binding reaction can then be monitored (Jerabek-Willemsen *et al.* 2014; Bartoschik *et al.* 2018).

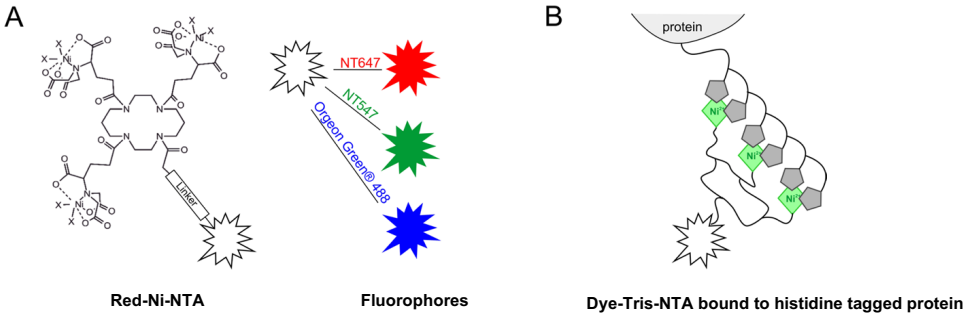

Figure 6.9: Labelling of protein with fluorescent dye. (A) Structure of Ni-NTA showing linker with bound fluorophore, typical fluorophores used in MST, NT647 (red), NT547 (green) and Orgeon green 488 (blue). (B) Schematic representation of the conjugate (Dye-Ni-NTA), which has Ni(II) ions enabling site specific labelling of the his-tagged protein (Bartoschik *et al.* 2018).

His-tagged *A. vinosum* CobQ was first labelled with the fluorescent dye (Red-Ni-NTA) using the protocol in Chapter 2 (2.5.1). The unlabelled molecule (HBAD) was then added to the enzyme. In total 16 eppendorf samples were labelled 1 to 16, in sample 1: 20 µL of the ligand solution is added. To the remaining 15 samples,10 µL of PBS was added. Serial dilutions are then employed, taking 10 µL from sample 1 and mixing with sample 2, removing 10 µL from sample 2 and mixing with sample 3 this is continued until all of the 16 samples have protein (protocol 2.5.2). The labelled samples are then loaded into glass capillaries using capillary action. Overview of the procedure is shown in Figure 2.1

Sixteen glass capillaries were loaded with increasing concentrations of labelled enzyme, these samples are used for analysis. (see protocol 2.5.2). The samples were run a number of times but did not give usable data. This indicates that *A. vinosum* CobQ from this sample did not bind HBAD.

6.5 Crystallisation of CobQ from *A. vinosum, B. melitensis* and *R. capsulatus*

The Molecular Dimensions screens 1 and 2 were used for initial screening of CobQ from *A. vinosum*, *B. melitensis* and *R. capsulatus* in crystallisation trials. Each of the three proteins was concentrated to 4 mg/mL in the presence of AMPPNP (5 uM) using purified protein. The protein to precipitant concentration was 2:1 (2 µL of protein and 1 µL of well solution). The crystal trays were monitored on a day to day basis.

6.5.1 Crystals of *A. vinosum* CobQ

After two days of screening, very fine needles were observed in a condition containing 1.6 M magnesium sulphate and 0.1 M MES, pH 6.5, for the *A. vinosum* CobQ (Figure 6.10). By optimisation of the magnesium sulphate concentration a usable crystal was obtained (Figure 6.10). This crystal was archived using well solution and 25% ethylene glycol and flash frozen in liquid nitrogen. The crystal was sent to the DLS but unfortunately this crystal showed no diffraction.

(a) (b)

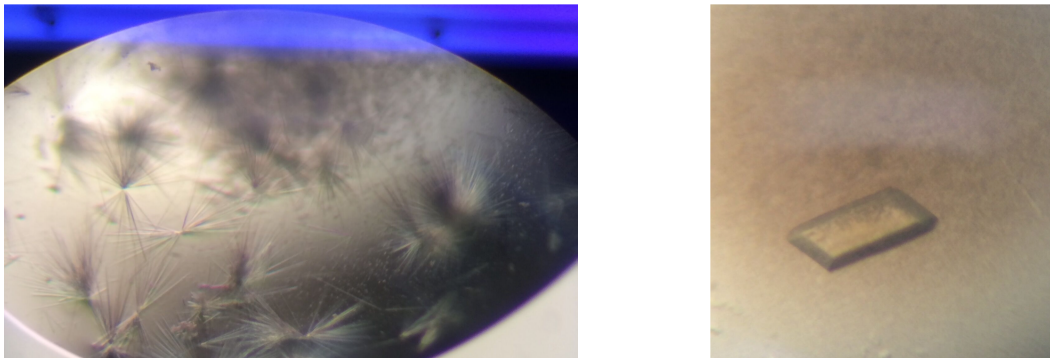

Figure 6.10: Crystals of *A. vinosum* CobQ. (a) Initial crystals appeared after two days, grown from 1.6 M magnesium sulphate and 0.1 M MES, pH 6.5 (very fine needles). (b) Optimisation of the above condition gave single crystals. This crystal was of a quality required for X-ray diffraction.

6.5.2 Crystallisation of CobQ from *R. capsulatus*

Crystallisation of the *R. capsulatus* CobQ was investigated using Molecular Dimensions screens 1 and 2 and from this a number of hits were identified. All of the hits in wells containing phosphate were found to be salt, however, in the presence of AMPPNP one condition containing 0.2 M magnesium formate with trans 4-hydroxyl-L-proline as an additive yielded a diffraction quality crystal (Figure 6.11). This crystal was archived and sent to the DLS for data collection.

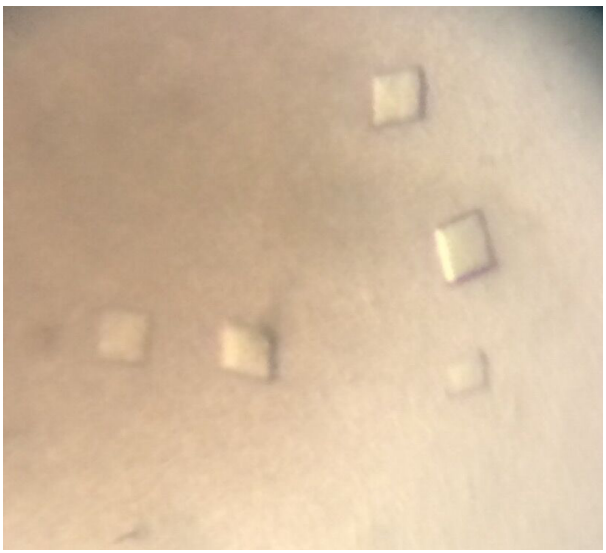

Figure 6.11: *R. capuslatus* crystals. Crystals were grown using 0.2 M Mg formate with trans 4-hydroxyl-L-proline as an additive. Crystals took three days to grow and were sent to the DLS for data collection.

This crystal diffracted to 4.5 Å, with a space group of $P6_1$ and cell dimensions of 174.12 Å. 174.12 Å 146.14 Å, α = 90.00, β = 90.00 and γ = 120.00. Although the structure was very low resolution an attempt was made to obtain the initial phases using the CobB structure. This, perhaps unsurprisingly, was unsuccessful since structure determination by molecular replacement generally requires much higher quality data. The best way forward would be to obtain higher quality CobQ crystals.

6.6 Production and purification of HBAD and HBAH

Adenosylcobyrinic acid *a, c*-diamide is the natural substrate for CobQ. This enzyme binds its substrate and amidates the carboxylates groups of position *b, d, e* and *g* of the ring resulting in the product adenosylcobyric acid. Crystals of the *R. capsulatus* of CobQ were obtained that diffracted to 4.5 Å, but due to poor resolution the structure was not solved. In order to increase the chance of obtaining crystals that would diffract to higher resolution, attempts were undertaken to make both the substrate and the product of the CobQ reaction, adenosylcobyrinic acid *a,c*-diamide and adenosylcobyric acid respectively. The binding of these compounds good potentially

stabilise the enzyme and lead to crystals that would diffract to higher resolution. As these molecules are not commercially available they must be produced in the lab. A

A plasmid containing all the necessary enzymes to produce both HBAD and HBAH was obtained from Evelyne Deery, University of Kent. The resulting strain (*E. coli* BGEC043 with (T7P)-AIG*JFLMKLH-A lvBQ-E*) was produced using 2YTNN broth and described in Chapter 2. After overnight production the culture was harvested by centrifugation and the pellet was resuspended in 30 mL of ethanol. The supernatant was then boiled for 30 minutes in order to denature the protein and separate the protein from its product and substrate (HBAD and HBAH). Centrifugation removed the denatured protein leaving HBA and HBAD in solution. The two compounds were separated using reverse phase chromatography. They were then separated on a DEAE column, with HBAH flowing through the column. HBAD was then removed from the column using an increasing concentration of NaCl, eluting in 100 mM NaCl. The compounds were dried and stored at -20°C until required.

6.6.1 Cobalt insertion to HBAD and HBAH

In order to bind these compounds to CobQ two separate samples were prepared, sample 1: HBAD and sample 2: HBAH were resuspended in 0.5 mM cobalt acetate at pH 6.0 and left at room temperature on a small shaker for up to 4 days to secure full insertion of the cobalt. Both reactions (HBAD and HBAH) were run of a spectrophotometer, and scanned from 300 nm to 700 nm (Figure 6.12) both samples are indistinguishable when run on a spectrophotometer (HBAH shown in Figure 6.12).

.

Cobalt insertion HBAH

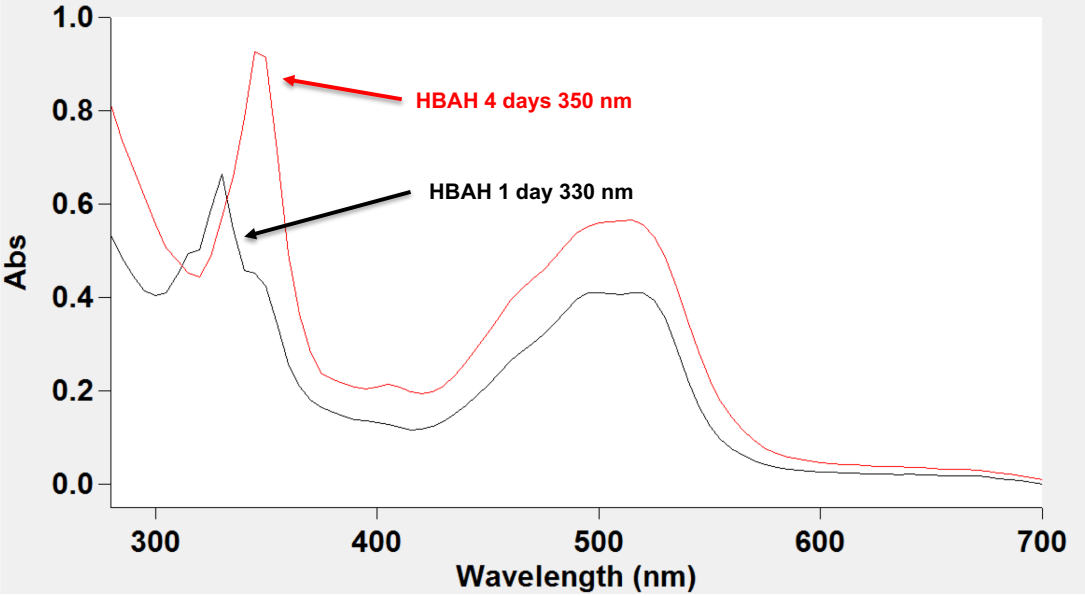

Figure 6.12: Cobalt insertion into HBAH. Trace shows HBAH after one day, with a typical absorption peak at 330 nm (black). After four days absorption peak moves from 330 nm to 350 nm (red) showing typical absorption peak at 350 nm which signifies full incorporation of cobalt.

6.7 Overexpression and purification of BtuR for adenosylation

In order to attach the upper ligand to cobyrinic acid *a,c*-diamide the expression of BtuR (CobR) is required, as BtuR is the enzyme involved in the attachment of the ligand to the enzyme (Lawrence *et al.* 2008b).

E. coli strain BL-21 (DE3) pLys*S* was transformed with pET14b carrying the BtuR gene resulting in the production of recombinant N-terminus His-tagged BtuR. The cells were grown in 2YT broth supplemented with ampicillin and chloramphenicol for 6 hours at 18 °C till an OD_{600} of 0.6 . The cells were induced with IPTG and were allowed to grow for a further 24 hours at 18°C (as described in Chapter 2). After harvesting by centrifugation the cell pellet was resuspended in Tris-HCl buffer, pH 8.0, containing 500 mM NaCl and 20 mM imidazole. The cells were then lysed by sonication and centrifuged for a second time to remove the cell debris. The protein was purified using a Ni chelate column and no further purification was necessary.

From a 1 L culture ~20 mg of protein was produced. BtuR was run on a 10 % SDS PAGE gel and appeared as a single band with a molecular mass of 22 kDa (Figure 6.13), which is in close agreement to the expected molecular mass of 21.986 kDa. The enzyme was found stable enough to be stored for periods of up to 6 months without any degradation.

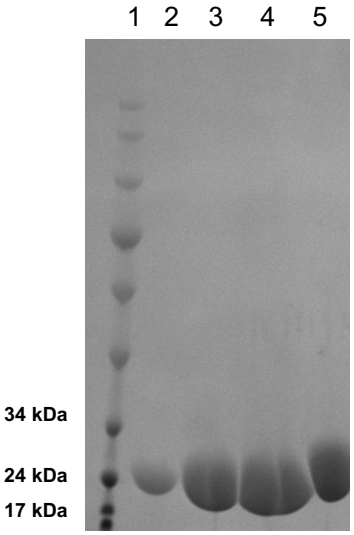

Figure 6.13: SDS PAGE gel of BtuR. Lane 1. contains protein markers of known molecular mass, as shown. Sample 2-5. 3 mL fractions from Ni column. All purified samples of BtuR were pulled and stored at -20 °C.

6.8 Adenosylation of cobalt HBAD and HBAH

As described in Chapter 2 all the components for the reaction buffer were placed in an anaerobic chamber for 24 hours before sample preparation, in order to make sure no oxygen was present in the samples. As this reaction is not only oxygen sensitive but also light sensitive everything was wrapped in tin foil. The cobyrinic acid *a,c*-diamide and cobyric acid with cobalt inserted were also placed in the chamber. The reactants were mixed and incubated again in the glove box for 24 hours. After incubation the sample was removed from the chamber, centrifuged and run through a reverse phase column (RP18), to remove any unbound material.

The product from the adenosylation assay using a UV-visible spectrometer was measured recorded 300 nm to 700 nm. The characteristic peak for the cobalt inserted substrate 350 nm was no longer present which signified that the adenosylation had been successful (Figure 6.14).

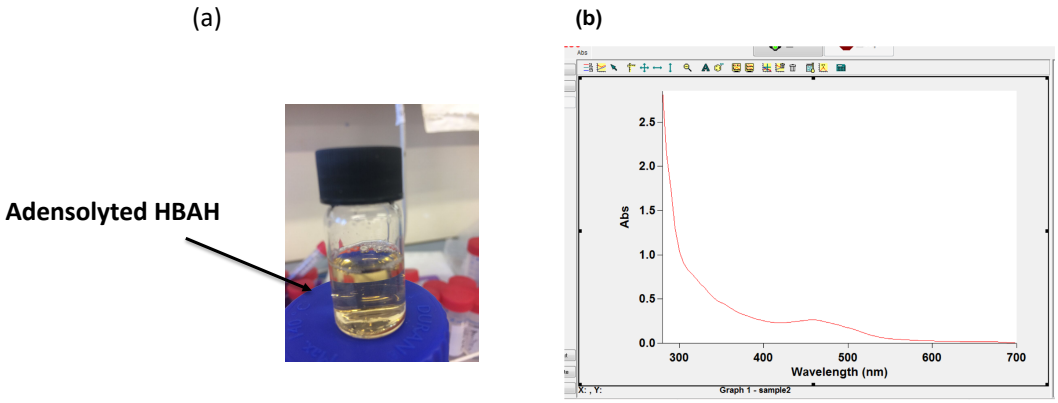

Figure 6.14: Adenosylation of HBAH. (a) Adensolyted sample removed from glove box, with characteristic yellow colour. (b) Adensolyted sample run on UV shows loss of 350 nm peak (see figure 6.12) indicating adensilation.

In order to verify that there was indeed adenosylation of the sample LC-MS analysis was undertaken (Dr. Andrew Lawrence, University of Kent). From the results there looks to be fragmentation of the sample in the run but there is a peak at 1186 Da which is the correct molecular mass for this product (Figure 6.15).

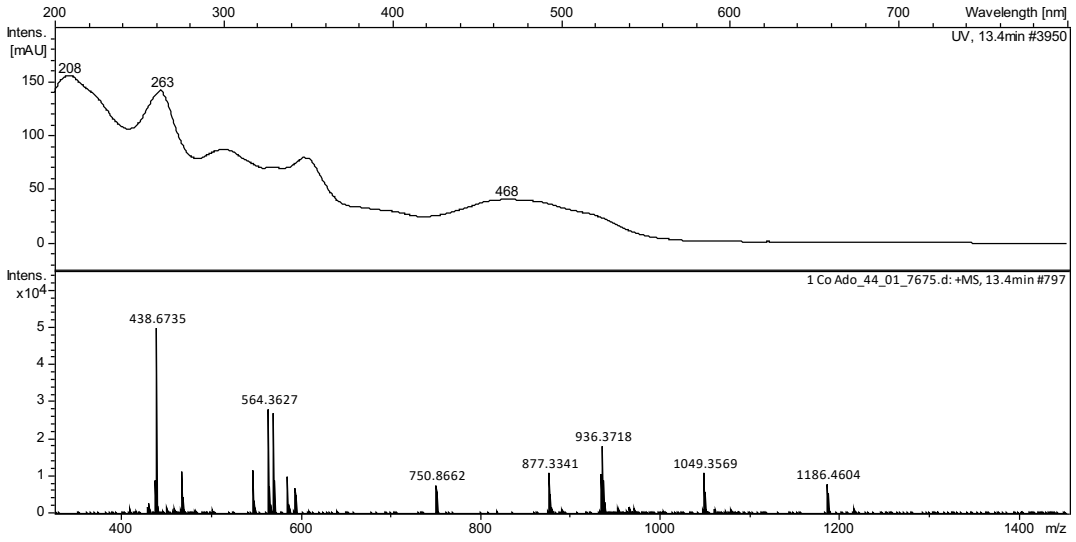

Figure 6.15: LC-MS analysis of adenosylated HBAH. LC-Ms shows a number of fragmented peaks, adensolyted HBAH peak at 1186.46 *m/z.*

6.9. Co-crystallisation trials of *Rhodobacter capsulitis* CobQ with adenosylcobyrinic acid a, c-diamide

To the purified *R. capsulatus* CobQ at a concentration of 4 mg/mL adenosylcobyrinic acid *a, c*-diamide (only) was added at a concentration of 100 µM. Co-crystallisation screens were set up using Molecular Dimension screens 1 and 2. A single tray was prepared using the condition that gave the initial diffracting crystals (0.2 M magnesium formate with trans 4-hydroxyl-L-proline) was also set up. Crystal trays were checked daily, but no crystals were observed. Further work is required to obtain adensolyted HBAD and HBAH that are of a purity and quality required for crystallisation.

6.10 Discussion

There are two enzymes involved in the six amidations of the side chains on the corrin ring, and these are CobB and CobQ. CobB has already been discussed in Chapter 3 and 4, whilst CobQ was the focus of this chapter. In order to increase the chances of obtaining structural information for CobQ, a number of CobQs from a range of bacteria were investigated for their suitability for crystallisation. Recombinant CobQs from *A. vinosum, B. melitensis* and *R. capsulatus* were expressed and purified from *E. coli*. Each of these proteins could be purified to homogeneity and behaved well when stored at -20 °C.

The added difficulty in obtaining a structure of CobQ is in the fact that binding of substrate only takes place after cobalt insertion and adenosylation. It was however reported that CobQ from *A. vinosum* was able to amidate the carboxylates on the corrin ring prior to cobalt insertion. When *A. vinosum* was supplemented with dimethylbenzimidazole (the lower ligand bound to cobalamin) this resulted in a compound that was identical to cobalamin (Koppenhagen and Pfiffner 1971).

In order to determine if this looked to be possible a thermofluor assay was set up. This assay did show an increase in stabilisation when ATP/Gln/HBAD were present, however, CobQ/ATP gave the same increase of 4 °C which could infer the stabilisation is due to the effects of ATP. In order to look more closely at this reaction an MST assay was run. No readable results were obtained which indicated that using this assay could not confirm binding.

A number of crystallisation trials were carried out which eventually resulted in a data set being collected for the *R. capsulatus* CobQ that was grown in the presence of AMPPNP. However, this crystal only diffracted to very low resolution (4.5 Å). Unfortunately, due to the low resolution and the fact that the CobB structure has only

15% identity between the two sequences no structural information was obtained.

In order to add stability to the enzyme and hopefully increase the chance of obtaining crystals, attempts were made to crystallise the protein in the presence of either its corrin substrate or corrin product. The substrate and product, adenosylcobyrinic acid a,c diamide and adenosylcobyric acid had to be produced from HBAD and HBAH. This synthesis was successful as determined by the UV visible analysis and the mass spectroscopy data (see Figure 6.14 and 6.15).

However, attempts to crystallise CobQ in the presence of either the corrin substrate or product were not successful. Due to the limited time in which to work with this complex no further trials have been attempted. However, there is still plenty of scope to explore the structure of CobQ in the future. Optimisation of the crystals that diffracted to 4.5 Å resolution would appear to be the best way forward.

CHAPTER 7

Discussion

7.1 General discussion

The knowledge and understanding of the biosynthetic pathways for cobalamin has come a great way since the structure of B_{12} was initially determined and the chemical synthesis of this molecule was first described (Woodward 1973.; Eschenmoser and Wintner 1977) (Quadros 2010). However, there are still several enzymes within the known biosynthetic pathways for cobalamin biogenesis that have not been fully characterised. A complete molecular understanding of the role played by the individual enzymes of the cobalamin pathway is important not only from a fundamental scientific standpoint, since it helps explain the molecular logic underpinning the process (Deery *et al.* 2013), but it can also be advantageous in exploiting the pathway to enable improved production of this essential nutrient and in the development of anti-vitamin molecules that interfere with B_{12}-dependent processes.

The aim of the research described in this thesis was to gain structural information on the enzymes that perform the amidations of the peripheral side chains of the corrin ring, namely CobB and CobQ. In fact, CobB proved to be the more amenable of the proteins to structural studies. This enzyme is responsible for amidating the *a* and *c* propionic acid side chains (Debuscche *et al.* 1990).

The X-ray crystal structure of *Brucella melitensis* CobB shows that the protein exists as a homodimer, where each subunit is composed of two globular domains. Dimer formation is mediated through interactions between helices 5 and 6 from each monomer (Chapter 3 Figure 3.23). CobB is composed of an N-terminal domain that binds ATP and the corrin substrate, and a C-terminal (GATase) domain that binds Gln as the amido donor (Debuscche *et al.* 1990).

In the C-terminal domain Gln is hydrolysed to glutamate and ammonia. The GATase domain belongs to the triad family of amidotransferase domains, which normally contain an active site with a conserved hydrogen bonded Cys-His-Glu arrangement (Raushel, Thoden and Holden 1999). However, in CobB the glutamic acid is not conserved when CobB is aligned with GATase family members (Raushel, Thoden and Holden 1999). Nonetheless, there is an alternative glutamic acid in the CobB family of proteins that is conserved (Glu326). From the structure of CobB it is clear that Glu326 is able to interact with His427 and Cys 327 and generate a catalytic triad (Figure 7.1). The glutamic acid acts to align and polarise His 427, which then activates the nucleophilic Cys327 (Bairagya and Bansal 2016). The triad reduces the pK_a of the nucleophilic cysteine which then attacks the substrate, allowing the release of ammonia from Gln and generating glutamic acid. Attack on the amido group of Gln leads to the formation of an oxyanion, which is stabilised in the oxyanion hole of CobB by the presence of positively charged backbone amides, all of which helps to stabilise the charge build up on the substrate transition state. Mechanistically, the active site His427 activates Cys327 for nucleophilic attack on the carboxyamide moiety of Gln to form a thioester intermediate, which leads to the release of ammonia (Bairagya and Bansal 2016).

The released ammonia is channelled from the GATase domain to the aminotransferase domain located in the N-terminal region of the protein so that it can be used to amidate the appropriate side chain on the corrin ring (Debuscche *et al.* 1990). The distance between the two domains is 17.7 Å (Chapter 3 Figure 3.30), and there appears to be a grove joining these two sites to help promote this channelling.

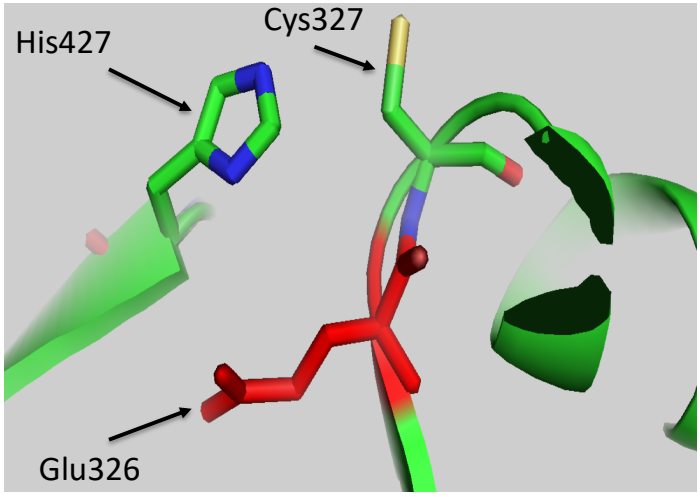

Figure 7.1 C-terminal binding site of CobB. Showing conserved histidine and cysteine, Glu326 conserved in CobB bacterial enzymes.

When CobB binds the corrin substrate in the N-terminal domain there is evidence of two distinct binding events, one of which is fast and one that is slow. This very likely represents the binding of corrin substrate to monomer A and then binding of a second corrin substrate to monomer B. This is evident from the observed kinetic data, which shows the rate of binding is much faster to monomer A than to B. This mechanism suggests negative co-operative feedback, which may be employed to control the rate of the enzyme, particularly its Gln hydrolysing activity since this could deplete levels of Gln within the cell if left unregulated.

CobB binds ATP in the same N-terminal active site of monomer A where the corrin substrate binds. The binding of ATP results in a slight change of conformation in the protein and decreases the rate at which HBA binds. HBA binds in an orientation that allows for the amidation of the C7 position on the ring to take place (Debussche *et al.* 1990). The carboxylate is able to promote the displacement of the terminal phosphate of ATP, generating ADP and a phosphorylated carboxylic acid. Ammonia, transferred to the active site from the GAT domain by a molecular tunnel, then acts as a nucleophile to displace the phosphate from the carboxylic acid, resulting in the amidation of the side chain and the release of inorganic phosphate. The HBAM then

leaves the active site, rotates 90° before being re-positioned in the active site with the C2 propionate side chain close to the ATP binding sight, and the process is repeated (Figure 7.2).

The negative cooperativity of substrate binding suggests that the enzyme follows a sequential model in which binding of substrate to one monomer induces a change in the other monomer. In the crystal structure the unstructured region (Phe176 to Leu183) from each monomer is involved in substrate binding to the opposite monomer. When there is no substrate in the active site, Arg177 in the unstructured region moves away from the HBA binding site of the opposite monomer and the other residues looks to fold round the ATP binding site of their own monomer. However, when HBA is present in the active site, Arg177 from the opposite monomer (B) interacts with the side chain attached to C18 of the corrin ring present in monomer A, whilst the other residues from Ala180 to Leu183 in monomer B flip away from the ATP binding site. This scissor like mechanism explains the difference in affinity and binding rate between the two monomers. When HBAM is in the active site and C2 is positioned in a conformation ready for amidation, the Arg177 now interacts with C13 on the ring.

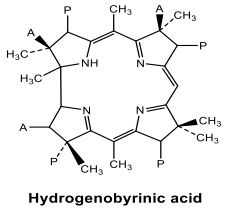

Hydrogenobyrinic acid

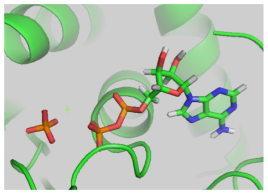

CobB binding ADP
and free phosphate

Mg-ATP

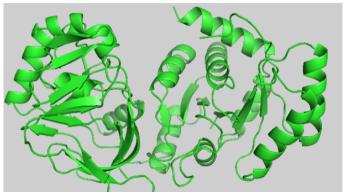

Monomer A of CobB

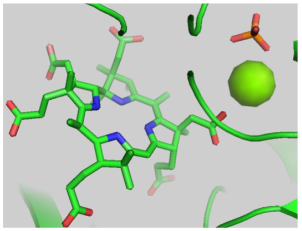

HBA binding CobB
Mg (ball) Phos. (orange)

ADP.Phos

[- COO-Ⓟ]
C7 on the ring

Gln Glu
NH_3

Amidation

HBAM leaves active site rotates 90 ° and re- binds

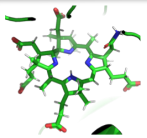

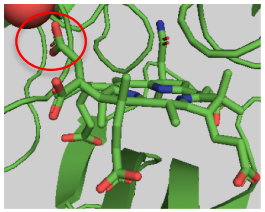

HBAM
C2 in position
for amidation

ADP.Phos

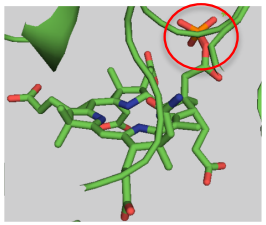

Phosphorylated
intermediate
C2 position on ring

NH_3

Glu Gln

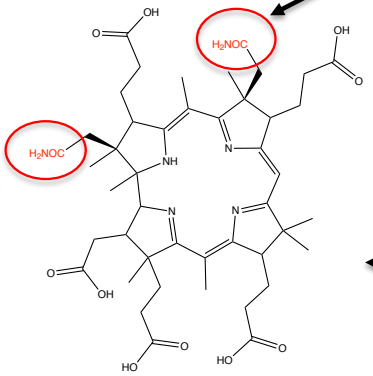

HBAD

C7

C2

270

Figure 7.2 Mechanism by which CobB binds HBA. The pathway shows the structure of CobB (only), binding Mg^{2+} and ATP which has been converted to ADP and free phosphate in the second structure. The third structure shows HBA binding CobB where the free phosphate and Mg^{2+} are visible. The next part of the reaction is the formation of a phosphorylated intermediate at position C7 (no crystal structure). This phosphorylated intermediate then undergoes amidation, and the mono amide leaves the active site rotates 90 °C and re-binds with the C2 position ready to be amidated (structure shown in pathway). The next structure shows the phosphorylated intermediate at the C2 position. Once this is amidated the product HBAD then leaves the active site.

CobQ, the second enzyme in the amidation process, amidates adenosylcobyrinic acid *a, c*-diamide to produce adenosylcobyric acid. As with CobB, CobQ is also a multifunctional enzyme, amidating four side chains on the ring (*b, d, e, g*) (Francis Blanche *et al.* 1991). Given the sequence similarity between CobB and CobQ it is highly likely that the these two enzymes will have a similar overall topology, reflecting the fact that they mediate a similar catalytic process albeit at different sites on the corrin ring. A crystal of CobQ was obtained, which diffracted to 4.5 Å resolution but unfortunately the structure could not be solved due to the poor resolution.

Obtaining a crystal structure of CobB enabled a closer look at the possible interaction that CobH may have with CobB since these two protein catalyse consecutive steps in the pathway. The crystal structures of CobH (Shipman *et al.* 2001) and CobB are such that it is plausible to suggest that an interaction may take place that enables CobH to release its product to CobB (Figure 5.9). CobH is known to binds its product, HBA, very tightly and it has been speculated that an interaction with the following enzyme in the pathway could allow for direct metabolite transfer (Miles, Rhee and Davies 1999; Huang, Holden and Raushel 2001). However, no strong interaction has been observed between CobH and CobB so therefore any interaction is likely to be transient. Indeed, attempts to generate a crystal of a complex between CobH and CobB were not successful. However, stopped-flow analysis was used to investigate the occurrence of transient interactions between the two proteins (Toseland and Geeves 2014), since the absorbance spectrum of HBA to CobH differed from HBA bound to CobB.

In this way it is possible, using HBA-loaded CobH, to follow the transfer of HBA to CobB. This provides the first evidence that a direct interaction between CobH and CobB takes place, but much more work is required to understand the molecular basis

of that specific interaction, which is favoured if CobB is also loaded with ATP and Gln. Further investigations, involving mutagenesis of specific amino acid residues, would be required in order to understand fully the process that leads to the release of HBA from CobH.

Obtaining structural and kinetic information on CobB has enabled a clearer insight of the mechanism by which the amidation process takes place during corrin ring synthesis. This project has, therefore, not only provided the first detailed structural characterisation of one of the amidases involved in cobalamin biogenesis but it has also opened the possibility of exploring, in molecular detail, the process by which the enzymes involved in the pathway are able to ensure that their precious biosynthetic intermediates are securely passed along the production line to generate the final product.

References

Acuner Ozbabacan, S.E. *et al.* (2011). Transient proteinprotein interactions. *Protein Engineering, Design and Selection* **24**:635–648.

Astner, I. *et al.* (2005). Crystal structure of 5-aminolevulinate synthase, the first enzyme of heme biosynthesis, and its link to XLSA in humans. *EMBO Journal* **24**:3166–3177.

Bairagya, H.R. and Bansal, M. (2016). New insight into the architecture of oxy-anion pocket in unliganded conformation of GAT domains: A MD-simulation study. *Proteins: Structure, Function and Bioinformatics* **84**:360–373.

Banerjee, R. and Ragsdale, S.W. (2003a). The Many Faces of Vitamin B 12 : Catalysis by Cobalamin-Dependent Enzymes. *Annual Review of Biochemistry* **72**:209–247.

Banerjee, R. and Ragsdale, S.W. (2003b). The Many Faces of Vitamin B_{12} : Catalysis by Cobalamin-Dependent Enzymes. *Annual Review of Biochemistry* **72**:209–247.

Barak, A.J., Beckenhauer, H.C. and Tuma, D.J. (2002). Methionine synthase. *Alcohol* **26**:65–67.

Bartoschik, T. *et al.* (2018). and purification-free protein labeling for quantitative protein interaction analysis by MicroScale Thermophoresis. *Nature Communications*:1–10.

Battersby, A.R. (2000). Tetrapyrroles : the pigments of life. *Natural Product Reports* **17**:507–526.

Battersby, A.R. (1978). The discovery of nature's biosynthetic pathways. *Experientia* **34**:1–13.

Beale, S.I. and Castelfranco, P.A. (1973). 14C incorporation from exogenous compounds into δ-aminolevulinic acid by greening cucumber cotyledons. *Biochemical and Biophysical Research Communications* **52**:143–149.

Blanche, F. *et al.* (1991). Biosynthesis of Vitamin B12 : Stepwise Amidation of Carboxyl Groups b , d , e , and g of Cobyrinic Acid a , c-Diamide Is Catalyzed by One Enzyme in Pseudomonas denitrificans. *Journal of Bacteriology* **173**:6046–6051.

Blanche, F. *et al.* (1993). Parallels and Decisive Differences in Vitamin B12 Biosyntheses. *Angewandte Chemie-international Edition - ANGEW CHEM INT ED* **32**:1651–1653.

Blanche, F. *et al.* (1992). Precorrin-6x Reductase from Pseudomonas. *Journal of Bacteriology* **174**:1036–1042.

Blanche, F. *et al.* (1991). Purification , Characterization , and Molecular Cloning of S-Adenosyl- L-Methionine : Uroporphyrinogen III Methyltransferase from Methanobacterium ivanovii. *Journal of Bacteriology* **173**:4637–4645.

Blanche, F. *et al.* (1995). Vitamin B12: How the Problem of Its Biosynthesis Was Solved. *Angewandte Chemie International Edition in English* **34**:383–411.

Bollivar, D.D. (2006). Recent advances in chlorophyll biosynthesis - Semantic Scholar. :173–194.

Briani, C. *et al.* (2013). Cobalamin Deficiency: Clinical Picture and Radiological Findings. *Nutrients* **5**:4521–4539.

Bridwell-Rabb, J., Grell, T.A.J. and Drennan, C.L. (2018). A Rich Man, Poor Man Story of S-Adenosylmethionine and Cobalamin Revisited. *Annual Review of Biochemistry* **87**:555–584.

Broderick, J.B. (2001). Coenzymes and Cofactors. *Encyclopedia of Life Sciences*.

Cameron, B. *et al.* (1991). Genetic analysis, nucleotide sequence, and products of two Pseudomonas denitrificans cob genes encoding nicotinate-nucleotide: dimethylbenzimidazole phosphoribosyltransferase and cobalamin (5'-phosphate) synthase. *Journal of Bacteriology* **173**:6066–6073.

Coot: model-building tools for molecular graphics - Emsley - 2004 - Acta Crystallographica Section D.

Cowtan, K. (2006). The Buccaneer software for automated model building. *Acta Crystallographica* **62**:1002–1011.

Crouzet, J. *et al.* (1991). Nucleotide Sequence and Genetic Analysis of a 13 . 1-Kilobase-Pair Pseudomonas denitrificans DNA Fragment Containing Five cob Genes and Identification of Structural Genes Encoding Cob (I) alamin Adenosyltransferase , Cobyric Acid Synthase , and Bifuncti. *Journal of Bacteriology* **173**:6074–6087.

Dailey, H.A. (2013). Illuminating the black box of B12 biosynthesis. *Proceedings of the National Academy of Sciences* **110**:14823–14824.

Dailey, H.A. *et al.* (2017). Prokaryotic Heme Biosynthesis: Multiple Pathways to a Common Essential Product. *Microbiology and Molecular Biology Reviews* **81**:1–62.

Debuscche, L. *et al.* (1990). Purification and characterization of cobyrinic acid a,c-diamide synthase from *Pseudomonas denitrificans*. *Journal of Bacteriology* **172**:6239–6244.

Debussche, L. *et al.* (1992a). Assay, purification, and characterization of cobaltochelatase, a unique complex enzyme catalyzing cobalt insertion in hydrogenobyrinic acid a,c- diamide during coenzyme B12 biosynthesis in Pseudomonas denitrificans. *Journal of Bacteriology* **174**:7445–7451.

Debussche, L. *et al.* (1992b). Assay, purification, and characterization of cobaltochelatase, a unique complex enzyme catalyzing cobalt insertion in hydrogenobyrinic acid a,c- diamide during coenzyme B12biosynthesis in Pseudomonas denitrificans. *Journal of Bacteriology* **174**:7445–7451.

Debussche, L. *et al.* (1993). Biosynthesis of the Corrin Macrocycle of Coenzyme B12 in Pseudomonas denitrificans NCO2H. *Journal of Applied Crystallography* **175**:7430–7440.

Debussche, L. *et al.* (1990). Purification and Characterization of Cobyrinic Acid a , c-Diamide Synthase from Pseudomonas denitrificans. *Journal of Bacteriology* **172**:6239–6244.

Debussche, L. *et al.* (1991). Purification and Partial Characterization of Cob (I) alamin Adenosyltransferase from Pseudomonas denitrificans. *Journal of Applied Crystallography* **173**:6300–6302.

Deery, E. *et al.* (2012). An enzyme-trap approach allows isolation of intermediates in cobalamin biosynthesis. *Nature chemical biology* **8**:933–40.

Deery, E. *et al.* (2013). Europe PMC Funders Group An enzyme-trap approach allows isolation of intermediates in cobalamin biosynthesis. *Nat Chem Biol.* **8**:933–940.

E. Neill. Marsh, G.D.R. (2012). Adenosylcobalamin enzymes: Theory and experiment begin to converge. *Biochimica et Biophysica Acta - Biomembranes* **11**:1154–1164.

Eccleston, J.F., Martin, S.R. and Schilstra, M.J. (2008). Rapid Kinetic Techniques. In: *Biophysical Tools for Biologists, Volume One: In Vitro Techniques*. Academic Press, pp. 445–477.

Emsley, P. and Cowtan, K. (2004). Coot: Model-building tools for molecular graphics. *Acta Crystallographica Section D: Biological Crystallography* **60**:2126–2132.

Eschenmoser, A. (1988). Vitamin B12: Experiments Concerning the Origin of Its Molecular Structure. *Angewandte Chemie International Edition in English* **27**:5–39. Eschenmoser, A. and Wintner, C.E. (1977). Natural product synthesis and vitamin B12. *Science* **196**:1410 LP-1420.

Evans, P. (2006). Scaling and assessment of data quality. *Acta crystallographica. Section D, Biological crystallography* **62**:72–82.

Fan, C. and Bobik, T.A. (2008). The PduX Enzyme of Salmonella enterica Is an L - Threonine Kinase Used for Coenzyme B 12 Synthesis *. *Journal of Biological Chemistry* **283**:11322–11329.

Fang, H., Kang, J. and Zhang, D. (2017). Microbial production of vitamin B12: a review and future perspectives. *Microbial Cell Factories* **16**:15.

Ferreira, G. and Gong, J. (1995). *5-Aminolevulinate Synthase and the First Step of Heme Biosynthesis*. Vol. 27.

Frankenberg, N., Moser, J. and Jahn, D. (2003). Bacterial heme biosynthesis and its biotechnological application. *Applied Microbiology and Biotechnology* **63**:115–127.

Fresquet, V., Williams, L. and Raushel, F.M. (2007). Partial Randomization of the Four Sequential Amidation Reactions Catalyzed by Cobyric Acid Synthetase with a Single Point Mutation †. *Biochemistry*:13983–13993.

Fresquet, V., Williams, L.K. and Raushel, F.M. (2004). Mechanism of cobyrinic acid a,c-diamide synthetase from Salmonella typhimurium LT2. *Biochemistry* **43**:10619–10627.

Galperin, M.Y. and Grishin, N. V. (2000). The synthetase domains of cobalamin biosynthesis amidotransferases CobB and CobQ belong to a new family of ATP-dependent amidoligases, related to dethiobiotin synthetase. *Proteins: Structure, Function and Genetics* **41**:238–247.

Gherasim, C., Lofgren, M. and Banerjee, R. (2013). Navigating the B 12 Road : Assimilation , Delivery , and Disorders of Cobalamin *. *Journal of Biological Chemistry* **288**:13186–13193.

Gu, S. *et al.* (2015). Crystal structure of CobK reveals strand-swapping between Rossmann-fold domains and molecular basis of the reduced precorrin product trap. *Scientific Reports* **5**:16943.

Hamza, I. and Dailey, H.A. (2012). One ring to rule them all: Trafficking of heme and heme synthesis intermediates in the metazoans. *Biochimica et Biophysica Acta - Molecular Cell Research* **1823**:1617–1632.

Hennig, M. *et al.* (1997). Crystal structure of glutamate-1-semialdehyde aminomutase : An ⎵ 2 -dimeric vitamin B 6 -dependent enzyme with asymmetry

in structure and active site reactivity. *PNAS* **94**:4866–4871.

Hodgkin, D.C. *et al.* (1955). Structure of Vitamin B12 : The Crystal Structure of the Hexacarboxylic Acid derived from B12 and the Molecular Structure of the Vitamin. *Nature* **176**:325–328.

Holden, H.M., Thoden, J.B. and Raushel, F.M. (1998). Carbamoyl phosphate synthetase: A tunnel runs through it. *Current Opinion in Structural Biology*:8:679-685.

Huang, D.D. *et al.* (1958). The enzymatic synthesis of d-aminolevulinic acid. *J Biological Chemistry* **233**:1214–1219.

Huang, X., Holden, H.M. and Raushel, F.M. (2001). Channeling of Substrates and Intermediates in Enzyme-Catalyzed Reactions. *Annual Review of Biochemistry* **70**:149–180.

Jahn, D. and Heinz, D.W. (2009). Biosynthesis of 5-Aminolevulinic Acid BT - Tetrapyrroles: Birth, Life and Death. In: Warren, M. J. and Smith, A. G. eds. *Springer New York*. New York, NY: Springer New York, pp. 29–42.

Jerabek-Willemsen, M. *et al.* (2014). MicroScale Thermophoresis: Interaction analysis and beyond. *Journal of Molecular Structure* **1077**:101–113.

Johnson, C.L. V *et al.* (2001). Functional Genomic , Biochemical , and Genetic Characterization of the Salmonella pduO Gene , an ATP : Cob (I) alamin Adenosyltransferase Gene †. *Journal of Bacteriology* **183**:1577–1584.

Jordan, P.M. and Berry, A. (1981). Mechanism of action of porphobilinogen deaminase. *Biochemical Journal* **1**:177–181.

Ko, Y.H., Hong, S. and Pedersen, P.L. (1999). Chemical Mechanism of ATP Synthase. *Journal of Biological Chemistry* **274**:28853–28856.

Koppenhagen, V.B. and Pfiffner, J. (1971). c11-(5,6 obamide and Its Copper and Zinc Analogues*. **246**.

Kranz, R.G. *et al.* (2009). Cytochrome c Biogenesis: Mechanisms for Covalent Modifications and Trafficking of Heme and for Heme-Iron Redox Control. *Microbiology and Molecular Biology Reviews* **73**:510–528.

Laemmli, U.K. (1970). Cleavage of Structural Proteins during the Assembly of the Head of Bacteriophage T4. *Nature***227**:680–685.

Lawrence, A.D. *et al.* (2008a). Identification , Characterization , and Structure / Function Analysis of a Corrin Reductase Involved in. *JBC* **283**:10813–10821.

Lawrence, A.D. *et al.* (2008b). JBC Papers in Press . Published on February 8 , 2008 as Manuscript M710431200. The latest version is at http://www.jbc.org/cgi/doi/10.1074/jbc.M710431200. *JBC*:1–22.

Leeper, J. (1987). The biosynthesis of porphyrins, chlorophylls, and vitamin B12. *Natural Product Reports* **2(6)**:561–580.

Leisico, F. *et al.* (2018). First insights of peptidoglycan amidation in Gram-positive bacteria-The high-resolution crystal structure of Staphylococcus aureus glutamine amidotransferase GatD. *Scientific Reports* **8**:1–13.

LENHERT, P.G. and HODGKIN, D.C. (1961). Structure of the 5,6-Dimethylbenzimidazolylcobamide Coenzyme. *Nature* **192**:937–938.

Leslie, A.G.W. (2006). The integration of macromolecular diffraction data. *Acta Crystallographica Section D: Biological Crystallography* **62**:48–57.

Lobo, S. a L. *et al.* (2015). Staphylococcus aureus haem biosynthesis: Characterisation of the enzymes involved in final steps of the pathway. *Molecular Microbiology* **97**:472–487.

Louie, G. V *et al.* (1992). Structure of porphobilinogen deaminase reveals a flexible multidomain polymerase with a single catalytic site. *Nature* **359**:33–39.

Ludwig, M.L., Drennan, C.L. and Matthews, R.G. (1996). The reactivity of B12 cofactors: The proteins make a difference. *Structure* **4**:505–512.

Lundqvist, J. *et al.* (2009). The AAA+ motor complex of subunits CobS and CobT of cobaltochelatase visualized by single particle electron microscopy. *Journal of Structural Biology* **167**:227–234.

Martens, J.H. *et al.* (2002). Microbial production of vitamin B12. *Applied Microbiology and Biotechnology* **58**:275–285.

Martens, J.H. *et al.* (2014). Microbial production of VitaminB Microbial production of vitamin B 12. *Applied Microbiology and Biotechnology* **58**:275.

Mathews, M.A.A. *et al.* (2001). Crystal structure of human uroporphyrinogen III synthase. *EMBO Journal* **20**.

McFerrin, M.B. and Snell, E.H. (2002). The development and application of a method to quantify the quality of cryoprotectant solutions using standard area-detector X-ray images. *Journal of Applied Crystallography* **35**:538–545.

Miles, E.W., Rhee, S. and Davies, D.R. (1999a). Channeling *. *Journal of Biological Chemistry* **274**:12193–12197.

Miles, E.W., Rhee, S. and Davies, D.R. (1999b). The molecular basis for substrate channeling. *J Biol Chem* **274**:12193–12197.

Moore, S.J. *et al.* (2012). Biochemical Society Annual Symposium No . 79 The anaerobic biosynthesis of vitamin B 12. :581–586.

Moore, S.J. *et al.* (2013). Elucidation of the anaerobic pathway for the corrin

component of cobalamin (vitamin B12). *Proceedings of the National Academy of Sciences of the United States of America* **110**:14906–11.

Moore, S.J. *et al.* (2017). Elucidation of the biosynthesis of the methane catalyst coenzyme F 430. *Nature* **543**:78–82.

Moser, È. *et al.* (2001). V-shaped structure of glutamyl-tRNA reductase, the first enzyme of tRNA-dependent tetrapyrrole biosynthesis. *EMBO Journal* **20**:6583–6590.

Mura, C. (2014). Development & Implementation of a PyMOL 'putty' Representation. *Department of Chemistry & Biochemistry, UCSD*:3–5.

Murooka, Y. *et al.* (2005). Production of tetrapyrrole compounds and vitamin B12 using genetically engineering of Propionibacterium freudenreichii . An overview To cite this version : HAL Id : hal-00895589 Production of tetrapyrrole compounds and vitamin B 12 using genetically engin. *Le Lait, INRA Editions* **85**:9–22.

Nordlander, J.E. and Mccrary, T.J. (1974). Additions and Corrections: Stereochemistry and Mechanism of Acetolysis of 4,4-Dimethylcyclohexyl Tosylate (J. Am. Chem. Soc. (1972) 94(14) (5133–5135) (10.1021/ja00769a084)). *Journal of the American Chemical Society* **96**:4066–4067.

O'Leary, F. and Samman, S. (2010). Vitamin B12 in health and disease. *Nutrients* **2**:299–316.

Parsons, J.B. *et al.* (2010). Characterisation of pdus, the pdu metabolosome corrin reductase, and evidence of substructural organisation within the bacterial microcompartment. *PLoS ONE* **5**.

Pravda, L. *et al.* (2014). Anatomy of enzyme channels. *BMC Bioinformatics* **15**:1–8.

Quadros, E. (2010). Advances in the Understanding of Cobalamin Assimilation and Metabolism. *Br J Haematol* **148(2)**:195–204.

Ragsdale, S.W. (2011). NIH Public Access. *NIH Public Access* **79**:293–324.

Raushel, F.M., Thoden, J.B. and Holden, H.M. (2003). Enzymes with molecular tunnels. *Accounts of Chemical Research*.

Raushel, F.M., Thoden, J.B. and Holden, H.M. (1999). The amidotransferase family of enzymes: Molecular machines for the production and delivery of ammonia. *Biochemistry* **38**:7891–7899.

Raux, E., Lanois, A. and Levillayer, F. (1996). Salmonella typhimurium Cobalamin (Vitamin B12) Biosynthetic Genes: Functional Studies in S. typhimurium and Escherichia coli. *J. Bacteriol.* **178**:753–767.

Rehms, A.A. and Callis, P.R. (1993). Two-photon fluorescence excitation spectra of aromatic amino acids. *Chemical Physics Letters* **208**:276–282.

Reid, J.D. and Hunter, C.N. (2002). Current understanding of the function of magnesium chelatase. *Biochemical Society Transactions* **30**:643–645.

Reinbothe, S. *et al.* (1996). Evolution of chlorophyll biosynthesis - The challenge to survive photooxidation. *Cell* **86**:703–705.

Rickes, E.L. *et al.* (1948). Crystalline vitamin B12. *Science* **107**:396–397.

Rickes, E.L. *et al.* (1948). Crystalline Vitamin B12 | Science. *Science* **107**:396–397.

Robscheit, F.S., Hooper, C.W. and Whipple, G.H. (1920). Blood regeneration following simple anemia IV. Influence of meat, liver and various extractives, alone or combined with standared diets. *Am. Journal of Physiol.* **53**:151.

Roth, J.R. *et al.* (1993). Characterization of the cobalamin (vitamin B12) biosynthetic genes of Salmonella typhimurium. *Journal of Bacteriology* **175**:3303–3316.

Roth, J.R. *et al.* (1993). Characterization of the Cobalamin (Vitamin B12) Biosynthetic Genes of Salmonella typhimurium. *Journal of Bacteriology* **175**:3303–3316.

Sampson, E.M., Johnson, C.L. V and Bobik, T.A. (2005). Biochemical evidence that the pduS gene encodes a bifunctional cobalamin reductase. **151**:1169–1177.

Santos, S.P. *et al.* (2012). Thermofluor-based optimization strategy for the stabilization and crystallization of Campylobacter jejuni desulforubrerythrin. *PROTEIN EXPRESSION AND PURIFICATION* **81**:193–200.

Scott, A. *et al.* (1993). Biosynthesis of vitamin B12. Discovery of the enzymes for oxidative ring contraction and insertion of the fourth methyl group. *FEBS Letters* **331**:105–108.

Senge, M.O. (2015). N-H Hydrogen Bonding in Porphyrins - from Conformational Design to Supramolecular Chemistry. *ECS Transactions* **66**:1–10.

Seyedarabi, A. *et al.* (2010). Cloning , purification and preliminary crystallographic analysis of cobalamin methyltransferases from Rhodobacter capsulatus crystallization communications Cloning , purification and preliminary crystallographic analysis of cobalamin methyltransferases fr. *Acta Crystallographica* **F66**:1652–1656.

Shemin, D. and Kikuchi, G. (1958). ENZYMATIC SYNTHESIS OF δ-AMINOLEVULINIC ACID*. *Annals of the New York Academy of Sciences* **75**:122–128.

Shin, J.A. *et al.* (2007). 5-Aminolevulinic Acid Biosynthesis in Coexpressing NADP-dependent Malic Enzyme and 5-Aminolevulinate Synthase. *Journal of Microbiol*

Biotechnol **17**:1579–1584.

Shipman, L.W. *et al.* (2001). Crystal structure of precorrin-8x methyl mutase. *Structure* **9**:587–596.

Shorb, M. (1948). The effects of dissociation in Lactobascillus lactis cultures on the requirements for vitamin B12. *J Biological Chemistry* **1607**:1463–1465.

Smith L. (1948). pubmed_result. *Nature* **24**:638.

Spencer, J.B. *et al.* (1993). The Escherichia coli cysG gene encodes the multifunctional protein, siroheme synthase - Spencer - 19. *FEBS Letters* **335**:57–60.

Suh, S.-J. and Escalante-Semerena, J.C. (1993). Cloning, sequencing and overexpression of cob A which encodes ATP:corrinoid adenosyltranferase in Salmonella typhimurium. *Gene* **129**:93–97.

Thauer, R.K. and Bonacker, L.G. (2007). Biosynthesis of Coenzyme F430, A Nickel Porphinoid Involved in Methanogenesis. In: *Ciba Foundation Symposium 180 - The Biosynthesis of the Tetrapyrrole Pigments*. John Wiley & Sons, Ltd, pp. 210–227.

Thibaut, D. *et al.* (1992). The final step in the biosynthesis of hydrogenobyrinic acid is catalyzed by the cobH gene product with precorrin-8x as the substrate. *Journal of Bacteriology* **174**:1043–1049.

Toseland, C.P. and Geeves, M.A. (2014). Rapid reaction kinetic techniques. In: Toseland, C. P. and Fili, N. eds. *Fluorescent Methods Applied to Molecular Motors: From Single Molecules to Whole Cells*. Springer, pp. 49–64.

Tripathy, B.C., Sherameti, I. and Oelmüller, R. (2010). Siroheme: An essential component for life on earth. *Plant Signaling and Behavior* **5**:14–20.

Trotta, P.P. *et al.* (1974). Glutamine-Binding Subunit of Glutamate Synthase and Partial Reactions. *Proceedings of the National Academy of Sciences* **71**:4607–4611.

Trzebiatowski, J.R., Toole, G.A.O. and Escalante-semerena, J.C. (1994). The cobT Gene of Salmonella typhimurium Encodes the NaMN : Responsible for the Synthesis of Nl- (5-Phospho-x-D-Ribosyl) - 5 , 6-Dimethylbenzimidazole , an Intermediate in the Synthesis of the Nucleotide Loop of Cobalamin. *Journal of Bacteriology* **176**:3568–3575.

Vagin, A.A. *et al.* (2004). REFMAC5 dictionary: Organization of prior chemical knowledge and guidelines for its use. *Acta Crystallographica Section D: Biological Crystallography* **60**:2184–2195.

Vishnu, P. *et al.* (2013). *A Method to Trap Transient and Weak Interacting A Method to Trap Transient and Weak Interacting Protein Complexes for Structural Studies*. Vol. 0707.

Walker, C. and Robert, W. (1997). Mechanism and regulation of Mg-chelatase. *Biochem J* **327**:321–333.

Walker, J.E. *et al.* (1982). Distantly related sequences in the alpha- and beta-subunits of ATP synthase, myosin, kinases and other ATP-requiring enzymes and a common nucleotide binding fold. *The EMBO Journal* **1**:945–951.

Warren, M.J. *et al.* (1992). Enzymic synthesis and structure of precorrin-3, a trimethyldipyrrocorphin intermediate in vitamin B12 biosynthesis. *Biochemistry* **31**:603–609.

Warren, M.J. *et al.* (2002). The biosynthesis of adenosylcobalamin (vitamin B12). *Natural Product Reports* **19**:390–412.

Woalder Xiwei Zheng, Cong Bi, Zhao Li, Maria Podariu, and D.S.H. (2017). NHS Public Access. *Physiology & behavior* **176**:139–148.

Woodward, R.B. (1973). The total synthesis of vitamin B12. *Pure and Applied Chemistry* **33(1)**:145–178.

Zayas, C.L. and Escalante-semerena, J.C. (2007). Reassessment of the Late Steps of Coenzyme B 12 Synthesis in Salmonella enterica : Evidence that Dephosphorylation of Adenosylcobalamin-5 J -Phosphate by the CobC Phosphatase Is the Last Step of the Pathway. *Journal of Bacteriology* **189**:2210–2218.

Zhoo, Q.K., Hartnett, M.S. and Slater, M.R. (2007). Selenomethionine Protein Labeling Using the Escherichia coli Strain KRX. *Promega Corporation*:24–26.